UNIVERSITY OF BIRMINGHAM

EFFECTS OF LOW-LEVEL LIGHT THERAPY ON EPITHELIAL PROGENITOR CELLS

by

Siti Aishah Zainal

A thesis submitted to
The University of Birmingham
for the degree of
DOCTOR OF PHILOSOPHY

Oral Biology
School of Dentistry
College of Medical & Dental Sciences
The University of Birmingham
September 2016

ABSTRACT

Low level light therapy has been widely used in the management of a range of human diseases. Light irradiation triggers a range of cellular signalling processes in a variety of cells, promoting wound healing and preventing cell death. The aim of this study was to investigate the photobiomodulatory effects of low level lasers and light-emitting diodes (LEDs) on human oral epithelial cells (H400 cells) as well as neutrophils, as a potential management strategy for periodontitis. Initially light sources were characterised to obtain dosage (radiant exposure) for light experiments. In addition, a model system utilising H400 cells was developed and characterised prior to laser and LEDs irradiation analysis. Biological responses were determined upon irradiation.

Results demonstrated that irradiation by laser and LEDs enhanced H400 cell growth. This was described by mitochondrial metabolic activity and cell proliferation marker, Ki-67. This supports the ability of low-level light to trigger cell growth for further healing inflammation in periodontal disease. Furthermore, ROS production by human neutrophils was attenuated following LEDs irradiation and this suggests this light therapy may decrease level of neutrophil ROS in inflamed tissue and improve wound healing.

Data suggested potential therapeutic benefits for enhancing healing in the gingival epithelium, which propose the possibility of the use of light therapy, a non-invasive tool in periodontal disease management.

Dedication

I dedicate this thesis to my husband Rusydi, my late father Zainal, my mother Normah, my daughter ‘Iffah and my parents-in law, Mohamad Noor and Chempawan. Special thanks to them for their endless love, prayer and support for me to complete this study.

Acknowledgement

My deepest appreciation is dedicated to my PhD supervisors, Dr Mike Milward, Professor Paul Cooper and Professor Will Palin for their endless support, patience, guidance and motivation throughout my study until I have completed my lab work and PhD thesis. My warm acknowledgment also goes to Mrs Michelle Holder and Dr M. A. Hadis, who spent much time teaching me on cell culture and laser and LEDs, Mrs Gay Smith, Ms Sue Finney, Dr Helen Wright, Dr Naomi Hubber and Mrs Khawla Doudin for kindly helping me with experimental works in Floor 7 lab.

I also would like to thank all staffs and postgraduate students at the School of Dentistry, particularly in Floor 7 and 8, who were there when I needed help, cheered me up when I was in tears. I wish to thank Perio group members, Pip, Helen Roberts, Ilaria and Iman, who have guided me doing neutrophils and special thanks to Kak Farha, who was there as a sister.

In addition, I would like to thank the Government of Malaysia and Universiti Sains Malaysia for funding my study.

TABLE OF CONTENTS

LIST OF FIGURES

CHAPTER 1: INTRODUCTION

CHAPTER 2: MATERIALS AND METHODS

CHAPTER 3: LIGHT SOUCE CHARACTERISATION

CHAPTER 4: ESTABLISHMENT OF ORAL EPITHELIAL CELL (OEC) H400s CULTURE

CHAPTER 5: H400 RESPONSES TO LASER IRRADIATION

CHAPTER 6: H400 RESPONSES TO SINGLE LED

CHAPTER 7: H400 RESPONSES TO 1ST GENERATION LED ARRAY IRRADIATION

LIST OF TABLES

CHAPTER 4: ESTABLISHMENT OF ORAL EPITHELIAL CELL (OEC) H400s CULTURE

CHAPTER 5: H400 RESPONSES TO LASER IRRADIATION

ABBREVIATIONS

AFU	Arbitrary fluorescence units
ANOVA	Analysis of variance
ATCC	American Type Culture Collection
ATP	Adenosine triphosphate
BHI	Brain heart infusion
BSA	Bovine serum albumin
cDNA	Complementary deoxyribonucleic acid
CCD	Charged coupled device
CCTV	Closed circuit television
DMEM/F-12	Dulbecco's modified Eagle's medium:nutrient mixture F-12
DMSO	Dimethyl sulfoxide
DNA	Deoxyribonucleic acid
DNase	Deoxyribonuclease
dTNPmix	Deoxynucleotide mix
ELISA	Enzyme linked immunosorbent assay
Fiji	Fiji is just Image J
GAPDH	Glyceraldehyde-3-phosphate dehydrogenase
H_2O_2	Hydrogen peroxide
IL-	Interleukin-
J	Joule
L	Litre
LDH	Lactase dehydrogenase
LPS	Lipopolysaccharide
M	Molar
min	Minutes
mm	Millimetre
MTT	3-(4,5-dimethylthiazol-2-yl)-2,5 diphenyl tetrazolium bromide
NAC	N-acetyl-cysteine

NADPH	Nicotinamide adenine dinucleotide phosphate
ND	Neutral density
NF-κB	Nuclear factor-kappa B
NIST	National Institute of Standards and Technology
nm	Nanometres
NO	Nitric oxide
OEC	Oral epithelium cell line
Oligo-dT	Oligonucleotide deoxy-thymine
PBS	Phosphate Buffered Saline
PCR	Polymerase chain reaction
PMA	Phorbol 12-myristate 13-acetate
RLU	Relative light units
RNA	Ribonucleic acid
RNase	Ribonuclease
ROS	Reactive oxygen species
rpm	Rotation per minute
RPMI	Roswell Park Memorial Institute
RT	Reverse transcriptase
s	Second
SD	Standard deviation
SMA	SubMiniature version A
SMD	Surface mount device
T-EDTA	Trypsin ethylenediaminetetraacetic acid

CHAPTER 1: INTRODUCTION

1.1 Introduction

The use of low-power light as a therapeutic modality is termed low-level light therapy (LLLT), photobiomodulation or phototherapy. LLLT has a wide range of healthcare applications (Kishen & Asundi 2007) and over the last 50 years it has been used for the management of a wide variety of medical and dental conditions including management of inflammation, promotion of wound healing and for pain relief (Barolet 2008, Parker 2007). The application of LLLT provides a safe, non-invasive, rapid and inexpensive method for delivering a therapeutic benefit (Kishen & Asundi 2007). Currently, LLLT devices are produced for treating a range of medical and dental diseases and utilise both laser and light-emitting diodes (LEDs) to deliver light therapy to target tissues.

LLLT utilises red and near-infrared (NIR) light (Figure 1.1). It is termed “low level” light therapy because the light applied utilises relatively low irradiances as compared with other forms of laser therapy used for ablation, cutting and tissue coagulation. As the low power densities used do not produce tissue heating, LLLT has also been termed “cold-laser” or “soft-laser” therapy. LLLT is therefore distinct in being non-ablative and non-thermal (Avci *et al.,* 2013, Gupta & Hamblin 2013, Greathouse *et al.,* 1985, Fork 1971).

A large number of both *in vivo* and *in vitro* studies have reported beneficial therapeutic outcomes following LLLT delivery (Parker 2007). However the potential of LLLT for oral therapy has received relatively little attention in comparison with its use in other clinical fields such as Medicine and Surgery (Kishen & Asundi 2007).

Notably, therapeutic benefits of LLLT have been shown in the treatment of inflamed oral tissues (Chor *et al.,* 2004), skin ulceration (Lagan *et al.,* 2000), dermatitis (Morita *et al.,* 1993), wound healing (Conlan *et al.,* 1996), chronic joint inflammatory disorder such as osteoarthritis and rheumatoid arthritis (Bjordal *et al.,* 2003), tinnitus (Salahaldin *et al.,* 2012) as well as in promoting nerve regeneration (Mohammed *et al.,* 2007) indicating the broad potential for this treatment modality.

The literature on light therapy is characterised by variable results which occur as a result of poor study design and due to an inadequate understanding of light delivery characteristics which lead to wide variations in light dose delivery at a cellular level (Hadis *et al.,* 2016). The key parameters which need to be considered for light delivery include wavelength (λ), irradiance (mW/cm^2), exposure time (s) and radiant exposure, or fluence (the product of irradiance and time, J/cm^2) which need to be optimised to ensure optimal therapeutic dose delivery (1.1.2.2).

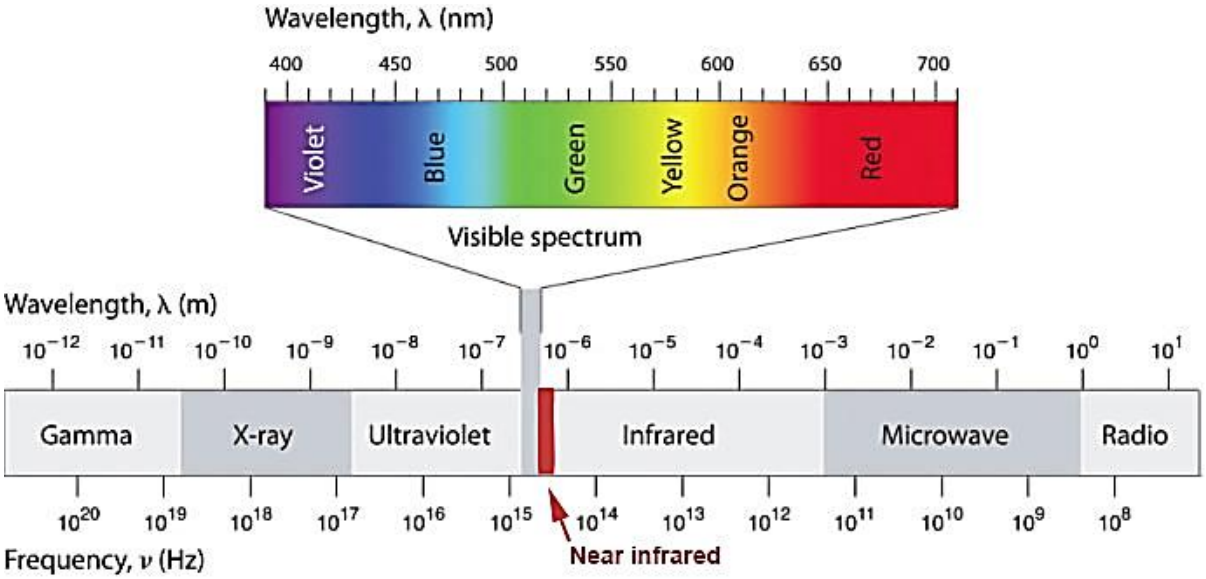

Figure 1.1: The electromagnetic spectrum showing visible light (blue, green and red) and invisible light (near-infrared) (www.resonantfm.com).

1.1.1 Historical perspective

Light therapy has been used to treat a wide range of diseases over many centuries. The first recorded report of the use of light therapy was in 1400 BC, where sunlight was used to treat skin diseases in combination with plant extracts. A number of other diseases have utilised sunlight for disease treatment in a wide range of countries including ancient Egypt, China, Rome and Greece (Roelandts 2002, Gupta & Hamblin 2013). The effective use of sunlight therapy was believed to occur due to the presence of red light and the sun's heat as the ultraviolet (UV) component of sunlight was not discovered until 1801 (Roelandts 2002).

In the second half of the 19th century, the interest in sunlight therapy markedly increased with a range of studies using sunlight to derive clinical benefit, examples include Downes and Blunt (1877) reporting that anthrax bacilli could be killed by sunlight. In addition, Palm from Edinburgh, in 1890, proposed that the sunlight could treat patients with rickets. Alongside this researchers became more aware of the effectiveness of UV rays present in sunlight and this lead to the use of filtered sunlight and development of artificial light sources (Roelandts 2002). Other applications of light therapy were later reported in 1893 by Niels Ryberg Finsen, a Danish physician and scientist who applied filtered sunlight for the treatment of lupus vulgaris (Roelandts 2005). Subsequently Finsen founded the Medical Light Institute in Copenhagen (later the Finsen Institute) in 1896 and continued to utilise natural sunlight filtered through glass lenses. A year later, he developed an artificial light source using a carbon arc lamp combined with quartz filters to treat patients with skin tuberculosis. His work in dermatology using light therapy resulted in him receiving the

1903 Nobel Prize for “Physiology of Medicine”. His work also demonstrated that red-light exposure reduced the incidence of smallpox pustules (Gupta & Hamblin 2013). Finsen is often called the ‘Father of Modern Phototherapy’ because he was the first clinician to utilise artificial light sources to treat a number of skin diseases (Roelandts 2005).

Following the development of first laser by Theodore H. Maiman in 1960 (Gaspar 2009; Carroll *et al.,* 2014) Professor Endre Mester, from Semmelweis Medical University in Budapest, Hungary began research into lasers as a therapeutic modality in 1965 (Hamblin & Demidova 2006). One of his first experiments aimed to determine whether the use of lasers could induce malignancy. In this initial experiment he used a ruby red laser (694nm) to irradiate mice. He shaved hair from two groups of mice; one as control (no laser exposure) and another group was treated using the ruby laser. To his surprise, the application of the low-powered laser did not induce tumour formation, but did enhance hair regrowth in the irradiated compared with non-irradiated mice (Gaspar 2009, Gupta & Hamblin 2013, Carroll *et al.*, 2014). This finding was the first demonstration of light to produce “photobiostimulation”. Mester is subsequently regarded as the ‘Father of Photobiomodulation’ as he was the first to describe the bio-stimulatory effects of laser light (Gaspar 2009). His research went on to utilise LLLT to manage patients with non-healing skin ulcers (Gaspar 2009, Gupta & Hamblin 2013).

The other main light source utilised in LLLT are LEDs (light emitting diodes) and initial studies by the National Aeronautics and Space Administration (NASA)

demonstrated that specific wavelengths enhanced plant growth. Further work aimed to promote wound healing in astronauts and Navy Seals and research with LEDs showed that light could also promote wound healing and had potential to treat various medical conditions (Barolet 2008) e.g accelerating skin wound healing (Weiss *et al.,* 2005), increasing cells viability in Parkinson's disease (Liang *et al.,* 2008) and positive respond on treating keratosis pilaris rubra (KPR) (Barolet 2008).

Following on from these early findings, LLLT using lasers and LEDs now benefit thousands of people worldwide who have a range of medical conditions (Gaspar 2009, Kishen & Asundi 2007, Barolet 2008).

1.1.2 Laser and LED

Most of the early research on LLLT utilised lasers, specifically HeNe (helium-neon) with a wavelength of 632.8nm. More recently LEDs have become popular for light delivery due to their flexibility in device design and relatively inexpensive. However one key difference is that laser devices produce coherent light whereas LEDs produce non-coherent light. It is proposed by some authors that coherence may play an important role in the effects produced by LLLT, however the literature also cites evidence that non-coherent light demonstrated enhanced clinical benefit when compared to coherent light treatment. It has been suggested that this finding may be due to the relatively broad spectrum of non-coherent light emitted by LEDs in comparison narrow spectrum produced by lasers. It is proposed that the wider range of wavelengths produced by LEDs may simultaneously excite multiple chromophores and stimulate multiple biochemical reactions which may not occur during coherent

laser irradiation. Likewise, irradiation using monochromatic coherent laser may not match the peak activation wavelength of the target chromophore, whereas LEDs producing a wider wavelength spectrum increase the chance of eliciting a positive chromophore response (Dall Agnol *et al.,* 2009; Karu 2003). So there is considerable confusion in the literature as to possible therapeutic differences between lasers and LEDs so this debate still needs to be fully resolved (Chung *et al.,* 2012).

1.1.2.1 Cellular mechanism of LLLT

The biological mechanism that underpins the cellular response to LLLT remains to be fully elucidated, however the most commonly proposed mechanism involves light absorption by the mitochondrial respiratory chain component cytochrome C oxidase (CCO). This photonic interaction causes release of bound nitric oxide (NO) from CCO allowing rebinding of oxygen and progression of respiration with downstream generation of adenosine triphosphate (ATP) and reactive oxygen species (ROS). This molecular response results in activation of a number of cell signalling pathways (Karu 2008, Karu 1989) and downstream protein synthesis resulting in enhanced cell proliferation / migration, and modulation of levels of cytokines, growth factors and inflammatory mediators as well as increased tissue oxygenation (Karu and Kolyakov 2005) (see Section 1.1.2.1).

LLLT was reported to promote wound healing by increasing cell proliferation (Hawkins & Abrahamse 2006). Karu (1999) indicated that biochemical reactions as well as whole cell metabolic activity can be stimulated by certain wavelengths of light. Proteins in mitochondria are likely to be the major molecules absorbing visible red

light and near infra-red (NIR) light used in LLLT; however the biological effects of LLLT are not yet fully understood (Walsh 1997). Notably within tissues, LLLT has also been shown to induce vasodilation resulting in increased blood flow allowing increased oxygen and immune cell trafficking to injured tissues which contributes to the wound healing (Walsh 1997).

Several authors have suggested that the mechanisms underpinning this form of biostimulation and induction of proliferation are derived from light absorption by key proteins (Gao & Xing 2009, Karu *et al.,* 2005). Karu proposed the mechanism of action is due to light absorption by a photoacceptor (chromophore), in particular CCO (cytochrome C oxidase) which plays an important role in the mitochondrial oxidative respiration cascade (Karu 2010), resulting in modulation of biochemical reactions (through signal transduction mechanisms) and cell proliferation (Gao & Xing 2009, Karu 1999). LLLT exposure of mitochondria (Greco *et al.,* 1989) reportedly results in release of NO from CCO which then allows oxygen to rebind and resume respiratory chain activity.

Two possible mechanisms which are linked are shown in Figure 1.2 and are described below.

1) Binding of NO to CCO results in down-regulation of cellular respiration, light is proposed to displace NO and allow binding of oxygen thereby promoting respiration and increased production of ATP (Karu 1999, Chung *et al.,* 2012).

2) A relatively new and alternate mechanism has been proposed for how the light improves NO bioavailability whereby CCO may act as a nitrite reductase enzyme (a

one electron reduction of nitrite gives NO) when the partial pressure of oxygen is low. The reaction which may subsequently take place is described by Equation 1.1.

Equation 1.1

$$NO_2^- + 2H^+ + e^- (CCO) \rightarrow NO + H_2O$$

In the electron transport chain, oxygen as the final electron accepter is converted to water. Oxygen metabolism produces reactive oxygen species (ROS) as a natural by-product and is actively involved in cell signalling, cell cycle progression, enzyme activation and protein synthesis. It is understood that LLLT stimulates oxygen metabolism thus increasing ROS production which trigger a range of transcription factors including NF-kB resulting in downstream gene expression changes and cytokine/growth factor production implicated in cellular proliferation and migration (Chung *et al.,* 2012).

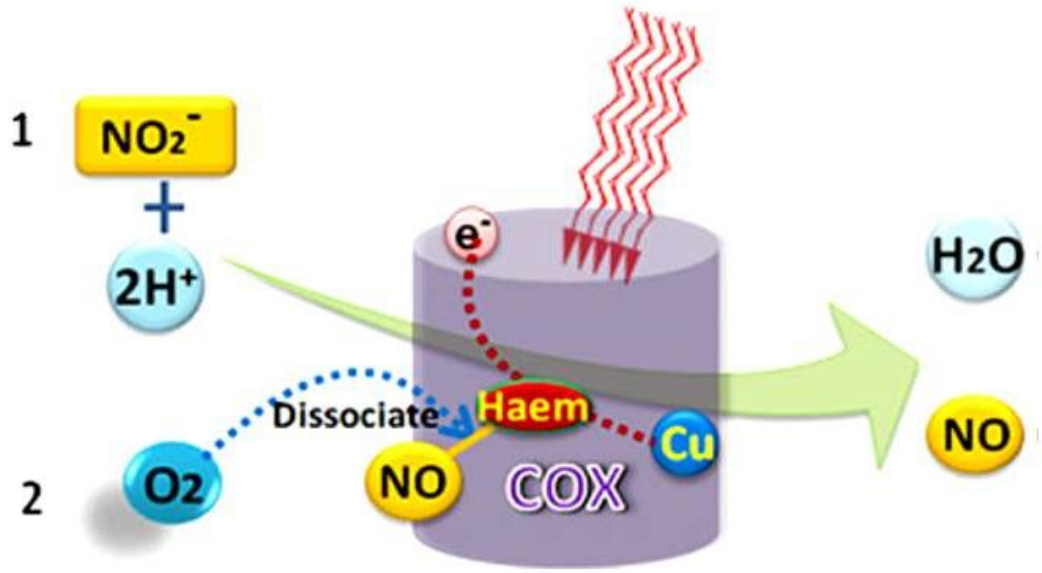

Figure 1.2: Diagram showing the possible mechanism of nitric oxide (NO) release from cytochrome c oxidase (CCO). Mechanism 1 indicates that CCO may act as a nitrite reductase enzyme and mechanism 2 shows the possible photodissociation of NO from CCO. Activation of both pathways may lead to the cellular and tissue responses associated with LLLT (Chung *et al.,* 2012).

1.1.2.2 LLLT radiometric parameters

As previously indicated, irradiation and dose parameters are key factors in successful application of LLLT. Incorrect parameter application and dose delivery may lead to less effective or even negative biological outcomes. Thus LLLT parameters need to be carefully defined to ensure accurate dose delivery can be achieved. There are two key components of this : (i) Irradiation parameters; which are wavelength, power, beam area, irradiance, pulse structure and coherence (Table 1.1) and (ii) Dose parameters; which are energy, radiant exposure, irradiation time and treatment interval (see Table 1.2) (Jenkins & Carroll 2011, Gupta & Hamblin 2013, Carroll *et al.*, 2014, Hadis *et al.,* 2016).

Notably, some studies published in the literature have not shown any significant correlation between LLLT and biological cell responses (Pogrel *et al.,* 1997). This is often due to inadequate determination of irradiation and dose parameters or lack of clarity with regard to light delivery and the types of cells being exposed (Posten *et al.,* 2005, Gao & Xing 2009, Hallman *et al.,* 1988, Pogrel *et al.,* 1997, Jenkins & Carroll 2011).

Table 1.1: Summary of parameters involved in defining LLLT irradiation (Huang *et al.,* 2009, Carroll *et al.,* 2014).

Parameter	Unit	Description
Wavelength	nm	Laser and LED devices utilised in LLLT emit in the spectrum range of 600-1000nm (red to NIR).
Power (Flux)	W	Power range 1mW to 10W.
Beam area	cm^2	Beam area is required for calculating irradiance.
Irradiance (Intensity)	W/cm^2	Often called Intensity or Power Density and it calculated as Irradiance = Power (W)/Area (cm^2). Typical irradiance is between $5mW/cm^2$ to $5W/cm^2$.
Pulse structure	Peak power (W) Pulse frequency (Hz) Pulse width (s) Duty cycle (%)	If the beam is pulsed then the power should be the average power and calculated as follows: Average Power (W) = Peak Power (W) x pulse width (s) x pulse frequency (Hz)
Coherence	Coherence length depends on spectral bandwidth	Coherent light produces laser speckle. Non-coherent light produces broader spectrum of wavelength.

Table 1.2: Summary of parameters involved in defining LLLT dose delivery (Huang *et al.,* 2009, Carroll *et al.,* 2014).

Parameter	Unit	Description
Energy (Joules)	J	Calculated as: Power (W) x time (s) = Energy (J).
Radiant exposure	J/cm^2	Calculated as: Power (W) x time (s)/beam area = Radiant exposure (J/cm^2).
Irradiation time	s	Irradiation time is to define the “dose” of LLLT after the other four parameters of the “medicine”.
Treatment interval	Hours, days or weeks	Evidence suggested that this is an important parameter.

1.1.3 LLLT versus photodynamic therapy (PDT)

The application of LLLT is different from photodynamic therapy (PDT). LLLT achieves its effect by direct interaction at a cellular level to reduce inflammation and promote healing. In contrast PDT uses light to activate an intermediary photosensitizer which generates active molecules that kill cells, e.g. bacteria or cancer cells. PDT utilises light with an appropriate wavelength which activates the photosensitising agent in target tissues to exert its killing effects. Arguably PDTs' most widely used application therapeutically is to kill pathogenic bacterial species that cause disease (Gursoy *et al.,* 2013). During exposure to light the photosensitizer undergoes transition from a low-energy-level (ground state) to a higher-energy (triplet state) with the higher-energy sensitizer reacting with biomolecules to produce free radicals and radical ions, or with molecular oxygen to generate singlet oxygen. The production of these cytotoxic species leads to oxidation of bacterial cellular components such as the cell membrane and it induces DNA damage, resulting in cell death (Gursoy *et al.,* 2013, Denis & Hamblin 2013).

LLLT is not as widely applied as PDT in the treatment of oral disease. While PDT can be used adjunctively for periodontitis, scaling and root planning are still considered the treatment of choice for the dentist to manage this chronic inflammatory disease. However, there is considerable potential for the use of LLLT in managing this and other oral diseases (Shivakumar *et al.,* 2012, Konopka & Goslinski 2007).

1.1.4 LLLT in treating disease

More than 2000 studies have been conducted and published where LLLT has been used for managing a range of diseases. Notably as previously mentioned LLLT has been used to treat inflamed oral tissues (Chor *et al.,* 2004), ulceration (Lagan *et al.,* 2000), dermatitis (Morita *et al.,* 1993), wound healing (Posten *et al.,* 2005), chronic inflammatory disease (Bjordal *et al.,* 2003), diseases of the ear (Salahaldin *et al.,* 2012) as well as in promoting nerve regeneration (Mohammed *et al.,* 2007) (see Table 1.3). However this thesis will focus on the specific oral application of LLLT and this will be explored in greater detail in the following text.

1.1.5 LLLT in oral disease management

Many positive clinical studies using LLLT have been reported over the last 40 years (Kishen & Asundi 2007, Barolet 2008). An advantage of LLLT is that it is non-invasive compared with other treatment approaches, however the application of LLLT in clinical dentistry has attracted limited research in comparison with other areas of medicine (Kishen & Asundi 2007).

Table 1.3: Selected examples of the application of LLLT for disease management.

Application	Effect of LLLT	Reference
Venous ulceration	Decrease in wound surface area	Lagan *et al.,* 2000
Dermatitis	Reduced skin lesions	Morita *et al.,* 1993
Tinnitus	Improved symptoms	Salahaldin *et al.,* 2012
Chronic joint disorder	Reduced inflammation, pain and improved function	Bjordal *et al.,* 2003
Degenerative peripheral nerve diseases	Improved nerve regeneration	Mohammed *et al.,* 2007

Low-level light based device application in dentistry has been used for treatment for diagnosis and therapy e.g., denture stomatitis (Maver-Biscanin *et al.,* 2004), healing regeneration (Naka & Yokose 2012, Kishen & Asundi 2007). It is known that light stimulates and triggers healing processes in wound tissues (Kishen & Asundi 2007) and in dentistry LLLT has been reported for several therapeutic applications including reduction of post-extraction oedema, dentin hypersensitivity (Gerschman *et al.,* 1994, Lizarelli *et al.,* 2007), oral mucositis (Cauwels & Martens 2011), oral stomatitis (Chor *et al.,* 2004) and candidiasis (Mima *et al.,* 2010). Considerable interest has been generated in exploring the application of LLLT as it allows simple non-invasive delivery, does not produce significant heat, sound or vibration and has no known detrimental effects on cells or tissues (Huang *et al.,* 2009, AlGhamdi *et al.,* 2012).

A range of lasers suitable for LLLT application are commercially available including ruby (694 nm), helium neon (HeNe; 632.8 nm), argon (Ar; 488 and 514 nm), krypton (521, 530, 568 and 647 nm), gallium aluminium arsenide (GaAlAs; 820 and 830 nm) and gallium arsenide (GaAs; 904 nm) (Posten *et al.,* 2005). While the scope of dental research for application of LLLT has been limited there are examples of long term therapeutic use with the countries of Japan and Russia having 10 and 30 years' experience respectively (Walsh 1997).

Positive effects of LLLT have been demonstrated in at cellular level with LLLT demonstrating enhanced cell proliferation in human dental pulp stem cells (hDPSC) (Eduardo *et al.,* 2008, Holder *et al.,* 2012) and human endothelial cells (Schindl *et al.,* 2003, AlGhamdi *et al.,* 2012, Hawkins & Abrahamse 2006). The published literature

also reports that LLLT has efficacy in reducing gingival inflammation (Bezerra 2015) and promoting tissue repair (Lins *et al.,* 2010). Combined, these cellular effects support the premise that LLLT has the potential for significant clinical efficacy in managing chronic oral inflammatory disease such as periodontitis.

1.2 Periodontal disease

Periodontal diseases result in damage to the periodontal tissues that support the teeth including gingivae, cementum, alveolar bone and the periodontal ligament (see Figure 1.3). Periodontal disease develops as a result of plaque interaction with the host immune/inflammatory response (Clerehugh *et al.,* 2009). Localised inflammation of the gingival tissues is known as gingivitis, this is a ubiquitous condition found in over 95% of the population and is associated with no loss of periodontal attachment (bone, periodontal ligament, or gingivae) and is completely reversible if the plaque biofilm is removed (Clerehugh *et al.,* 2009). In contrast periodontitis is caused by an aberrant host immune/inflammatory response to the plaque biofilm and is characterised by a non-resolving chronic inflammatory lesion which in contrast to gingivitis, results in irreversible local tissue damage (Pihlstrom *et al.,* 2005).

Table 1.4: Examples of the application of LLLT relevant to the dental research field (*in vivo* and *vitro*) (Carroll *et al.*, 2014).

Application	Effect of LLLT	Reference
Soft tissue healing	Induced proliferation of human gingival fibroblasts	Kreisler *et al.,* 2002
Oral mucositis	Reduced severity and pain	Cauwels & Martens 2011
Dentin hypersensitivity	Reduced thermal sensitivity	Lizarelli *et al.,* 2007
Oral stomatitis	Reduced pain and severity	Chor *et al.,* 2004
Chronic gingivitis	Reduced inflammation	Igic *et al.,* 2012
Periodontitis	Less inflammation & improved clinical outcomes	Makhlouf *et al.,* 2012
Implants	Promoted bone formation	Naka & Yokose 2012
Dental pulp cell responses	Increased mitochondrial activity in dental pulp cell	Holder *et al.,* 2012

Periodontitis is characterised by infiltration of immune cells such as polymorphonuclear (PMN) leukocytes, monocytes, lymphocytes, plasma and mast cells as well as local increases in cytokines. Cytokines comprise of signalling molecules such as chemokines, interferons, interleukins and tumour necrosis factors (Silva *et al.,* 2007, Milward 2010). Dysregulation of cytokine production has been implicated in the pathogenesis of several oral inflammatory diseases, including periodontitis (Konstan & Berger 1997) (see Section 1.2.5.2, 1.2.5.3 and 1.2.5.4).

1.2.1 Anatomy of the periodontal tissues

The periodontal tissues comprise of the gingivae, periodontal ligament, root cementum and alveolar bone (Milward 2010 & Clerehugh *et al.,* 2009) (see Figure 1.3). The periodontal ligament allows attachment of the tooth to the alveolar bone as well as providing support for the teeth during function (Palumbo 2011). The gingival tissues are part of oral mucosa (Palumbo 2011) and are essential to protect periodontal tissues from the external oral environment (Nanci & Bosshardt 2006).

The junction between gingival tissue and tooth enamel is termed the dentogingival junction and comprises epithelial and connective tissue components. The epithelium attachment is further subdivided into three functional zones – gingival, crevicular and junctional epithelium – and the connective tissue is subdivided into superficial and basal compartments. The junctional epithelium provides a barrier protecting the periodontal tissues from the external oral environment (Nanci & Bosshardt 2006, Milward 2010).

1.2.2 Impact of periodontal disease

Periodontitis occurs in susceptible individuals and while initiated by the plaque biofilm it is characterised by an exaggerated host inflammatory/immune response. A range of risk factors have also been identified which increase the likelihood of a subject experiencing disease such as smoking (Palmer *et al.,* 2005), plaque accumulation and systemic diseases, such as diabetes (Akalın *et al.,* 2008, Palmer *et al.,* 2005).

Periodontitis, due to its ability to cause loss of tissue support is a major cause of tooth loss (Pihlstrom *et al.,* 2005) if not correctly managed. The identification and severity of periodontal disease is defined by clinical parameters which are probing depth and attachment level. In recent years periodontitis has been associated with a range of systemic inflammatory diseases that share common pathogenic pathways, e.g. cardiovascular disease (Scannapeico *et al.,* 2003), diabetes (Seymour *et al.,* 2007) and rheumatoid arthritis (Clark 2000). In addition periodontitis has been shown to have a significant negative impact on the quality of life of patients. Indeed a life quality assessment was undertaken by Needleman and colleagues in 2004 using the UK oral health-related quality-of-life measure (OHQoL-UK©) showed how periodontal disease impacted on the day to day life of the patients. Notably the oral health condition affected their physiological state and appearance (Needleman *et al.,* 2004) (Table 1.5). Besides the uncomfortable condition produced by the oral disease frequently impacting and reducing the quality of life in terms of physical, physiological and social aspects.

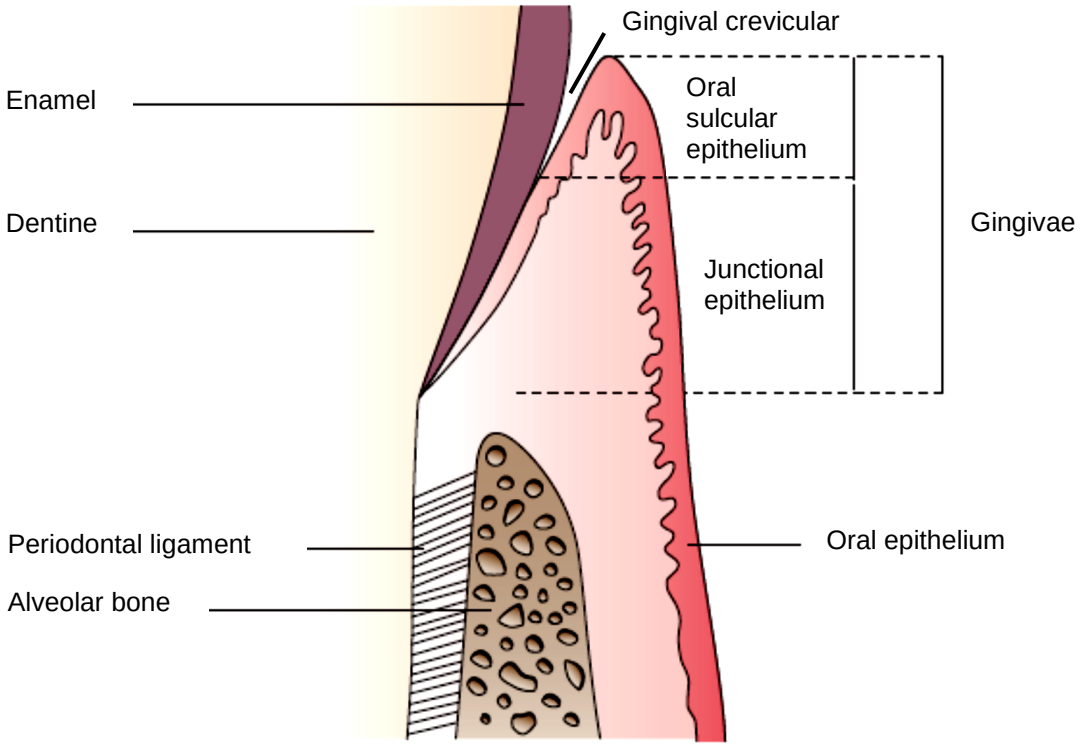

Figure 1.3: A longitudinal section of a tooth showing the adjacent healthy periodontal tissue and its components (Clerehugh *et al.,* 2009).

1.2.3 Epidemiology

The recent UK Adult Dental Health Survey (2009) indicated that 45% of adults have evidence of periodontal disease, with some 8% of individual exhibiting severe disease. Table 1.5 describes the oral health effect on patients' epidemiological survey (Needleman *et al.,* 2004) whilst Figure 1.4 demonstrates periodontal pocketing at three levels of severity (White *et al.,* 2012). A similar pattern can be seen in the United States of America where 47% of the population has evidence of periodontitis (Eke *et al.,* 2012). Given the large numbers of the UK and global populations affected by periodontal disease, improving therapeutic strategies would have significant positive influences upon treatment outcomes.

1.2.4 Disease pathogenesis

1.2.4.1 Inflammation

The word "inflammation" is derived from the Latin word '*inflammare*' (to set on fire) (Ferrero-Miliani *et al.,* 2006). Clinically the signs of inflammation include *rubor* (redness), *calor* (heat), *tumor* (swelling), and *dolor* (pain) and were defined initially by Cornelius Celsus, a Roman encyclopaedist almost 2000 years ago. Later a fifth sign of inflammation; (*functio laesa*) loss of function was included by Rudolf Virchow, one of the 19th century's notable leaders in medicine and pathology (Ferrero-Miliani *et al.,* 2006, Medzhitov 2008, Schultz 2008, Nathan 2002). Mechanistically these signs of inflammation are characterised by vasodilatation resulting in increased blood flow, elevated cellular metabolism, release of soluble mediators, and extravasation of fluids and cellular matrix (Ferrero-Miliani *et al.,* 2006).

Table 1.5: Data demonstrates how periodontal oral disease affects patient quality of life in percentage (Needleman *et al.,* 2004).

OHQoL-UK© items	Very bad effect % (number)	Bad effect % (number)	No effect % (number)	Good effect % (number)	Very good effect % (number)
Symptoms					
comfort	1 (2)	18 (37)	41 (83)	21 (43)	20 (40)
breath odour	2 (3)	16 (33)	44 (91)	22 (44)	17 (35)
Physical aspects					
eating	0 (0)	14 (28)	49 (100)	24 (49)	14 (28)
appearance	< 1 (1)	18 (37)	35 (72)	29 (60)	18 (37)
general health	0 (0)	7 (15)	53 (108)	25 (51)	15 (30)
speech	0 (0)	3 (6)	69 (142)	15 (30)	13 (27)
smiling or laughing	0 (0)	3 (7)	66 (135)	21 (43)	10 (20)
Psychological aspects					
relax or sleep	0 (0)	7 (15)	75 (154)	12 (25)	5 (11)
confidence	2 (3)	10 (21)	58 (119)	20 (41)	10 (21)
mood	< 1 (1)	12 (25)	55 (112)	25 (51)	8 (16)
carefree manner	1 (2)	14 (28)	58 (119)	21 (42)	7 (14)
personality	< 1 (1)	5 (10)	66 (136)	21 (42)	8 (16)
Social aspects					
work	< 1 (1)	2 (3)	80 (163)	14 (29)	4 (9)
social life	0 (0)	3 (7)	66 (135)	21 (43)	10 (20
finances	5 (11)	27 (55)	59 (120)	6 (12)	3 (7)
romantic relationships	1 (2)	3 (6)	67 (138)	18 (37)	11 (23)

.

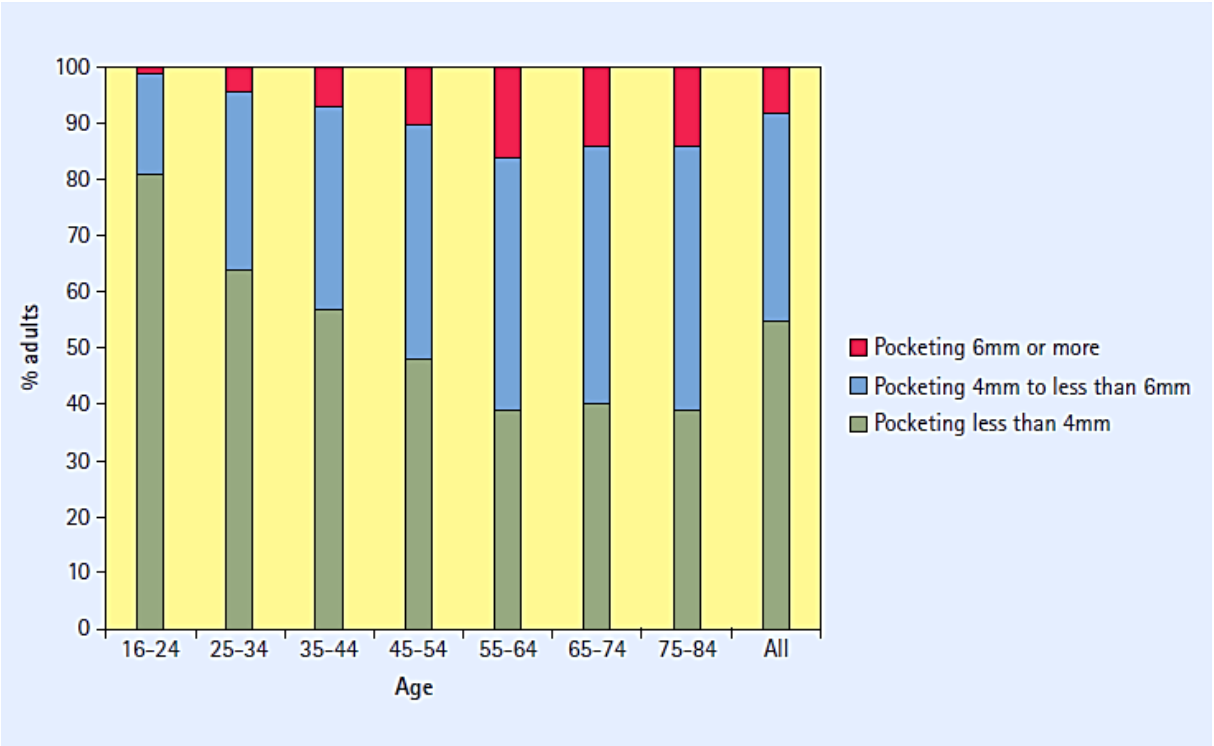

Figure 1.4: Diagram represents the percentage of prevalence of pocketing in periodontal disease patients in the UK (White *et al.,* 2012).

Inflammation is a crucial host response by the immune system that enables tissue to heal following infection or injury. It is essential for maintenance of normal tissue homeostasis as well as restoring tissue integrity and function (Medzhitov 2010, Ahmed 2011). The process of the inflammatory response involves selective expression of pro-inflammatory molecules which generate a multifactorial network of chemical signals (cytokines & chemokines). These molecules are released from a range of host cells including immune cells and structural tissue cells such as fibroblasts, epithelial and endothelial cells which are central to the process of tissue healing (Coussens & Werb 2002, Basso *et al.,* 2012, Davidson 1992). There are four principal components in an inflammatory response ; (a) Inducers of inflammation, (b) Sensors which detect the inducer, (c) Mediators of inflammation which are induced by the sensors and (d) Target tissues which are affected by the mediators (Medzhitov 2010).

1.2.4.1.1 The central role of Nuclear factor kappa-B signalling in the inflammatory response

Nuclear factor kappa-B (NF-κB) is an important transcription factor which regulates the expression of a wide range of pro-inflammatory genes. It has been shown to be a key factor in host defence responses and chronic inflammatory diseases (Siebenlist *et al.,* 1994, Barnes 1997). NF-κB activation is triggered by many extracellular stimuli including viruses, oxidants, inflammatory cytokines, immune stimuli (Barnes 1997) and bacterial stimulation via toll-like receptors (TLRs) (Milward 2010) .

The NF-κB family comprises dimeric proteins which are generated from monomers of ~300 amino acids which belong to the Rel protein family. The active form of NF-κB is usually comprised of two DNA binding subunits, a p50 subunit and a p65 (Rel A) subunit. Other Rel family related proteins that have also been identified include: c-Rel, Rel B, v-Rel and p52. Inactive NF-κB is located in the cytoplasm bound to an inhibitory protein, IκB (inhibitor of kappa-B) and this molecule is also comprised of a range of types including, IκB-α, IκB-β, IκB-γ and Bcl-3 (Barnes 1997, Verma *et al.,* 1995, Baeuerle & Henkel 1994).

Activation of NF-κB occurs following cell stimulation by a range of extracellular stimuli such as inflammatory cytokines which stimulate IκB kinases via signal receptors which then enhance the process of phosphorylation and proteolysis (degradation) of the inhibitory protein, IκB by specific IκB kinases. The phosphorylated IκB protein then allows free NF-κB subunits (p50 and p65) to enter into the nucleus. In the nucleus, the transcription factor binds to κB sites in the promoter regions of specific target genes for pro-inflammatory proteins such as cytokines (Figure 1.5) (Barnes & Karin 1997,Gilmore 2006, Tak & Firestein 2001). NF-κB binding enhances the mRNA transcription of these target genes and the mRNA is then translated in the ribosomes to proteins, e.g. pro-inflammatory cytokines. The pro-inflammatory cytokines, such as IL-1β, IL-8 and TNF-α, are then released from the cell and modulate the inflammatory response (as described in section 1.2.3). High activation of NF-κB at sites of inflammation can result in chronic inflammatory diseases such as rheumatoid arthritis, multiple sclerosis, inflammatory bowel disease (Tak & Firestein 2001) and periodontitis (Chapple 1997).

1.2.4.1.2 Activator protein-1 (AP-1)

AP-1, activator protein-1 is a pro-inflammatory transcription factor which regulates gene expression during immune responses as well modulating the production of cytokines, growth factors and stress signals. AP-1 has been shown to play a pivotal role in normal cellular development (proliferation) or neoplastic transformation leading to cancer (Hess *et al.,* 2004). AP-1 is comprised of a family of Jun, Fos or ATF (activating transcription factor) subunits which bind to AP-1 binding site (Karin *et al.,* 1997).

1.2.4.1.3 Nuclear factor erythroid 2- related factor 2 (Nrf2)

Nrf2 is a basic leucine zipper redox-sensitive transcriptional factor which regulates the expression of many antioxidant and detoxification genes (Bellezza *et al.,* 2010, Rangasamy *et al.,* 2004). Prior to activation of Nrf2 transcription factor, antioxidant response element (ARE) signals detach Nrf2 from its inhibitor, Keap1 and enters the nucleus, then attaches to the antioxidant response element (ARE), leading to up-regulation of molecular target proteins which boost cellular detoxification processes and antioxidant potential (Nguyen *et al.,* 2003, Rangasamy *et al.,* 2004, Lee *et al.,* 2005).

The Nrf2/ARE pathway has been proposed to play important functions in cellular antioxidant defence system and anti-carcinogenicity (Lee & Johnson 2004). Chen and colleagues have shown that Nrf2/ARE pathway can protect cells from oxidant-mediated injury and inhibit the suppression of key redox-sensitive inflammatory

responses which play a pivotal role in chronic inflammatory diseases (Chen *et al.,* 2006).

1.2.4.2 Role of oral epithelium in periodontal disease

The crevicular (health) or pocket epithelium (disease) lines the gingival sulcus or pocket and is intimately associated with the plaque biofilm which develops on the root surface. This epithelium, as with all epithelia acts as a barrier to protect the underlying connective tissues from the external environment. However studies investigating lung epithelium (Bals & Hiemstra 2004) and more recent studies utilising gingival epithelium (Milward *et al.,* 2007) have indicated a role in initiating and propagating an inflammatory response. Following stimulation by the plaque biofilm, gingival epithelial cells become activated via NF-kB and produce a wide range of pro-inflammatory cytokines and chemokines including interleukin-8 (IL-8), interleukin-1β (IL-1β) and tumor necrosis factor-α (TNF-α). These mediators released locally drive a range of pro-inflammatory events including the recruitment of a range of immune cell types, including neutrophils, to the site of challenge (Dale 2002, Milward *et al.,* 2007,). These responses form part of the innate immune system which serve to maintain the integrity of pocket epithelium (Dale 2002). Importantly increases in oral epithelial cell proliferation, alterations in cell signalling (further details in section 1.2.6.1) and promotion of tissue homeostasis are also essential to this process and occur to help maintain tissue defence (Dale 2002).

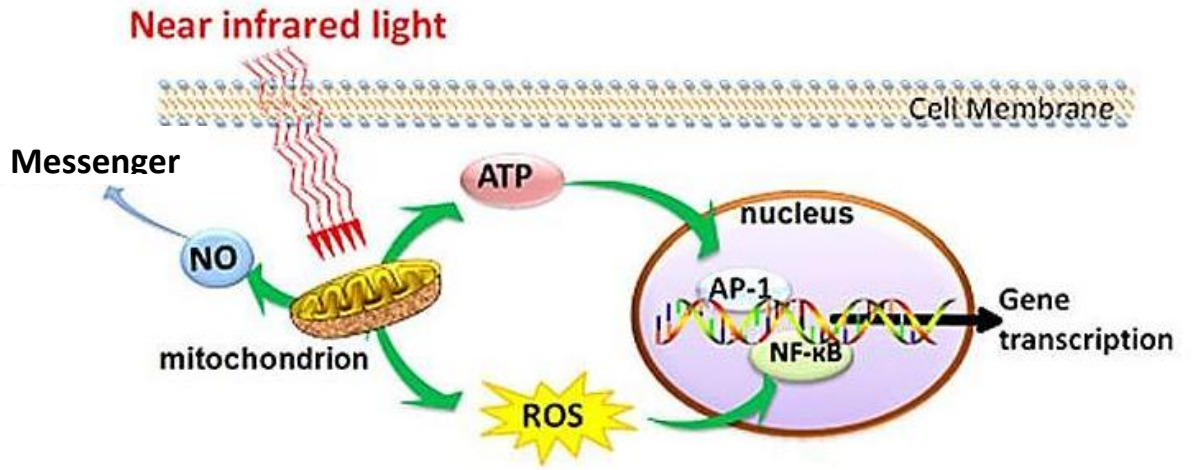

Figure 1.5: Diagram showing the proposed cellular mechanism of LLLT. Activation of transcription factors such as NF-κB and AP-1 induces gene transcriptional *(Chung et al.,* 2012).

Therapeutic interventions (e.g. LLLT) which enhance barrier function and modulate the hyper inflammatory response seen in periodontitis patients may offer a potential therapeutic target in the management of periodontal disease.

The presence of an intact oral epithelium provides a physical barrier to prevent bacteria present in the plaque biofilm from invading the underlying host tissues. This barrier is provided by the oral epithelial cells which are tightly attached to each other (by junctional epithelium) and are keratinised. Notably during disease progression the junctional epithelium exhibits a pocket-lining epithelium phenotype, with microulcerations and a leaky structure, therefore the protective function is compromised (Clerehugh *et al.,* 2009). When this first line of defence is compromised the chemokines and cytokines released serve to activate an immune response to eliminate disease and restore tissue homeostasis (Milward 2010).

1.2.4.3 Role of plaque biofilm in periodontal disease

A complex plaque biofilm containing approximately 700 species of bacteria develops on the teeth (Aas *et al.,* 2005). The plaque biofilm comprises a matrix of polymers made up from bacteria and its components and also constituents from saliva. Research has demonstrated that accumulation of dental plaque resulted in local inflammation of gingival tissue (gingivitis) which resolves on plaque removal. This situation differs from patients with periodontitis where the initial inflammation progresses to loss of periodontal tissues and is irreversible. Plaque accumulation is key to initiation and propagation of the inflammatory lesion but development of periodontitis is dependent on an aberrant exaggerated host response i.e. such

patients are said to be susceptible to periodontitis. Therefore clinically we can observe patients with relatively high levels of plaque who do not have periodontitis and conversely patients with good plaque control who have disease. This indicates the importance of host response in disease initiation and progression but also underlines the need for bacteria to initiate this host response. However specific bacterial species are critically involved in the aetiology of periodontitis (Milward 2010). There are five major bacterial complexes which have been recognised by Socransky and Haffajee (2005) and classified in coloured complexes; red, orange, yellow, green and purple (Figure 1.6). The complexes described the relationship between the species and severity of periodontal disease and also explained the distribution in different regions of periodontal pocket or gingival sulcus (Socransky *et al.,* 1998). The red complex bacteria are mostly strongly associated with periodontal disease. Two of listed bacteria in Figure 1.6 were employed in this study, *P. gingivalis* and *F. nucleatum*.

F. nucleatum is a Gram-negative anaerobic bacterium which implicated in periodontal disease, notably dominant in dental plaque biofilms and one of the oral species associated with periodontitis constantly (Signat *et al.,* 1995). *P. gingivalis* also a Gram-negative anaerobic bacterium which contributes to development of periodontitis (Griffen *et al.,* 1998, How *et al.,* 2016). The bacterium modulates host inflammatory response causing periodontal tissue disruption (How *et al.,* 2016).

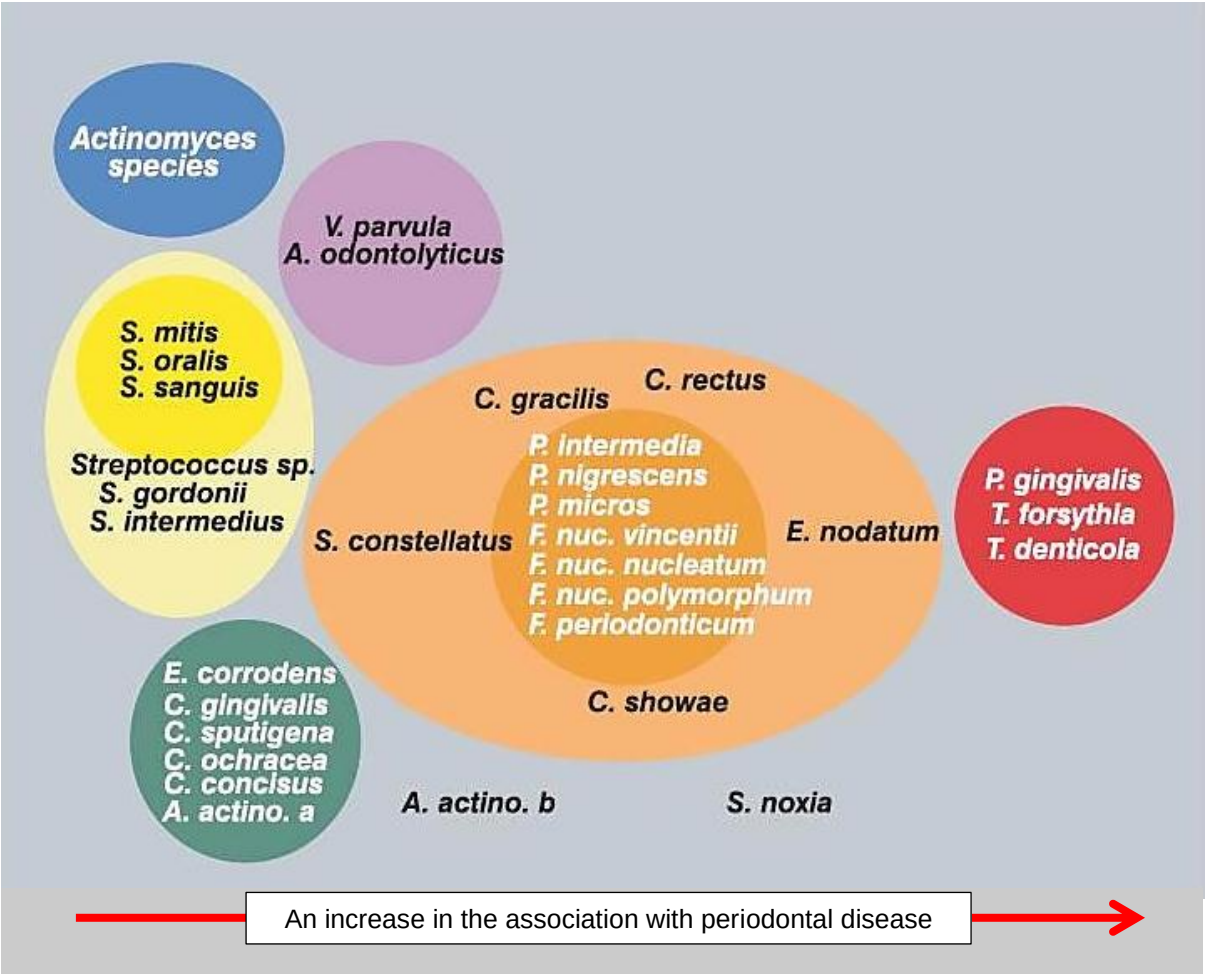

Figure 1.6: The microbial complexes and their association with periodontal disease where diagrammatic representation also illustrates the relationship of bacterial species within and between the microbial complexes (Socransky & Haffajee 2005).

1.2.4.4 Role of neutrophils in periodontal disease

Neutrophils are key cells in the 'first line' defence to infection and are a key component of the innate immune response. They are a type of leukocytes which kill bacteria by phagocytosis, degranulation and by the formation of neutrophil extracellular traps (NETs). In the periodontal tissues, neutrophils are the main protective cell, which are found abundantly within the gingival crevice and epithelium (Scott & Krauss 2012).

Neutrophils contribute to protection of the junctional epithelium from the pathogen-rich plaque biofilm. It is proposed that this is achieved by 2 mechanisms i) a robust secretory structure releasing reactive oxygen species (ROS) and bacteriocidal proteins, and ii) phagocytic mechanisms . The overall protective role of these cells is provided by a combination of these processes (Scott & Krauss 2012). Neutrophils develop in the bone marrow, with in the region of $5\text{-}10x10^{10}$ new neutrophils produced daily. Mature neutrophils enter the blood circulation after differentiation which occurs over approximately 14 days. At sites of inflamed tissue, such as in the periodontium, neutrophils are recruited from the blood circulation along a concentration gradient of chemotactic cytokines released locally from cells present in the inflamed periodontium. Once present neutrophils kill invading bacteria using the mechanisms previously described. The final stage of the inflammatory response involves resolution of inflammation and wound healing (Scott & Kraus 2012). In periodontitis patients' neutrophils have been shown to be hyper active and hyper reactive producing excess levels of free radicals such as reactive oxygen species (ROS) and enzymes that are implicated in the local tissue damage that is

characteristic of the periodontal lesion. The activity of these cells in terms of their hyper-active response will likely impede resolution of inflammation thereby inhibiting and frustrating periodontal tissue healing processes (Milward 2010, Fujimaki *et al.,* 2003).

1.2.5 Current management strategies for periodontitis

Treatment of periodontitis currently involves optimising the patient's oral hygiene regimen, removing risk factors such as smoking and providing professional cleaning (scaling and root planning). In certain types of periodontal disease (aggressive periodontitis) antimicrobial therapy and periodontal surgery may be indicated alongside conventional treatment. Currently no therapies are available that directly modulate the hyper-inflammatory response, promote healing or sustain the functional barrier of epithelium (Slot *et al.,* 2014).

1.2.6 Potential for use of LLLT in periodontal disease

Thus, LLLT may have a potential for use in periodontal disease management alongside non-surgical therapy. Notably light therapy is painless and non-ablative (Chang *et al.,* 2013) and may enhance and stimulate tissue repair. Interestingly preliminary reports indicate that light delivered at 660nm and at 10J/cm^2 may facilitate periodontal tissue repair by reducing inflammation, stimulating bone deposition and promoting collagen fibre alignment (Chang *et al.,* 2013). These findings reported by Chang *et al.,* (2013) demonstrate the potential positive effects of LLLT in promoting periodontal healing using a LED device.

Furthermore, a study has shown that certain wavelengths promote proliferation during wound repair (Sperandio *et al.,* 2014). Karu (1999) driven by the expression of the anti-inflammatory cytokines and the subsequent downstream reduction in inflammation and subsequent promotion of wound healing. In order to optimise this potential careful consideration is required as to how light is delivered to tissues and cells in order to deliver maximal clinical benefit.

1.2.7 Light-tissue interaction

Understanding the interaction of light with tissues is a key factor in determining dose delivery at a cellular level. When tissue is exposed to light, it can be absorbed, reflected transmitted and / or scattered. This interaction is dependent on both light characteristics and also the composition of the tissue. Optimising tissue light energy absorption has been shown to be important in unlocking the therapeutic potential of light therapy (Gupta & Hamblin 2013).

One of the important factors in how light interacts with tissue is light wavelength (nm). Different wavelengths will interact with different chromophores found in different tissue types. Chromophores are light-absorbing chemical compounds and among these are melanin and haemoglobin which absorb light in visible range (Igarashi *et al*., (2005). Light wavelength is often characterised by using their associated visible spectrum, i.e. blue (400-470nm), green (470-550nm), red (630-700nm) and NIR (700-1200nm) (Barolet 2008) (Figure 1.1). Tissue penetration will depend wavelength for example 400nm will penetrate less than 1mm, 630nm penetrates 1-6mm, and

700-900nm will produce the deepest level of tissue penetration (6mm and more) (Barolet 2008) (Figure 1.8).

The optical characteristics of tissue and how light interacts with it is central to the therapeutic success of LLLT, therefore there is a so-called “optical/therapeutic window” in tissue covering the red and NIR wavelengths in which the effective tissue penetration of light is maximised (Figure 1.9) (Gupta & Hamblin 2013). Within the light spectrum, blue, green and yellow light wavelengths may have significant effects on cell behaviour. However, the use of red and NIR light in LLLT has shown significant efficacy in treating both humans and animals (Gupta & Hamblin 2013).

The literature indicates that there is an optimum dose delivery for any particular biological system with dose levels outside this range not delivering any beneficial or detrimental effect. Evidence gained on cellular response has led to proposal of the Arndt-Schultz curve (Figure 1.7) (Sommer *et al.,* 2001). In 1887, Hugo Schulz published a paper demonstrating that different types of poisons (such as iodine, bromine, mercuric chloride and arsenious acid) produces a stimulatory effect on yeast metabolism when given in low doses. Following on from this Rudolph Arndt, a psychiatrist, they developed a principle known as “Arndt-Schulz law”, stating that weak stimuli increases activity this will increase further as the level of stimulation increases up to a threshold beyond which activity is reduced (Huang *et al.,* 2009).

The concept of a biphasic dose response has been frequently observed in respect to LLLT where low levels of light dose demonstrate an enhanced effect on stimulating

and repairing tissues in comparison to higher doses (Huang *et al.,* 2009). The “Arndt–Schulz law” is frequently used to describe this biphasic dose response (Huang *et al.,* 2009). The key parameters such as wavelength, radiant exposure, irradiance value and exposure time are key to delivering effective LLLT treatment (Sommer *et al.,* 2001).

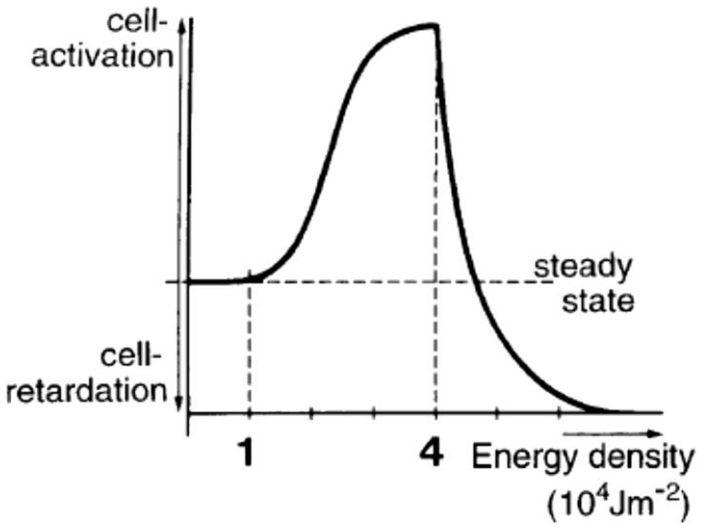

Figure 1.7: Graph representing Arndt-Schulz law shows biphasic modes of cell responses at different levels of energy density (radiant exposure) (Sommer *et al.*, 2001).

1.2.7.1 The effect of LLLT on epithelial cells

Biostimulatory effects of light on cell proliferation and wound healing *in vivo* and *in vitro* is well established with healing triggered *in vivo* via stimulation of a variety of cell types including epithelial cells (Walsh 1997). Epithelial cells provide a barrier between the organism and the external environment (e.g. epidermis, bronchial, alveolar epithelium) or between an organ and a fluid space (e.g. oral epithelium in the mouth). Epithelial cells play a key role in the regulation of permeability, transport, endocytosis and exocytosis (Maas-Szabowski *et al.,* 2002) in addition epithelial cells have been shown to produce a pro-inflammatory response when stimulated with bacteria, e.g. the crevicular epithelium in the gingival crevice, thereby orchestrating protection for the host from invading bacteria. Functionally, recent studies using LLLT have shown the ability of epithelial cells to respond to light which enhances cell proliferation and increases the motility of human keratinocytes (Haas *et al.,* 1990). Notably LLLT did not modify keratinocyte differentiation or interfere with the normal function (Rood *et al.,* 1992). Thus, light (laser/LEDs) therapy potentially can accelerate keratinocytes proliferation and restore the physical integrity of the tissue (Walsh 1997).

1.2.7.2 The effect of LLLT on neutrophils

The numbers of neutrophils increase in inflamed tissue due to local release of chemotactic agents. Increased numbers of neutrophils result in increased production of ROS, which if in excess as seen in periodontitis patients can lead to local tissue damage. Fujimaki and colleagues (2003) found significant reduction of ROS by human neutrophils when irradiated with Ga-Al-As laser which was carried out 60min

before stimulation by opsonized zymosan (OZ) and calcium-ionophore (Ca-i). They also demonstrated that ROS production in smokers was highly decreased than non-smokers. Another study also indicated that neutrophil numbers are reduced following the use of LLLT. This may have implications in decreasing the excess inflammation seen in periodontitis and other chronic inflammatory diseases (Morgan & Rashid 2009). Thus, it seems that LLLT may attenuate ROS production by neutrophils and thereby increase the efficacy of LLLT in wound healing. Hence, neutrophil modulation may play a significant role in treatment of inflammatory driven diseases (Fujimaki *et al.,* 2003).

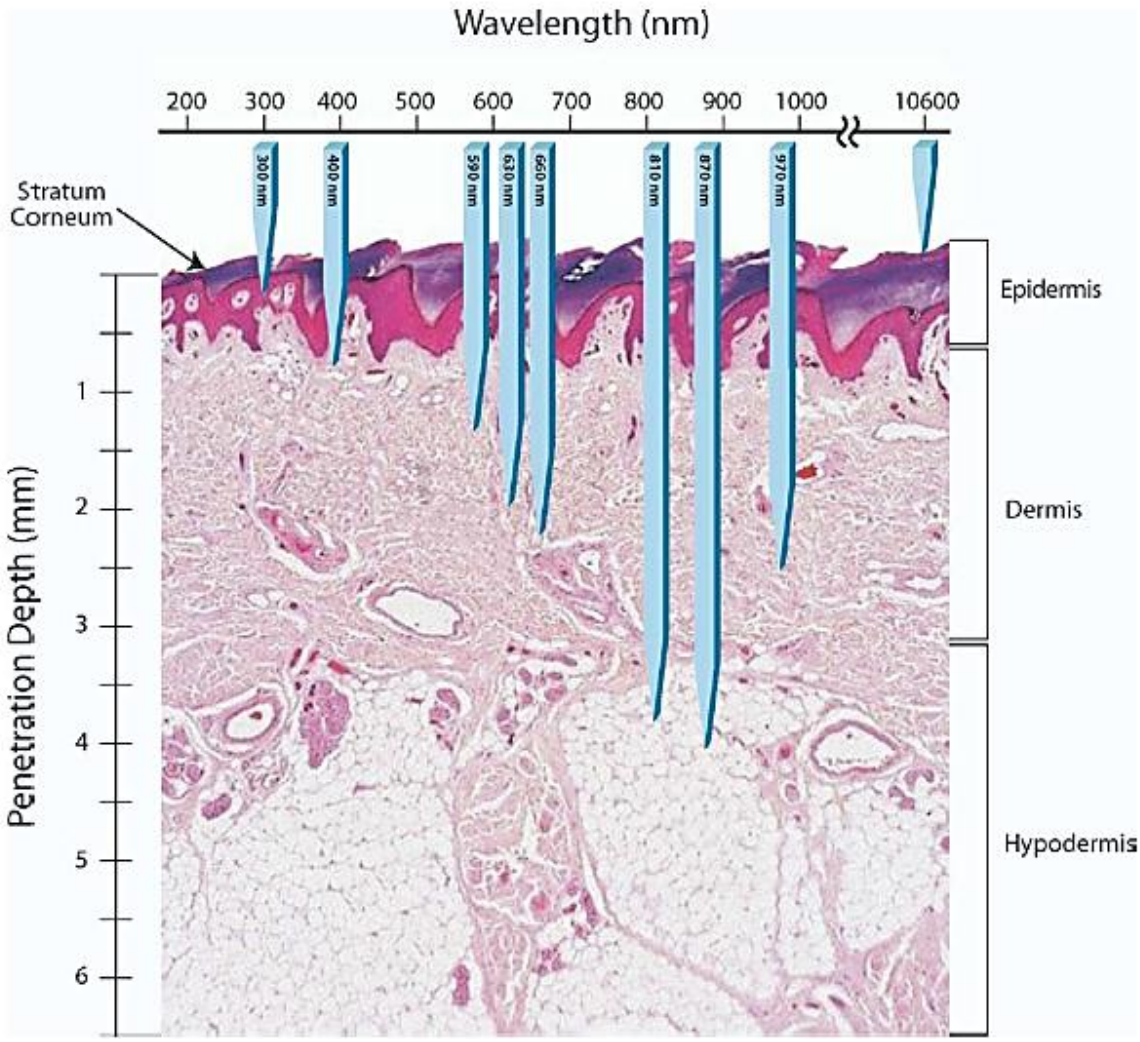

Figure 1.8: This schematic indicates the optical penetration depth for a range of wavelengths (Barolet 2008).

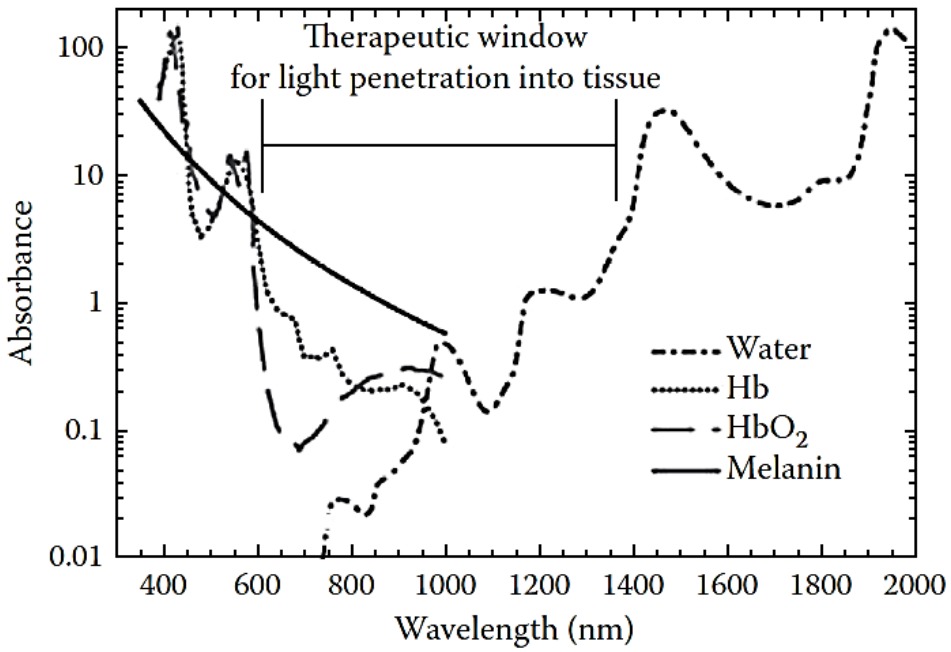

Figure 1.9: Light absorption by tissue chromophores indicating the therapeutic window in which visible and NIR light can penetrate deepest into tissue (Adapted from Gupta & Hamblin 2013). Hb: Hemoglobin, HbO2: Oxyhemoglobin.

1.3 Aims & objectives

This thesis proposes the potential for the use of LLLT as a therapy in the management of periodontitis. Therefore this thesis aims to investigate the effect of low-level laser or LEDs on:

(a) Human oral epithelial cells in terms cell proliferation, promoting healing-associated responses and reducing the inflammatory response.

(b) Investigate the modulation of neutrophil responses.

In order to achieve these overarching aims the study will have the following objectives:

1. Development and characterisation of range of LED and laser-based light sources
2. Determination of light irradiation parameters in order to fully understand light delivery at a cellular level
3. Assessment and determination of a range of biological responses; i.e. cell proliferation, mitochondrial metabolic activity, and gene expression of human oral epithelial cells following irradiation
4. Assessment of neutrophil ROS response following LED irradiation
5. Determination of inflammatory response following irradiation on bacterial stimulated human oral epithelial cells.

CHAPTER 2: MATERIALS AND METHODS

2.1 Materials

2.1.1 Light sources

This section describes the characterisation approaches used for all the optical devices used to irradiate cell cultures during the studies described in this thesis.

2.1.1.1 Laser

The laser device utilised in this study was a red light laser (OFL173, Odic Force Lasers, UK) (Figure 2.1). The manufacturer reported wavelength was 650nm ± 5nm and delivers a ‘circular’ laser pattern. This laser is mounted in a stainless steel housing which acts as a heat sink enabling heat dissipation and allows consistent orientation of cell culture ware. The laser is powered using a stabilised 5V DC 80mA power supply (mains power; 240v AC). Cell culture vessels can be placed directly on top of the laser and positioned a measured distance away in order to vary the light delivered to the cell monolayer.

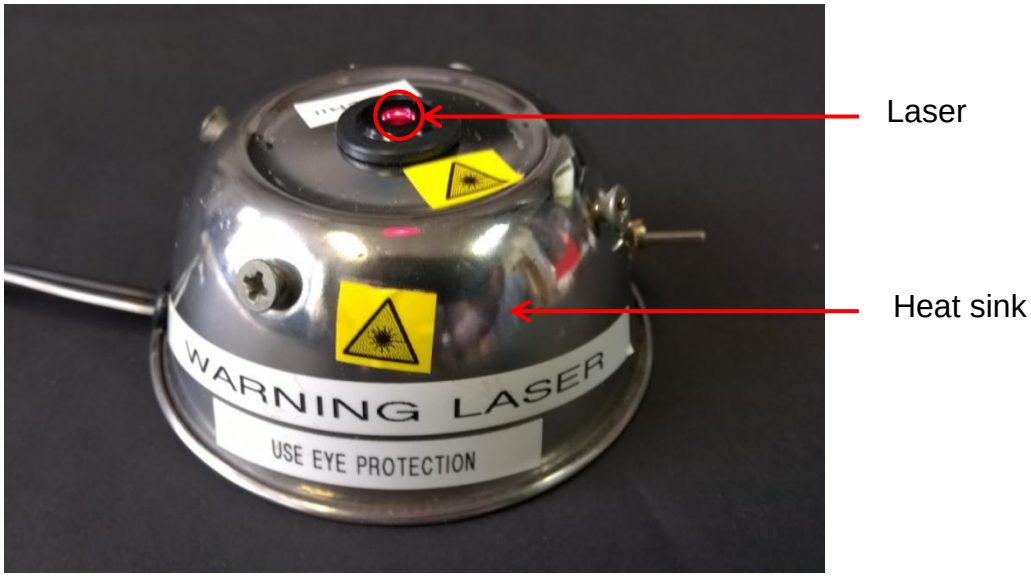

Figure 2.1: Laser light source housed in a bespoke stainless steel housing which acts as a heat sink to dissipate laser heat generation.

2.1.1.2 LED

The bespoke single LED device used a high power (10 watt) red surface mount device (SMD) LED (Model: JLLU20-W140-R600lm, JELED Electronic Co Ltd., Hong Kong) that was mounted on a heat sink (Figure 2.2). The manufacturer's quoted wavelength was 630nm. The LED was powered using a stabilised 6v DC, 750mA power supply run from 240v AC mains voltage.

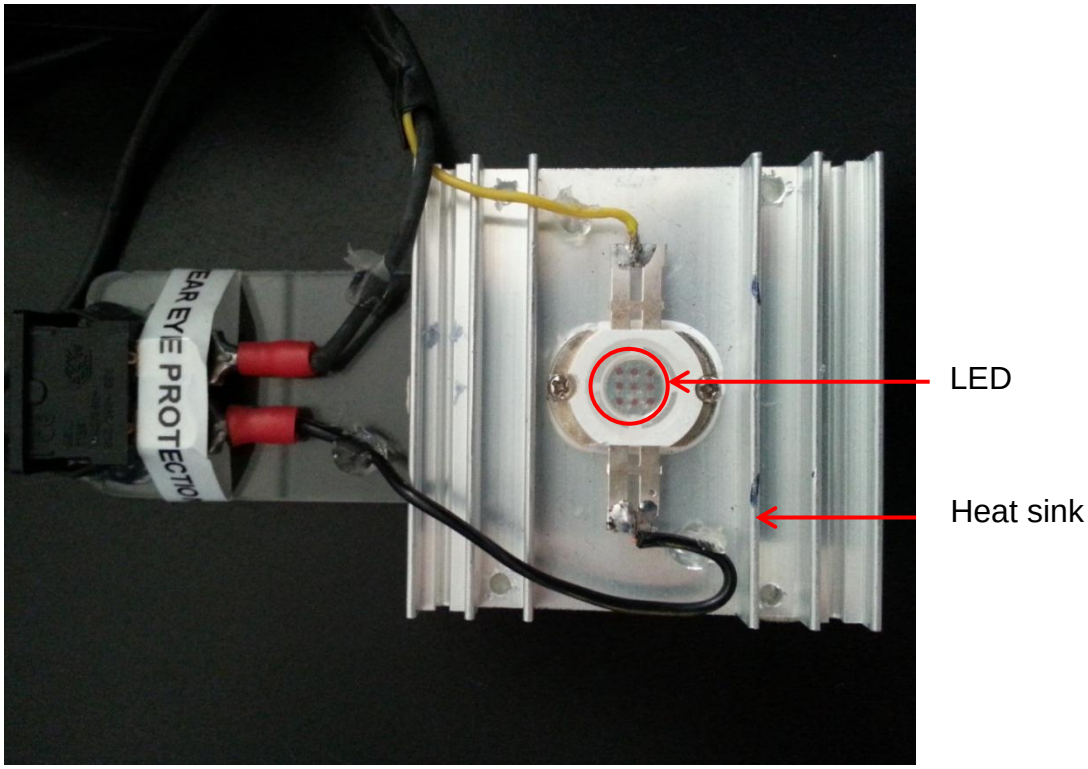

Figure 2.2: Single LED light source mounted on a heat sink to dissipate heat generated by the high power LED.

2.1.1.3 LED arrays

Bespoke LED arrays were developed utilising multiple 60x5mm epoxy encased LEDs (Roithner Lasertechnik, Austria), each of the 10 columns contained different LED wavelengths (n=6 per wavelength) (Figure 2.3 (a)). The wavelengths of the LED used ranged from 625-830nm (Table 2.1) (Figure 2.3 (b)). LEDs were mounted on a custom designed and manufactured printed circuit board. Resistors were used for each of the different LED wavelengths to standardise the voltage and optimise light output. The unit was designed to allow each column of LEDs to be individually controlled (Table 2.1) to enable variation in exposure time and subsequent dose delivery. The LED array was driven by a stabilised 5V, DC 500mA power supply run off mains voltage (240v AC).

(a)

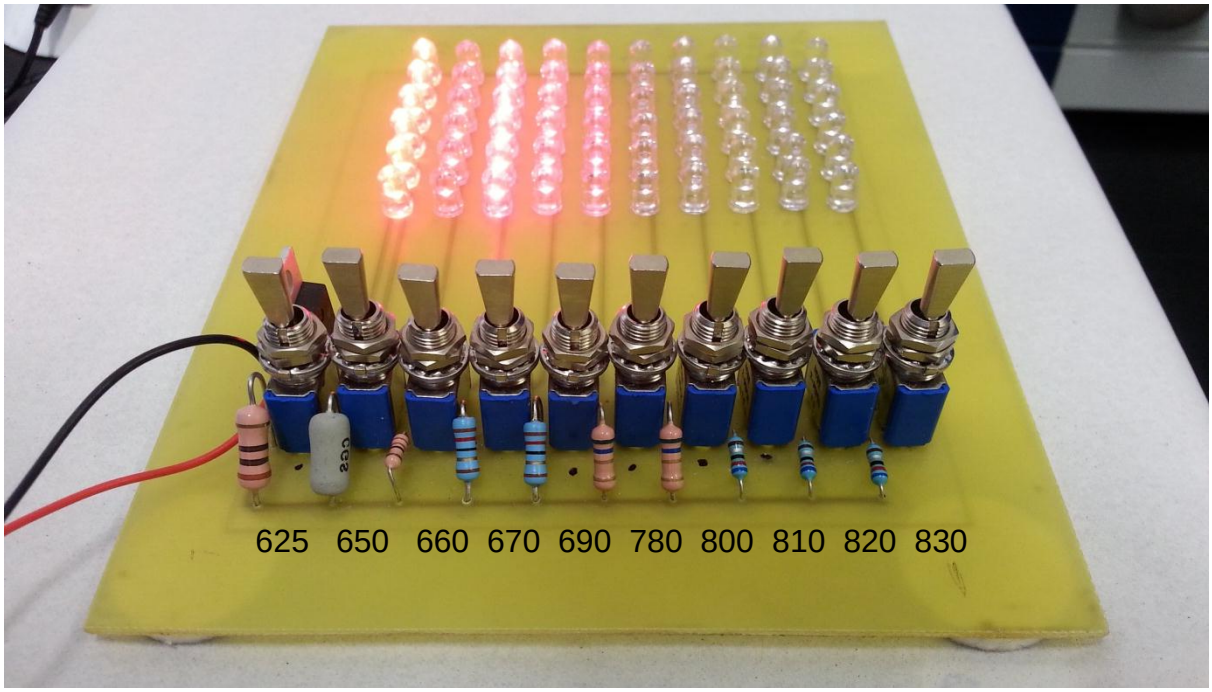

(b)

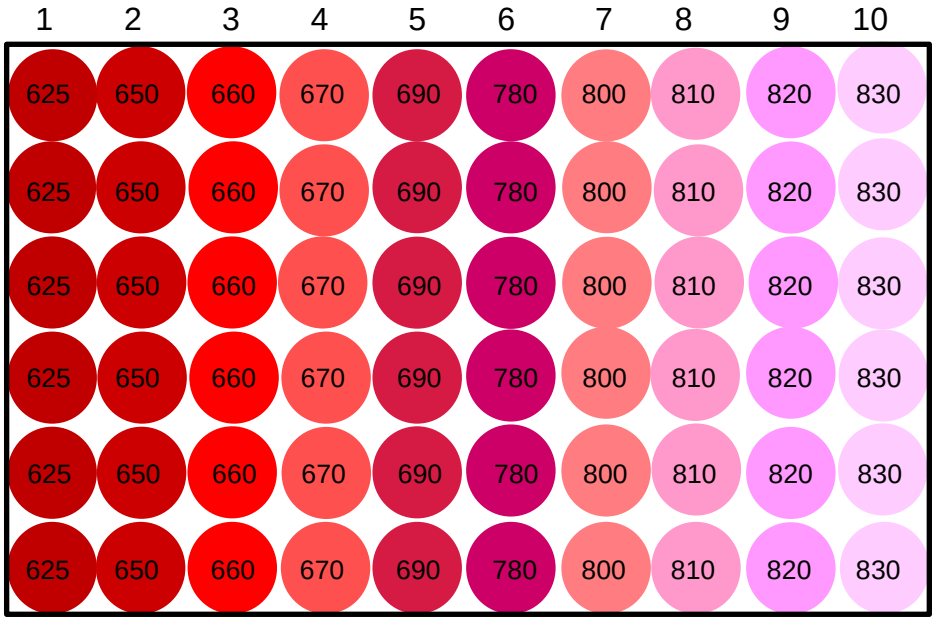

Figure 2.3: (a) The multiple LED array emitting wavelengths ranging from 625 to 830nm. (b) Schematic diagram showing the distribution of wavelengths emitted across the device.

Table 2.1: Published manufacturer's LED data and resistance used to standardise voltage delivery for each wavelength of LED for the device shown in Figure 2.3.

No. of Column	Centre Wavelength (nm)	Optical Power (mW)	Viewing Angle (degree, °)	Resistance (Ohms, Ω)
1	625	$1.46x10^{-3}$	15	11
2	650	$1.46x10^{-4}$	20	14.7
3	660	15	24	11
4	670	3.5	20	12
5	690	4	15	12
6	780	18	20	6.8
7	800	22	10	6.8
8	810	45	20	6.8
9	820	18	10	6.8
10	830	20	15	6.8

A second, power-adjustable LED array was developed to standardise the irradiance value (mW/cm^2) for each LED (Figure 2.4) (Table 2.2), which was set at an output of 24mW/cm^2. However, the LEDs in columns 4 and 6 were not used in subsequent experiments as it was not possible for these LEDs to deliver the required irradiance of 24mW/cm^2. The standard irradiance value was achieved by using different resistors to control voltage delivered to each group of LEDs, thereby standardising light output (irradiance value). The major difference between the first LED array and second multi-well LED device was the ability of the second device to standardise light output for all the wavelengths. The first device developed delivered standard voltage to each wavelength of LEDs however this resulted in different levels of irradiance for each wavelength. In addition the second device developed contained a wider range of wavelengths.

(a)

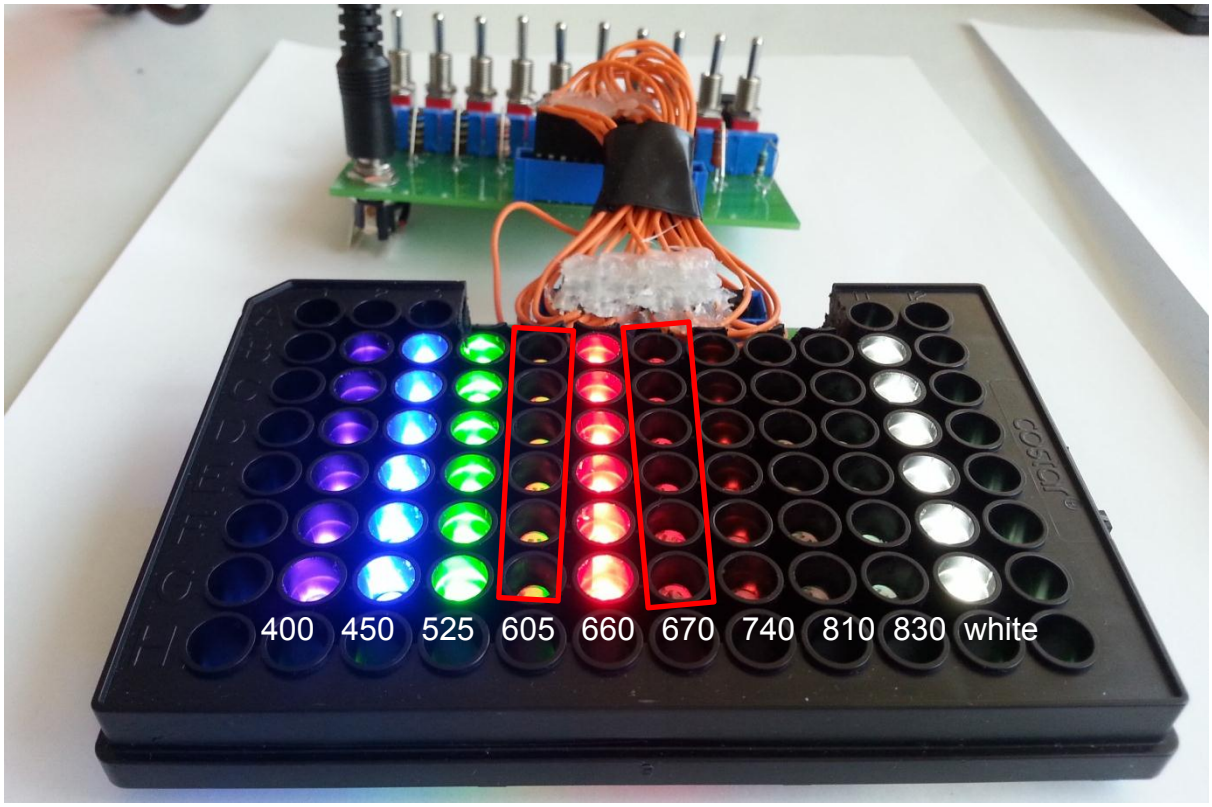

(b)

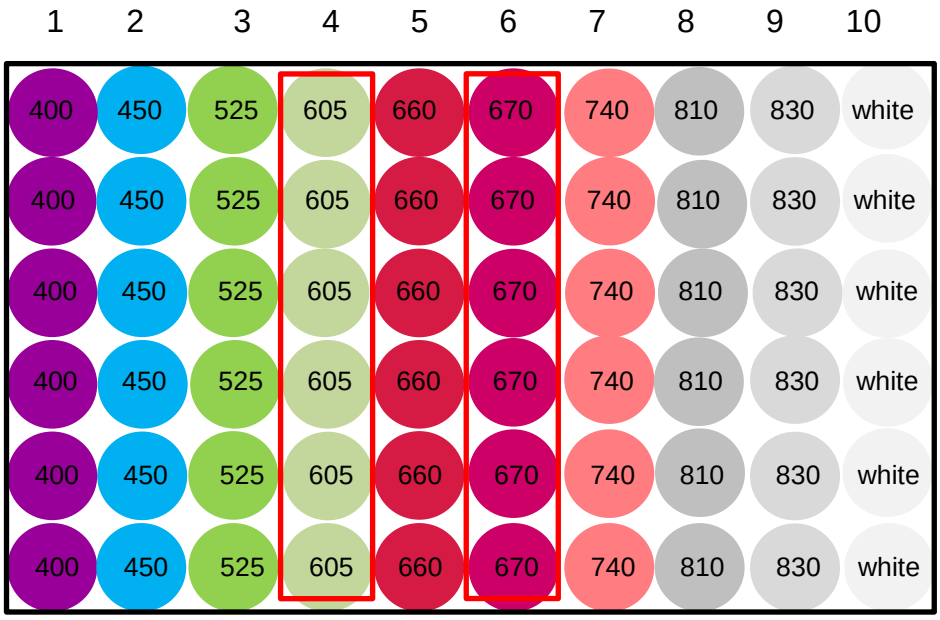

Figure 2.4: (a) Second generation LED array emitting wavelengths between 400-830nm (included white LEDs – producing a range of wavelengths.). (b) Schematic diagram showing the range of wavelengths used. LEDs in column 4 and 6 were unused as where unable to deliver sufficient irradiance.

Table 2.2: Manufacturers published data for each LED used in the second generation array and the resistors used to standardise irradiance (mW/cm^2) for the device shown in Figure 2.4.

No. of Column	Centre Wavelength (nm)	Optical Power (mW)	Viewing Angle (degree, ^{o})	Resistance (Ohms, Ω)
1	400	21-29	15	16.9
2	450	20	25	6.8
3	525	$1.17x10^{-2}$-$1.46x10^{-2}$	15	6.8
5	660	15	24	11
7	740	18	20	8.2
8	810	45	20	6.8
9	800	20	15	6.8
10	white	$1.1x10^{-2}$	15	6.8

2.1.2 Cell culture

2.1.2.1 Reagents

2.1.2.1.1 Supplemented Dulbecco's modification of Eagle's growth medium (DMEM)

Dulbecco's Modified Eagle's Medium/Ham's Nutrient Mixture F12 (DMEM) (SAFC Biosciences, USA) 1000ml was supplemented with sterile 20ml L-glutamine (final concentration, 200mM) (Sigma, UK), 50µl hydrocortisone of 10mg/ml stock solution (final concentration, 0.0005mg/ml) (Sigma-Aldrich, MO, USA) [increase proliferation (Suda & Dexter 1981)] and foetal calf serum (5 or 10% v/v) (Labtech, UK) and used to culture oral epithelial cells (H400). All growth media was checked for sterility by overnight incubation (at 37^{o}C, 5% CO_2) of a 5ml aliquot and inspected for turbidity. Phenol red-free media (Gibco, Life technologies, UK) was used to culture cells in 96-well plates. The media was supplemented prior to use with L-glutamine, hydrocortisone and foetal calf serum at the same concentration as phenol red containing DMEM. All media were stored at 4^{o}C and warmed to 37^{o}C prior to use.

2.1.2.1.2 Phosphate-buffered saline (PBS)

Sterilised PBS buffer was prepared for use in washing cells, preparation of MTT solution and also in the luminol (section 2.1.3.1.4), isoluminol (section 2.1.3.1.5) and lucigenin (section 2.1.3.1.6) reagent preparation. PBS was prepared using 8g NaCl (Sigma-Aldrich, UK), 2g KH_2PO_4 (Sigma-Aldrich, UK), 1.15g Na_2HPO_4 and 2g KCl which were dissolved in 1000ml of distilled water and pH adjusted to 7.4 using 1M

NaOH. The solution was sterilised by autoclaving at 121°C for 15min and stored at room temperature prior to use.

2.1.2.1.3 Trypsin ethylenediaminetetraacetic acid (Trypsin-EDTA) solution

Trypsin-EDTA was used to detach the adherent H400 epithelial cell monolayer to produce a single cell suspension for cell counting, archiving and reseeding. Trypsin-EDTA 0.25% (w/v) was sterile filtered and contained 2.5g porcine trypsin and 0.2g EDTA·4Na per litre of Hanks' balanced salt solution with phenol red (Sigma-Aldrich, MO, USA). The reagent was stored in 3ml & 1ml aliquots at -20°C and pre-warmed to 37°C in a water bath prior to use.

2.1.2.1.4 *E.coli* LPS

Escherichia coli LPS (lipopolysaccharide) (Sigma-Aldrich, UK) was used in immunocytochemistry studies (section 2.2.4.4) to stimulate activation of NF-κB (as described in Milward 2010) in H400 cells. A 1mg/ml stock solution was prepared by combining 10mg of *E.coli* LPS with 10ml of sterile DMEM. This was then aliquoted into 500µl siliconised Eppendorf tubes (to minimise LPS attachment to plastic tube) and frozen (-20°C) prior to use. A concentration of 20µg/ml (final concentration) was used for cell stimulation experiments.

2.1.2.1.5 Cryogenic solution

Cryogenic solution was used for cell storage by mixing 700µl of DMEM (section 2.1.2.2.1), 200µl of foetal calf serum (section 2.1.2.2.1) and 100µl of dimethyl sulphoxide (DMSO) (Sigma, USA).

2.1.3 Neutrophil ROS production

2.1.3.1 Reagents

2.1.3.1.1 Percoll

Percoll solution contains a 1130g/ml colloidal silica suspension coated with polyvinylpyrolidone (GE Healthcare Life Sciences, UK). Two discontinuous Percoll gradients of densities 1.079 and 1.098 were used to isolate neutrophils, these gradients were stored at 4^{o}C prior to use. Details of the constituents of each gradient are provided in Table 2.3.

2.1.3.1.2 Lysis buffer

1000ml of lysis buffer was prepared containing 8.3g of NH_4Cl, 1g of $KHCO_3$, 0.04g Na_2 EDTA $2H_2O$ and 2.5g of bovine serum albumin (BSA) in 1000ml sterile water. Each reagent was thoroughly mixed prior to the addition of the subsequent component. Lysis buffer was used to lyse red blood cells as part of the process to obtain a pure neutrophil preparation. The buffer was stored at 4^{o}C prior to use.

Table 2.3: Percoll gradient constituents.

Density / Solution	1.079	1.098
Percoll	19.708ml	24.823ml
Water	11.792ml	6.677ml
NaCl (1.5M)	3.5ml	3.5ml

2.1.3.1.3 Blocking buffer

Blocking buffer was prepared by adding 10g of BSA (Sigma-Aldrich, UK) to 1000ml of PBS. The buffer was used to coat and block the surface of the plate for subsequent experimental analysis. The solution then was aliquoted and stored at -20^{o}C. Prior to use the bottle was thawed at room temperature.

2.1.3.1.4 Luminol

A stock solution of 30mM luminol (Sigma-Aldrich, UK) was produced by diluting 0.5g luminol in 94.05ml 1mM NaOH and stored at 4^{o}C wrapped in foil (to protect from photo-degradation). 1ml of this stock solution was added to 9ml of PBS (3mmol/L) to produce a working solution and the pH was adjusted to 7.3. The working solution was foil wrapped and stored at 4^{o}C for up to 6 weeks. Luminol was used to measure total (intracellular and extracellular) neutrophil ROS.

2.1.3.1.5 Isoluminol

Isoluminol (Sigma-Aldrich, UK) 0.5g was dissolved in 94.05ml 0.1M NaOH to produce a 30mM stock solution which was wrapped with foil and stored at 4^{o}C prior to use. A 3mM working solution was prepared by diluting 1ml of isoluminol stock in 9ml of PBS and pH adjusted to 7.3. This working solution was foil wrapped and stored at 4^{o}C for up to 6 weeks.

2.1.3.1.6 HRP

Horseradish peroxidase (HRP) (Sigma, UK) was applied at 1.5 units/well (of 96-well plate). A master stock solution (1000units/ml) of HRP was prepared by adding 5ml PBS to 5000KU HRP powder. Before applying to each well, 1.5µl of the master stock and 13.5µl of PBS were combined. Aliquots of the master stock were stored at -20^{o}C prior to use. HRP was used with isoluminol to detect extracellular neutrophil ROS.

2.1.3.1.7 Lucigenin

A 1mg/ml stock solution was prepared by combining 0.005g with lucigenin (Sigma, UK) to 5ml PBS. The stock solution was foil-wrapped and stored at 4^{o}C prior to use and up to 6 months. A working solution was prepared on the day of the experiment by diluting 1:3 in PBS. Lucigenin was used to detect neutrophil superoxide.

2.1.3.1.8 PMA

A stock solution of PMA (phorbol 12-myristate 13-acetate) (Sigma-Aldrich, UK) was prepared by dissolving 1mg PMA in 1ml of DMSO (1mg/ml) (1.6212mM) and diluted further to achieve a 25nM concentration in each well (96 well plate). The initial stock solution was stored at -20^{o}C and thawed immediately prior to use.

2.1.3.1.9 gPBS (supplemented PBS with glucose and cations)

The gPBS solution was generated in 1L by adding 1.8g glucose (Sigma-Aldrich, UK), 0.15g $CaCl_2$ (BDH, UK), 1.5ml 1M $MgCl_2$ (BDH, UK) to 1L of PBS (2.1.2.2.2). The mixture was prepared by adding reagents in order and mixed well before adding the

next component. The resulting solution was kept at 4°C prior to use and used within 1 month.

2.1.4 Bacterial culture

2.1.4.1 Bacterial stock

Bacterial stocks of *P. gingivalis* (ATCC 33277) and *F. nucleatum* (ATCC 10953) were originally purchased from the American Type Culture Collection (ATCC, USA).

2.1.4.2 Blood agar

Prepared blood agar plates were purchased (Base no.2 with 5% horse blood, proteose peptone, liver digest, yeast extract and sodium chloride) (Oxoid, UK) and kept at 4°C prior to use. Plates were allowed to reach room temperature prior to use. All the plates were utilised before the manufacturer's expiry date.

2.1.4.3 Brain heart infusion (BHI) broth

Brain heart infusion (BHI) broth (with 10% horse serum, brain infusion solids, beef heart infusion solids, proteose peptone, glucose, sodium chloride and disodium phosphate) (Oxoid, UK) was prepared by dissolving 37g BHI dehydrated culture medium in 1L of distilled water, mixed and autoclaved (121°C for 15min) and kept at 4°C prior to use.

2.1.4.4 Crystal violet

Crystal violet (Sigma-Aldrich, UK) 2g was added to 20ml of 95% ethanol (Sigma-Aldrich, UK). 1% ammonium oxalate was prepared by dissolving 0.8g ammonium oxalate in 80ml of distilled water and added to crystal violet solution in a 1:1 ratio. The resultant solution was stored at room temperature prior to use. Crystal violet is a bacterial stain used in Gram staining (Beveridge 2001).

2.1.4.5 Carbol fuchsin

Carbol fuchsin (or safranin) (Sigma-Aldrich, UK) solution was prepared by mixing the 1ml stock with 9ml of distilled water. The mixture was kept at room temperature. This solution was used in Gram staining and differentially stains Gram negative bacteria a red colouration (Beveridge 2001).

2.2 Methods

2.2.1 Light characterisation

2.2.1.1 Wavelength measurement

The light sources used in this study were purchased based on optical data published by the manufacturer. However all light sources were validated using UV-Vis spectrophotometry methods to determine actual light delivery characteristics. Spectral irradiance for each light source was measured using a fibre-based UV-Vis spectrometer (USB4000, Ocean Optics, UK) equipped with an optical fibre (8µm) and a 3.9mm diameter opal glass cosine corrector attachment (CC3, Ocean Optics, UK)

that was calibrated to NIST (National Institute of Standards and Technology) standards against a NIST traceable deuterium-tungsten light source (Mikropack DH2000-Cal, Ocean Optics, Dunedin, USA). The cosine corrector probe was placed above 35mm culture dishes or 96-well black-walled plates to determine the irradiance delivered to the cultureware surfaces, i.e. where the cell monolayer was grown. The spectrometer system was connected to a computer running SpectraSuite software (Ocean Optics, UK) (Figure 2.5). Results allowed determination of wavelength and irradiance values. Specific details of this procedure are discussed later in this section.

During laser measurement, filters (ND 03B and ND 06B) were used to reduce the irradiance reaching the spectrometer to avoid sensor saturation resulting in inaccurate results. The ND filters were positioned between the light collector and culture dish to attenuate the light resulting in a six-fold reduction in irradiance, therefore the measured irradiance was multiplied by 6 to obtain the actual irradiance value for the light source being measured. For single LED measurement, ND filters were not required due to the lower irradiance produced and therefore the cosine corrector was positioned directly above the cultureware. Spectral irradiance measurements for laser and single LED were performed using two conditions; (a) cultureware placed at a distance of 33mm from the light source, and (b) cultureware positioned directly above the light source. In addition, the spectral irradiance measurements for the LED arrays were undertaken using the same experimental protocol as that described for the ‘single LED’, i.e. without the use of ND filters.

To perform spectral irradiance measurement of the LED array, a 96-well black plate was fixed directly above the bespoke LED array aligning the wells of the upper plate with the wells of the LED array sleeve. Wells of 96-well plate had diameters of 6mm which were appropriately suited to the diameter of the cosine corrector (3.9mm diameter) which was used to measure delivered irradiance. Black 96 well plates were used in these and other experiments to prevent light bleeding between wells.

All spectral measurements were determined using the SpectraSuite software (Ocean Optics, UK). SigmaPlot 12.0 (Systat Software, Inc, Illinois, USA) which calculated the light source irradiance value. Figure 2.5 shows the experimental set-up used for wavelength measurement.

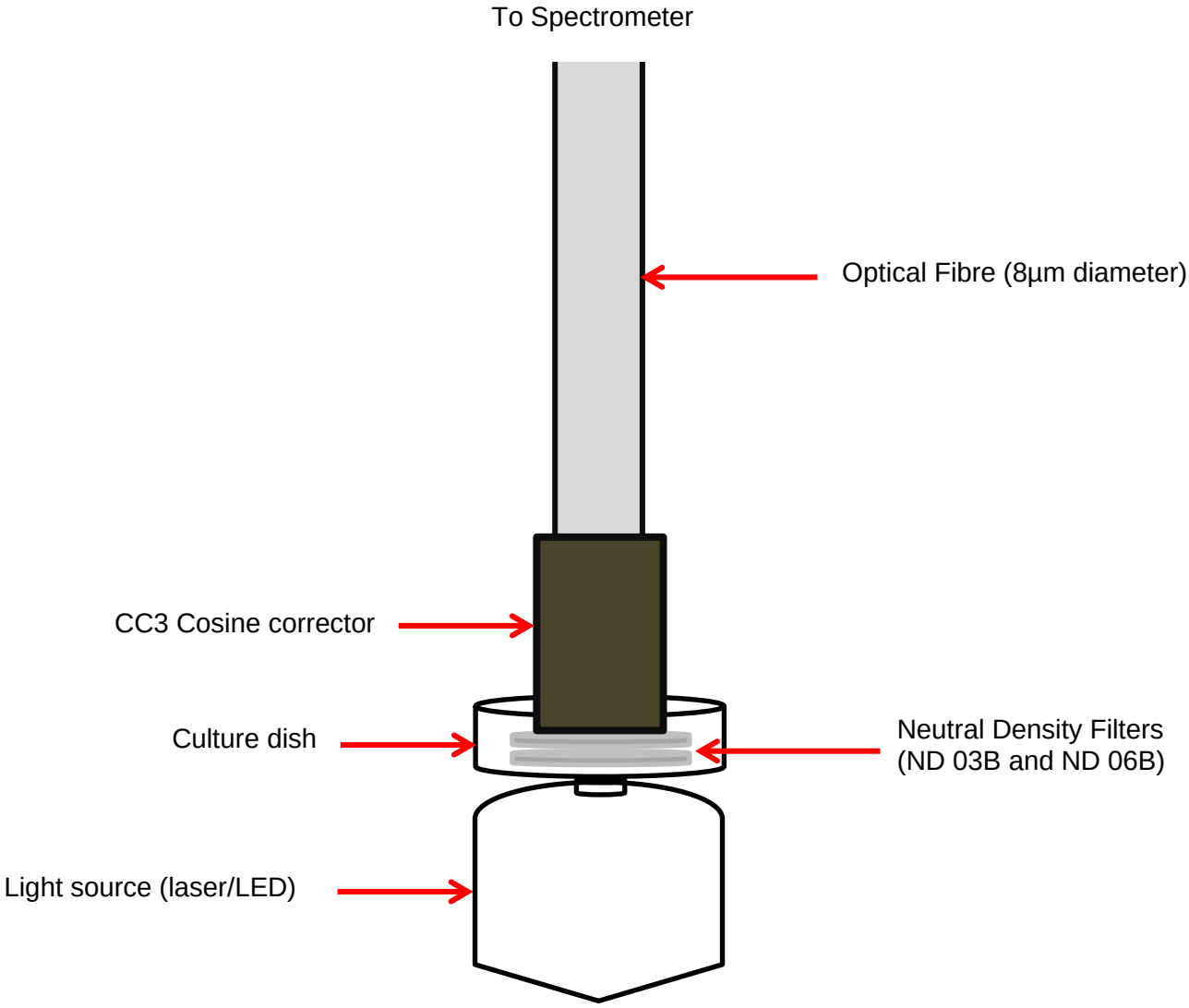

Figure 2.5: Schematic diagram of experimental set-up of light source wavelength measurement and irradiance value (distance of 0mm or 33mm between sensor and light source).

2.2.1.2 Exposure time and dosimetry (radiant exposure)

Oral epithelial cell cultures or neutrophils were exposed to the respective light source; (laser, single LED or LED arrays) 24h post seeding for single dosing experiments and 24h and 48h for double dosing experiments. The light exposure time differed for each light source, for the laser and single LED, cell cultures were irradiated for between 4-60s (Table 2.5 and Table 2.6), the first generation LED array cultures were irradiated for between 8-120s (Table 2.7). Whilst the second generation LED array used exposure times of between 30-480s (Table 2.8). Initial experiments were performed to identify the optimal exposure conditions with each light source and these conditions were then used for all future experimentation (Appendix 1).

Exposure time will determine the dose or radiant exposure delivered and this has been reported to produce differential cell responses (Vinck *et al.,* 2003, Bolton *et al.,* 1991). Details of the experimental protocol used for each individual light source are provided in the following sections. To identify radiant exposure (J/cm^2) (dose), the following calculation was applied according to Equation 2.1. The irradiance value (intensity) was obtained alongside wavelength measurements (Section 2.2.1).

Equation 2.1

$$\text{Radiant exposure } (J/cm^2) = \text{Irradiance value } (W/cm^2) \times \text{time } (s)$$

For example, the irradiance value for the laser was $1788mW/cm^2$ and the time of exposure was 60s. Therefore, the radiant exposure was:

$1788mW/cm^2 \times 60s$
$= 107J/cm^2$

2.2.1.3 Beam profiling

Light beam profiling was undertaken to characterise light field distribution which is of relevance as the light dose delivered to cells in a monolayer will vary across the light source field of illumination which may result in different cellular responses. The experimental set-up used was similar to that reported for the spectral irradiance measurements (Figure 2.6). A silicon based CCD (charged coupled device) camera beam profiler (SP620, Ophir, Spiricon, Israel) was used to capture images of light distribution for each light source (laser, single LED and LED arrays). The camera was equipped with a 50mm CCTV lens (Ophir, Spiricon, Israel) (Figure 2.6 (a) and (b)) which focused on the circular base of the tested light. Spacer rings were attached to the CCD in order to enlarge/reduce the beam image by adjusting the focal length. The more spacers used reduced the distance between the target and the camera, thereby enlarging the image on the screen. Use of less spacers means that the distance between the target and the screen had to increase in order to be in focus. Before beam measurements were undertaken, power value (Watt) of each source was determined using a photodiode (PD300, Ophir, Spiricon, Israel). Prior to measuring the beam profile of the light sources, the beam profile system was corrected for ambient light and the pixel response using a function, UltraCal in the Beam Gage software (Ophir, Spiricon, Israel). The calibration and measurements were monitored in using Beam Gage software (Ophir, Spiricon, Israel). The data of power values (obtained using the photodiode, as described above) were inputted into the software before beam measurements were obtained and used to calculate the spectral irradiance (mW/cm^2).

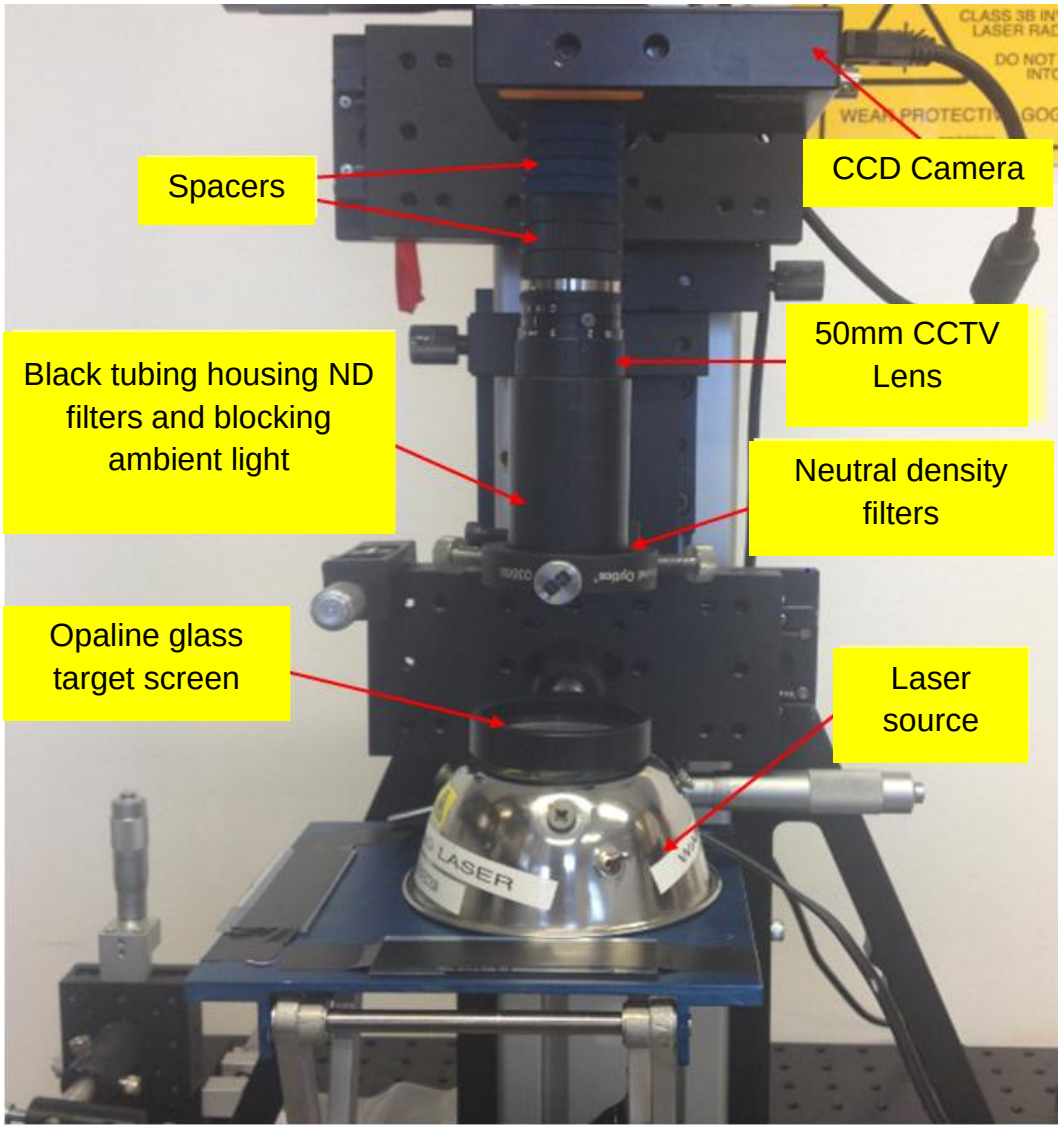

Figure 2.6 (a): Experimental set-up used for laser beam profiling.

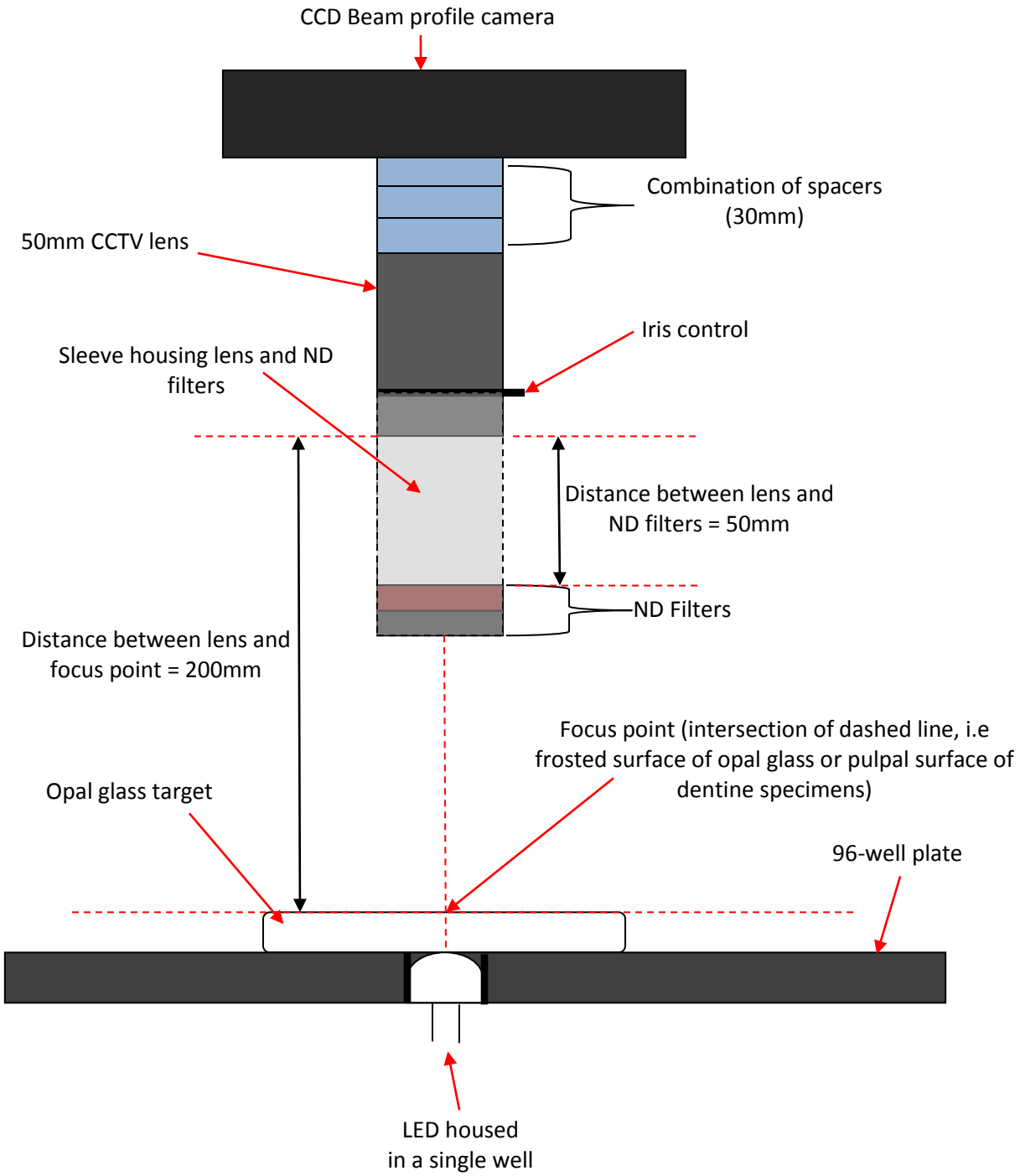

Figure 2.6 (b): Diagram of beam profiler set up for light source beam profiling (kindly provided by Dr. M. A. Hadis).

2.2.1.4 Temperature measurement

Temperature measurements were performed to determine any thermal changes which may occur during cell culture exposure by the laser, single LED or LED arrays. Analysis was performed in real-time utilising a K-type thermocouple (diameter: 1.21mm) (Maplin, UK) which was embedded into a SubMiniature version A (SMA) connector (outer diameter: 6.3mm). The cultureware with/without media was irradiated from beneath (at a distance of 0mm or 33mm for laser and single LED and 0mm for LED arrays). Temperature measurements were undertaken under the two conditions of; (a) at room temperature, and (b) following removal from a 37^{o}C incubator to replicate experimental conditions. The temperature was continuously measured using a multimeter (Iso-Tech, IDM 207, UK) and the data was monitored using Virtual DMM software (National Instruments, UK) (Figure 2.7).

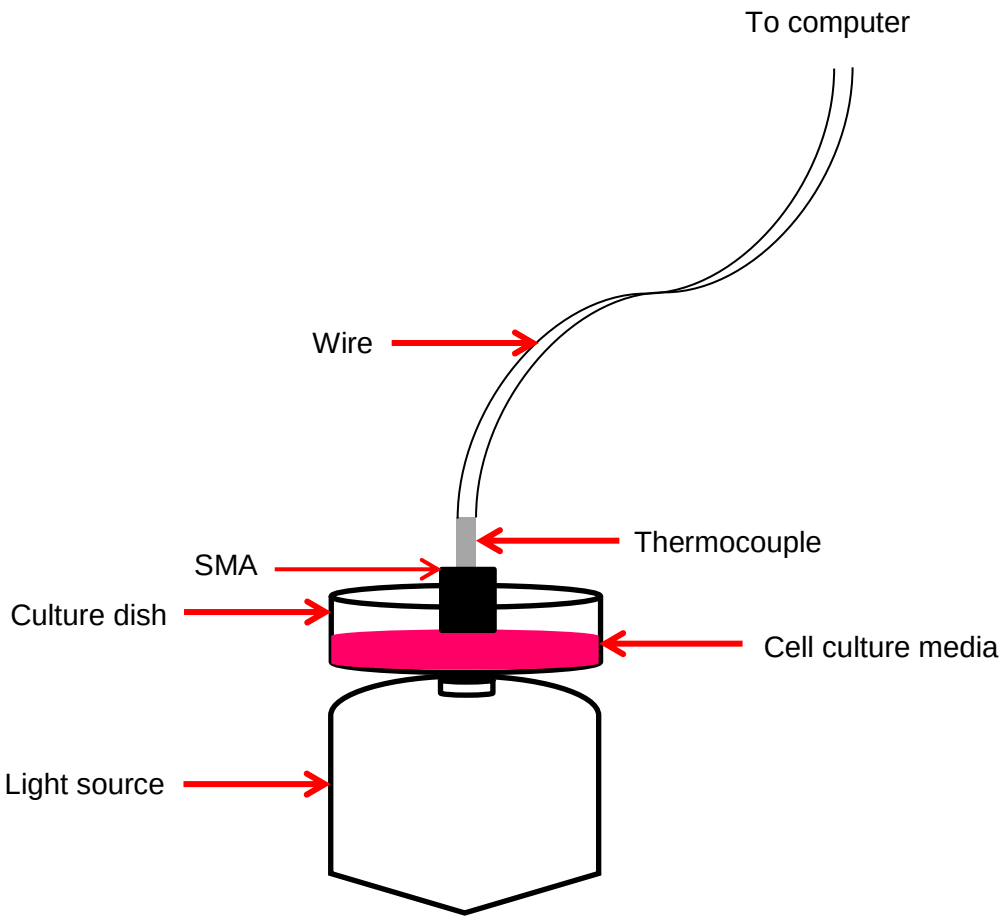

Figure 2.7: Schematic diagram of experimental set-up used for temperature measurement (distance: 0mm or 33mm) in cell culture systems.

2.2.2 Oral epithelial cell (OEC) H400 culture

A well characterised immortal epithelial cell line (H400) was utilised for all experimental work. This cell line was derived from the gingival epithelium of a female patient (Prime *et al.,* 1990) diagnosed with oral squamous cell carcinoma (SCC) and classified as a grade II tumour based on the STNMP system (S-site, T-size, N-lymph node, M-metastatic and P-nature of the tumour pathology). This H400 cell line was kindly donated by Dr S. Prime (University of Bristol, United Kingdom). All cell culture work required the use of well-established aseptic techniques to avoid microbial contamination. All experiments were undertaken in a positive pressure lamina flow hood (Gelaire, ICN Biomedicals, UK) and sterile plastic- / glass-ware were used to minimise the potential for contamination.

2.2.2.1 Cell storage and retrieval

To ensure sufficient cells were available for experimentation, cells were grown to confluence in a $75cm^2$ (T75) flask (Corning, UK). Following trypsinisation a cell suspension was produced, cell counts performed and $1x10^5$ cells were suspended in 1ml cryogenic solution (see Section 2.1.2.2.5). Suspensions were transferred to a cryovial and the DMSO (Sigma, USA) was added last to the suspension due to its cytotoxicity. Cells were frozen at -80^{o}C overnight before long term storage in liquid nitrogen.

Cell retrieval involved removal of a cryovial from liquid nitrogen followed by rapid thawing (over approximately 60s) in a 37^{o}C water bath. Once thawed the cell suspension was carefully transferred into a sterile 15ml tube containing 1ml pre-

warmed (37°C) DMEM (containing 10% of FCS) and gently mixed. This was then centrifuged (Jouan, France) at 800rpm for 10min, the resultant supernatant carefully decanted using a Pasteur pipette and the pellet was re-suspended in 1ml of fresh warmed (37°C) DMEM. The suspension was used to seed 75cm^2 flasks containing 14ml of DMEM culture media with 10% of FCS and incubated at 37°C in 5% CO_2. Flasks were inspected microscopically (Zeiss Axiovert 25, Zeiss, UK) for fungal/bacterial contamination during incubation. After 2-3 days culture, media was replaced with fresh media and re-incubated at 37°C in 5% CO_2 until approximately 80% confluence was achieved. Cell passage was performed to maintain cell growth and to allow seeding of a range of cultureware for subsequent experiments.

2.2.2.2 Cell passage

Cell passage is required when cells near confluence to allow continued propagation. Following media removal, the attached cell monolayer was washed using pre-warmed PBS (37°C) and trypsin-EDTA 0.25% (w/v) (1ml for 25cm^2 and 3ml for 75cm^2 flasks) was added and incubated for 5min and monitored to determine dissolution of the cell monolayer, gentle agitation of the flask aids dispersion of cell clumps. The production of a single cell suspension was confirmed microscopically and the subsequent cell suspension pipetted into a 15ml tube containing an equal volume of warm (37°C) DMEM growth media (to stop further action of trypsin-EDTA). This mixture was gently mixed and centrifuged at 800rpm for 4min. After centrifugation, the supernatant was discarded and the resultant pellet was re-suspended in 10ml warm (37°C) DMEM growth media. Cell counts were performed and then cells were seeded into a variety of cell culture vessels at a range of seeding

densities (Table 2.4) dependent of the experimental requirements. Experiments were undertaken between passages 10-40.

2.2.2.3 Determination of suitable foetal calf serum (FCS) concentration and cell inoculation densities for cell proliferation experiments

Epithelial cell culture routinely utilises 10% FCS supplementation, which allows rapid cell growth due to the abundant nutritional levels this concentration provides. Such optimal growth conditions may mask any proliferation benefit that light irradiation may deliver therefore reduced concentrations of FCS were utilised to investigate this premise. Initial experiments to examine growth effects of FCS supplementation used two different concentrations of FCS (5% and 10%). 35mm dishes were seeded with $2x10^4$ cells (in 2ml of DMEM) (for each concentration, n=4). Cell counts were performed 3 and 5 days post seeding and the growth rate indicated that 5% of FCS supplementation would be optimal to get 20-30% confluence (see Section 4.2) for future experimentation investigating irradiation effects on cell growth.

Following FCS concentration effect determination, investigations on initial cell seeding number influence on cell growth were performed. Cells were seeded at a range of seeding densities to determine the optimum seeding concentration for cell growth studies in a range of cell culture vessels. It is important to determine the seeding concentration for each culture vessel and at what time points cells achieve confluence in order to define the ideal experimental time frame for future experiments. At day 0, cells were seeded in 2ml of DMEM supplemented with 5% FCS at concentrations of $2x10^2$, $2x10^3$, $10x10^3$ and $2x10^4$ cells ($1x10^2$, $1x10^3$, $5x10^3$

and $1x10^4$ cells/ml, respectively) in 35mm dishes, $1x10^3$ – $10x10^3$ cells in 150µl of the growth media in 96-well plates ($6.6x10^3$ – $6.6x10^4$ cells/ml) and $2x10^5$ and $4x10^5$ in standard sized Petri dish with 15ml of the supplemented media ($1.3x10^4$ cells/ml and $2.6x10^4$ cells/ml).

In order to undertake these studies cells needed to be seeded into a variety of cell cultureware to allow irradiation with different light sources. Cells were grown at 37°C in 5% CO_2. Table 2.4 summarises the initial seeding densities/numbers used.

Cell counts were performed on days 1, 3, 4 and/or 5 following seeding (day 0) according to the cultureware used, for a range of FCS concentrations and initial seeding densities in order to determine optimal conditions to investigate the effects of light irradiation.

Table 2.4: Cell seeding densities/numbers for the range of culture ware used in this project.

Culture dish/plate	Volume of DMEM	Cell seeding number
25cm^2 cell culture flask	5ml	2x10^5
75cm^2 cell culture flask	12ml	5x10^5
35mm dish	2ml	2x10^4
96-well plate	150µl (per well)	3x10^3
100ml dish (standard Petri dish) (including a 4 well glass microscope slide)	15ml	2x10^5

2.2.2.4 Culture of cells in 35mm dishes

For experiments using laser and single LED light sources, cells were grown in 35mm sterile culture dishes (Sarstedt, Leicester, UK). Following seeding with 2ml DMEM containing $2x10^4$ cells, dishes were incubated at 37°C in 5% CO_2 and cell counts performed 1-4 days post irradiation. In addition RNA was isolated to investigate potential gene expression changes 24h post irradiation. In order to reduce confounding factors cell growth media was not changed during the experimentation period (see Section 2.2.3.1 and 2.2.3.2).

2.2.2.5 Culture of cells in 96-well plates

In order to investigate mitochondrial metabolic responses and reactive oxygen species (ROS) production post LED array irradiation, cells were cultured in black walled (Costar, UK) 96-well plates. Cells were seeded at a density of $3x10^3$ cells in 150µl of DMEM (per well) and incubated at 37°C in 5% CO_2 for 24h prior to LED array irradiation for further treatment (see Section 2.2.3.3).

2.2.2.6 Culture of cells in 4-well glass slides

Prior to laser irradiation for immunocytochemistry staining (section 2.2.3.1.2), H400 cells were seeded in standard Petri dish containing 4-well glass slide with two different initial inoculums to identify the optimum concentration for further study. The dishes were cultured with $2x10^5$ and $4x10^5$ cells in 15ml per dish ($1.3x10^4$ and $2.6x10^4$ per ml).

2.2.3 Cellular light irradiation

2.2.3.1 Laser irradiation

2.2.3.1.1 Laser irradiation of H400 cells in a 35mm dish

To perform laser irradiation, H400 cells were cultured in 35mm dishes and irradiated using the red laser from beneath the culture dish at a distance of either 0 or 33mm (Figure 2.8 (a)) 24h after initial seeding.

Initial optimisation experiments were performed to investigate the optimum value of radiant exposure for further laser irradiation work with H400 cells. Results from these initial experiments (see Appendix 1) enabled determination of radiant exposure for laser irradiation, i.e. utilising different radiant exposures (at 0mm) of 7, 10 and 14J/cm^2 which equated to 4, 6 and 8s irradiation respectively (Table 2.5). A further parameter that was modified was the distance between the light source and cultureware for laser irradiation (0 or 33mm). Laser irradiation with at a 33mm distance delivered decreased radiant exposure and minimised any potential effect from heat generated by the laser compared with a distance of 0mm. From the distance of 33mm, cell cultures in 35mm dishes were exposed to the laser with exposure times of 80, 100 and 120s to generate 27, 34 and 41J/cm^2 of radiant exposure 24h post-seeding (Table 2.5).

Another reported method of promoting enhanced biological response is by using a 'double dosing regimen' for light irradiation (Holder *et al.,* 2012). This protocol was

investigated in comparison with non-irradiated negative control and 'single dosing' experimental protocols. Single dosing occurred 24h post seeding whereas double dosing introduced a second light exposure 24h after the first dose (48h post cell seeding).

2.2.3.1.2 Laser irradiation for immunocytochemical staining

Laser irradiation was performed on H400 cells cultured in 4-well slides prior to immunocytochemical staining (see section 2.2.4.4) to study the effect of irradiation on NF-κB translocation of post-irradiation +/- stimulation with *E. coli* LPS. A total of $2x10^5$ of H400 cells (in 15ml media) were seeded in a Petri dish (containing a sterile 4-well glass microscope slide) and grown for 48h at which point irradiation was carried out for 80 and 120s (27 and 41J/cm^2 of radiant exposure) (Table 2.5).

2.2.3.1.3 Laser irradiation for IL-8 ELISA

For ELISA IL-8 investigation, H400 cells were seeded (see Section 2.2.2.4) and 24h later, *P. gingivalis* and *F. nucleatum* (whole dead bacteria) ($2x10^6$ bugs per $2x10^4$ cells) were used to stimulate cells (negative controls were included). Stimulated and unstimulated dishes were then irradiated using the laser for 80-120s (27-41J/cm^2) (Table 2.5) at 24h post-bacterial exposure and again at a further 24h for a "double dosing" regime. Culture media was collected 24h post single and double irradiation for quantification of interleukin-8 (IL-8) levels in culture media (see section 2.2.7).

2.2.3.2 LED irradiation

A similar experimental protocol was employed for single LED irradiation whereby H400 cells were exposed at 33 or 0mm distance from the underside of the cell culture dish (Figure 2.8 (b) and Figure 2.9). Initial experiments were performed (section Appendix 2) applying both distances in order to determine the optimum irradiation parameters. As a result of these initial experiments studies using this single LED were performed at a distance of 33mm and exposure time of 90 and 181s (0.5 and 1.0 J/cm^2 of radiant exposure) (Table 2.6).

Table 2.5: Calculation of radiant exposure for the laser by utilising irradiance value and time.

Light source	Distance (mm)	Irradiance value (mW/cm^2)	Exposure time (sec)	Radiant exposure (J/cm^2)
Laser	0	1788	4	7
			6	10
			8	14
	33	344	80	27
			100	34
			120	41

Table 2.6: The radiant exposure for the single LED by utilising irradiance value and time.

Light source	Distance (mm)	Irradiance value (mW/cm^2)	Exposure time (sec)	Radiant exposure (J/cm^2)
Single LED	33	5.5	90	0.5
			181	1.0

(a)

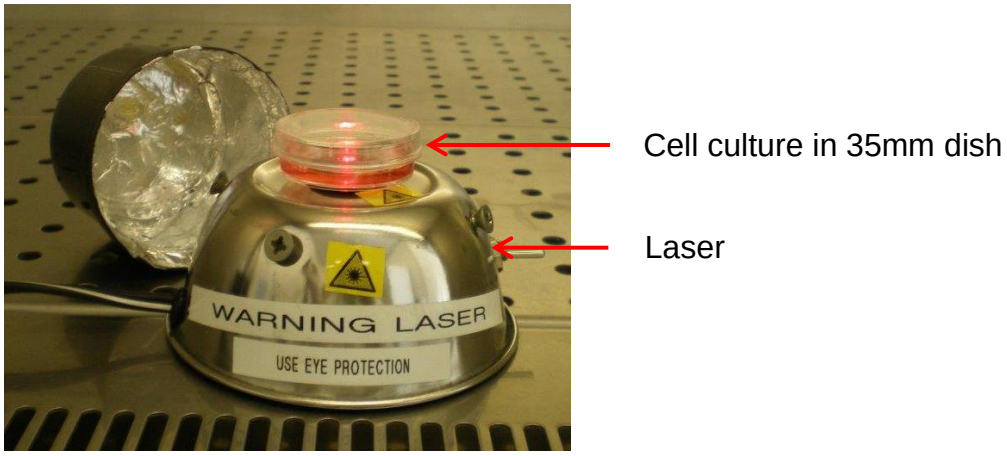

(b)

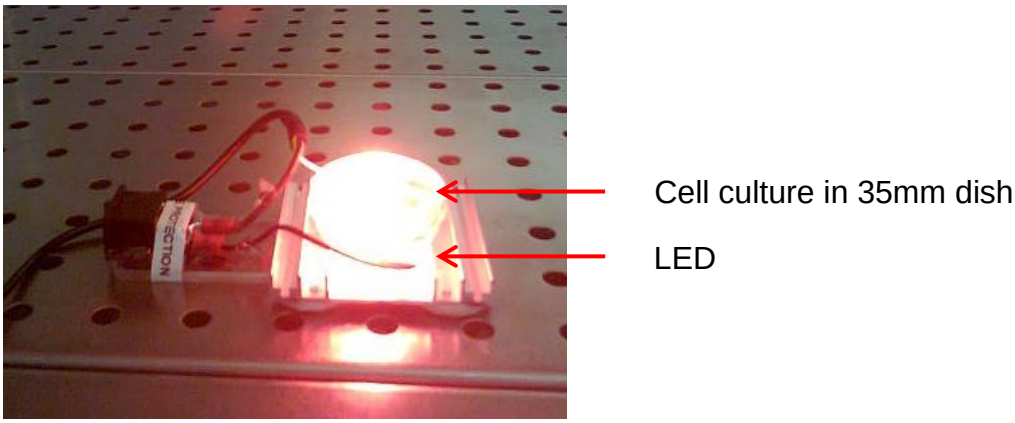

Figure 2.8: Irradiation of H400 cells (35mm dishes) using (a) laser and (b) single SMD LED.

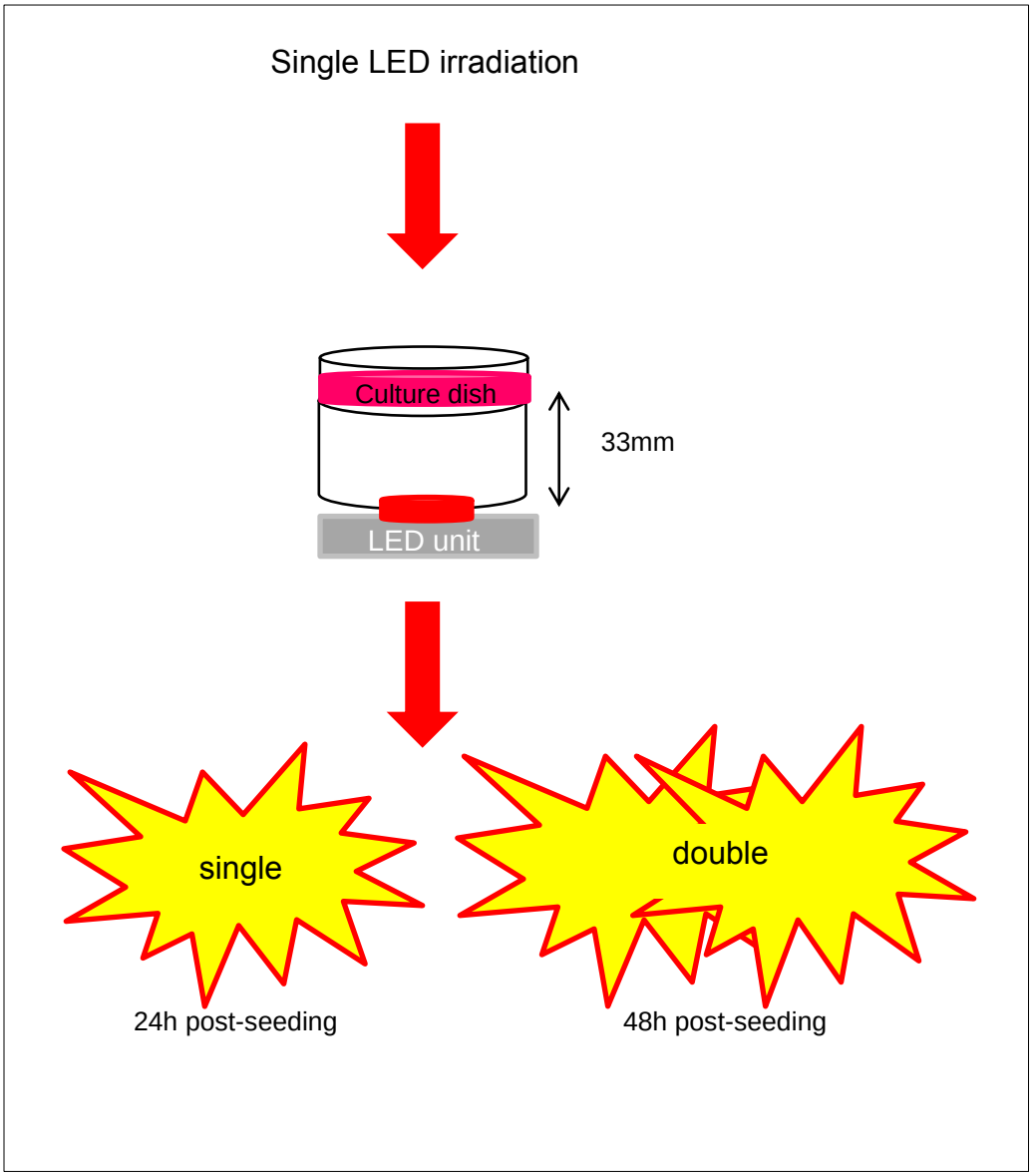

Figure 2.9: Diagram summarising the exposure regimes for single LED irradiation with single and double dosage at a distance of 33mm from the culture.

2.2.3.2.1 Single LED irradiation for ELISA IL-8

H400 cells were cultured and stimulated with heat-killed *P. gingivalis* and *F. nucleatum* and culture media collected and stored at -80^{o}C before use as described in Section 2.2.3.1.3. Single LED irradiation was carried out 24h and 24h & 48h post stimulation for single and double dosage, respectively. H400 cell cultures were irradiated for 90 and 181s (0.5 and 1.0 J/cm^2 of radiant exposure).

2.2.3.3 LED arrays

Experiments utilising LED arrays were conducted using 96-well black walled plates. H400 cells were seeded in 96-well plates and illuminated directly from beneath (the distance between LED and cell monolayer was 3mm) (Figure 2.10 (a)). Each column (1-10) of the first generation 96 LED array exhibited different wavelengths (625, 650, 660, 670, 690, 780, 800, 810, 820 and 830nm) (Figure 2.3) (section Appendix 3). However, due to variety of radiant exposures delivered by the first generation device later experiments controlled each LED individually in order to deliver a similar radiant exposure value across the range of wavelengths used. The experimental conditions used were 2, 5 and 10J/cm^2 radiant exposure and a single dosing regimen (see Table 2.7).

Initial experiments used the first generation LED array where the radiant exposure varied between the different wavelengths, results obtained therefore could not directly be attributed to differences in wavelength, therefore future experiments used a bespoke second generation LED array where radiant exposure could be standardised across the range of different wavelengths used in the device. The

second generation LED array was set up to deliver a radiant exposure of 24mW/cm^2 (except 2 diodes; 605 and 670nm where this radiant exposure could not be achieved, as a result these wavelengths were omitted in subsequent experiments) (Figure 2.10(b)). Changes in exposure time with the second generation array allowed delivery of standard radiant exposures across all wavelengths. Exposure times of between 30-480s were used which equated to a radiant exposure range of between 0.7-11.6J/cm^2 (Table 2.8). Single and double dosing irradiance regimes were also investigated using this second generation LED array.

2.2.3.3.1 Second generation LED array irradiation on stimulated H400 cells for MTT analysis and ELISA IL-8

Oral epithelial H400 cells were seeded (Section 2.2.2.5) and stimulated with heat-killed *P. gingivalis* and *F. nucleatum* (2.2.6.2) 24h post seeding. LED array irradiation was undertaken for 480s (Table 2.8) 24h post stimulation. Following 24h incubation at 37^{o}C in 5% of CO_2, culture media was collected as in Section 2.2.3.1.3 for ELISA IL-8 (2.2.7) and the plate then prepared for MTT assay (see Section 2.2.4.3). MTT assays were undertaken according to Table 2.9.

Table 2.7: Exposure conditions for first generation LED array. For each wavelength the exposure parameters required to deliver radiant exposures of 2J/cm^2, 5J/cm^2 and 10J/cm^2 are provided.

Wavelength (nm)	Irradiance value (mW/cm^2)	Time (s) for		
		2J/cm^2	5J/cm^2	10J/cm^2
625	65	30	76	153
650	9	222	555	1111
660	48	41	104	208
670	23	86	217	434
690	52	38	96	192
780	126	15	39	79
800	142	14	35	70
810	67	29	74	149
820	114	17	43	87
830	116	17	43	86

Table 2.8: The radiant exposures, J/cm^2 and exposure times for the second generation array in order to deliver an irradiance value of 24mW/cm^2.

Irradiance value	30s	60s	120s	240s	480s
24mW/cm^2	0.7	1.5	2.9	5.8	11.6

(a)

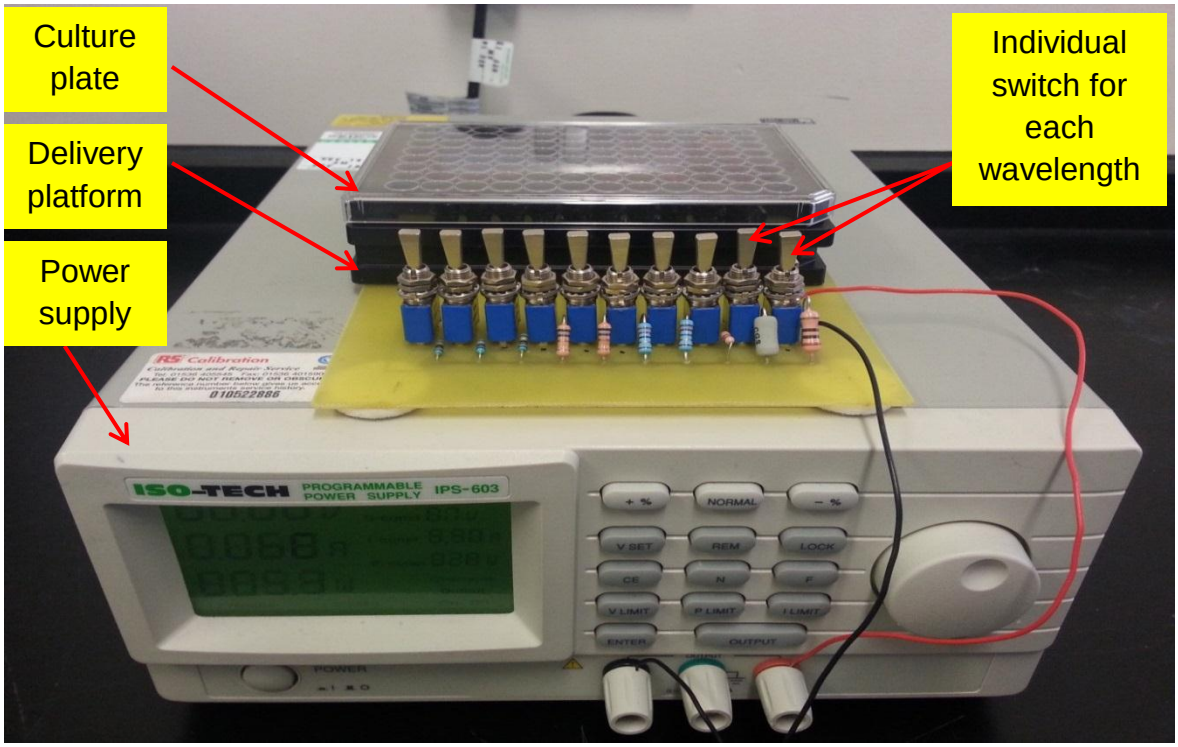

(b)

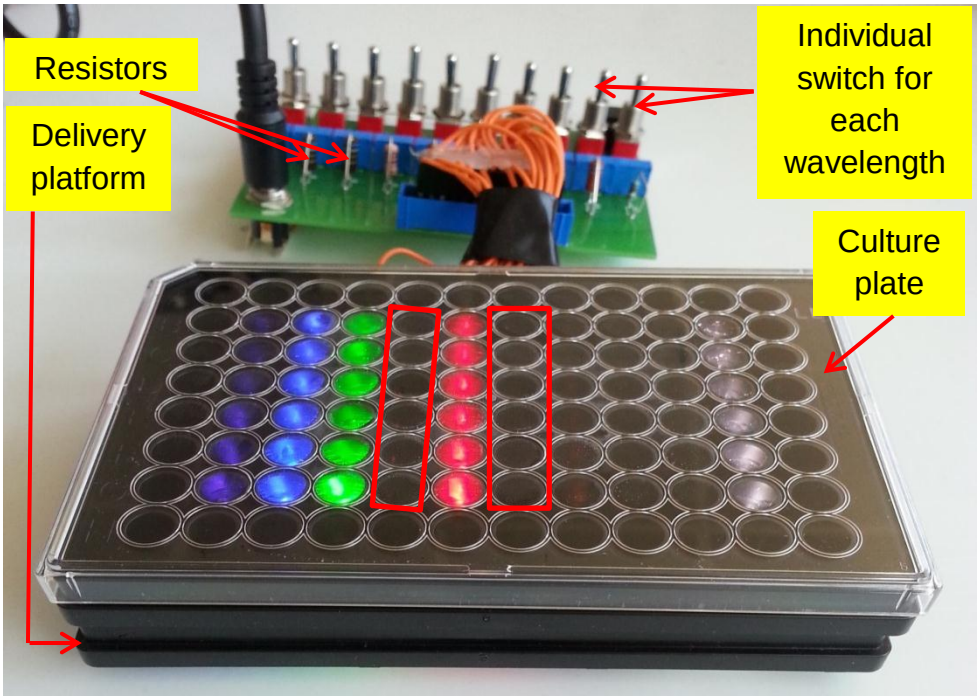

Figure 2.10: (a) First generation LED array with power supply (b) The second generation LED array with standardised irradiance of 24mW/cm^2 except for diodes in red rectangle (605 and 670nm).

Table 2.9: Different conditions of plates for MTT after stimulation and irradiation (h-k: heat-killed, *P.g*: *P. gingivalis*, *F.n*: *F. nucleatum*).

Day \ Plate	1	2	3	4	5	6
Day 0	Seeded	Seeded	Seeded	Seeded	Seeded	Seeded
Day 1	h-k *P.g* in	h-k *P.g* in	h-k *P.g* in	h-k *F.n* in	h-k *F.n* in	h-k *F.n* in
Day 2	Irradiated	-	Irradiated	Irradiated	-	Irradiated
Day 3	MTT	Irradiated	-	MTT	Irradiated	-
Day 4	-	MTT	MTT	-	MTT	MTT

2.2.4 Biological assays

2.2.4.1 Cell counts and viability analysis

Assessment of cell number was performed using two approaches (a) conventional manual counting using a haemocytometer (Neubauer, Hawksley, UK) (Figure 2.11) where cells are counted under a microscope, (Zeiss Axiovert 25, Zeiss, UK) and (b) using an automatic cell counter (Luna™, Logos Biosystems, Inc, Republic of Korea) (Figure 2.13 (b)) (see Section 2.2.2.2).

Cell counts were performed using 10µl of cell suspension (see Section 2.2.2.2) and loaded into a Neubauer haemocytometer (Hawksley, UK) and viewed at 10x magnification under a Zeiss Axiovert 25 microscope (Zeiss, UK). Data from the haemocytometer counts gave a value of $x10^4$ cells per ml. Each sample was counted 6 times and the average value calculated. To determine cell viability, trypan blue exclusion staining (0.4%; Gibco, UK) was utilised. A 10µl cell suspension was added to 10µl of 0.4% (w/v) Trypan blue and thoroughly mixed before transferring to a haemocytometer. Trypan blue is taken up by non-viable cells as they lack cell membrane continuity (Louis & Siegel 2011) and not by viable cells as they have intact cell membranes. Cells stained with trypan blue along with total cell count was performed in order to determine total cell number and percentage of cell viability.

Counts performed using the Luna automated cell counter used a disposable counting chamber (Figure 2.13 (a)). 10µl of sample was gently mixed with 10µl of trypan blue and then 10µl of the mixture was loaded into the chamber. The slide was then loaded

into the reader port of the instrument (Figure 2.13 (b)). Manual focusing was performed to ensure a well-focused image denoted by viable cells having dark edges and bright centres and non-viable cells were stained blue. Once automated counting was complete results were obtained for total number of viable & non-viable cells as well as percentage viability. For automated cell counting at least 6 individual counts were performed from each cell suspension. Initial validation experiments were performed to establish accuracy of automated cell counting in comparison with the well-established manual counting technique. This was confirmed by generation of a correlation graph between data from Luna and manual cell counting (Figure 2.12).

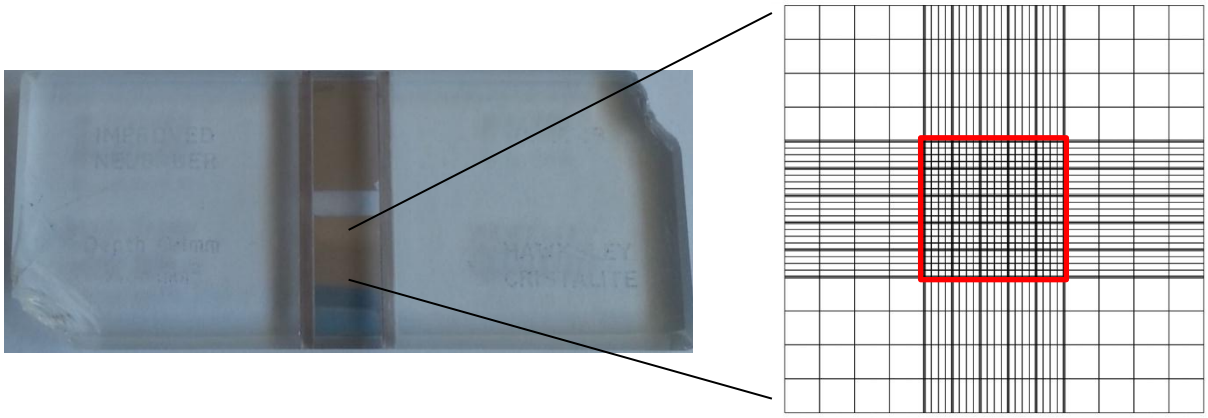

Figure 2.11: The diagram of Neubauer haemocytometer (www.microbehunter.com). Cell counting was undertaken by counting live cells included in the red square area. The counted cell represented x10^4 per ml of cells.

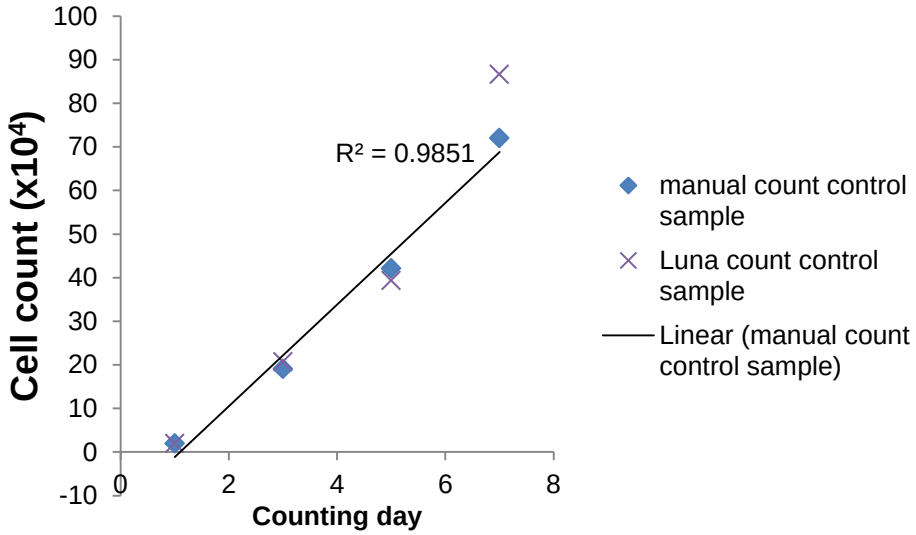

Figure 2.12: Comparison of H400 cell counts obtained using Luna automated cell count and manual direct counting. Linear regression analysis with R^2 showing a value 0.9851, indicating good correlation between manual and Luna counts.

(a)

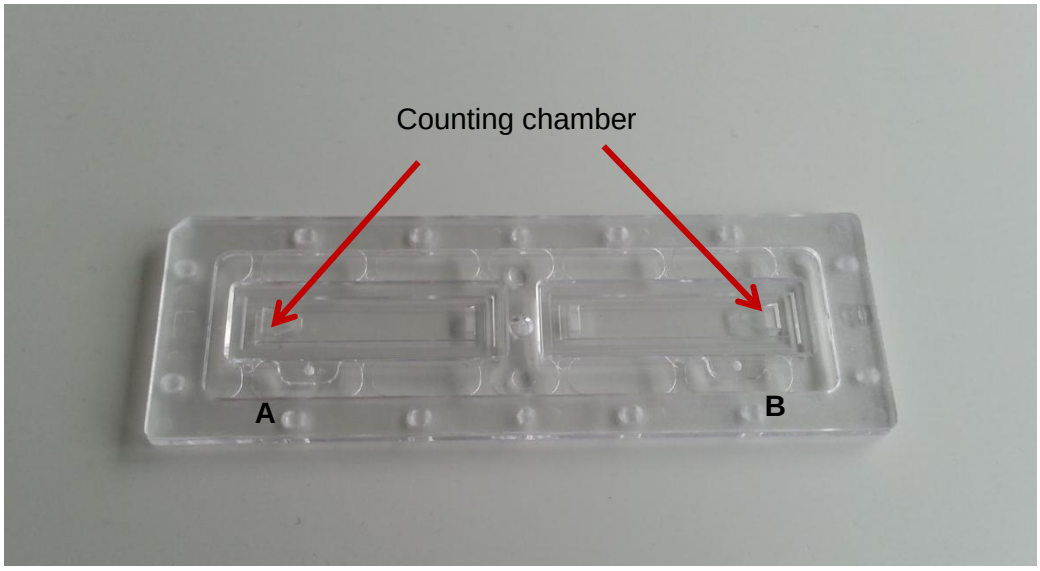

(b)

Figure 2.13: Luna^{TM} automated cell counting device (a) cell counting slide, (b) Automated cell count reader.

2.2.4.2 Methylene blue staining

Methylene blue staining of cell culture monolayers was performed to investigate the potential effect of variation in LED and laser beam profile on patterns of cell growth. Cells were seeded in 35mm dishes ($2x10^4$ cells) and cultured for 24h before irradiation. Staining was performed 48 and 76h post exposure. Methylene blue solution (2%) was prepared by dissolving methylene blue powder (Tocris Bioscience, UK) in 50% ethanol (Fisher Scientific, UK) and then passing through a 0.2µM filter (Fisher Scientific, UK). DMEM was removed from the culture dish and the cell monolayer fixed for 10min with 10% formalin solution (Sigma-Aldrich, UK). The formalin was then removed and 1ml of methylene blue solution added and incubated at room temperature for 30min. The solution was then removed and the monolayer washed 3 times with deionised water and the stained cultures air dried at room temperature. Images of the cultures were captured using a tripod mounted digital camera (D40, Nikon, Japan) with a18-55mm lens manually set at 55mm and an aperture of f8 to ensure sufficient depth of field. The cell culture dish was back illuminated with a light box. The resulting images were compared to determine any differences in the patterns of cell growth between irradiated and non-irradiated cell culture plates.

2.2.4.3 MTT assay

The MTT (3-[4,5-dimethylthiazol-2-yl]-2,5 diphenyl tetrazolium bromide) assay provides two potential readouts: (a) to determine mitochondrial metabolic activity (Mosmann 1983) and (b) as a surrogate marker of viable cell number. If MTT is assessed at early time points (e.g. 4h post irradiation) it is considered a measure of

metabolic activity. At longer time points MTT (e.g. over 24h) it can be used as a measure of viable cell number (Mosmann 1983).

Cells were seeded ($3x10^3$ cells in 150µl per well) into black walled flat bottom 96-well plates and irradiated using both the first and second generation LED arrays as described previously at 24h post seeding where double dosing applied for 1st generation array. Prior to use, the MTT solution was prepared by dissolving 5mg of MTT powder in 1ml of PBS. The mixture was filtered using a 0.2µM filter and stored in the dark at 4°C. After a further 24h, 15µl of MTT solution (to achieve a 1:10 dilution MTT to growth media) was added to each well and the plate incubated at 37°C for 4h (Sylvester 2011). The MTT solution and media was removed from wells and 50µl of DMSO (Sigma-Aldrich, Gillingham, UK) pipetted into each well. The plate was then incubated at room temperature for 5min on an orbital shaker (R100/TW Rotatest Shaker, Luckham LTD, England) to ensure formazan crystals were fully dissolved. The optical density (O.D) @ 570nm was measured using an ELx800 Universal Microplate reader (Bio-Tek Instruments, UK)**.**

2.2.4.4 Immunocytochemical staining

For immunocytochemical analysis cells were cultured on multi-well glass slides (C.A Hendley Ltd, UK) (Figure 2.14 (a)) for 48h. Slides were irradiated 1h prior to bacterial (*E.coli* LPS) stimulation (1h incubation at 37°C). The slides were washed with PBS (3x), then fixed in dry acetone for 15min at room temperature. Slides were then air dried (15min) and placed in a humidity chamber prior to staining. Primary antibodies were prepared (NF-κB p65 subunit (clone F-6, Santa Cruz Biotechnology, US) and

Ki-67 (clone MM1, Novacastra™, UK) in a ratio of 1:100 in PBS with 1% BSA. NF-κB antibodies were added to experimental wells and Ki-67 and PBS (with 1% of BSA) were included as positive and negative controls, respectively (Figure 2.14 (b)). After 60min incubation, slides were washed with PBS (3x10min) and air dried. Multilink (biotin-labelled goat anti-mouse/rabbit Ig, BioGenex, US) was applied and incubated for a further 20min. The slides were then washed with PBS (3x10min) and overlaid with label (peroxidase linked to avidin, BioGenex, US) and incubated for a further 20min. Following washing with PBS (3x10min) slides were stained with DAB (diaminobenzidene) reagent and incubated at room temperature for 5min, before washing carefully under running water for 2min and then counterstained with hematoxylin (BioGenex, US) for 5min. Slides were rinsed in deionised water prior to dehydration in graded alcohols, cleared with xylene and mounted in XAM.

(a)

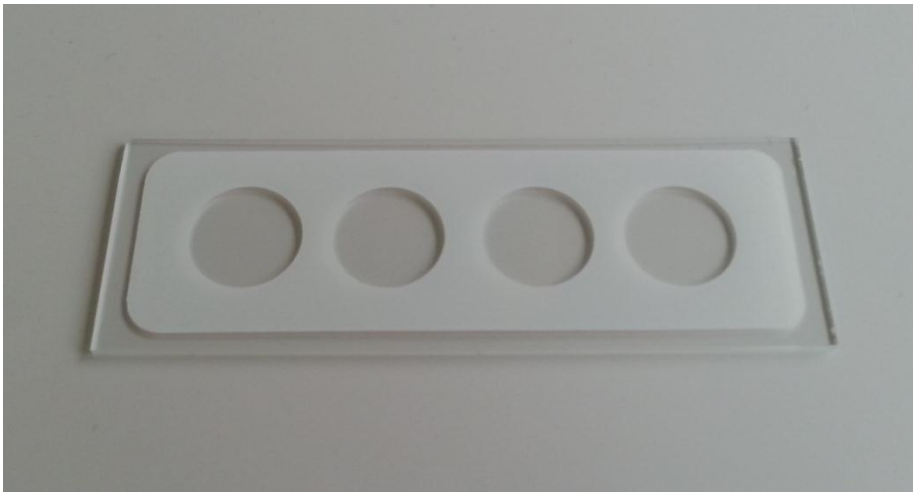

(b)

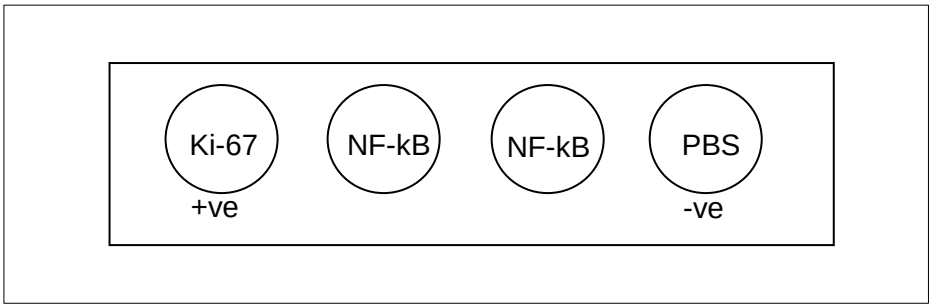

Figure 2.14: (a) Four well glass slide (C.A Hendley Ltd, UK). (b) Slide staining key: positive control (Ki-67), negative staining control (PBS) and specific NF-kB antibody.

2.2.4.5 BrdU cell proliferation assay

Cell proliferation rates were determined using a 5-bromo-2-deoxy-uridine (BrdU) labelling/detection kit (Roche Applied Science, Burgess Hill, UK). Cells were seeded ($2x10^4$ cells per dish ($1x10^4$ cells/ml)) in 35mm cell culture dishes (see Section 2.2.2.4) (for laser irradiation) and ($3x10^3$ cells per well ($2x10^4$ cells/ml)) in 96-well black walled plates (see Section 2.2.2.5) (for LED array irradiation) and cultured for 24h prior to irradiation. 24h following irradiation culture media was removed and 1ml of BrdU labelling medium was added to the 35mm dish and 100µl to each well of 96-well black plate (ratio of BrdU labelling medium in sterile media 1:1000). Similar amounts of reagent for 35mm dish and 96-well plate were applied for the rest of the assay. Cultures were incubated for 60min, following which BrdU labelling media was removed and washed (3x) in washing buffer (1:10 with double distilled water). Cells were then fixed with ethanol glycine (30ml of 50mM glycine (0.375g in 100ml distilled water, pH 2.0) to 70ml absolute ethanol, pH 2.0 with HCl, stored at 4^{o}C) for 20min at room temperature. After removing all liquid, the plates were placed at -20^{o}C for 30min and the anti-BrdU reagent (1:20 in incubation buffer) was prepared. Plates were then washed (3x) with wash buffer, and anti BrdU added followed by 30min incubation at room temperature. Plates were then washed 3x (wash buffer) and anti-mouse Ig-AP conjugate (1:20 with PBS) added to the dishes. Following incubation at 37^{o}C for 30min, dishes were washed (3x with washing buffer). The colour substrate buffer (13µl NBT + 10µl BCIP + 3ml substrate buffer (100mM Tris HCl (1.6g) + 100mM NaCl (0.58g) + 50mM $MgCl_2$ (1.15g) in 100ml distilled water, pH 9.5)) was mixed and added prior to incubation at room temperature for 30min. Following a final wash (3x) plates were examined microscopically using a 20x objective (Zeiss

Axiovert 25, Zeiss, UK) and images captured. Brown stained and unstained cells were then counted using cell counter application in Image J software (http://fiji.sc/Fiji) and data analysed (section 2.2.8).

2.2.4.6 Chemiluminescent ROS assay for H400 cultures

2.2.4.6.1 ROS detection using Luminol

A chemiluminescent ROS assay was used to determine total ROS release from H400 cells following light exposure using the 1st generation LED array. Cells were seeded (3x10^3 cells in 150µl DMEM per well) in black walled flat bottom 96-well plates (Costar, UK) (2.2.2.5) and grown for 24h. Prior to absorbance determination, Luminol working solutions (3mmol/L pH 7.3) were prepared by addition of 1ml Luminol stock solution (30mmol/L in 0.1M NaOH) to 9ml of PBS and stored at 4^{o}C for up to 6 weeks.

Prior to treatment, the media was removed and the cells washed with PBS to remove any remaining media. Following the washing, a total of 170µl of PBS was added to each well. The plate was then irradiated using the first generation LED array for 8s. Following this 30µl of Luminol solution was rapidly added to the wells (giving a final volume of 200µl per well). The plate was then read at 37^{o}C in a luminometer (Berthold LB96v, Bad Wildbad, Germany) over the next 2h. Raw data was recorded and transferred to Excel spread sheet (Microsoft, US) for analysis.

2.2.4.6.2 ROS detection using CM-H_2DCFDA

ROS determination in H400 cells utilised the reagent, CM-H_2DCFDA (5-(and-6)-chloromethyl-2',7'-dichlorodihydrofluorescein diacetate, acetyl ester) (Life Technologies, UK). H400 cells were seeded (section 2.2.2.5) and incubated at 37^{o}C for 24h. The media was then removed and cells washed with PBS (1x), 50µl of clear fresh media was added followed by 2nd generation LED array irradiation (480s irradiation – 11.6J/cm^2 radiant exposure) (2.2.2.5). Another 50µl of clear fresh media containing 10µM CM-H_2DCFDA was then added to the plate. At 30min before the 1h incubation had ended, 0.5µl of H_2O_2 was added into empty wells in triplicate as ROS production control (H_2O_2 acts as a positive ROS control for this study. The plate was read at an excitation of 485nm and an emission of 535nm using a fluorometer (Berthold Twinkle, Germany).

2.2.4.7 Isolation of RNA and preparation of DNA

2.2.4.7.1 Isolation of RNA

RNA was isolated from cells cultured in 35mm plasticware using an RNA extraction kit (RNeasy® protect mini kit, Qiagen UK) according to the manufacturer's instructions. A total of 10 culture dishes (35mm) (2x10^4 cells in 2ml) were used to generate sufficient cells for RNA isolation for cultures irradiated with laser and single LED (Sections 2.2.3.1.1 and 2.2.3.2, respectively).

Cell monolayers were washed with PBS following culture media removal to minimise inhibition of lysis and enhance RNA yield. A total of 350µl of lysis buffer (RLT buffer)

containing 1% β-mercaptoethanol (β-ME) was added to the culture dishes and agitated to ensure complete cell lysis. The lysate was collected by pipette and transferred to a clean 2ml centrifuge tube. An equal volume of 70% ethanol was added to the lysate and mixed well by pipetting. The mixture was transferred onto an RNeasy® spin column in a 2ml collection tube. The tube was centrifuged at 10000rpm for 30s in a 5415D micro-centrifuge (Eppendorf, UK). The flow-through was discarded, 350µl of RW1 wash buffer was added onto the column and then spun at 10000rpm for 30s. DNase I was prepared by mixing 10µl of DNase I to 70µl of buffer RDD (to be used with DNase I - provided in kit) and gently mixed by inverting tube and then briefly centrifuged (1000rpm for 2s). DNase I solution was added to the spin column membrane and incubated at room temperature for 15min. Samples were then washed with 350µl of buffer RW1 (buffer for washing membrane-bound RNA) and centrifuged at 10000rpm for 30s. 500µl of buffer RPE (buffer for washing membrane-bound RNA) was pipetted into the spin column for further washing and centrifuged at 10000rpm for 30s and then re-washed with 500µl of buffer RPE and centrifuged at 10000rpm for 2min. The column was then placed into a new collection tube and centrifuged at 10000rpm for 1min. Following addition of 30µl of RNase free water to the membrane, the column which was placed into a 1.5ml collection tube was spun at 10000rpm for a 1min to elute RNA. Quantification of RNA yield was then performed (see Section 2.2.4.7.4).

2.2.4.7.2 Reverse transcription

Reverse transcription of RNA was performed using a commercially available kit, (Bioline Tetro, UK) following manufacturer's instructions. Transcription was

undertaken to generate complementary DNA (cDNA) from RNA. All the reagents in Table 2.10 were combined in a sterile 1.5ml Eppendorf tube. The mixture containing the RNA template were incubated in a thermal cycler, Eppendorf (Eppendorf, UK) at 45^{o}C for 30min followed by 85^{o}C for 5 min and then placed at 4^{o}C. cDNA samples were stored at -80^{o}C prior to use.

2.2.4.7.3 Concentration of cDNA

500µl of water was added to the 1.5ml tube containing cDNA and transferred to a Microcon YM-30 centifugal filter unit (Milipore, UK) and centrifuged at 10000rpm for 2min. The sample was re-centrifuged at 8000rpm for 1min. At this point, the cDNA is predicted to be in a total volume of 50-60µl. The filter was then inverted into a new 1.5ml collection tube and centrifuged at 0.8rpm for 1min to collect the cDNA. The cDNA quality and concentration was determined using a spectrophotometer and agarose gel electrophoresis (see following sections).

2.2.4.7.4 Quantification of RNA and cDNA

The quantification of RNA and complementary DNA was performed using a spectrophotometer (Biophotometer, Eppendorf, UK). The measurement was obtained by diluting the sample into RNase free water (2µl sample to 68µl RNAse free water). The diluted sample was then pipetted into a cuvette (Eppendorf, UK) and the sample concentration determined at an absorbance of 260nm. The purity of sample was assessed by reading the 260nm : 280nm ratio. High cDNA purity ranges are from 1.6 to 1.8.

Table 2.10: Reagents and volumes used in the reverse transcription reaction.

Reagents	**Volume (µl)**
5X RT buffer	4
10mM dNTP mix	1
Oligo $(dT)_{18}$	1
RNase inhibitor	1
Reverse transcriptase	1
RNA template	variable
RNase free water	to a total volume of 20µl
Total volume	20

2.2.4.7.5 Agarose gel electrophoresis

Isolated RNA, cDNA and PCR products were visualised by agarose gel electrophoresis. 1.5% of agarose gels were prepared by adding 0.9g of agarose to 60ml of 1X Tris-acetate-EDTA (TAE) buffer (Helena Biosciences, UK) in a large conical flask. The solution was mixed and then heated in a microwave with 30s mixing cycles. The solution was then allowed to cool at room temperature to approximately 60^{o}C before addition of 3µl of SYBR Gold to enable visualisation of nucleic acids under UV light. A comb was inserted into the liquid agarose to form wells and the gel was allowed to set at room temperature for at least 30min.

Prior to performing electrophoresis, the gel was placed in the tank containing sufficient 1X TAE (Tris base, acetic acid and EDTA) to ensure coverage of the gel and wells. The comb was then carefully removed to produce a series of wells. The first well was loaded with 3µl of 100bp Hyperladder IV (Bioline, UK) to allow size determination of DNA products. 6µl of sample was then loaded into the remaining wells. The gel was electrophoresed at 120 volts for 40min. The resulting gel was visualised under UV light (300nm) in a G:Box gel documentation unit (Syngene, UK) and captured using Genesnap software (Syngene, UK) and the bands present were analysed using GeneTools software (Syngene, UK).

2.2.4.8 Polymerase chain reaction (PCR)

2.2.4.8.1 Sample normalisation

The concentration of cDNA present in samples will be variable and reflect the initial concentration of RNA extracted. By normalising the cDNA the gene expression levels may be effectively compared between control and experimental samples. During normalisation, the optimum number of PCR cycles were determined. The normalisation utilised the expression level of the house keeping gene, glyceraldehyde-3-phosphate-dehydrogenase (GAPDH). Quantification of expression level of target genes using a housekeeping gene as standard is important for normalisation of expression levels (Pfaffl 2001).

Prior to use, a primer master mix was prepared. A total of 10µl of 100µM forward and 10µl of 100µM reverse primer were added to 60µl of RNAse free water. A PCR master mix was prepared by mixing the following components; 12.5µl of REDTaq® ReadyMix™ PCR Reaction Mix (Sigma, United Kingdom), 2µl of forward and reverse of target gene primer mix, 9.5µl of RNase free water and 1µl of cDNA template. The reaction was performed using Eppendorf thermal cycler (Mastercycler Gradient, Eppendorf, UK).

The programme used for the amplification consisted of initial denaturation at 94^{o}C for 5min, followed by cycles of denaturation at 94^{o}C for 30s, annealing at appropriate temperature (according to the melting temperature provided by the manufacturer) for 30s, extension at 72^{o}C for 30s and final extension at 72^{o}C for 10min. The programme

was set on hold at 4°C before the samples were taken out of the thermal cycler. Initial experiment used 18, 21 and 24 cycles. A total of 6µl of sample was collected at each time point and stored in a 96 well plate on ice until all cycles had completed. The PCR products then were visualised using gel electrophoresis, as described previously. The gel image was captured and the intensity of bands determined using GeneTools software (Syngene, UK). The required number of PCR cycles for the target gene were determined and the required amount of cDNA calculated based on the gel image for GAPDH normalisation (as previously described) in order to obtain products with equal intensity. The following equation was used to calculate the volume of cDNA required for normalisation in order to ensure the similar amount of cDNA template is generated in the PCR:

$$\frac{\text{Intensity of standard band}}{\text{Intensity of band to normalise}} \times \text{Volume of standard sample} = \text{Volume of cDNA required to normalise}$$

2.2.4.8.2 PCR primers

All PCR primers were designed using primer-BLAST (NCBI, USA) according to published accession number except for the NF-κB gene primers, which utilised the NF-κB gene primers reported by Milward *et al.,* (2007). All primers were synthesized by Invitrogen, Life Technologies, UK. Table 2.11 provides the details of the primer assays used.

All PCR assays were performed using REDTaq® ReadyMix™ PCRMix (Sigma-Aldrich, UK) as described in section 2.2.4.8.1. PCR products were visualised by electrophoresis in 1.5% agarose gel, imaged and analysed (see Section 2.2.4.7.5).

2.2.4.8.3 PCR semi-quantification

PCR semi-quantification was analysed using GeneTools software (Syngene, UK) according to the image captured using Genesnap software (Syngene, UK). There was a red box which was used to determine PCR bands to be assessed. The software then generated value; molecular weight, raw volume and % raw volume. However, only raw volume data is used for semi-quantification. The value for each band was then exported to Excel (Microsoft, US) documentation.

Table 2.11: Details for PCR primers used in assays.

Gene	Symbol	Primer sequence	PCR product (bp)	Reference
NADH dehydrogenase (ubiquinone) 1 alpha subcomplex, 11	**NDUFA11**	F: 5'-GTCATTTGAAGCTGGGCTGC-3' R: 3'-GCTCACACCTTGGGTTTTGC-5'	410	(Houreld *et al.,* 2012, Masha *et al.,* 2013)
NADH dehydrogenase (ubiquinone) Fe-S protein 7	**NDUFS7**	F: 5'-GGATGACCTCGTCAACTGGG-3' R: 3'-ACAACCTCACGGGACACAAG-5'	511	
Cytochrome c oxidase subunit VIb polypeptide 2	**COX6B2**	F: 5'-GCAGCCCTGCGAGTACTATT-3' R: 3'-TCTCGCCCATACAGACAGGA-5'	524	
Cytochrome c oxidase subunit Vic	**COX6C**	F: 5'-TGCACATGGTTTGGGACTCT-3' R: 3'-CCCCAGGGATAGCACGAATG-5'	415	
Pyrophospatase	**PPA1**	F: 5'-CCTTCTCCCTGGAGTACCGA-3' R: 3'-TAGCCAGGTTTCAGCCGTTT-5'	511	
ATP synthase, H +transporting, mitochondrial Fo complex, subunit B1	**ATP5F1**	F: 5'-GCATTGCGGACCTAAAGCTG-3' R: 3'-ATCAGCCAGAAACAGTTCACCA-5'	519	
ATP synthase, H +transporting, mitochondrial Fo complex, subunit C2 (subunit 9)	**ATP5G2**	F: 5'-TCCTAGACTGTCCCAGGAGC-3' R: 3'-AGAGAGGATCAGCTCAGGCA-5'	557	

Table 2.11: continued.

Gene	Symbol	Primer sequence	PCR product (bp)	Reference
NF-KappaB1	**NFKB1**	F: 5'-CCTGGATGACTCTTGGGAAA-3' R: 3'-CTTCGGTGTAGCCCATTTGT-5'	366	(Milward *et al.,* 2007)
NF-KappaB2	**NFKB2**	F: 5'-CGTACCGACAGACAACCTCA-3' R: 3'-CCGTACGCACTGTCTTCCTT-5'	186	
NF-KappaB1 epsilon	**NFKB1E**	F: 5'-GTGAAGCCTGTTTGCCTCTC-3' R: 3'-AGGGTCCTCAACAGCAAGAA-5'	172	
Mitogen-activated protein kinase 11-isoform of p38 MAPK	**MAPK11**	F: 5'-GGACAACCACCAGGTGTCAA-3' R: 3'-GCAGAAGTGTCCGAGTCCAA-5'	424	(Zhang *et al.*, 2003)

2.2.4.9 PCR array

PCR array was carried out using RT^2 Profiler PCR Arrays, Qiagen (Germany). This array is designed to analyse a range of genes associated to a disease or biological pathway. A type of RT^2 Profiler PCR Array was selected, Human Mitochondrial Energy Metabolism Plus (Code number PAHS-008YA). This array profiles 84 key genes expression involved in mitochondrial respiration specifically electron transport chain and oxidative phosphorylation complexes (Figure 2.15 and 2.16).

This array was undertaken according to manufacturer's provided protocol and only using RNA sample of irradiated H400s 120s laser. RNA was isolated (see section 2.2.4.7.1) and RT^2 First Strand kit thawed. A total of 10µl Genomic DNA elimination mix was then prepared by mixing 2µl of RNA, 2µl of Buffer GE (provided in kit) and 6µl of RNase-free water. Following incubation at 42°C for 5min, the mixture immediately placed on ice for 1min. Subsequently, 10µl of reverse transcription mix (4µl of 5x Buffer BC3 + 1µl Control P2 + 2µl RE3 Reverse Transcriptase Mix + 3µl RNase-free water) was mixed to genomic DNA elimination mix and incubated at 42°C for 15min. Then the reaction was stopped immediately by incubating at 95°C for 5min. A total of 91µl RNase-free water was added to reaction and placed on ice to proceed with real-time PCR protocol.

RT2 SYBR Green mastermix was centrifuged to bring the contents to the bottom of tube. PCR components mix was then prepared in a loading reservoir by adding 1350µl 2x RT2 SYBR Green mastermix, 102µl cDNA synthesis reaction and 1248µl RNase-free water followed by loading the PCR component into the RT^2 Profiler PCR array sealed tightly using Optical Adhesive Film. The array was centrifuged for 1min

at 1000g at room temperature to remove bubbles and kept on ice while setting up the PCR cycling program (Table 2.12). PCR array was performed using Roche LightCycler® 480 PCR system (Roche, Germany). The result, CT values then was exported to Excel® spreadsheet and analysed using web-based software, www.SABiosciences.com/pcrarraydataanalysis.php.

Table 2.12: PCR cycling conditions specifically for Roche LightCycler® 480 PCR system.

Cycles	Duration	Temperature
1	10min	95°C
45	15s	95°C
	1min	60°C

	1	2	3	4	5	6	7	8	9	10	11	12
A	ATP5A1	ATP5B	ATP5C1	ATP5F1	ATP5G1	ATP5G2	ATP5G3	ATP5H	ATP5I	ATP5J	ATP5J2	ATP5L
B	ATP5O	COX4I1	COX5A	COX5B	COX6A1	COX6A2	COX6B1	COX6C	COX7A2	COX7A2L	COX7B	COX8A
C	CYC1	NDUFA1	NDUFA10	NDUFA11	NDUFA2	NDUFA3	NDUFA4	NDUFA5	NDUFA6	NDUFA8	NDUFAB1	NDUFB10
D	NDUFB2	NDUFB3	NDUFB4	NDUFB5	NDUFB6	NDUFB7	NDUFB8	NDUFB9	NDUFC1	NDUFC2	NDUFS1	NDUFS2
E	NDUFS3	NDUFS4	NDUFS5	NDUFS6	NDUFS7	NDUFS8	NDUFV1	NDUFV2	NDUFV3	PPA1	SDHA	SDHB
F	SDHC	SDHD	UQCR11	UQCRC1	UQCRC2	UQCRFS1	UQCRH	UQCRQ	ARRDC3	ASB1	CYB561D1	DNAJB1
G	EDN1	GADD45B	HSPA1A	HSPA1B	LRP5L	MitoH1	MitoH2_1210 6	MitoH2_1457 3	MitoH2_4162	MitoH2_5726	RNU11	SLC25A25
H	ACTB	B2M	GAPDH	HPRT1	RPLP0	HGDC	RTC	RTC	RTC	PPC	PPC	PPC

Figure 2.15: Genes are involved in RT2 Profiler PCR Array, Human Mitochondrial Energy Metabolism Plus.

Position	UniGene	GenBank	Symbol	Description
A01	Hs.298280	NM_004046	ATP5A1	ATP synthase, H+ transporting, mitochondrial F1 complex, alpha subunit 1, cardiac muscle
A02	Hs.406510	NM_001686	ATP5B	ATP synthase, H+ transporting, mitochondrial F1 complex, beta polypeptide
A03	Hs.271135	NM_005174	ATP5C1	ATP synthase, H+ transporting, mitochondrial F1 complex, gamma polypeptide 1
A04	Hs.514870	NM_001688	ATP5F1	ATP synthase, H+ transporting, mitochondrial Fo complex, subunit B1
A05	Hs.80986	NM_005175	ATP5G1	ATP synthase, H+ transporting, mitochondrial Fo complex, subunit C1 (subunit 9)
A06	Hs.524464	NM_001002031	ATP5G2	ATP synthase, H+ transporting, mitochondrial Fo complex, subunit C2 (subunit 9)
A07	Hs.429	NM_001689	ATP5G3	ATP synthase, H+ transporting, mitochondrial Fo complex, subunit C3 (subunit 9)
A08	Hs.514465	NM_006356	ATP5H	ATP synthase, H+ transporting, mitochondrial Fo complex, subunit d
A09	Hs.85539	NM_007100	ATP5I	ATP synthase, H+ transporting, mitochondrial Fo complex, subunit E
A10	Hs.246310	NM_001685	ATP5J	ATP synthase, H+ transporting, mitochondrial Fo complex, subunit F6
A11	Hs.656515	NM_004889	ATP5J2	ATP synthase, H+ transporting, mitochondrial Fo complex, subunit F2
A12	Hs.486360	NM_006476	ATP5L	ATP synthase, H+ transporting, mitochondrial Fo complex, subunit G
B01	Hs.409140	NM_001697	ATP5O	ATP synthase, H+ transporting, mitochondrial F1 complex, O subunit
B02	Hs.433419	NM_001861	COX4I1	Cytochrome c oxidase subunit IV isoform 1
B03	Hs.401903	NM_004255	COX5A	Cytochrome c oxidase subunit Va
B04	Hs.1342	NM_001862	COX5B	Cytochrome c oxidase subunit Vb
B05	Hs.706889	NM_004373	COX6A1	Cytochrome c oxidase subunit VIa polypeptide 1
B06	Hs.250760	NM_005205	COX6A2	Cytochrome c oxidase subunit VIa polypeptide 2
B07	Hs.431668	NM_001863	COX6B1	Cytochrome c oxidase subunit VIb polypeptide 1 (ubiquitous)
B08	Hs.351875	NM_004374	COX6C	Cytochrome c oxidase subunit VIc
B09	Hs.70312	NM_001865	COX7A2	Cytochrome c oxidase subunit VIIa polypeptide 2 (liver)
B10	Hs.744101	NM_004718	COX7A2L	Cytochrome c oxidase subunit VIIa polypeptide 2 like
B11	Hs.522699	NM_001866	COX7B	Cytochrome c oxidase subunit VIIb
B12	Hs.743989	NM_004074	COX8A	Cytochrome c oxidase subunit VIIIA (ubiquitous)
C01	Hs.289271	NM_001916	CYC1	Cytochrome c-1
C02	Hs.534168	NM_004541	NDUFA1	NADH dehydrogenase (ubiquinone) 1 alpha subcomplex, 1, 7.5kDa
C03	Hs.277677	NM_004544	NDUFA10	NADH dehydrogenase (ubiquinone) 1 alpha subcomplex, 10, 42kDa
C04	Hs.406062	NM_175614	NDUFA11	NADH dehydrogenase (ubiquinone) 1 alpha subcomplex, 11, 14.7kDa
C05	Hs.75914	NM_002488	NDUFA2	NADH dehydrogenase (ubiquinone) 1 alpha subcomplex, 2, 8kDa
C06	Hs.198269	NM_004542	NDUFA3	NADH dehydrogenase (ubiquinone) 1 alpha subcomplex, 3, 9kDa
C07	Hs.50098	NM_002489	NDUFA4	NADH dehydrogenase (ubiquinone) 1 alpha subcomplex, 4, 9kDa
C08	Hs.651219	NM_005000	NDUFA5	NADH dehydrogenase (ubiquinone) 1 alpha subcomplex, 5, 13kDa
C09	Hs.274416	NM_002490	NDUFA6	NADH dehydrogenase (ubiquinone) 1 alpha subcomplex, 6, 14kDa
C10	Hs.495039	NM_014222	NDUFA8	NADH dehydrogenase (ubiquinone) 1 alpha subcomplex, 8, 19kDa
C11	Hs.189716	NM_005003	NDUFAB1	NADH dehydrogenase (ubiquinone) 1, alpha/beta subcomplex, 1, 8kDa
C12	Hs.513266	NM_004548	NDUFB10	NADH dehydrogenase (ubiquinone) 1 beta subcomplex, 10, 22kDa
D01	Hs.655788	NM_004546	NDUFB2	NADH dehydrogenase (ubiquinone) 1 beta subcomplex, 2, 8kDa
D02	Hs.109760	NM_002491	NDUFB3	NADH dehydrogenase (ubiquinone) 1 beta subcomplex, 3, 12kDa

Figure 2.16: List of genes and description of Human Mitochondrial Energy Metabolism Plus.

Position	UniGene	GenBank	Symbol	Description
D03	Hs.304613	NM_004547	NDUFB4	NADH dehydrogenase (ubiquinone) 1 beta subcomplex, 4, 15kDa
D04	Hs.730674	NM_002492	NDUFB5	NADH dehydrogenase (ubiquinone) 1 beta subcomplex, 5, 16kDa
D05	Hs.493668	NM_182739	NDUFB6	NADH dehydrogenase (ubiquinone) 1 beta subcomplex, 6, 17kDa
D06	Hs.532853	NM_004146	NDUFB7	NADH dehydrogenase (ubiquinone) 1 beta subcomplex, 7, 18kDa
D07	Hs.523215	NM_005004	NDUFB8	NADH dehydrogenase (ubiquinone) 1 beta subcomplex, 8, 19kDa
D08	Hs.15977	NM_005005	NDUFB9	NADH dehydrogenase (ubiquinone) 1 beta subcomplex, 9, 22kDa
D09	Hs.84549	NM_002494	NDUFC1	NADH dehydrogenase (ubiquinone) 1, subcomplex unknown, 1, 6kDa
D10	Hs.407860	NM_004549	NDUFC2	NADH dehydrogenase (ubiquinone) 1, subcomplex unknown, 2, 14.5kDa
D11	Hs.598436	NM_005006	NDUFS1	NADH dehydrogenase (ubiquinone) Fe-S protein 1, 75kDa (NADH-coenzyme Q reductase)
D12	Hs.173611	NM_004550	NDUFS2	NADH dehydrogenase (ubiquinone) Fe-S protein 2, 49kDa (NADH-coenzyme Q reductase)
E01	Hs.502528	NM_004551	NDUFS3	NADH dehydrogenase (ubiquinone) Fe-S protein 3, 30kDa (NADH-coenzyme Q reductase)
E02	Hs.528222	NM_002495	NDUFS4	NADH dehydrogenase (ubiquinone) Fe-S protein 4, 18kDa (NADH-coenzyme Q reductase)
E03	Hs.632385	NM_004552	NDUFS5	NADH dehydrogenase (ubiquinone) Fe-S protein 5, 15kDa (NADH-coenzyme Q reductase)
E04	Hs.408257	NM_004553	NDUFS6	NADH dehydrogenase (ubiquinone) Fe-S protein 6, 13kDa (NADH-coenzyme Q reductase)
E05	Hs.211914	NM_024407	NDUFS7	NADH dehydrogenase (ubiquinone) Fe-S protein 7, 20kDa (NADH-coenzyme Q reductase)
E06	Hs.90443	NM_002496	NDUFS8	NADH dehydrogenase (ubiquinone) Fe-S protein 8, 23kDa (NADH-coenzyme Q reductase)
E07	Hs.7744	NM_007103	NDUFV1	NADH dehydrogenase (ubiquinone) flavoprotein 1, 51kDa
E08	Hs.464572	NM_021074	NDUFV2	NADH dehydrogenase (ubiquinone) flavoprotein 2, 24kDa
E09	Hs.473937	NM_021075	NDUFV3	NADH dehydrogenase (ubiquinone) flavoprotein 3, 10kDa
E10	Hs.437403	NM_021129	PPA1	Pyrophosphatase (inorganic) 1
E11	Hs.440475	NM_004168	SDHA	Succinate dehydrogenase complex, subunit A, flavoprotein (Fp)
E12	Hs.465924	NM_003000	SDHB	Succinate dehydrogenase complex, subunit B, iron sulfur (Ip)
F01	Hs.444472	NM_003001	SDHC	Succinate dehydrogenase complex, subunit C, integral membrane protein, 15kDa
F02	Hs.744039	NM_003002	SDHD	Succinate dehydrogenase complex, subunit D, integral membrane protein
F03	Hs.8372	NM_006830	UQCR11	Ubiquinol-cytochrome c reductase, complex III subunit XI
F04	Hs.119251	NM_003365	UQCRC1	Ubiquinol-cytochrome c reductase core protein I
F05	Hs.528803	NM_003366	UQCRC2	Ubiquinol-cytochrome c reductase core protein II
F06	Hs.743307	NM_006003	UQCRFS1	Ubiquinol-cytochrome c reductase, Rieske iron-sulfur polypeptide 1
F07	Hs.481571	NM_006004	UQCRH	Ubiquinol-cytochrome c reductase hinge protein
F08	Hs.146602	NM_014402	UQCRQ	Ubiquinol-cytochrome c reductase, complex III subunit VII, 9.5kDa
F09	Hs.24684	NM_020801	ARRDC3	Arrestin domain containing 3
F10	Hs.516788	NM_001040445	ASB1	Ankyrin repeat and SOCS box containing 1
F11	Hs.514682	NM_182580	CYB561D1	Cytochrome b-561 domain containing 1
F12	Hs.515210	NM_006145	DNAJB1	DnaJ (Hsp40) homolog, subfamily B, member 1
G01	Hs.713645	NM_001955	EDN1	Endothelin 1
G02	Hs.110571	NM_015675	GADD45B	Growth arrest and DNA-damage-inducible, beta
G03	Hs.702139	NM_005345	HSPA1A	Heat shock 70kDa protein 1A
G04	Hs.719966	NM_005346	HSPA1B	Heat shock 70kDa protein 1B
G05	Hs.634058	NM_182492	LRP5L	Low density lipoprotein receptor-related protein 5-like
G06	N/A	r4_NC_012920	MitoH1	Polycistronic_H1_3
G07	N/A	r3_NC_012920	MitoH2_12106	Polycistronic_H2_200_12106_1
G08	N/A	r2_NC_012920	MitoH2_14573	Polycistronic_H2_200_14573_3
G09	N/A	r1_NC_012920	MitoH2_4162	Polycistronic_H2_200_4162_1
G10	N/A	r5_NC_012920	MitoH2_5726	Polycistronic_H2_200_5726_3
G11	Hs.640266	NR_004407	RNU11	RNU11
G12	Hs.729700	NM_052901	SLC25A25	Solute carrier family 25 (mitochondrial carrier; phosphate carrier), member 25
H01	Hs.520640	NM_001101	ACTB	Actin, beta
H02	Hs.534255	NM_004048	B2M	Beta-2-microglobulin
H03	Hs.544577	NM_002046	GAPDH	Glyceraldehyde-3-phosphate dehydrogenase
H04	Hs.412707	NM_000194	HPRT1	Hypoxanthine phosphoribosyltransferase 1
H05	Hs.546285	NM_001002	RPLP0	Ribosomal protein, large, P0
H06	N/A	SA_00105	HGDC	Human Genomic DNA Contamination
H07	N/A	SA_00104	RTC	Reverse Transcription Control
H08	N/A	SA_00104	RTC	Reverse Transcription Control
H09	N/A	SA_00104	RTC	Reverse Transcription Control
H10	N/A	SA_00103	PPC	Positive PCR Control
H11	N/A	SA_00103	PPC	Positive PCR Control
H12	N/A	SA_00103	PPC	Positive PCR Control

Figure 2.16: continued

2.2.5 Neutrophil isolation

Percoll gradients were prepared prior to blood collection. Two discontinuous gradients were used for neutrophil isolation (see Section 2.1.3.1.1). A total of 8ml of 1.098 density Percoll was layered under 8ml of 1.079 density Percoll in a 25ml universal tube. Blood was then carefully layered on top of the gradient using a Pasteur pipette. The tube was centrifuged for 8min at 980rpm (150g) followed by 10min at 2700rpm (1200g). Layers of Percoll containing plasma, monocytes, and lymphocytes were discarded. The neutrophil layer was gently aspirated using a Pasteur pipette and transferred to a Falcon tube containing 30ml of lysis buffer, the resulting solution was gently inverted several times and incubated at room temperature for 10min to allow erythrocyte lysis.

Cells were then pelleted at 1750rpm (500g) for 6min and re-suspended in 4ml of lysis buffer and incubated at room temperature for 3min. This mix was centrifuged at 1750rpm (500g) for 6min and washed with 4ml PBS and re-centrifuged under the same conditions. The supernatant was discarded and the pellet was re-suspend in 3ml of PBS.

Prior to the chemiluminescence assay, the neutrophils were manually counted using a haemocytometer (2.2.4.1). The central square of haemocytometer ($1mm^2$) is subdivided into 25 smaller squares ($0.04mm^2$), neutrophils were counted in 9 of the $0.04mm^2$ squares. Total cells were calculated using the formulae (Equation 2.2) below where 25 represents the number of squares, $1x10^4$ refers the haemocytometer dimensions and 9 is the number of squares counted (White 2015).

Equation 2.2

$$\frac{\text{Cell count} \times 25 \times 1\times10^{4}}{9} = \text{number of cells/ml}$$

2.2.5.1 Chemiluminescent ROS assay for neutrophils

Initially, a 96-well black walled plate was blocked overnight with PBS-BSA (1%) at 4^{o}C. The plate was washed with PBS prior to use. A total of 10^5 neutrophils were seeded into each well (volume of cells refers to cell suspension) and then irradiated using 2nd generation LED arrays at a radiant exposure of 11.6J/cm^2 followed by addition of luminol (30µl), isoluminol (60µl) and HRP (15µl) and lucigenin (30µl) to the appropriate wells. Control wells were not irradiated. gPBS was added to wells to give a final volume of 200µl for each well. The plate was placed into luminometer, Berthold LB96v (Berthold Technologies, Germany) at 37^{o}C and maintained at that temperature for 30min prior stimulation with 25µl PMA which was added immediately following the 30min incubation. The plate was then returned to the luminometer and incubated for 3h.

2.2.5.2 Neutrophil ROS detection using CM-H_2DCFDA

A 96-well black plate was blocked using 1% of BSA in PBS for 24h and discarded prior to use followed by adding 100µl of Ploy-L-lysine (Sigma-Aldrich, UK) to coat the plate. After 10min incubation at room temperature, the plate was washed twice with PBS. Subsequent to neutrophils isolation, cells were prepared and applied to 96-well black plate as described in 2.2.5.1. A total of 37.5µl neutrophil in gPBS was added to

the wells and incubated 37°C for 30min. The plate then was irradiated by 480s 2nd generation LED array and immediately added 50µl of gPBS and 10 µM CM-H_2DCFDA. Before 1h incubation ended, 1.5µl PMA was put and plate read at 0, 10, 20, 30 and 60min upon PMA added. The plate then was read at an excitation of 485nm and an emission of 535nm using a fluorometer (Berthold Twinkle, Germany).

2.2.5.3 Determination of neutrophil cell viability post 2nd generation LED array irradiation

Pierce LDH (lactate dehydrogenase) Cytotoxicity Assay (Thermo Scientific, USA)) was used to determine neutrophil viability after 2nd generation LED array irradiation. Lactate dehydrogenase is released from cells when the plasma membrane is damaged. Isolated neutrophils (2.2.5) in gPBS were loaded ($1x10^5$ cells/well) into a 96-well black plate for in triplicate. The plate was incubated at 37°C in 5% CO_2 for 30min. The plate was then prepared as follows: 10µl of ultrapure water was added as negative control and same amount of Lysis Buffer (10x) (kit reagent) was employed as positive control. Following irradiation with the 2nd generation (section 2.2.3.3) LED array, the plate was incubated for 45min at 37°C in 5% CO_2. A total of 50µl of each sample medium were transferred to a new 96-well white flat bottom plate and an equal amount of Reaction Mixture (manufacturer kit supplied reagent) was added to each sample. The plate was then covered to protect from light and incubated for 30min at room temperature. 50µl of stop solution (manufacturer kit supplied reagent) was added to each sample and the absorbance read at 490nm and 630nm (ELx800 Universal Microplate reader, Bio-Tek Instruments, UK).

2.2.6 Bacterial culture growth

Archived bacterial stock, *P. gingivalis* and *F. nucleatum* (section 2.1.4.1) was thawed at room temperature. 100µl of this bacterial suspension was inoculated onto blood agar plates (section 2.1.4.2) and spread using a disposable pre-sterilised plastic loop. Plates were incubated at 37^{o}C in an anaerobic chamber (Don Whitley, UK). Cultures were grown for at least 3 days to allow sufficient bacterial growth. The resulting colonies were checked for purity and typical morphology before Gram staining to determine microscopic morphology (section 2.2.6.1).

2.2.6.1 Determination of bacterial growth

In order to estimate the amount of bacterial growth, bacterial suspensions in broth (2.1.4.3) were measured at 600nm optical density (OD_{600nm}) (Jenway 6300, Keison, UK) using a non-inoculated broth as standard for calibration of the spectrophotometer. The relationship between turbidity and OD is species dependent and bacterial counts were determined using data generated by the Forsyth Institute (Boston) (White 2015).

2.2.6.2 Heat-killing of bacteria

A single colony was inoculated in BHI broth and incubated anaerobically at 37^{o}C for 24h. Following incubation and bacterial growth, the broth was thoroughly mixed and aliquoted to 50ml centrifuge tubes. Gram staining, microscopy and colony morphology analysis were performed to aid confirmation of strain and purity. Tubes were centrifuged at 3000rpm for 10min (Harrier 18/80, DJB Labcare, UK). Post centrifugation, supernatant was discarded and the pellet was re-suspended in 10ml

PBS (2.1.2.2.2). This step was repeated and the final pellet re-suspended in 10ml PBS. The concentration of bacteria was determined (section 2.2.6.1) and diluted to $1x10^7$ bacteria in PBS. Heat-killing of bacteria was achieved by heating the bacterial suspension in a water bath at 100°C for 1h. To confirm success of heat killing, 50µl of the mixture was inoculated onto a blood agar plate (section 2.1.4.2) and incubated at 37°C anaerobically for 3 days. The remaining heat-killed bacterial suspension was aliquoted into 1ml volumes and stored at -20°C until required.

2.2.6.3 Gram-staining protocol

Gram staining was performed to determine the microscopic morphology, colour (Gram positive or negative) and bacterial size. Gram-positive bacteria appear in purple/blue while Gram-negative bacteria will appear in red/pink (White 2015). The bacterial suspension was spread onto a microscope slide and quickly heat-fixed using a Bunsen burner. The slide was then flooded with crystal violet (see section 2.1.4.4) for 30s, then rinsed with deionised water and stained with Lugol's iodine (Sigma-Aldrich, UK) for a further 30s before rinsing with distilled water. The slide was then rapidly decolourised using acetone, washed and then stained carbol fuchsin (see 2.1.4.5) for 30s, rinsed with distilled water and dried. The slide was visualised under oil immersion microscope at 100x magnification (Leitz Dialux 22) and images captured using Nikon Coolpix 1990 (Japan).

2.2.7 Quantification of IL-8 in culture media

Culture media from H400 cells exposed to bacteria (or unstimulated – negative control) and exposed to 2^{nd} generation LED array (sections 2.2.3.1, 2.2.3.2 and

2.2.3.3) were transferred to 1.5ml tubes and centrifuged at 1500rpm for 15min. Following centrifugation, supernatant was collected in cryotubes in 500µl aliquots and stored at -80^{o}C. Prior to assay, aliquots were defrosted and centrifuged at 800rpm for 1min. A commercial ELISA kit (R&D Systems, UK) was used to quantify IL-8 in media samples. All reagents were diluted according to the manufacturer's protocol and equilibrated to room temperature prior to use. A total of 100µl of diluted capture antibody was added to each well (provided by manufacturer). The remaining 100µl of capture antibody was mixed with 12ml of PBS and vortexed. Wash buffer was prepared by adding 24ml of the buffer to 576ml of deionised water (prepared the previous day) The plate was washed three times followed by blocking the plate using 300µl of reagent diluent (3ml of stock reagent diluent was mixed with 30ml of deionised water) and left for 1h. The plate was then washed three times. Standards for the plate were prepared. 50µl of standard was added to 2ml of reagent diluent and mixed. The standard was further serially diluted from 80ng/ml to 2ng/ml for experimentation and added to the appropriate wells. The experimental samples were added to the remaining wells. The plate was covered and incubated at room temperature for 2h. After incubation (37^{o}C), the plate was washed three times and 100µl of Streptavidin HRP (kit reagent) added, covered and kept at room temperature for 25min. The plate was again washed three times and 100µl substrate solution added to each well, this was incubated (37^{o}C) in the dark for 25min. To stop the reaction, 50µl of stop solution was added to all wells and the absorbance read at 450nm and 570nm (ELx800 Universal Microplate reader (Bio-Tek Instruments, UK).

2.2.8 Statistical analysis

IBM SPSS Statistics 20 statistical software (IBM Software Group, Chicago, USA) was used for data analysis. Differences between light sources (laser/LED) and non-irradiated controls were compared using one-way ANOVA (Analysis of Variance) and subsequent Tukey's *post hoc* tests. The level of significant was set at 0.05 (*p*-value).

CHAPTER 3: LIGHT SOURCE CHARACTERISATION

3.1 Introduction

In order to be able to determine the light dose delivered to cells it is of fundamental importance to characterise any light delivery device. This is often omitted or poorly performed in the literature resulting in unreliable outcomes. Therefore this section carefully details the characterisation of all the light delivery devices used in this study i.e. laser, single (SMD) LED, and 1st and 2nd generation 96 well LED arrays. All of these light sources were measured to determine wavelength (nm), irradiance (mW/cm^2), radiant exposure (J/cm^2), beam profile and temperature change (^{o}C).

Light sources utilised in this thesis are provided with manufacturer supplied optical characterisation data sheet, however these are not always accurate so it is essential that careful measurement of a range of optical parameters are undertaken prior to use to ensure accurate light delivery. Another important factor is heat generation, any light source will produce heat which could be responsible for the cellular responses rather than the direct action of light, it is therefore essential to carefully determine and control heat changes in the cell culture system.

The wavelength peak of each light source was verified using a spectrometer (see Section 2.2.1.1) and the irradiance value was obtained using the SpectraSuite software (2.2.1.1) whilst any temperature increase during irradiation was measured using a thermocouple based system (2.2.1.4). Additionally, beam profile was determined using a beam profiler (2.2.1.3). This chapter will thoroughly determine light parameters for each of the light sources used and identify the optimum radiant exposure for use in future experiments.

3.2 Light characterisation

This initial study characterised a 670nm laser (2.1.1.1), 630nm single (SMD) LED (2.1.1.2) and two different LED arrays, 1st (2.1.1.3) and 2nd (2.1.1.4) generation LED array which both had a different wavelength ranges (625-830nm and 400-830nm, respectively).

3.2.1 Wavelength peak, irradiance value and radiant exposure

3.2.1.1 Introduction

Peak wavelength measurements (2.2.1.1) were carried out in order to compare manufacturer's quoted wavelength to the measured wavelength monitored in real time using Spectrasuite software and the irradiance value for each light source were determined using the same software (2.2.1.1). This value is crucial for the calculation of radiant exposure prior light irradiation.

3.2.1.2 Results

The following results show the (i) comparison of peak wavelength and for manufacturers quoted data and those measured during this thesis and (ii) irradiance for (a) laser, (b) single LED, (c) 1st generation LED array and (d) 2nd generation LED array. The measured emitted peaks revealed differences in the peak spectral output between those values (Figure 3.1 (a), (b) (c) and (d) and the difference are presented in Table 3.1. From the numbers generated by the Spectrometer and calculated using SigmaPlot 12.0 software, the obtained irradiance value and was applied to present the radiant exposure (see Section 2.2.1.2, 2.2.3.1.1, 2.2.3.2, 2.2.3.3).

Following wavelength measurement, comparison between measured peak and manufacturer quoted wavelengths were made. This comparison is shown in Table 3.1 (a), (b) and (c).

3.2.1.3 Discussion

Data generated from spectrometer demonstrated slight differences from the manufacturer quoted wavelength. The peak wavelength for the quoted 670nm laser was measured at 666nm, whilst the quoted 630nm single LED was measured as 628nm. Similar variations were seen in the 1st and 2nd generation LED arrays with measured wavelengths showing differences from the manufacturer data (Table 3.1 (c) and (d).

It is critical to have accurate assessment of light delivery before exposing H400 cells to light in order to ensure correct does delivery at a cellular level and to compare results found in the literature, as well as allowing reproducibility between different experiments.

(a) 670nm laser

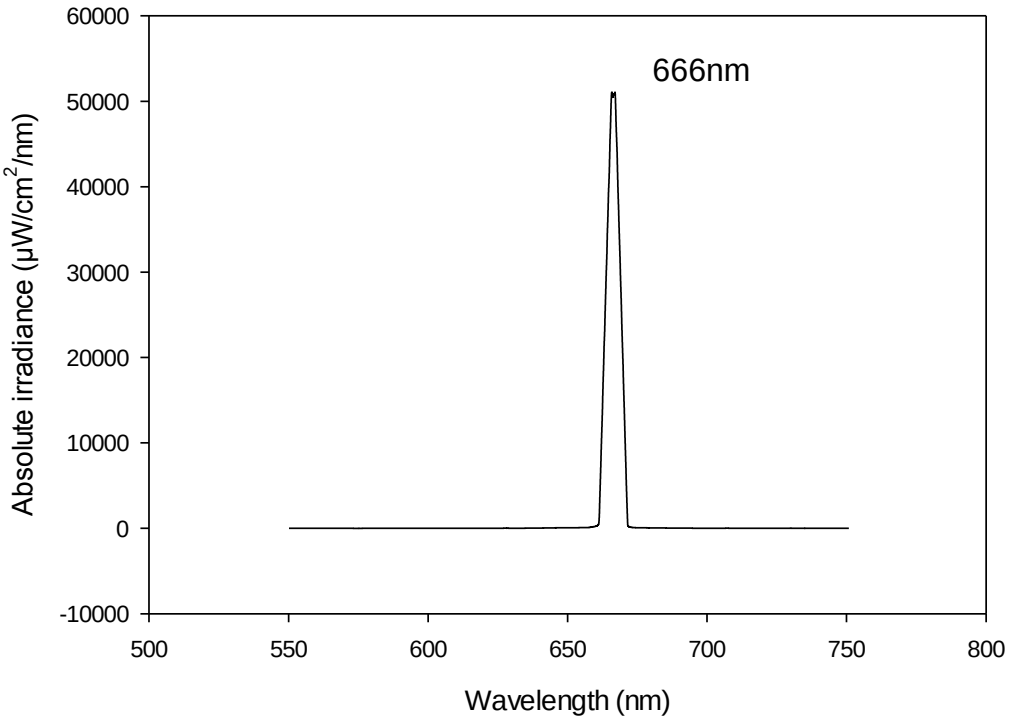

(b) 630nm single LED

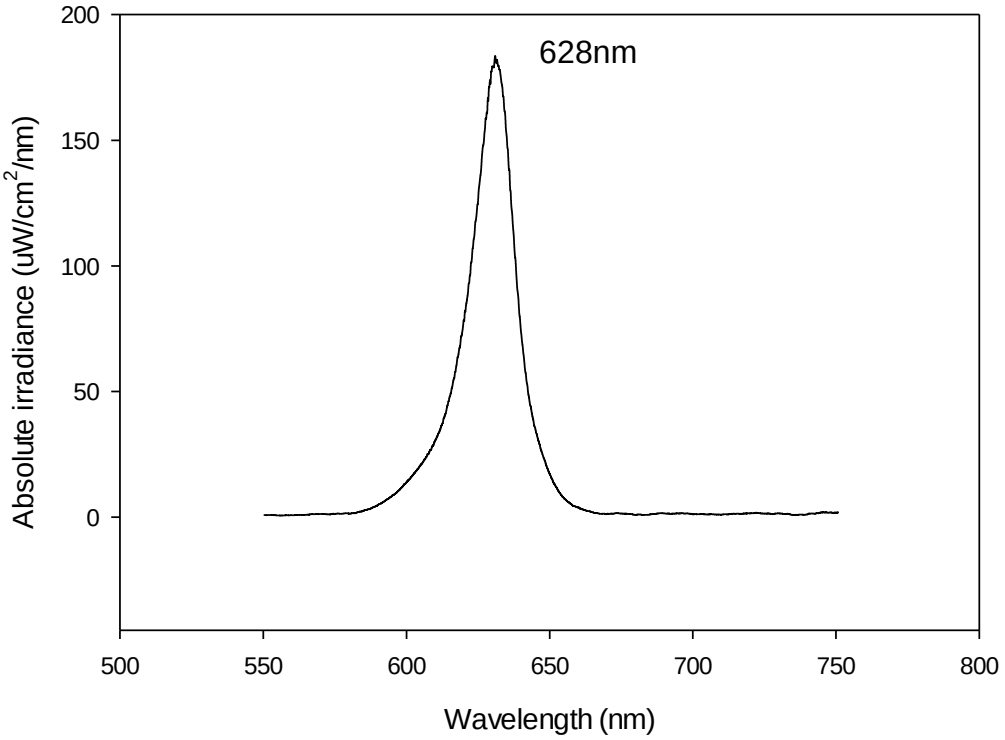

(c) 1st generation LED array

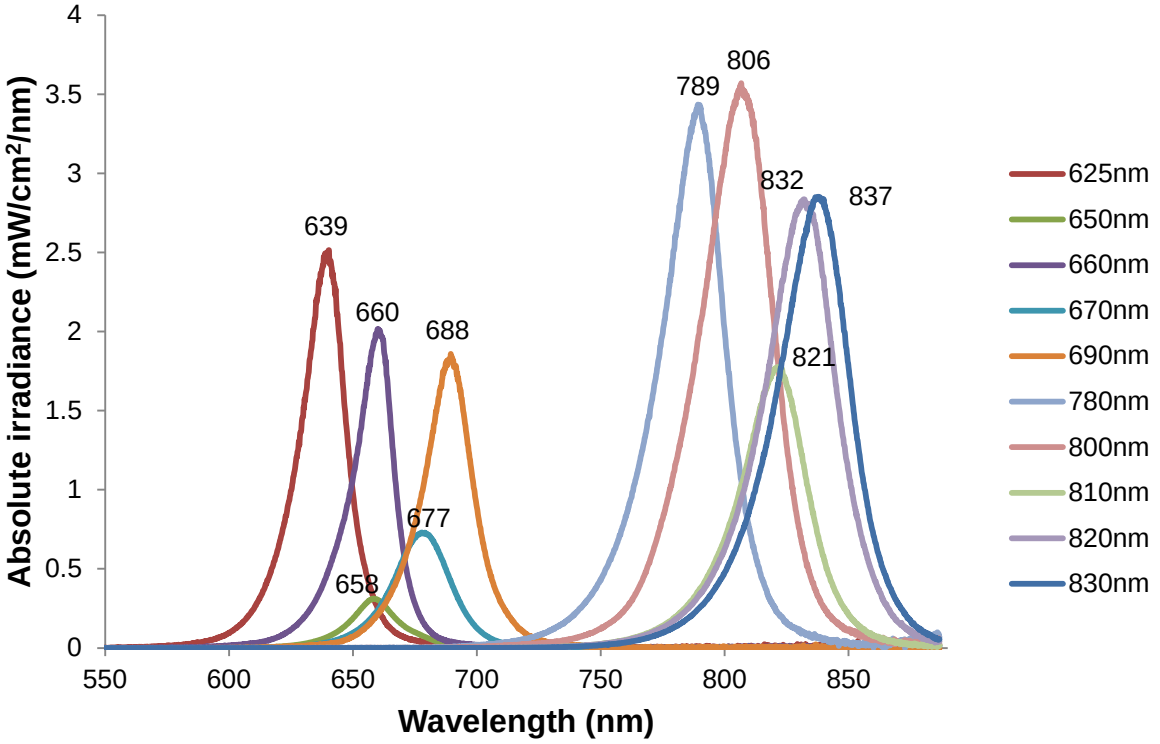

(d) 2nd generation LED array

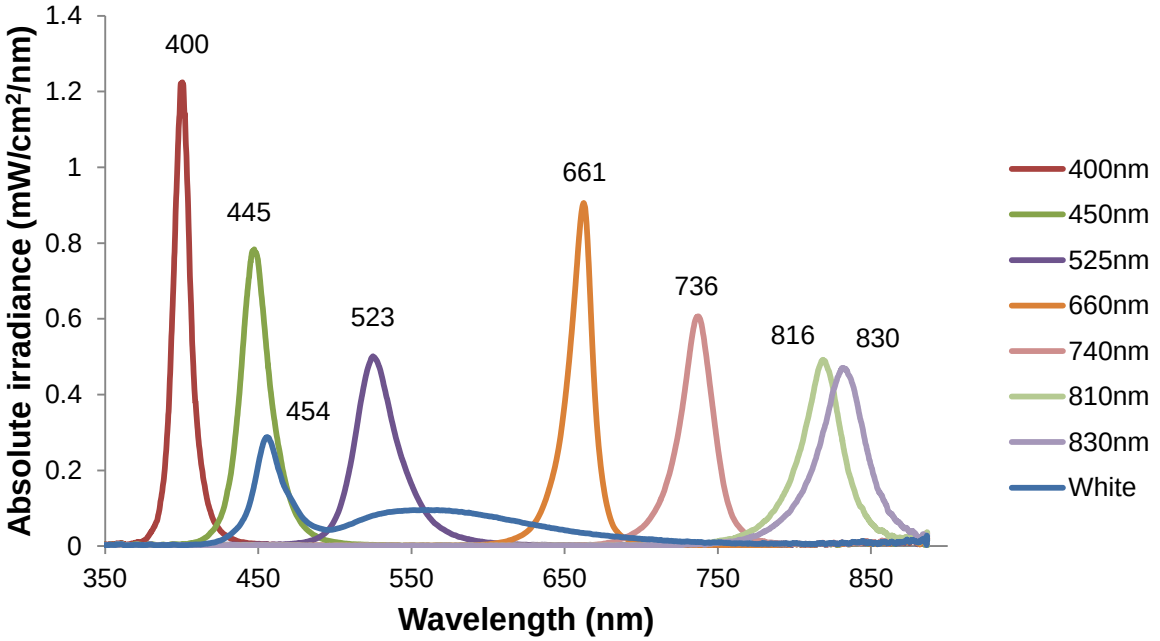

Figure 3.1: The graphs show the average measured wavelength peak of (a) 670nm laser (n=3 in duplicate); (b) 630nm single LED (n=3 in duplicate); (c) 1st generation LED array (n=6 in duplicate) and (d); 2nd generation LED array (n=6 in duplicate).

Table 3.1: Differences of peak wavelength between measured and manufacturer quoted (a) laser, (b) single LED, (c) 1st generation LED array and (d) 2nd generation LED array (St. Dev: standard deviation).

(a) laser

Manufacturer quoted peak wavelength (nm)	670
Average measured peak wavelength (nm) (n=3)	666
St. Dev	0.00

(b) single LED

Manufacturer quoted peak wavelength (nm)	630
Average measured peak wavelength (nm) (n=3)	628
St. Dev	0.58

(c) 1st generation LED array

Line	1	2	3	4	5	6	7	8	9	10	11	12
A		Measured peak wavelength (nm)										
B		638	657	659	671	682	788	802	820	829	835	
C		638	658	661	680	688	787	810	822	831	836	
D		640	657	659	674	690	790	804	823	832	836	
E		640	657	660	683	690	789	809	819	831	837	
F		642	659	661	681	689	789	808	821	836	840	
G		638	658	661	673	688	790	803	818	831	838	
H												

Quoted wavelength (nm)	625	650	660	670	690	780	800	810	820	830	
Average measured peak wavelength (nm)	639	658	660	677	688	789	806	821	832	837	
St. Dev	1.63	0.82	0.98	4.94	2.99	1.17	3.41	1.87	2.34	1.79	

(d) 2nd generation LED array

Line	1	2	3	4	5	6	7	8	9	10	11	12
A		Measured peak wavelength (nm)										
B		399	444	522		660		737	817	831	454	
C		399	444	523		661		736	817	829	452	
D		400	444	523		661		737	816	829	455	
E		399	445	524		662		738	817	830	455	
F		400	444	524		661		735	816	836	455	
G		400	449	521		660		734	814	827	453	
H												

Quoted wavelength (nm)	400	450	525		660		740	810	830	400 - 600	
Average measured peak wavelength (nm)	400	445	523		661		736	816	830	454	
St. Dev	0.55	2.00	1.17		0.75		1.47	1.17	3.08	1.26	

3.2.2 Beam profile

3.2.2.1 Introduction

Beam profiling shows the spatial distribution of irradiance and was undertaken using beam profiler (2.2.1.3). This process enabled measurement of the area and intensity of light delivered by the particular light source thereby allowing optimisation to the particular cell culture model used i.e. to ensure that the cell monolayer received adequate levels of irradiation.

3.2.2.2 Results

Spatial distribution of each light source produced a range of different beam profiles. The colours represented in the following beam profile images indicate different irradiance values at particular point across the irradiation area, the lowest irradiance in grey and the highest value in white. This technique also allowed estimation of light distribution across the irradiation area which varied between uniform and even (see Section 2.2.1.1 and 3.2.1).

(a) Laser-0mm (b) Laser-33mm (c) colour scale

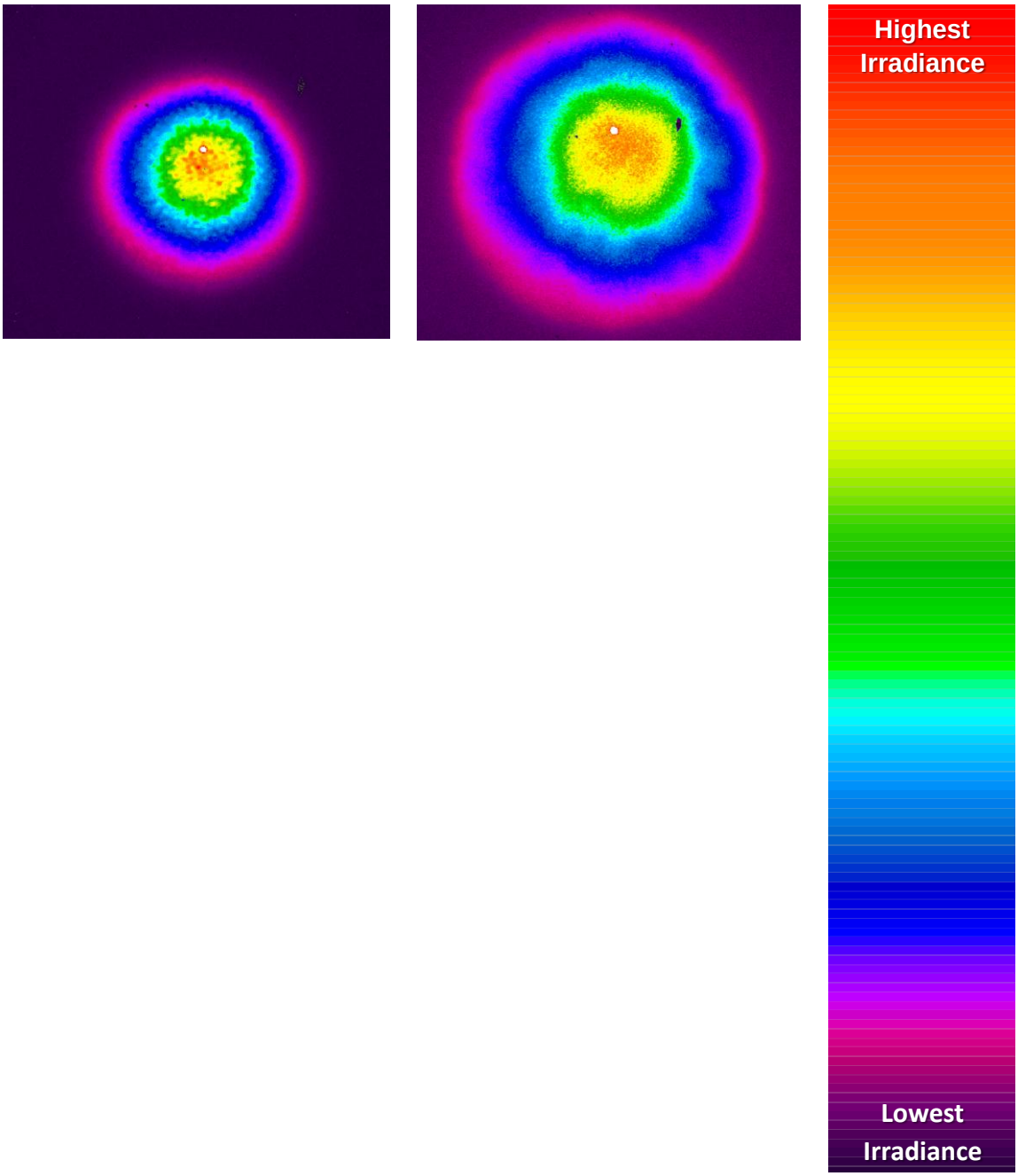

Figure 3.2: Beam profile for 670nm laser at (a) 0mm and (b) 33mm distance from light source; (c) Scale to indicate colours that represent irradiance at various points across the irradiation area.

(a) LED-0mm (b) LED-33mm

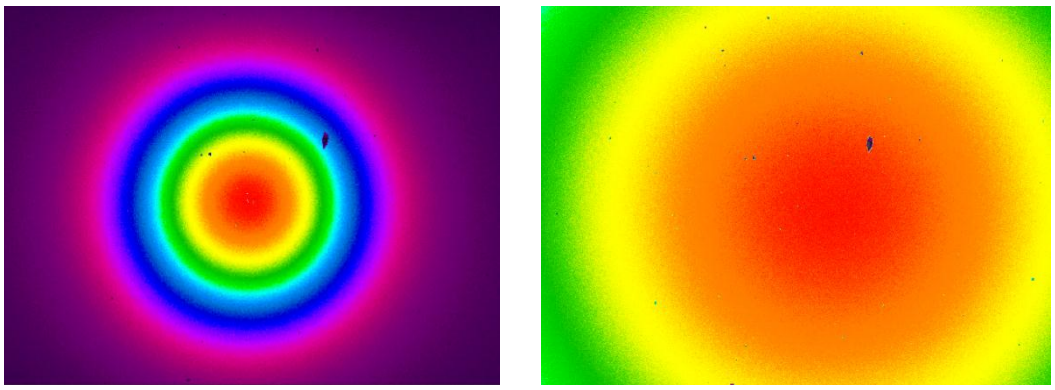

Figure 3.3: The diagram demonstrates profile for 630nm single LED (a) 0mm and (b) 33mm (see Figure 3.2 (c) for irradiance colour scale).

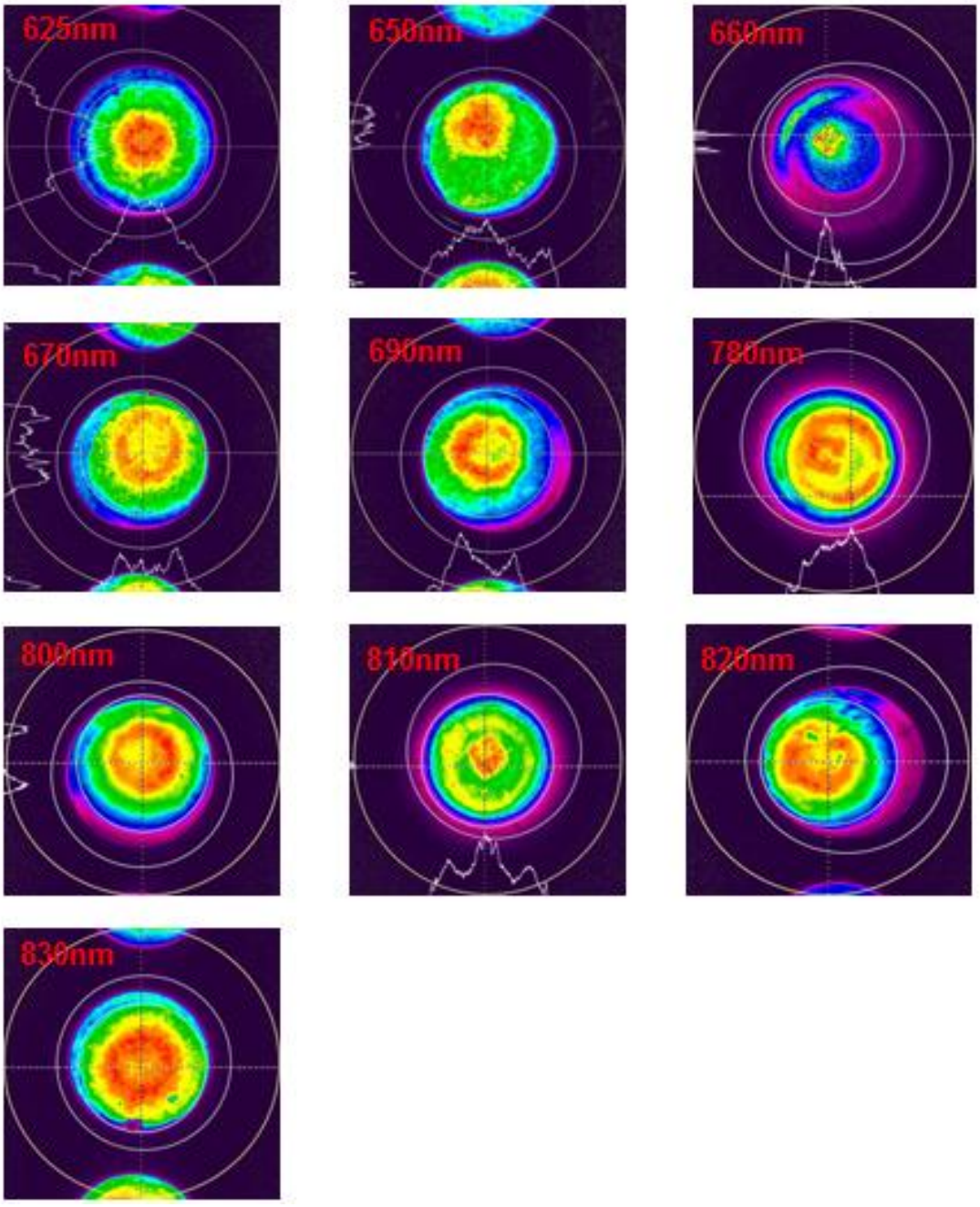

Figure 3.4: Beam profile of LEDs from 1st generation LED array, (625-830nm) (see Figure 3.2 (c) irradiance colour scale).

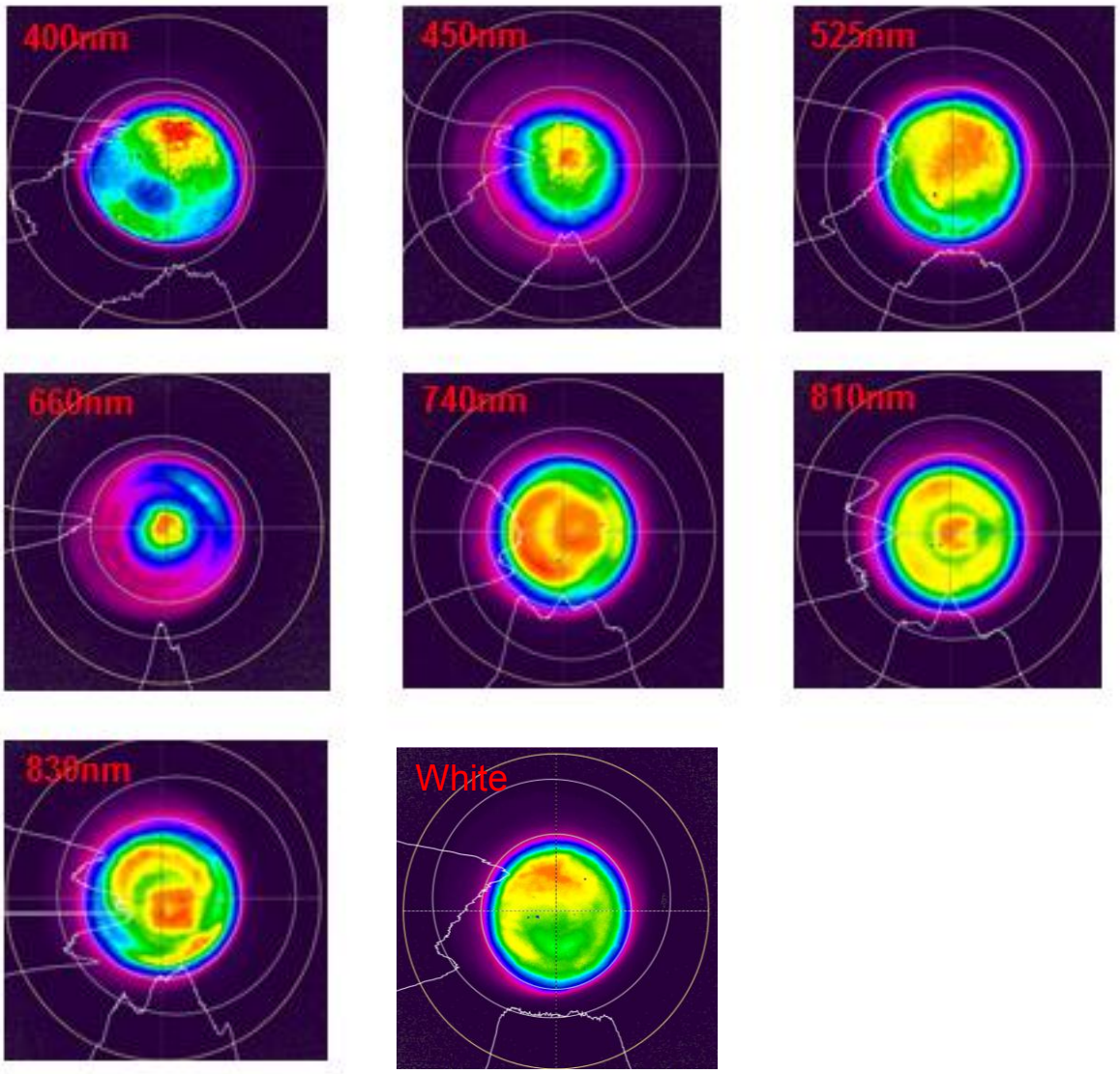

Figure 3.5: These diagrams show the beam profile of 2nd generation LED array used in this study (see Figure 3.2 (c) irradiance colour scale).

3.2.2.3 Discussion

This data measures the beam distribution and levels of irradiance over the irradiated area for each light source. Figure 3.3 and 3.4 show differences between 1st and 2nd generation LED array (Figure 3.5 and 3.6). This is likely due to the differences in the diameter in the LED used. It was necessary to change the beam profiler experimental set up for measurement of the laser and single LED, by using spacer rings to adjust the distance between light and camera (see Section 2.2.1.3).

These data on wavelength, irradiance and beam profile are essential to allow accurate dose delivery to cells in subsequent experiments and to determine the best cell culture vessels to grow cells in to optimise light delivery at a cellular level.

3.2.3 Temperature measurement

3.2.3.1 Introduction

Measuring temperature changes (2.2.1.4) following light irradiation is important in interpreting cellular biological changes following light exposure, as any changes may be a function of temperature rather that the direct effect of light. Measurements were taken in a range of conditions and at different time points for each light source in order to determine the magnitude of any temperature changes and the possible relevance to the experimental set up used. In order to mimic experimental conditions cell culture ware was pre-incubated (37^{o}C and 5% of CO_2) removed from the incubator and exposed to various light sources for differing amounts of time.

3.2.3.2 Results

In order to determine the potential relevance of temperature as a confounding factor in downstream cell changes, temperature was measured in the cell culture system with or without light irradiation. Temperature was assessed in real time following light exposure using either the laser, single LED, or 1st and 2nd generation LED arrays. These data showed variation of temperature change (^{o}C) with different irradiation times (Figure 3.6; laser, Figure 3.7; single LED, Figure 3.8; 1st generation LED array and Figure 3.9; 2nd generation LED array). The cell culture media temperature dropped on removal from the incubator 37^{o}C, comparison was then seen when irradiation began (Figure 3.10).

(a) 60s exposure at 0mm distance

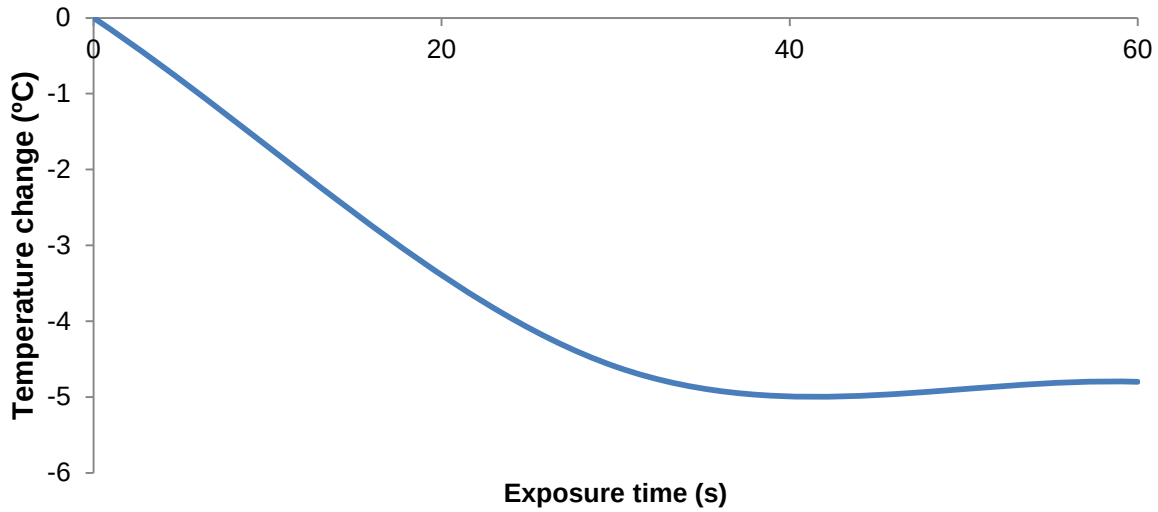

(b) 120s exposure time at 33mm

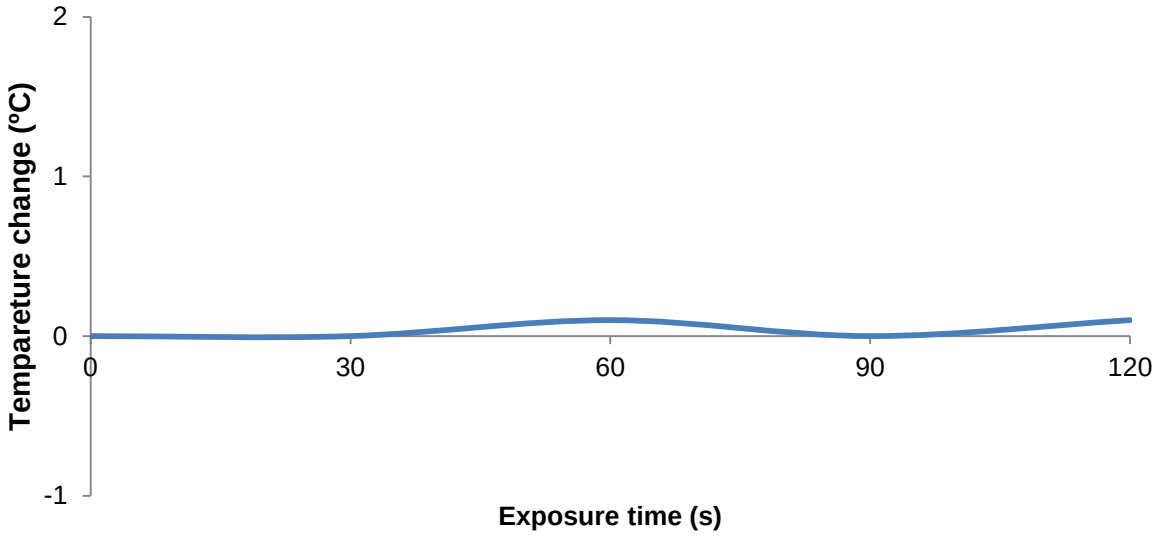

Figure 3.6: Change in temperature during 670nm laser irradiation (a) 60s exposure at 0mm distance between light source and culture ware (n=3 in triplicate) (b) 120s exposure time at 33mm distance (n=3 in triplicate).

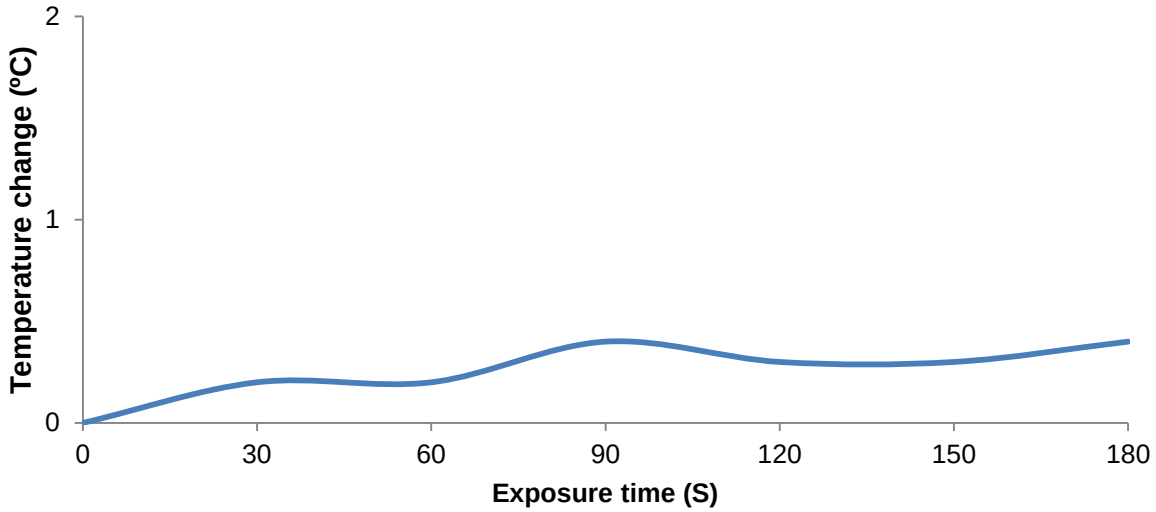

Figure 3.7: Temperature change during 180s of single LED irradiation at a distance 33mm (n=3 in triplicate).

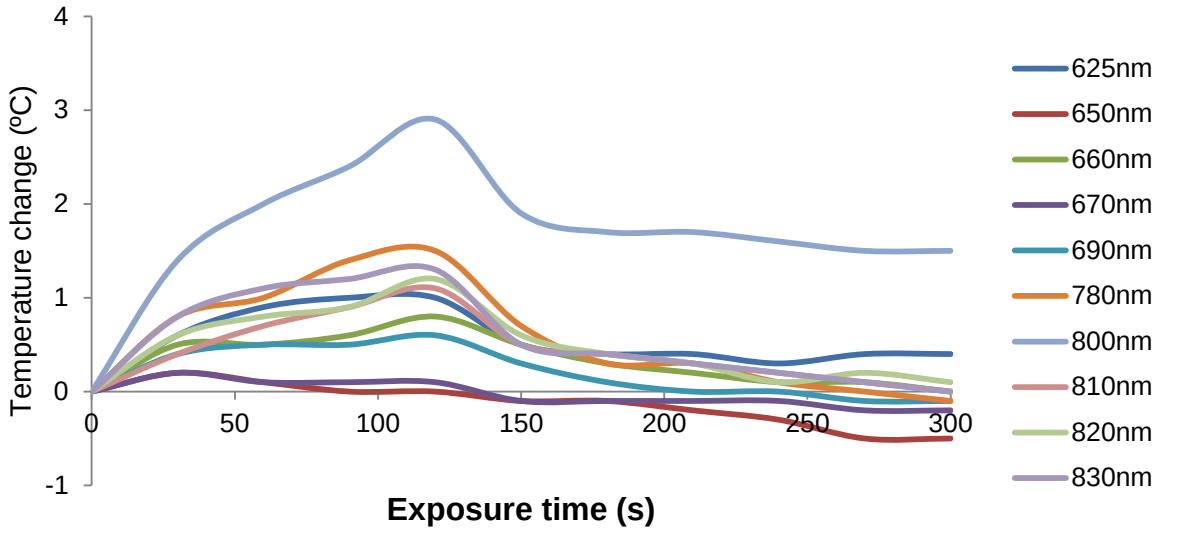

Figure 3.8: Temperature change with 1st generation LED array with 300s continuous exposure (n=3 in duplicate).

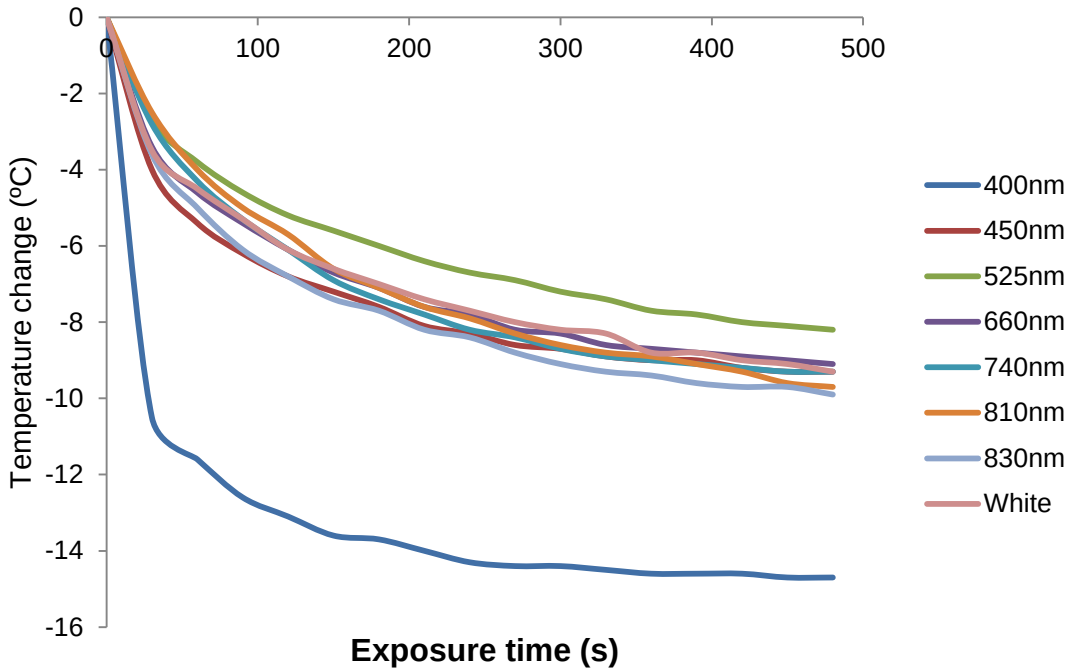

Figure 3.9: Temperature change using 2nd generation LED array with continuous exposure over 480s (n=3 in duplicate).

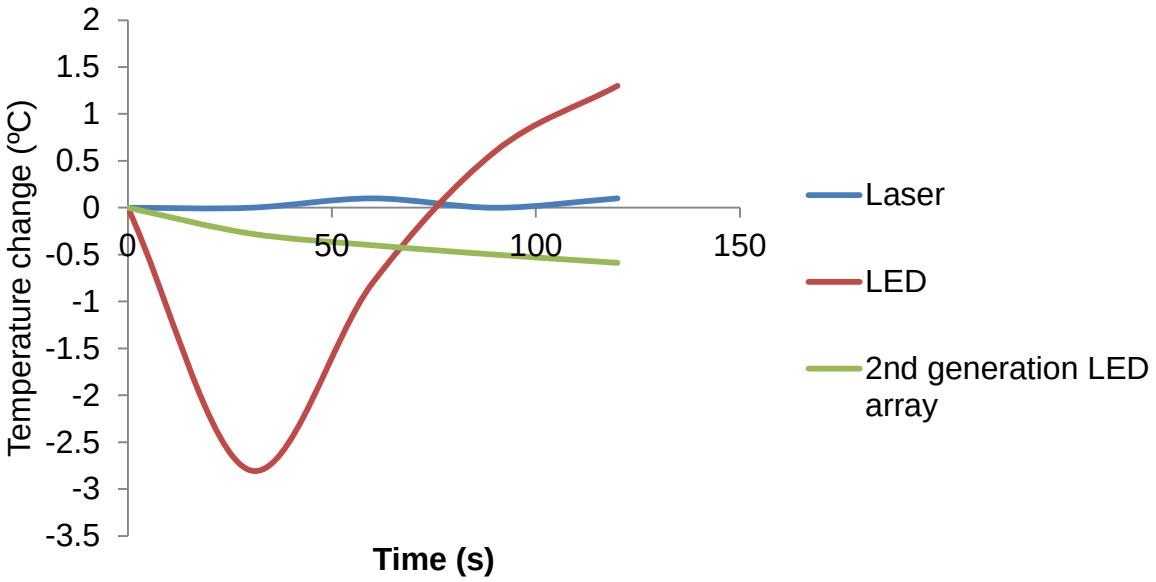

Figure 3.10: Temperature change upon removal from incubator and irradiation started after 30s (n=3 in duplicate).

3.2.3.3 Discussion

For the 670nm laser (Figure 3.6 (a) and (b)), the temperature measurement was carried out at 0 and 33mm distance. It was proposed that the temperature during light irradiation at a distance of 0mm might be increased and that by increasing the distance between the light source and cell culture vessel this could be minimised. However these data suggest that increasing distance actually resulted in a slight increase in media temperature at an increased distance. The purpose of these experiments was to investigate temperature change as a confounding factor for any cell biological changes seen following irradiation and to determine strategies to minimise this effect.

Overall these data showed that for the single LED revealed temperature increases of less than 1^{o}C while 1st generation LED array showed slight increase within 120s irradiation time. However, temperature change for 2nd generation LED array showed a small decrease with the 480s exposure.

From these experiments it suggests that temperature change with light exposure in these model systems is small and unlikely to have a significant effect on cell metabolism.

CHAPTER 4: ESTABLISHMENT OF ORAL EPITHELIAL CELL (OEC) H400s CULTURE

4.1 Introduction

This chapter describes the initial experiments to determine the growth characteristics of the human oral epithelial cell line, H400s in order to develop a model to investigate biological responses following irradiation. A range of different cell culture vessels will be utilised so a detailed understanding of cell growth in each of these will required for the range of experiments required. The immortal human oral epithelial cell line (H400) was selected because it is well characterised and has been used as a model system for studying cell behaviour in periodontal disease (Prime *et al.,* 1990, Milward 2010). Cell growth characteristics were investigated including seeding density, media serum concentration, cell viability and time to reach confluence in a range of cell culture vessels (as described in Table 2.4). It is proposed that if cells have an excess of nutrition provided that the additive effects of light exposure may be masked, therefore experiments were included to limit nutrient availability (modification of media serum content). Also cell number will plateau once a confluent monolayer is achieved at which point no further effects on cell number will be detectable, so it is essential that all experiments are correctly timed to ensure irradiated cultures can still proliferate.

As described in Section 2.2.4.1, cell counting was performed using Luna automated cell counter following comparison between Luna and manual count as illustrated by Figure 2.1.2. The Luna cell counter generated cell number and viability which appeared on device monitor.

4.2 Determination of level of confluence and foetal calf serum (FCS) concentration

In order to find the correlation between level of confluence and days, culturing cell was initially applied $2x10^4$ cells in DMEM supplemented with 10% of FCS in 35mm dish and cell counting performed on days 2-7. Cells were nearly fully confluence on day 7 (Table 4.1 and Figure 4.1). Subsequently, cells were seeded at $2x10^4$ cells per dish ($1x10^4$ cells/ml) in 35mm dishes with media containing either 5 or 10% FCS. Figure 4.2 shows the cell counts at days 3 and 5 post seeding of H400s grown on DMEM supplemented by 5 and 10% FCS (Table 4.2 and Figure 4.2). Cell growth was seen with both concentration but there was increased proliferation with 10% FCS, as this concentration is the most widely used for H400 cells and gave suitable growth characteristics (Milward 2010, Almeida-Lopes *et al.,* 2001). However, it was decided that the suitable concentration for growing H400s in this study would be 5% because there should be spaces for H400s to grow following irradiation and used for subsequent experiments.

Table 4.1: Cell number observed on days 2-7 to perform growth curve of seeded H400s with $2x10^4$ cell inoculation in 35mm dish.

Day	Cell number ($1x10^4$)	Cell viability (%)
2	6	77.8
3	11	74.2
4	35	87.9
5	51	91.8
6	68	93.5
7	77	96.1

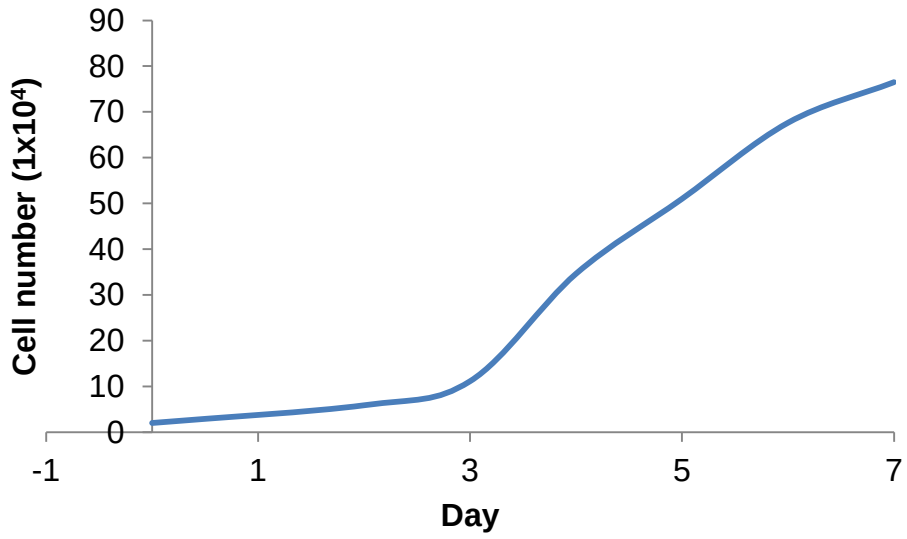

Figure 4.1: Cell growth curve of cell count on days 2-7 cultured in DMEM with 10% FCS (n=4 in duplicate).

Table 4.2: Cell number and viability generated following H400s seeding with different concentration of FCS.

	Cell number ($1x10^4$)		Cell viability (%)	
Seeding condition	**Day 3**	**Day 5**	**Day 3**	**Day 5**
20000 cells - 10% FCS	7.5	43.5	63.3	90.6
20000 cells - 5% FCS	8	30.5	60.9	91.2

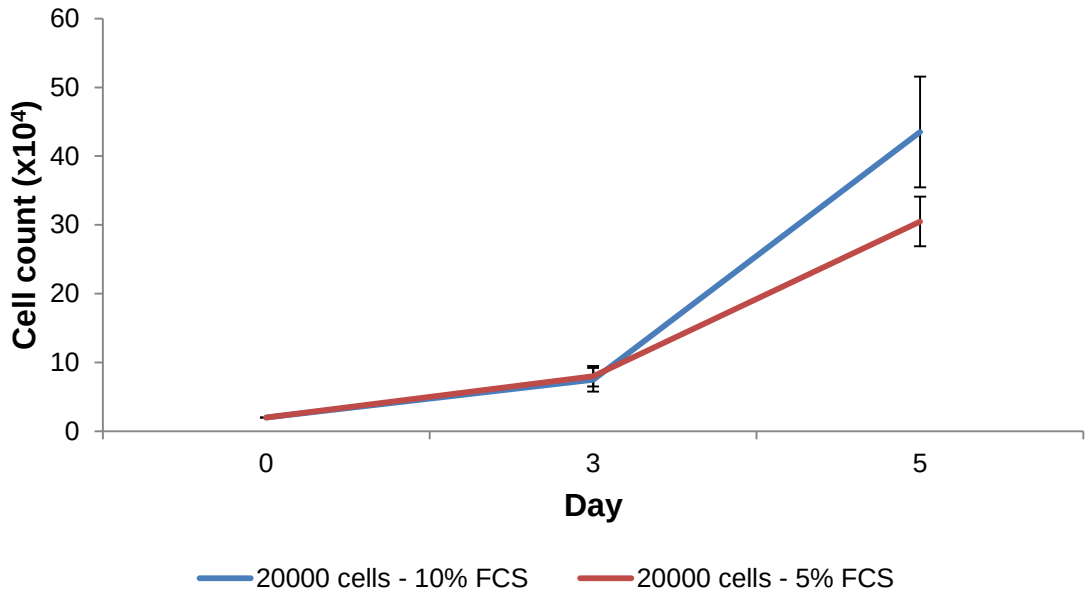

Figure 4.2: H400s which were supplemented with 10% of FCS showed higher growth than 5%. Results are mean ± SD (n=4 duplicate).

4.3 Determination of optimal cell seeding density

4.3.1 Determination of cell seeding in 35mm Petri dish

For 35mm dish cultureware, cell seeding density was determined using DMEM supplemented with 5% FCS. Cell were seeded at $2x10^2$, $2x10^3$, $10x10^3$ and $2x10^4$ cells per dish in 2ml of growth media and incubated at 37°C in 5% CO_2 for up to 5 days. Four replicates were included for each seeding density. Data from days 4 and 5 post seeding indicated that the lowest growth rate was observed with an initial seeding density of $2x10^2$ cells (100 cells/ml), while the highest growth could be seen from inoculation with $2x10^4$ cells (10000 cells/ml) (Table 4.3 and Figure 4.3). The lowest seeding density ($2x10^2$ cells) resulted in no detectable growth at days 4 and 5. This was possibly due to scanty cell seeding resulting in inadequate cell-cell interaction and lack of extracellular protein signalling molecules which is essential for survival and proliferation (Alberts *et al.,* 2002). The highest level of proliferation was observed in cells seeded at $2x10^4$ cells (10000 cells/ml) and this seeding density resulted in cells not reaching confluence within the time frame of the experiment so provided optimal conditions for the irradiation experiments and was used for all future experiments in 35mm.

Table 4.3: Cell count and viability data when assessed on days 4 and 5 after cultured with different seeding inoculation.

Cell seeding concentration	Cell number		Cell viability (%)	
	Day 4	Day 5	Day 4	Day 5
200	0	0	0	0
2000	1250	1875	74.2	81.9
10000	10010	10149	76.9	93.7
20000	53750	154375	70.5	92.2

(a)

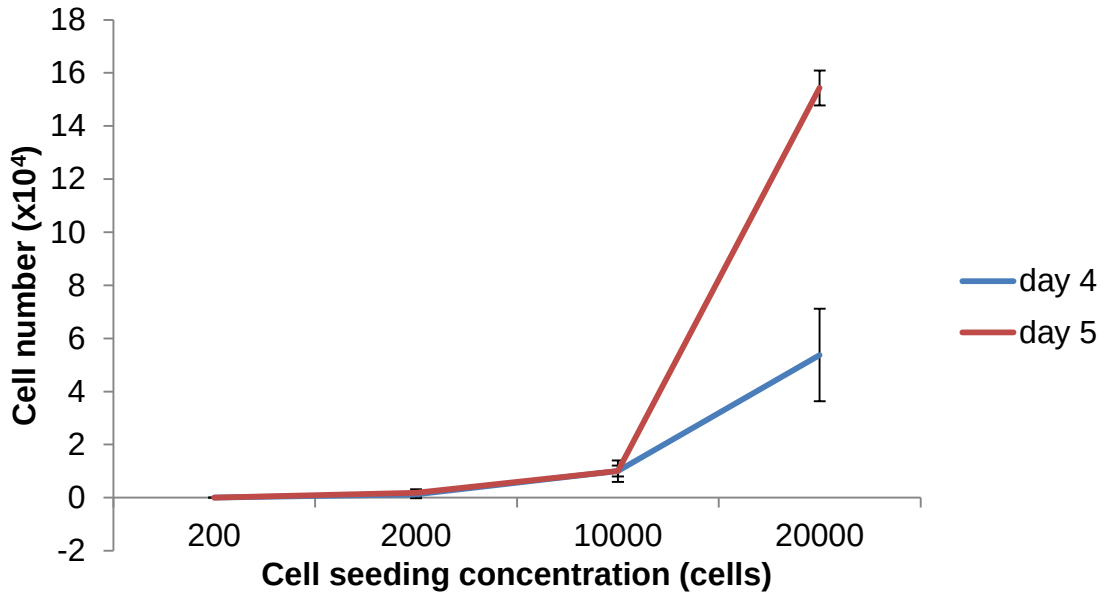

(b)

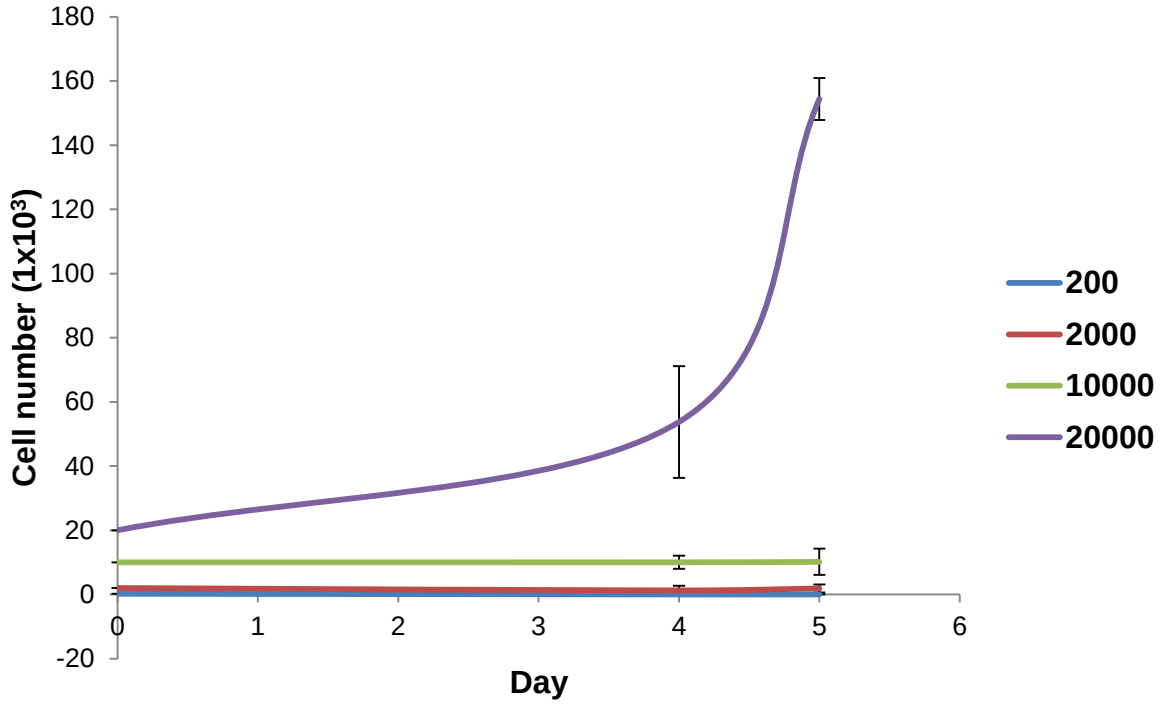

Figure 4.3: (a) Growth characteristics of H400 cells with different cell seeding concentrations ($2x10^2$, $2x10^3$, $10x10^3$ and $2x10^4$ cells per dish) and (b) cell number increase for each different seeding inoculation. Results are mean ± SD (n=4 in duplicate).

4.3.2 Determination of cell seeding in 96-well plates

96-well plates were seeded with a range of cell densities (1000, 1200, 1400, 1600, 1800, 2000, 4000, 6000, 8000, 10000, 12000 and 15000 cells/well (in 150µl) and grown for 4 days to determine the best conditions for growth (produce sufficient growth without reaching confluence during irradiation experiments). Cell counts were performed on day 1 and this demonstrated linear growth whilst day 4 showed almost similar cell numbers for initial inoculum of 4000 cells/well and above (Figure 4.4, 4.5 and Table 4.4). From the result, for the 96-well black plate and the culture conditions it was suggested that the best seeding concentration was between 2000 - 4000 cells/well. Therefore, 3000 cells/well was chosen to seed the plate.

Table 4.4: Cell counting data at days 1 and 4 for 96-well black plate with different cell inoculation.

	Cell number	
Cell seeding concentration	**Day 1**	**Day 4**
1000	814	13730
1200	867	19154
1400	927	20444
1600	1070	24850
1800	1010	18396
2000	1093	20292
4000	1606	39980
6000	2246	42752
8000	2902	42810
10000	3452	42670
12000	4357	36214
15000	5947	41116

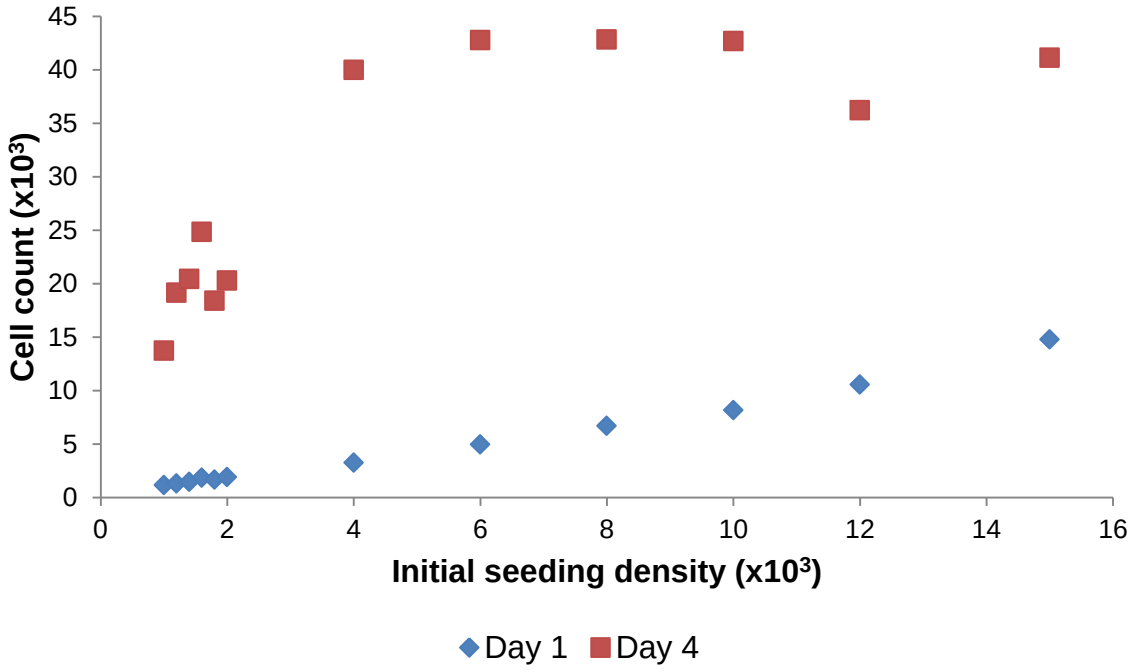

Figure 4.4: H400s data collection at (a) day 1 and (b) day 4 with a range of seeding concentration (n=2 in duplicate).

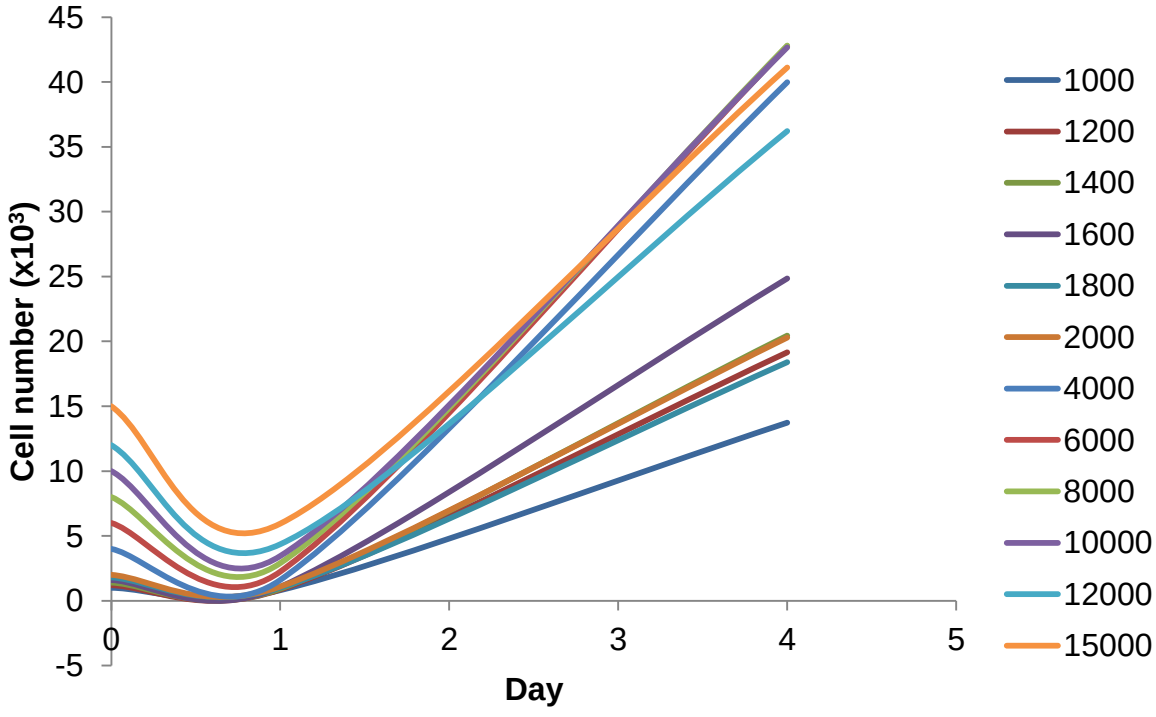

Figure 4.5: Cell counting for different seeding cells relative to day growth (n=2 in duplicate).

4.3.3 Determination of cell seeding density for 4-well glass slide

Prior to immunocytochemistry staining, a pilot experiment to determine initial seeding density for the 4-well glass slide which was housed in a standard Petri dish was performed. The H400s were cultured at two different initial seeding densities, $2x10^5$ and $4x10^5$ cells in 15ml and grown at 37°C in 5% CO_2 for 2 days. On day 2, the percentage confluence and cell attachment was analysed under microscope (Zeiss Axiovert 25, Zeiss, UK) with 20x magnification (data not shown). According to the microscopic assessment and the growth curves generated it was determined that initial seeding with $2x10^5$ would be most appropriate for the immunocytochemistry study.

4.4 Discussion

The result of these experiments demonstrated that to reach the 70% level of confluence with more than 90% of viability for subsequent experiments, the 35mm culture dish should be seeded with $2x10^4$ cells per dish ($1x10^4$ cells/ml) and 4-well slide in Petri dish with $2x10^5$ cells (in 15ml) in DMEM with 5% FCS while for the 96-well black plate with $3x10^3$ cells per well ($2x10^4$ cells/ml). Considering the time of incubation and level of confluence, it was decided that the ideal cell confluence should be in the region of 20-30% prior to light irradiation to allow sufficient substrate area not to impede cell growth and to give the best possibility of demonstrating increases in cell proliferation on light exposure.

In this section of work H400 cell growth has been carefully characterised so that conditions for subsequent experiments can be optimised in order to investigate cell responses upon light irradiation.

CHAPTER 5: H400 RESPONSES TO LASER IRRADIATION

5.1 H400 cells responses upon laser irradiation

5.1.1 Introduction

The aim of the current study was to investigate possible stimulatory effect of light on epithelial cell growth (H400). H400s which have been well characterised in a number of previous studies and offer a useful study model for investigating epithelial responses in the periodontal tissues. The resulting findings may have application in dental therapy. Initial experimentation aimed to explore growth responses of H400 cells to the range of light sources utilised in this study.

The previously determined cell seeding density (see Section 4.3.1) appropriate for these experimental conditions were utilised in these experiments. Laser irradiation parameters utilised were as discussed in Appendix 1. H400s were cultured at $2x10^4$ cell in 35mm dish ($1x10^4$ cells/ml). Briefly, H400 cell cultures was irradiated (a) at distance 0mm between the laser and cell monolayer for 4, 6 and 8s (which equated to 7, 10 and 14J/cm^2 radiant exposure) and (b) at 33mm distance between the laser and cell monolayer for 80, 100 and 120s exposure time (which equated to 27, 34 and 41J/cm^2 radiant exposure respectively).

5.1.2 Results

H400 cellular responses following laser irradiation were assessed by cell counts, MTT assay, BrdU assay, NF-κB translocation and downstream gene expression changes using SQ-PCR. The incubation post-seeding were varied according to

different assay and discussed later. The data is presented as percentage increase or decrease when normalised to control (non-irradiated) sample.

5.1.2.1 Cell count

Cell counts were determined 3 days post seeding (48h post irradiation) using Luna automated cell counter. Results showed (Figures 5.1 & 5.2) a significant increase (p<0.05) in cell number (compared to non-irradiated controls) following irradiation for 100s (34 J/cm^2 radiant exposure) & 120s (41 J/cm2 radiant exposure).

5.1.2.2 MTT assay

In addition to cell counts mitochondrial metabolic activity of the irradiated cells were assessed. Figures 5.3 and 5.4 show the percentage MTT increase in irradiated cells in comparison to non-irradiated controls. H400 cells irradiated for 120s (41J/cm^2) resulted significant increase in MTT and this result so a similar trend when compared to the manual cell count data (Figure 5.2).

5.1.2.3 BrdU assay

This assay is a surrogate measure of cell proliferation where the substrate bromodeoxyuridine (BrdU) is incorporated into newly synthesized DNA of actively proliferating cells. The BrdU assay was carried out 24h following 4, 6 and 8s laser irradiation (7, 10 and 14J/cm^2 of radiant exposure respectively) to determine any significant increase following laser exposure. The results indicated a significant increase in H400 cell proliferation when cells were irradiated at 0mm distance utilising a 6s exposure time (10J/cm^2). These results are shown in Figure 5.5.

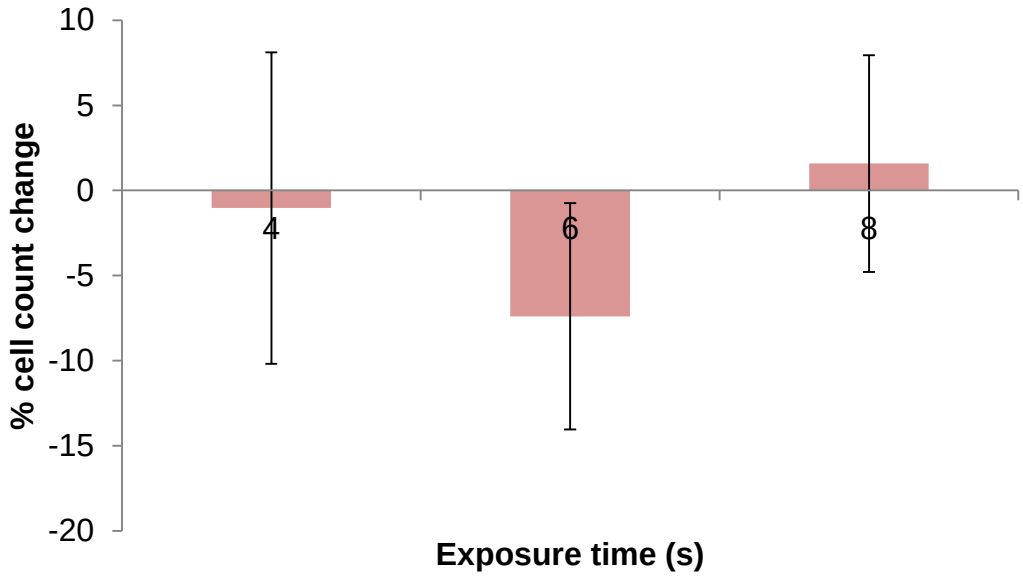

Figure 5.1: Percentage cell count change when normalised to non-irradiated control (n=3 in triplicate) of H400 cells irradiated for 4, 6 and 8s exposure time (7, 10 and 14J/cm^2 of radiant exposure respectively). Results are mean ± SD.

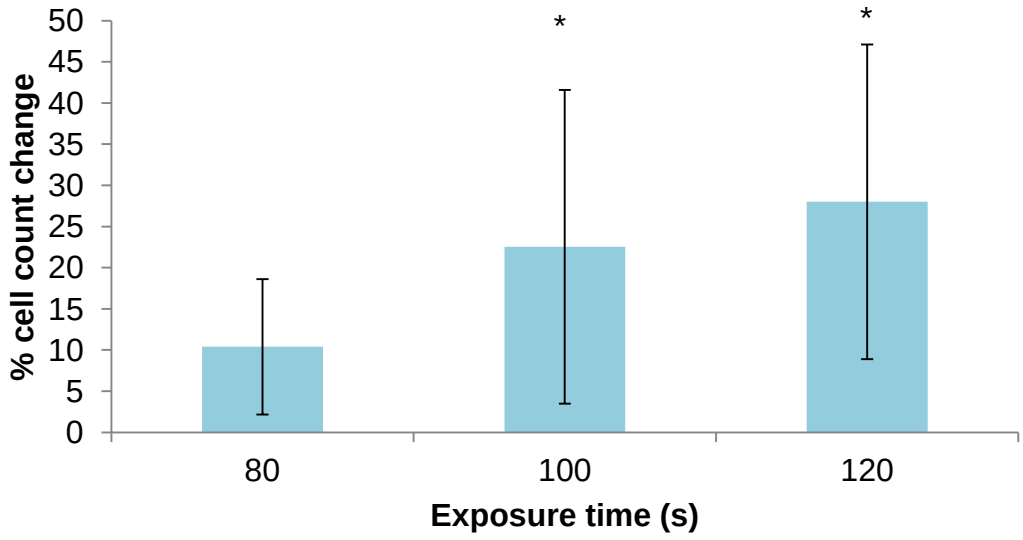

Figure 5.2: Percentage cell count increase when normalised to non-control (n=4 in duplicate). Following 80, 100 and 120s laser exposure time (radiant exposure 27, 34 and 41J/cm^2, respectively). Results are mean ± SD. *p<0.05.

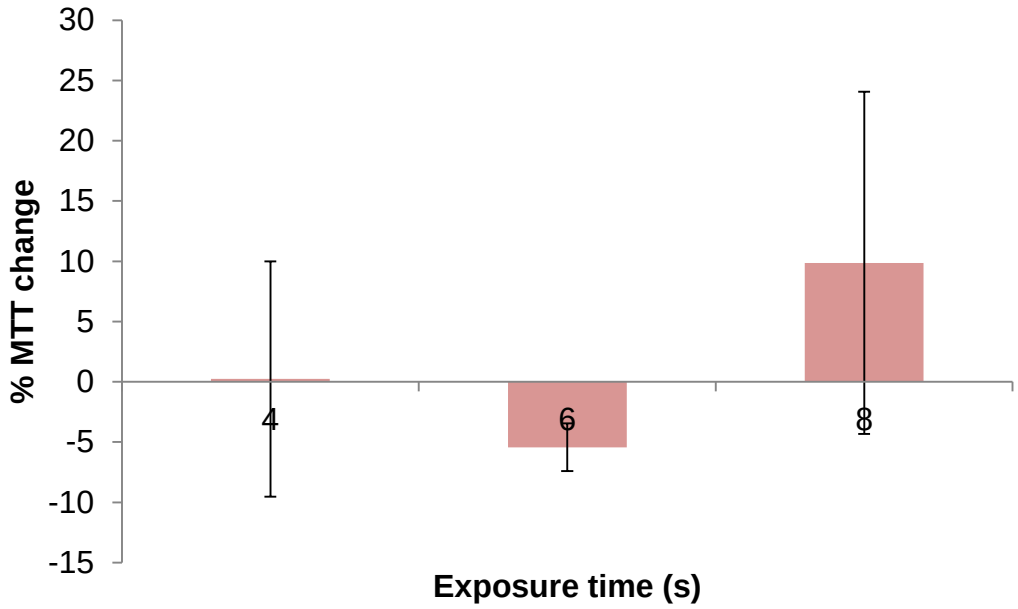

Figure 5.3: Percentage of MTT change when normalised to non-irradiated control following 4, 6 and 8s laser irradiation (7, 10 and 14J/cm^2 of radiant exposure respectively). Results are mean ± SD (n=4 in duplicate).

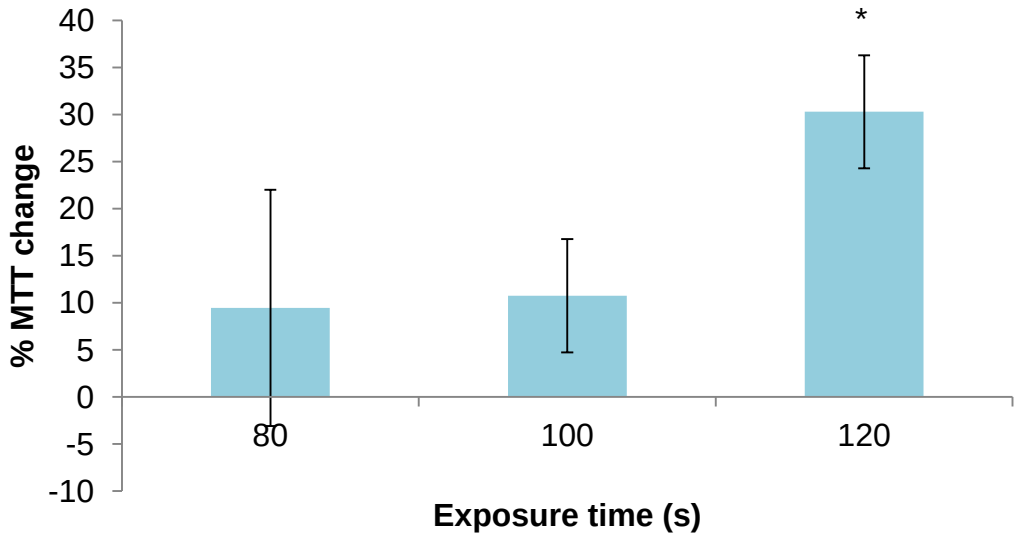

Figure 5.4: Percentage increase in MTT for H400 cells irradiated for 80, 100 and 120s time of exposure (27, 34 and 41J/cm^2 radiant exposure respectively) (n=4 in duplicate). Results are mean ± SD. *p<0.05

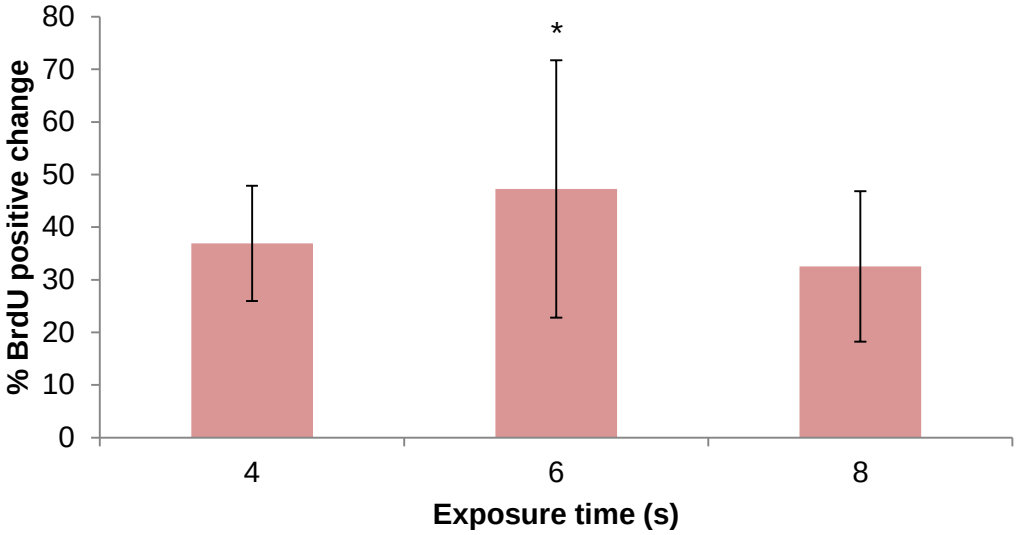

Figure 5.5: Percentage increase in BrdU compared to non-irradiated cells. 4, 6 and 8s served 7, 10 and 14J/cm^2 radiant exposure. Results are mean ± SD (n=4 in duplicate). *p<0.05.

5.1.2.4 NF-κB activation

H400s cell culture were also grown on 4-well glass microscope slides (Figure 2.15) to determine NF-κB activation using immunocytochemistry in cells stimulated (including non-stimulated controls) with *E. coli* LPS and laser irradiated (including non-irradiated controls). H400 cells were irradiated for 120s (41J/cm^2 radiant exposure) at a distance of 33mm, at both 1 and 24h prior to stimulation with *E. coli* LPS (or non-stimulated control). Figure 5.6 illustrates representative immunocytochemical images, Figure 5.7 shows semi-quantitative analysis of cell images with percentage increase in NF-κB activation normalised to non-stimulated and non-irradiated controls. Positive and negative control were included to ensure specificity of staining. Activation of NF-κB turned the nucleus brown and 6 fields were counted using Image J software (as described in Section 2.2.4.5).

These results depicted in figures 5.6 and 5.7 suggest that in this experimental model laser irradiation reduces NF-kB activation following stimulation with *E.coli* LPS.

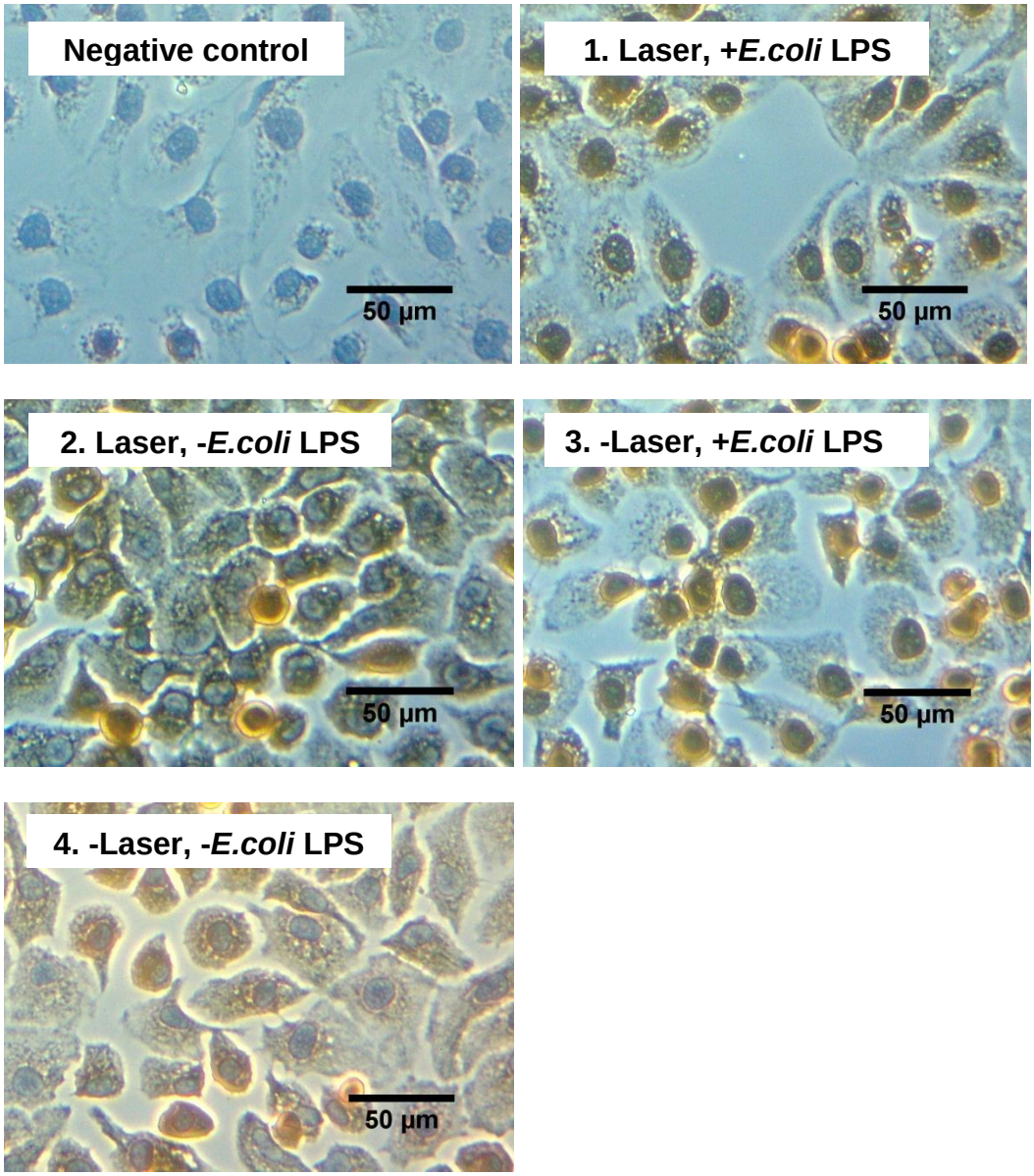

Figure 5.6: Representative H400 cell images with or without 120s laser irradiation (41J/cm^2) 1h before stimulation with *E.coli* LPS (1h incubation) or unstimulated control [1. 120s laser irradiation with *E.coli* LPS stimulation, 2. 120s laser without *E. coli* LPS stimulation, 3. No laser with *E.coli* LPS stimulation, 4. No laser without *E. coli* LPS stimulation (un-stimulated control)].

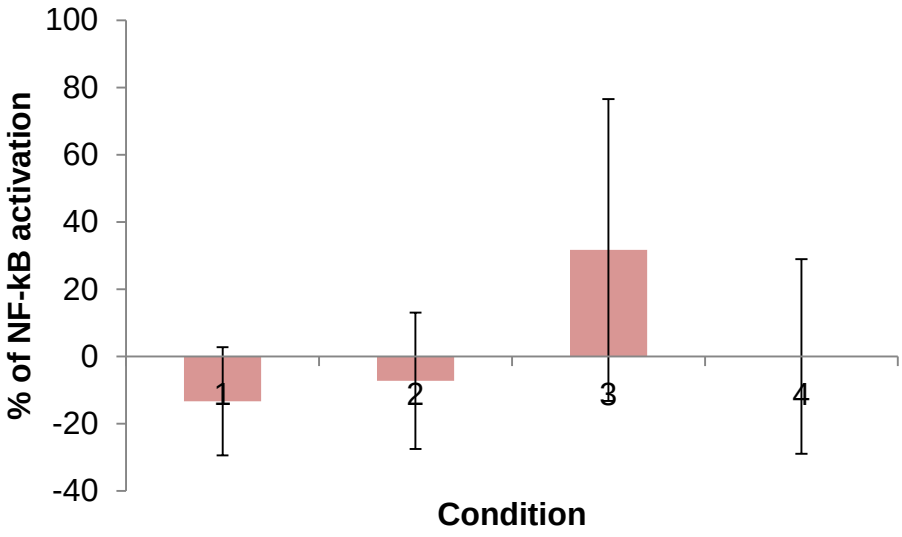

Figure 5.7: Stimulated or non-stimulated (*E. coli* LPS 1h incubation) and irradiated or non-irradiated (for 120s) H400 cells graph shows percentage of NF-kB activation compared to unstimulated control. Labelling 1-4 refers to image legends in Figure 5.6. Results are mean ± SD (n=2 in single).

5.1.2.5 Gene expression by PCR

Data from the previous experiments have shown the ability of the 670nm laser irradiation at distance 33mm to enhance H400 cell growth. The next part of this project aimed to assess gene expression changes following laser irradiation for 80, 100 and 120s (27, 34 and 41J/cm^2 radiant exposure). The genes selected were based on a literature search for genes implicated in cell proliferation, tissue healing and inflammatory response especially in regard to periodontal disease (Table 2.11).

H400 cells were grown in 35mm dishes, laser irradiated 24h post-seeding and RNA extracted 48h later. RNA was processed as discussed in section 2.2.4.7 materials and methods and converted to cDNA. Gene expression was examined utilising SQ RT-PCR normalised to the housekeeping gene GAPDH.

Figure 5.8 shows percentage gene expression (normalised to non-irradiated control). These data demonstrated low level gene expression of cells irradiated for 80s (27J/cm^2) with the exception of COX6C, MAPK11, NF-κB1E and NDUFA11 genes. However cells laser irradiated for 100s and 120s demonstrated higher level of genes expression in the majority of genes investigated.

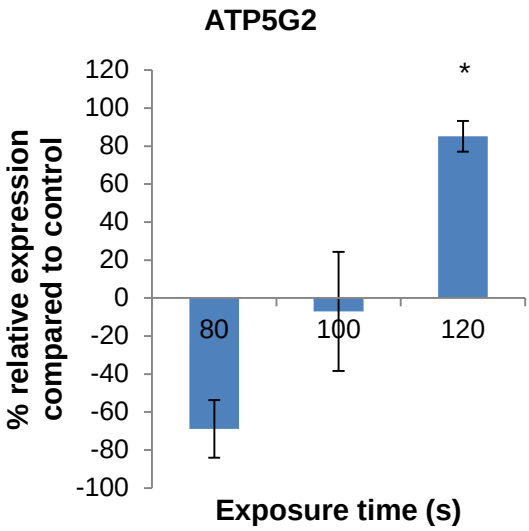
ATP5G2
% relative expression compared to control
120
100
80
60
40
20
0
-20
-40
-60
-80
-100
80
100
120
*
Exposure time (s)

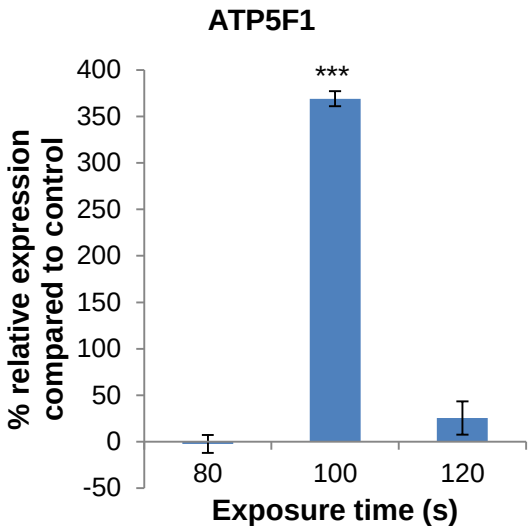
ATP5F1
% relative expression compared to control
400
350
300
250
200
150
100
50
0
-50
80
100
120
***
Exposure time (s)

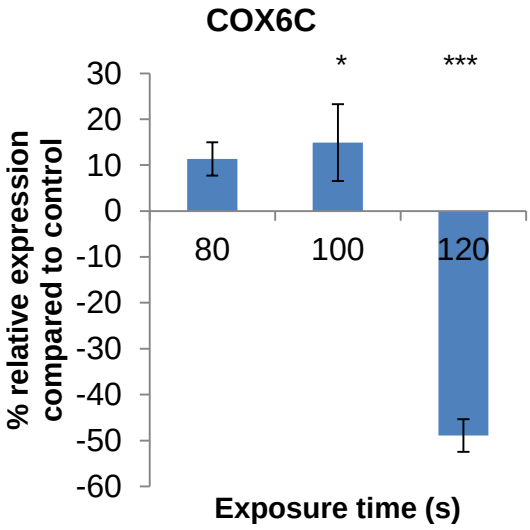
COX6C
% relative expression compared to control
30
20
10
0
-10
-20
-30
-40
-50
-60
80
100
120
*
***
Exposure time (s)

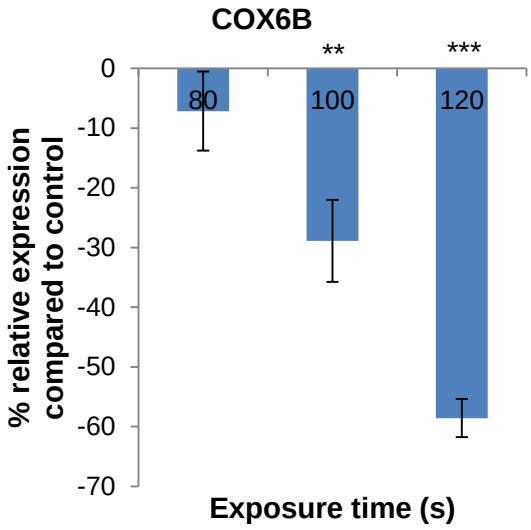
COX6B
% relative expression compared to control
0
-10
-20
-30
-40
-50
-60
-70
80
100
120
**
***
Exposure time (s)

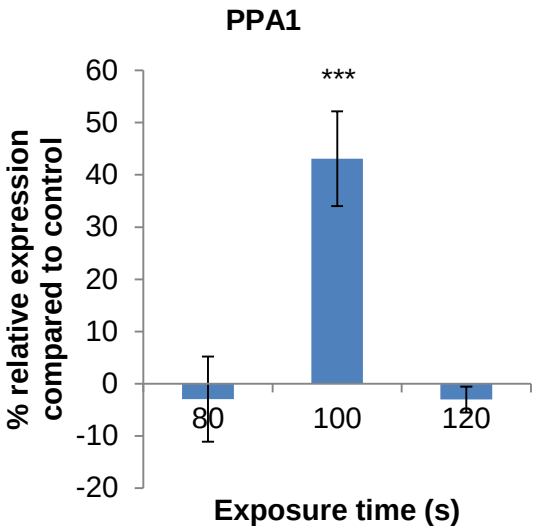
PPA1
% relative expression compared to control
60
50
40
30
20
10
0
-10
-20
***
80
100
120
Exposure time (s)

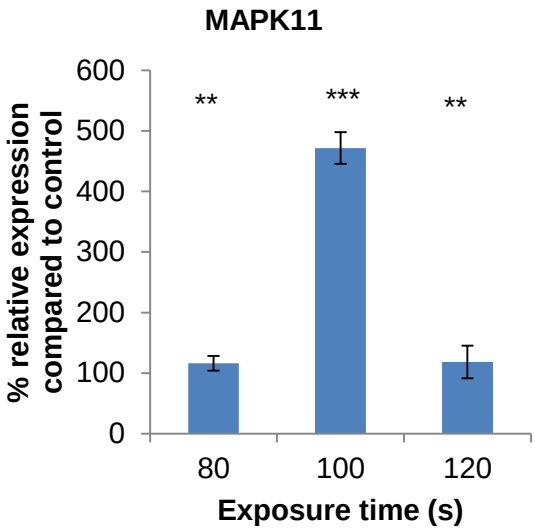
MAPK11
% relative expression compared to control
600
500
400
300
200
100
0
**
***
**
80
100
120
Exposure time (s)

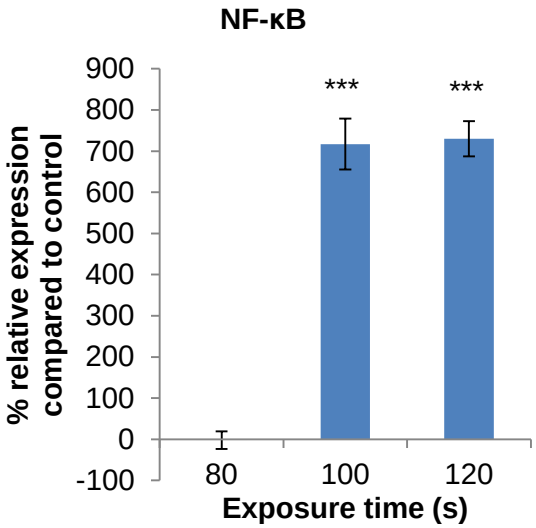
NF-κB
% relative expression compared to control
900
800
700
600
500
400
300
200
100
0
-100
***
***
80
100
120
Exposure time (s)

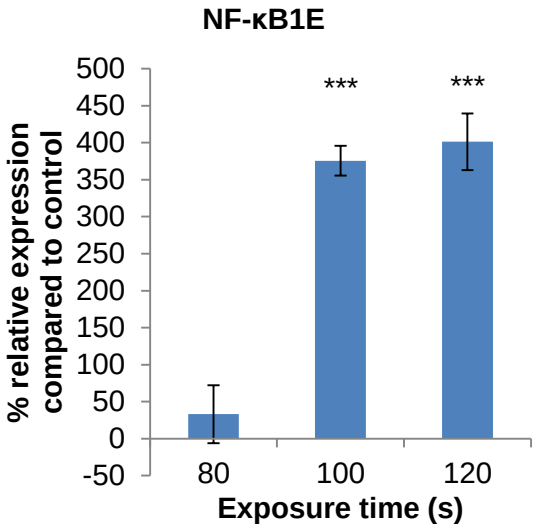
NF-κB1E
% relative expression compared to control
500
450
400
350
300
250
200
150
100
50
0
-50
***
***
80
100
120
Exposure time (s)

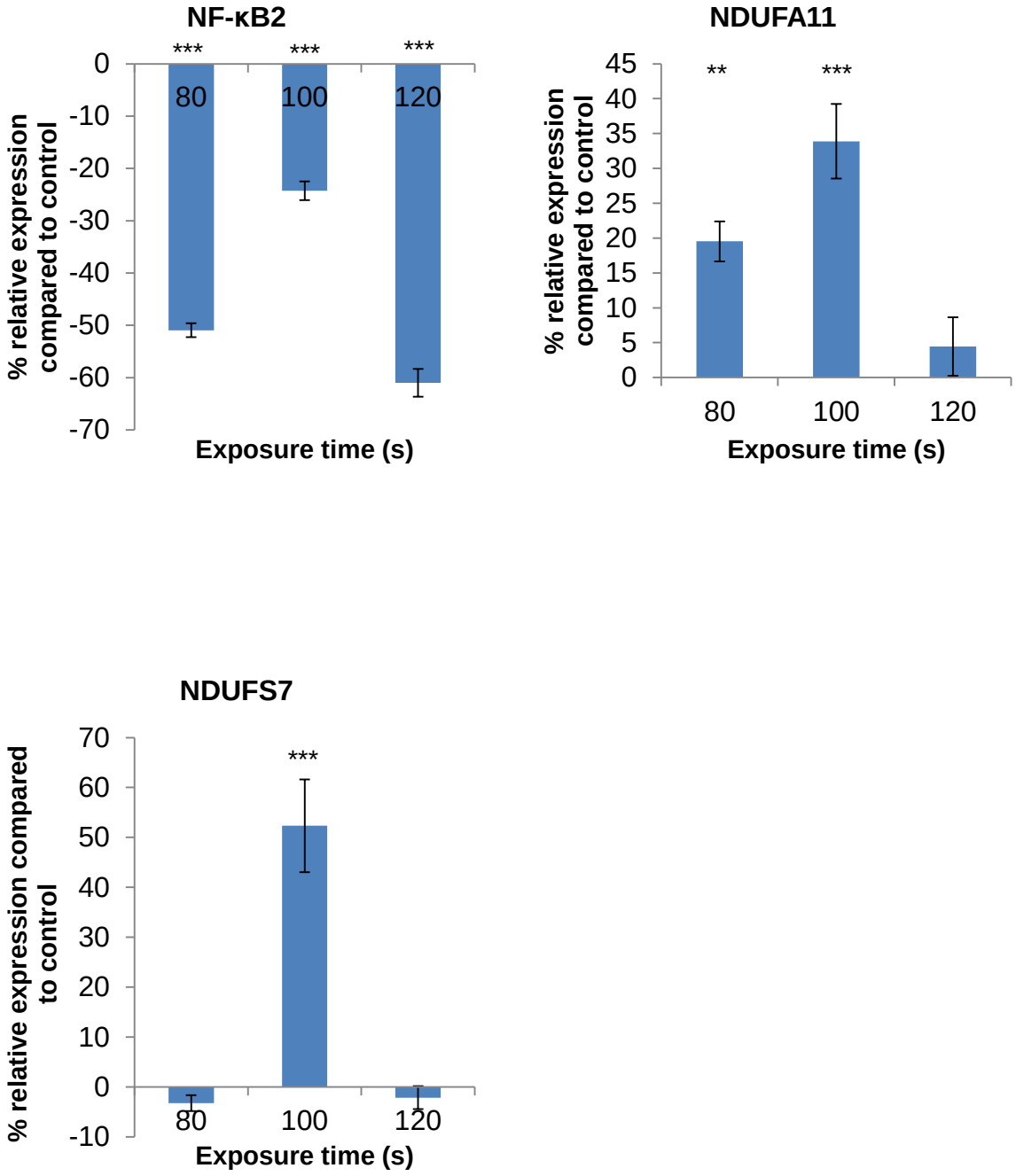

Figure 5.8: Gene expression levels of 11 genes expressed by H400 cells laser irradiated for 80, 100 and 120s (n=3 in duplicate). Results are mean ± SD. *p<0.05, **p<0.01, ***p<0.001.

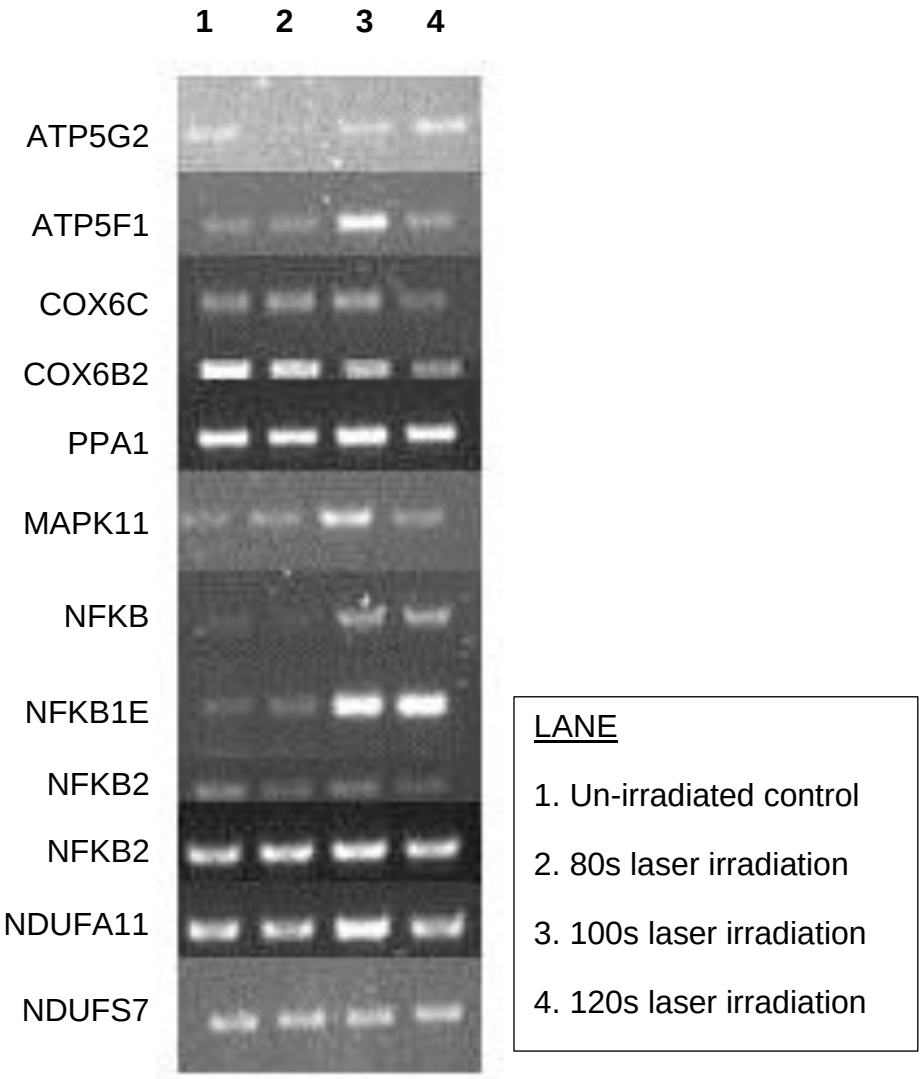

Figure 5.9: Agarose gel electrophoresis of laser irradiated H400 cells.

5.1.2.6 PCR array

The use of PCR array allows high throughput screening of large numbers of genes in biological samples offering the potential to investigate pathways and identify novel genes that may be important in light irradiation effects.

The Human Mitochondrial Energy Metabolism Plus RT^2 Profiler PCR Array was chosen as it investigates 84 key genes involved in mitochondrial respiration, which includes genes encoding components of the electron transport chain and oxidative phosphorylation complexes, also determination of a change of mitochondrial energy metabolism activity. This PCR array was undertaken to compare gene expression levels in comparison to controls following 120s laser irradiation.

The fold changes of the 84 genes of the array in comparison to non-irradiated control are shown in Figure 5.10. Two genes demonstrated increased expression compared to control (Table 5.1), two genes showed reduced levels of expression (Table 5.2) while the rest of the genes showed no significant change in expression.

Layout	01	02	03	04	05	06	07	08	09	10	11	12
A	ATP5A1 1.02 C	ATP5B -1.10	ATP5C1 -1.12	ATP5F1 -1.04	ATP5G1 -1.11	ATP5G2 2.03	ATP5G3 -1.21	ATP5H -1.15	ATP5I -1.15	ATP5J -1.12	ATP5J2 -1.21	ATP5L -1.04
B	ATP5O -1.16	COX4I1 -1.09	COX5A -1.20	COX5B -1.23	COX6A1 -1.00	COX6A2 1.02 C	COX6B1 -1.08	COX6C 1.02 C	COX7A2 -1.10	COX7A2L -1.16	COX7B -1.17	COX8A -1.08
C	CYC1 -1.03	NDUFA1 -1.36	NDUFA10 -1.17	NDUFA11 -1.24	NDUFA2 -1.13	NDUFA3 -1.12	NDUFA4 -1.19	NDUFA5 1.05	NDUFA6 -1.14	NDUFA8 -1.28	NDUFAB1 -1.15	NDUFB10 -1.24
D	NDUFB2 -1.08	NDUFB3 -1.17	NDUFB4 -1.15	NDUFB5 -1.18	NDUFB6 2.33 A	NDUFB7 -1.17	NDUFB8 -1.13	NDUFB9 -1.25	NDUFC1 -1.18	NDUFC2 -1.02	NDUFS1 -1.13	NDUFS2 -1.20
E	NDUFS3 -1.15	NDUFS4 -1.45	NDUFS5 -1.07	NDUFS6 -1.19	NDUFS7 -1.02	NDUFS8 -1.26	NDUFV1 -1.14	NDUFV2 -1.11	NDUFV3 -1.29	PPA1 -1.24	SDHA -1.18	SDHB -1.08
F	SDHC -1.01	SDHD -1.14	UQCR11 -1.13	UQCRC1 -1.26	UQCRC2 -1.28	UQCRFS1 -1.13	UQCRH -1.27	UQCRQ -1.07	ARRDC3 1.31	ASB1 -1.16	CYB561D 1 -1.09	DNAJB1 -1.24
G	EDN1 1.26	GADD45B 1.41	HSPA1A -1.10	HSPA1B -1.08	LRP5L -1.59	MitoH1 1.12	MitoH2_1 2106 1.47	MitoH2_1 4573 -2.85	MitoH2_4 162 -2.10	MitoH2_5 726 -1.45	RNU11 1.41	SLC25A25 -1.08

Figure 5.10: Fold changes in gene expression between the non-irradiated control and 120s laser irradiation for the 84 genes in the array. The above grid indicated the plate layout used for this experiment.

Table 5.1: Genes significantly up-regulated in H400s following 120s laser irradiation.

Position	Gene Symbol	Fold Regulation
D05	**NDUFB6**	**2.33**
A06	**ATP5G2**	**2.03**

Table 5.2: Genes relatively down-regulated in H400s following 120s laser irradiation.

Position	Gene Symbol	Fold Regulation
G08	**MitoH2_14573**	**-2.85**
G09	**MitoH2_4162**	**-2.10**

5.1.2.7 ELISA IL-8 detection with or without stimulation of *F. nucleatum* and *P. gingivalis*

IL-8 is a pro-inflammatory cytokine which is a surrogate marker of NF-κB activation (Uehara & Takada 2007, Milward 2010). H400 cells were stimulated with *F. nucleatum* and *P. gingivalis*, for then irradiated with laser for 80, 100 and 120s and IL-8 expression determined. Culture media was collected 48h post-irradiation and prepared as in Section 2.2.7.

Standard curve is illustrated in Figure 5.11 and results represented in Figure 5.12 shows the percentage of un-stimulated IL-8 absorbance (450-570nm) of 120s laser normalised to control with Figure 5.13 (a) demonstrates that IL-8 levels following laser irradiation for 80, 100 and 120s following *F. nucleatum* stimulation, with cells exposed to laser for 120s showing a significant increase ($p<0.05$). However, following stimulation with *P. gingivalis* and laser irradiation, the result showed reduced levels of IL-8 production compared to non-irradiated controls following 80 and 100s irradiation whilst IL-8 production rose following 120s irradiation.

These data suggest the ability of laser irradiation to modulate IL-8 production which could offer potential for management of inflammatory lesions.

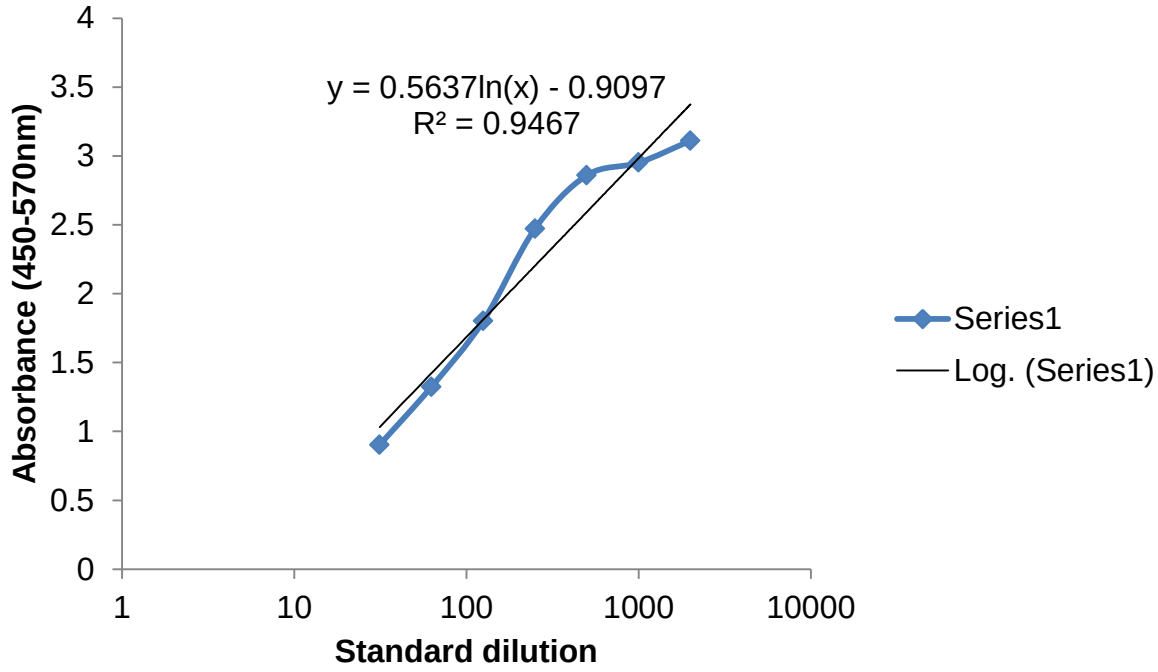

Figure 5.11: Standard curve of IL-8 absorbance with standard dilution.

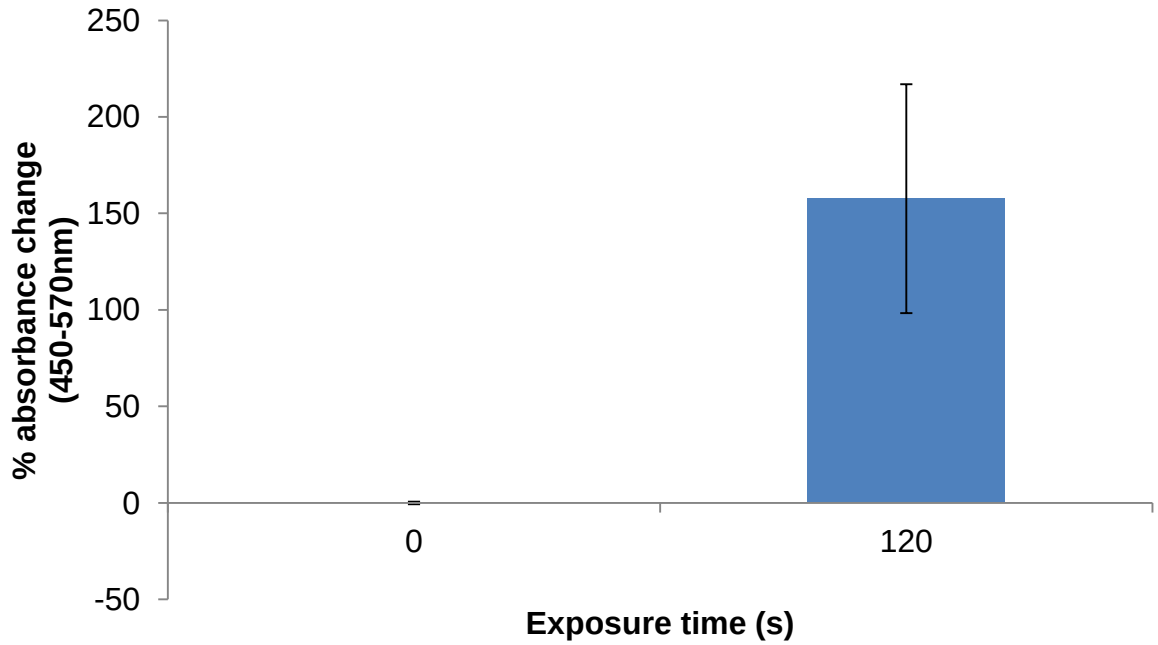

Figure 5.12: ELISA IL-8 percentage of absorbance increase of un-irradiated H400s control (n=3 in single).

(a)

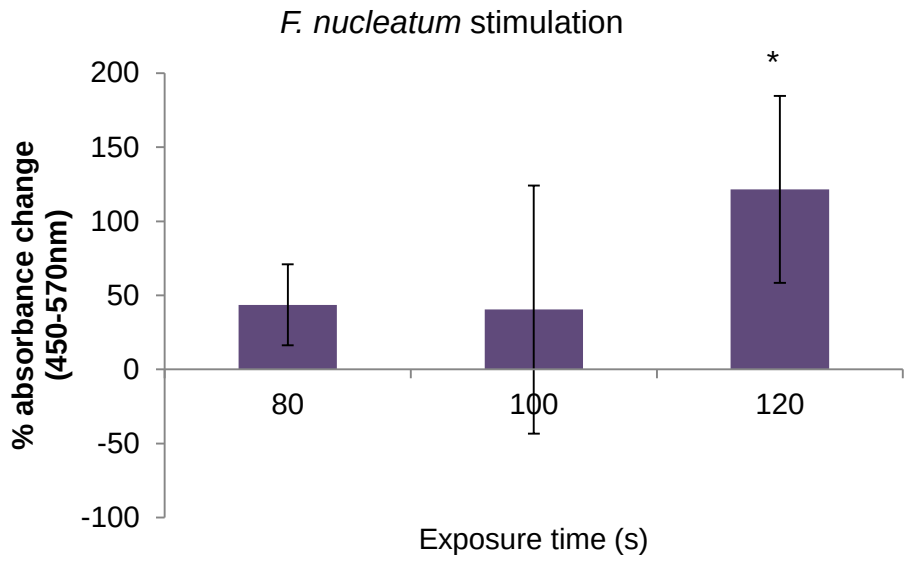

(b)

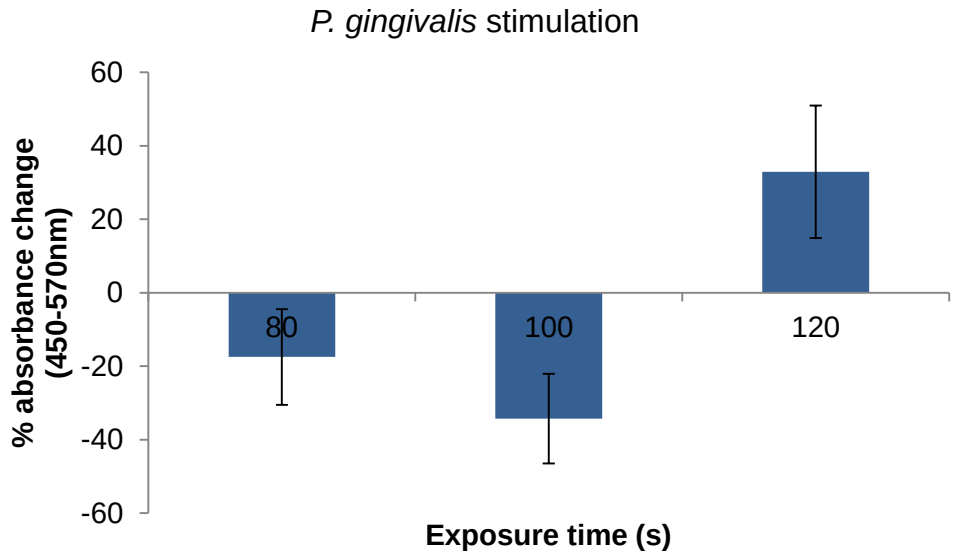

Figure 5.13: IL-8 production as a percentage of non-irradiated controls in cells stimulated with (a) *F. nucleatum* and (b) *P. gingivalis* and laser irradiated for 80, 100 and 120s. IL-8 of *F. nucleatum* stimulated was significantly increased at 120s while not in *P. gingivalis* stimulated. Results are mean ± SD. *p<0.05 (n=3 single).

5.1.2.8 Methylene blue staining

It was determined that the laser irradiation profile was small in comparison to the cell monolayer exposed in the cultureware which was used for this experiment resulting in the potential for sub optimal dosing of cells outside the beam area. In order to determine if this would result in differential cell proliferation across the cell monolayer methylene blue staining was performed. Cell staining appeared to show no significant variation across the culture dish suggesting that irradiation area did not differentially influence cell growth in cell culture monolayer (Figure 5.14 and 5.15).

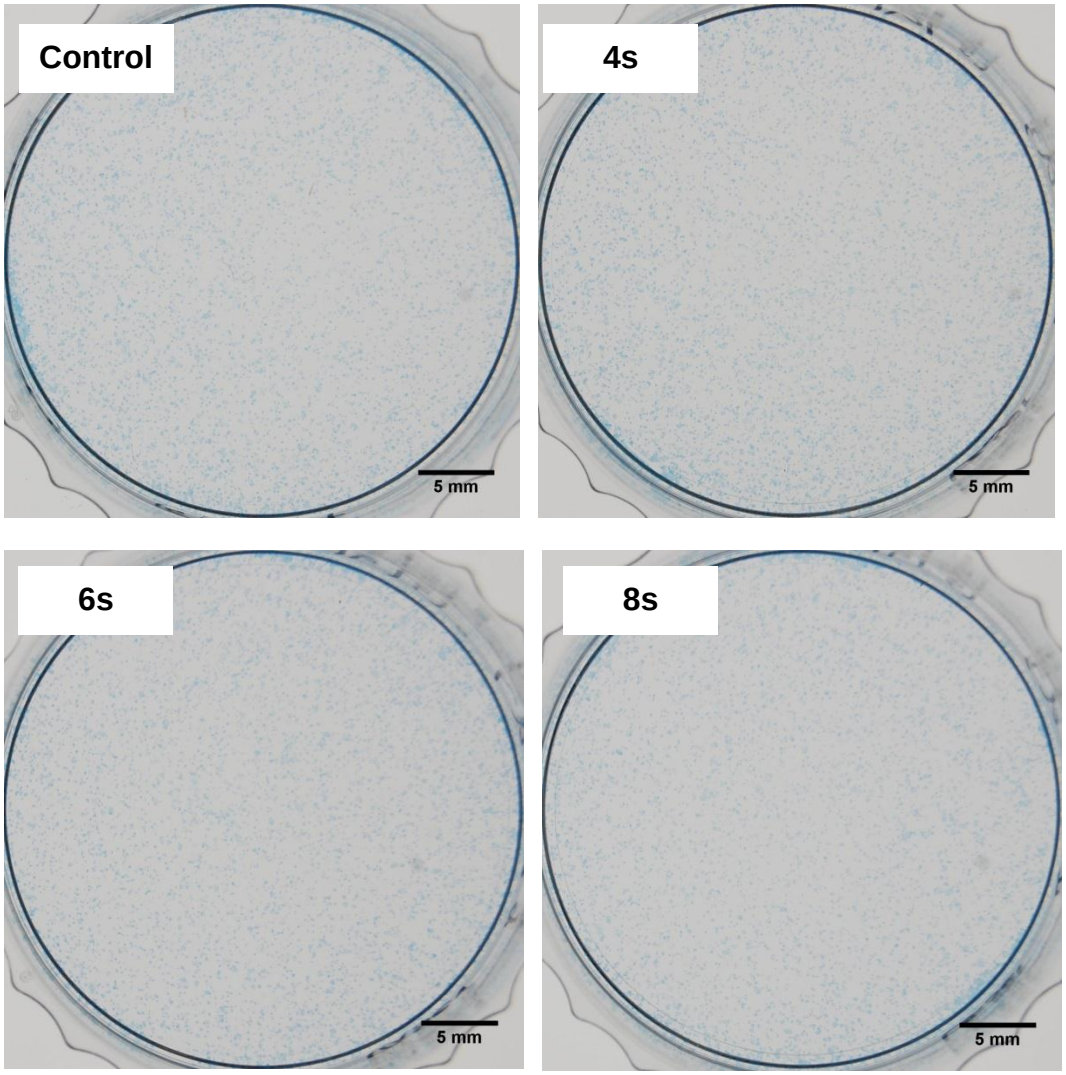

Figure 5.14: Methylene blue staining at day 3 for H400s laser irradiated for 4, 6 and 8s laser (7, 10 and 14J/cm^2) (n=3 in duplicate).

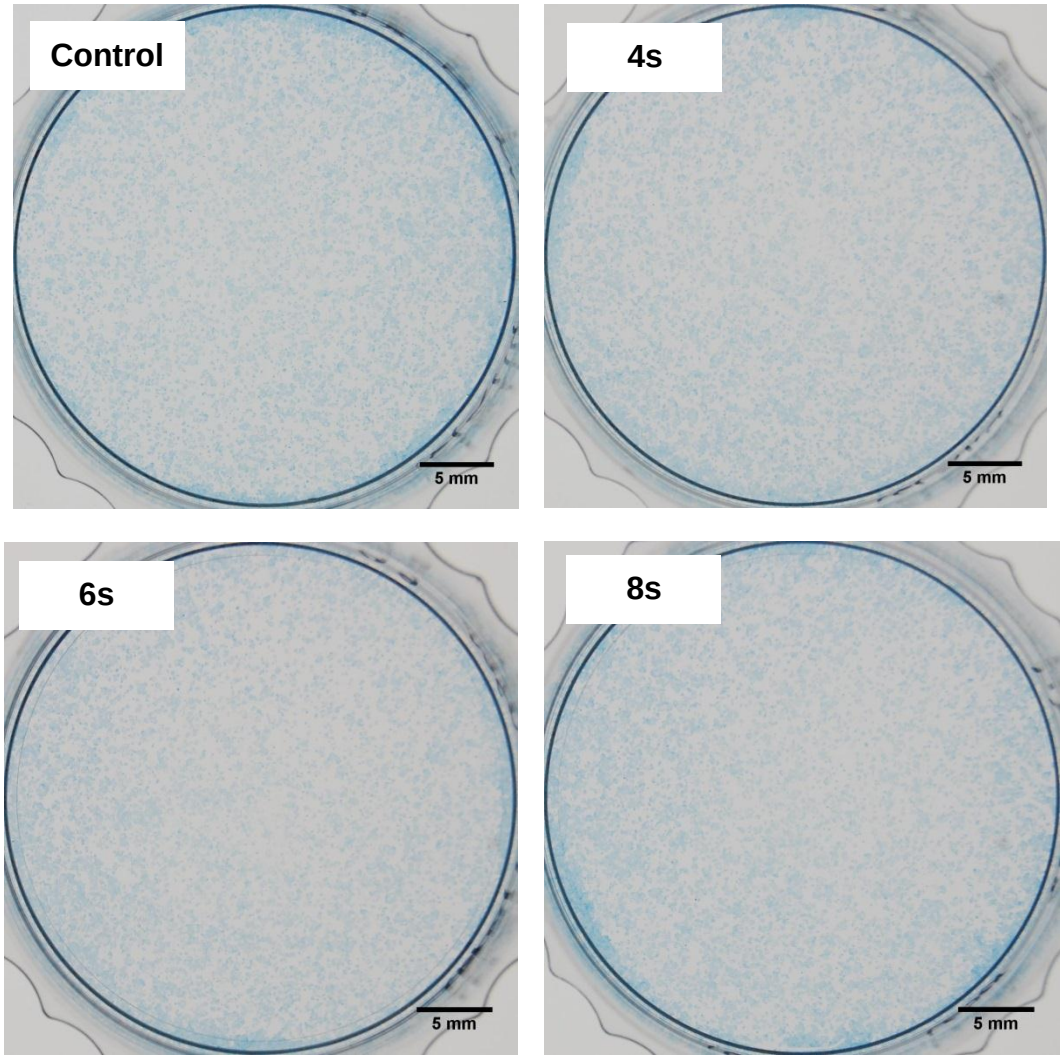

Figure 5.15: Methylene blue staining at day 4 for H400s laser irradiated for 4, 6 and 8s laser (7, 10 and 14J/cm^2) (n=3 in duplicate).

5.2 Discussion

This chapter describes 670nm laser irradiation in attempt to look at the possible biological responses of irradiated cells. Following optimisation, the cell count results showed increase cell number following 100 and 120s laser irradiation at a distance 33mm. The reason these two different distances were utilised was to determine the optimum condition when irradiating. Experimental conditions used cultureware directly on top of laser (0mm) or at a distance of 33mm. It was calculated for 0mm distance, irradiation time of 4, 6 and 8s where the irradiance value was 1788mW/cm^2 resulting in a radiant exposure of 7, 10 and 14J/cm^2 and at 33mm, 80, 100 and 120s were the irradiance value of 344mW/cm^2 resulted in 27, 34 and 41J/cm^2 radiant exposure. The irradiation at a distance of 33mm produced significant results in comparison to 0mm irradiation distance for cell counts and MTT assay (Figure 5.2 and 5.4). 120s irradiation at 33mm distance demonstrated significant result in these experiments. However, BrdU assay showed that laser irradiation for 6s (10J/cm^2 radiant exposure) at a distance of 0mm (Figure 5.5) was significantly increased. BrdU assay was performed following 4, 6 and 8s irradiation to examine the potential of those exposure times to trigger proliferation of H400s where cell count and MTT had shown no increase in cell number.

To further investigate H400 cellular responses and based on the significant results obtained utilising cell counts and MTT, immunocytochemical staining was performed on cells irradiated for 120s irradiation (41J/cm^2 – at 33mm distance) in order to explore NF-κB activation following irradiation and stimulation with *E. coli* LPS. Interestingly, the activation of NF- κB in non-irradiated H400 cells (Figure 5.7 no. 3)

was higher than irradiated (Figure 5.7 no. 1 and 2) and control (Figure 5.7 no. 4). However, this did not reach statistical significance compared to control. It is known that *E. coli* LPS stimulation results in activation of NF-κB indicated by translocation to the nucleus (Milward 2010), it would be of considerable interest if laser irradiation could modulate NF-kB activation, low level increases in non-stimulated cells may increase cellular protection by causing a downstream low grade inflammatory response. A study published by Chen *et al.,* (2011) observed significant activation of NF-κB in fibroblasts in response to 810nm laser irradiation and it is believed that different cell types may exhibit different patterns of NF-κB activation following laser irradiation (Chen *et al.,* 2011). More work is required to clarify the role of lasers in NF-kB activation in this experimental model system. NO and NF-κB assay kits would be essential to undergo for better understanding.

Selection of genes was chosen based on reports on gene expression related to cytochrome C oxidase and ATP synthesis (Houreld *et al.,* 2012, Masha *et al.,* 2013) and NF-κB activation in H400 oral epithelial cell line (Milward *et al.,* 2007). The ATP5G2 gene which role is to encode ATP synthase (Masha *et al.,* 2013) demonstrated significantly increased levels of expression after 120s laser exposure. Additionally, other genes; ATP5F1, COX6C, PPA1, MAPK11, NF-κB, NF-κB1E, NDUFA11 and NDUFS7; were observed showing upregulated either by 100 or 120s irradiation. The pattern of differential gene expression will allow further investigation in order to elucidate the pathways involved in cellular response to irradiation.

Activation of NF-kB and resulting gene expression changes may ultimately lead to increase levels of cellular cytokine release, this was assessed using a known surrogate marker of NF-kB activation and a key pro-inflammatory cytokine IL-8 by ELISA. Using a commercially available ELISA kit, IL-8 was determined in media from laser irradiated and stimulated by *F. nucleatum* and *P. gingivalis,* both bacteria playing central roles in the pathogenesis of periodontal disease. IL-8 was significantly upregulated in H400s irradiated for 120s following *F. nucleatum* stimulation [Figure 5.13 (a)] and downregulated in cells irradiated for 100s and stimulated with *P. gingivalis* [Figure 5.13 (b)]. These differential response may be important in developing a light based therapeutic strategy for managing periodontal disease and further work is required to determine how light might act on the hyper inflammation characteristic of the periodontal.

It was proposed that due to the narrow light beam generated by laser devices that this may limit the number of cell that receive light exposure and may reduce any cellular responses seen in a cell monolayer, i.e. laser beam is approximately 5mm whereas the dishes used to culture cells was 35mm. However by using methylene blue staining it appears to indicate that cells grow evenly across the cell culture plate and are not just influenced by the laser beam diameter.

This chapter utilised a single wavelength laser (670nm) the prospect of what influences different wavelengths of light would make was raised in subsequent chapters the cellular influences of LED were determined as these offer a far wider range of wavelengths than lasers.

CHAPTER 6: H400 RESPONSES TO SINGLE LED

6.1 H400s responses following LED irradiation

6.1.1 Introduction

Following on from the previous chapter which investigated cellular responses to irradiation by lasers, this chapter will investigate the effects generated in H400 cells exposed to single LED irradiation. This work utilised an LED with a wavelength of 630nm and cells were irradiated for 90 and 181s (control was non-irradiated cells) this equated to a radiant exposure of 0.5 and 1.0J/cm^2 respectively (see Section 3.2.1.3 and Table 2.6). Cell cultureware was placed at a distance above the LED of 33mm where the irradiance value obtained was 5.5mW/cm^2 (see Table 2.6). Both single and double dosing experimental conditions were investigated in order to optimise cellular responses (Section 2.2.3.2).

6.1.2 Results

H400s cells culture were irradiated 24h post-seeding and biological responses examined by cell counting, MTT assay, NF-κB activation, gene expression and IL-8 detection. The results are presented as a percentage of the non-irradiated control.

6.1.2.1 Cell count

These data indicate an increase in cell growth following single dosing (90 and 181s) at 3 days post irradiation and with double dosing (181s) at 5 days post irradiation, using LED irradiation but they did not reach statistical significance (Figure 6.1). Data for single dosing (90 and 181s) and double dosing (90s) showed no significant differences compared to non-irradiated control (Figure 6.1 (b)).

(a) day 3 post irradiation-single dosing

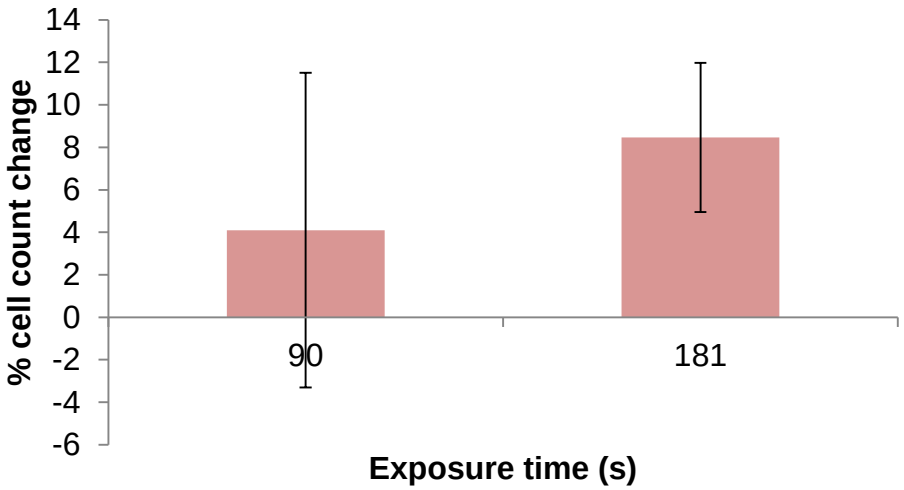

(b) day 5 post-irradiation-single and double dosing

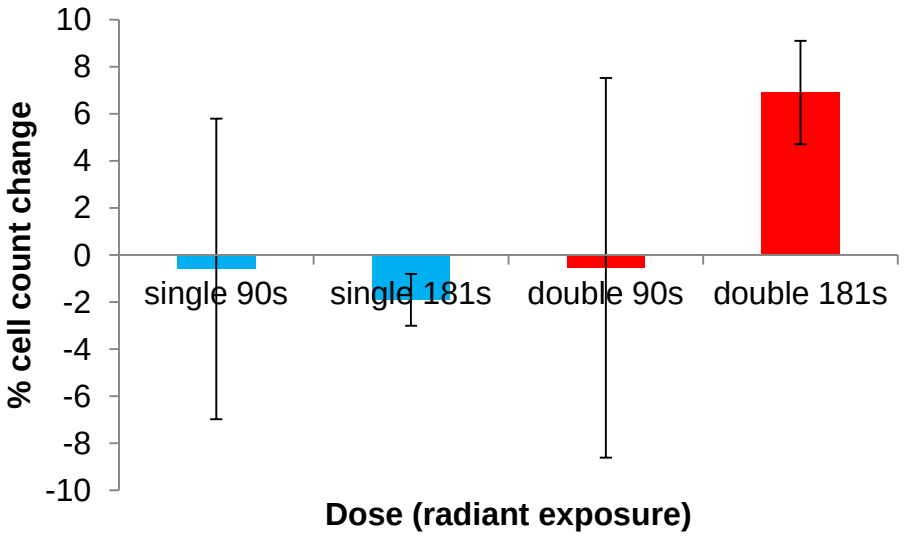

Figure 6.1: Effect of LED irradiation on H400 cell growth determined by cell counting at (a) day 3 post irradiation for single dosing and (b) day 5 post-irradiation for single and double dosing. Cells were irradiated for 90 or 181s at days 1 and 3 post-seeding. Results are represented as a percentage of non-irradiated control. Results are mean ± SD (n=4 in duplicate).

6.1.2.2 MTT assay

MTT assay was performed on the same day as the cell counts were determined. Results for day 3 post exposure (Figure 6.2 (a)) indicated an increase in mitochondrial activity for both 90 and 181s LED irradiation, however these differences were not significant. The MTT data generated on day 5 for single and double dosing regimens was variable, with single 90s irradiation and double dosing for 181s showing a reduction in MTT activity, whereas single dose of 181s and double dose of 90s showed increases over the non-irradiated controls. These data did however not reach significance.

6.1.2.3 NF-κB activation

Activation of NF-κB in H400 cells LED irradiated and stimulated with *E. coli* LPS was assessed using immunocytochemical anaysis. Cells were grown on 4 well glass slides and were irradiated for 191s (1J/cm^2 at a distance of 33mm) 1h before *E. coli* LPS stimulation (20µg/ml). These results indicated the ability of *E. coli* LPS to activate NF-kB as demonstrated by nuclear translocation. Exposure to LED in the absence of *E. coli* stimulation did not show NF-kB activation. The use of LED irradiation in cells exposed to *E. coli* stimulation did not alter the levels of NF-kB activation (Figures 6.3 and 6.4).

(a) day 3 post irradiation-single dosing

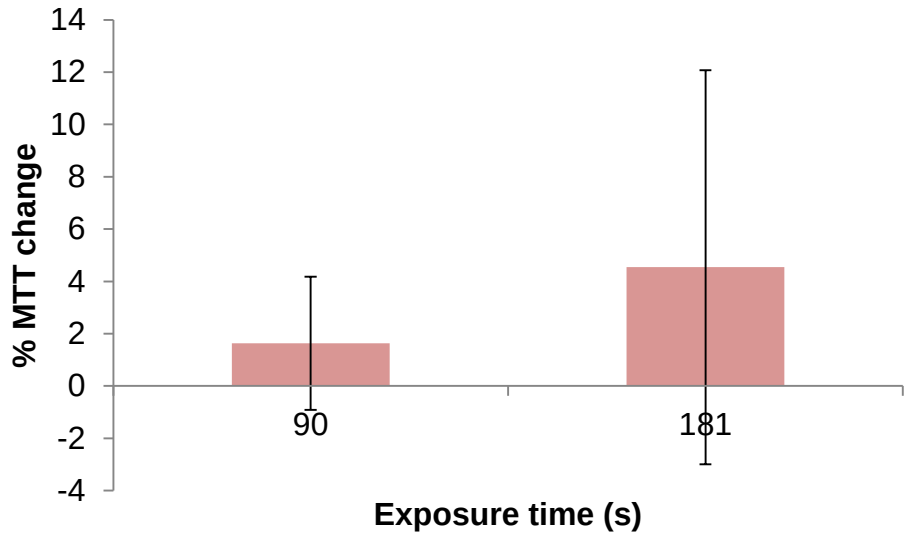

(b) day 5 post-irradiation-single and double dosing

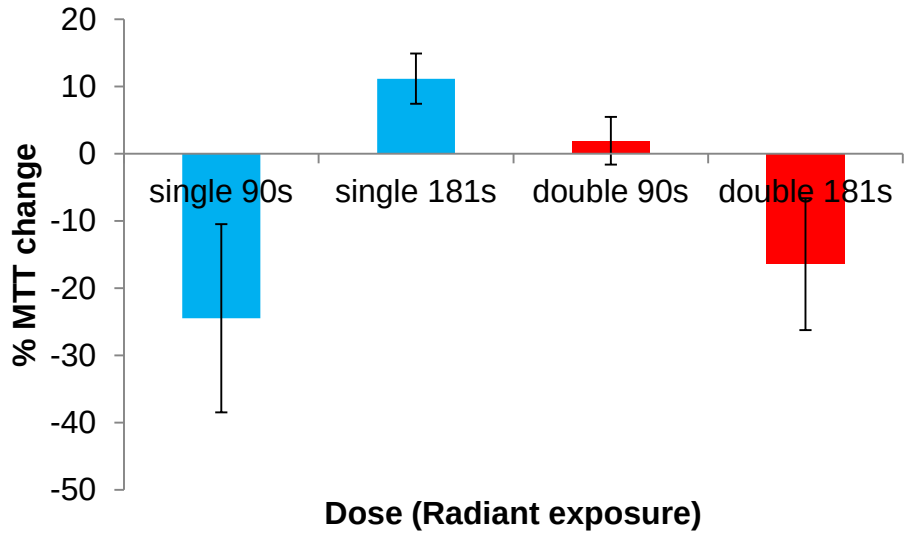

Figure 6.2: Cell counts at (a) day 3 for single dose and (b) day 5 for single and double dose for culture irradiated for 90 and 181s at days 1 and 3 post-inoculation. Results are mean ± SD (n=3 in duplicate).

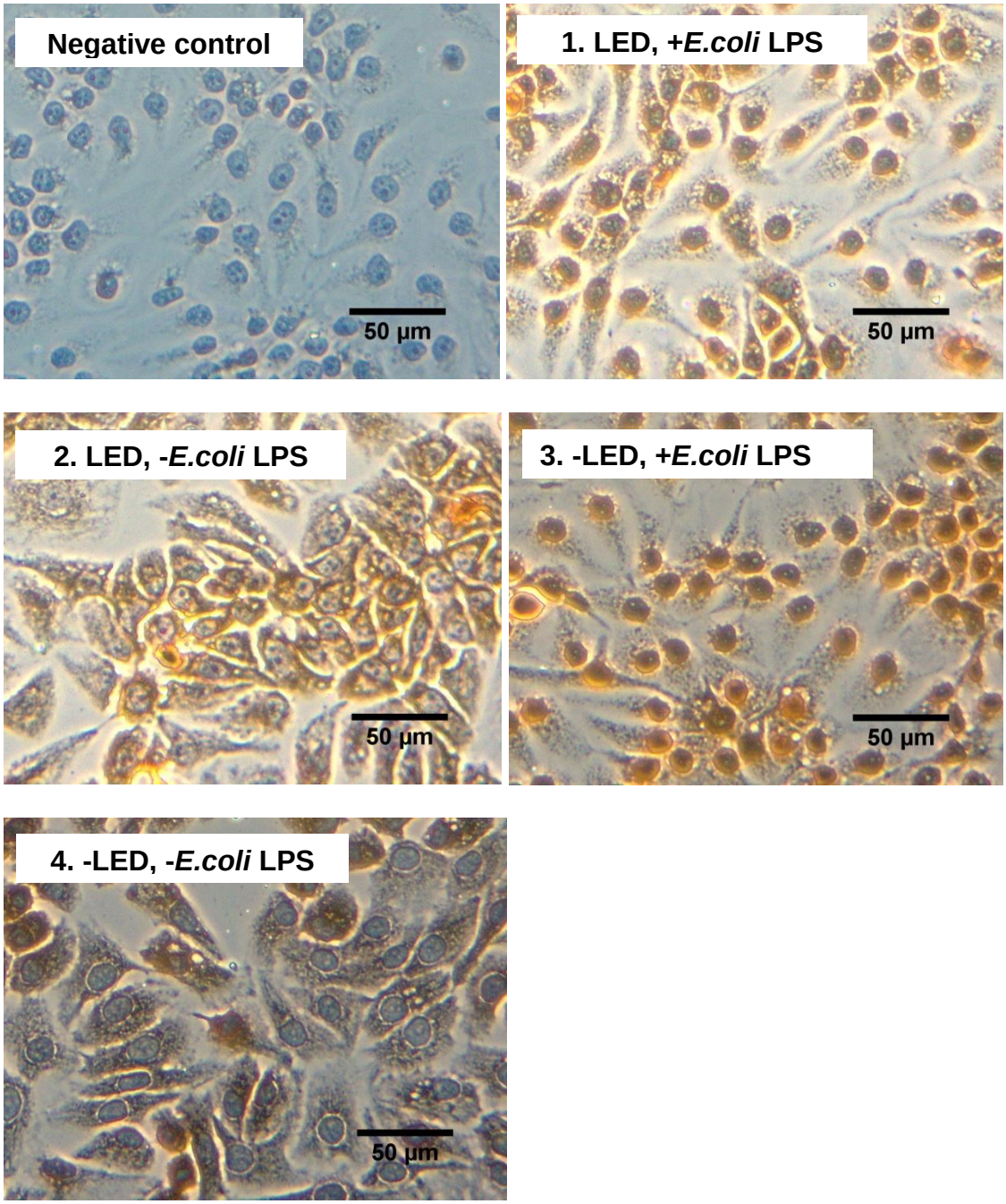

Figure 6.3: Photos of H400 cells irradiated for 181s (or with no irradiation) with 630nm LED (1J/cm^2) 1h prior to *E. coli* stimulation for 1h (or non-stimulated control). Cells were stained for NF-kB using immunocytochemistry (+ indicates with condition and – means without) (Level of magnification - 20x).

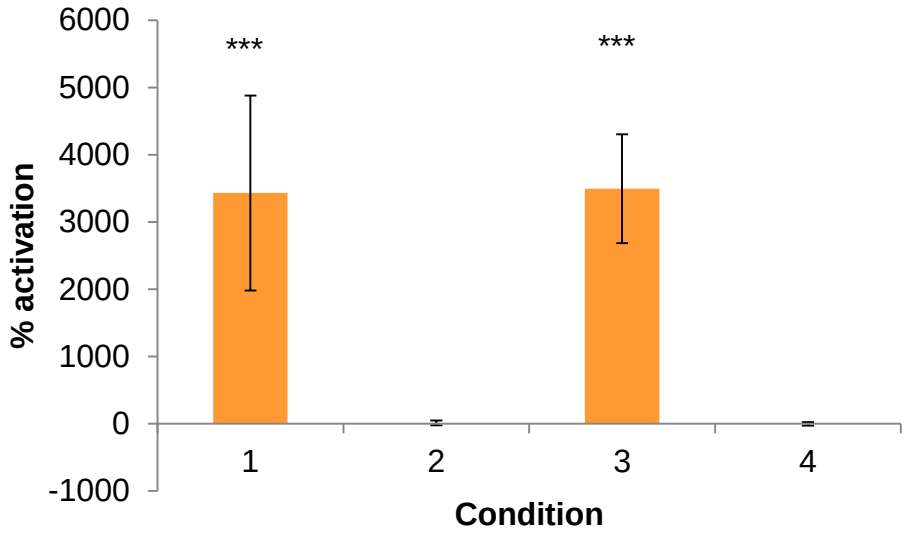

Figure 6.4: H400 cells irradiated and non-irradiated with 181s 630nm LED and stimulated (or non-stimulated) for 1h with *E. coli* LPS. The percentage of NF-kB activated cells was compared to control (non-irradiated and non-stimulated). X axis labels relate to immunocytochemical images in figure 6.3 (n=2 in single). Results are mean ± SD. ****p*<0.001.

6.1.2.4 PCR gene expression

As in previous chapter, gene expression changes following irradiation using the single LED light source by PCR were determined for both single and double dosing regimens. H400 cells were irradiated for 90 and 181s for both single and double dosing and harvested at days 3 (single dose) and 5 (single and double dose). Data generated for the single dosing regimen at day 3 post exposure (Figures 6.5 & 6.6) indicated a number of changes in gene expression in comparison to the non-irradiated control, there was also differences between the two irradiation times used. Looking at the data for the majority of genes investigated increased irradiation time resulted in a decrease in relative gene expression with the exception of COX6B2 and NF-kB1E which showed a significant increase in gene expression.

Gene expression data generated for single and double dosing regimens at 5 days post exposure (Figures 6.7 & 6.8) also showed variable results. In single dose experiments 5 days post irradiation increased levels of gene expression were seen with longer irradiation times (181s) in ATP5G2, ATP5F1, NF-kB, NDUFS7, NDUFA11, with other genes showing reduced or unchanged levels of activation. For double dosing experiments increased levels of gene expression were seen at the longer exposure time point of 181s (in comparison to 90s) in COX6C, COX6B2, NF-kB2, NDUFA11, NDUFS7 and MAPK11 with other genes showing reduced or unchanged levels. These results have the potential to help understand the pathways that may be activated as a result of LED irradiation and will be fully discussed later in this thesis.

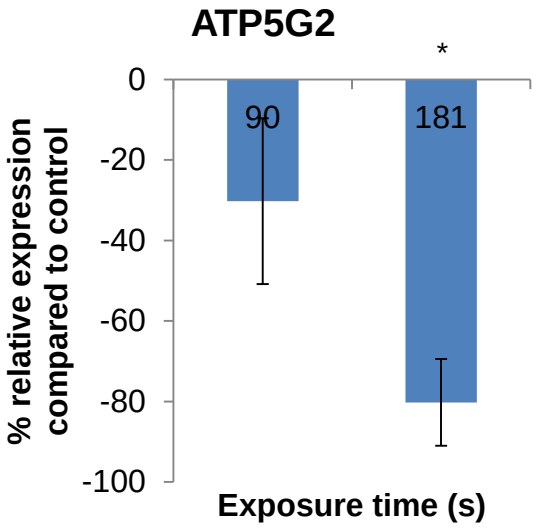
ATP5G2
*
0
-20
-40
-60
-80
-100
90
181
% relative expression compared to control
Exposure time (s)

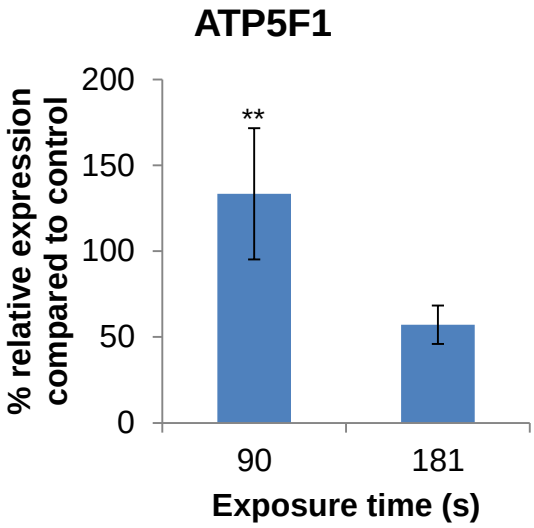
ATP5F1
200
150
100
50
0
**
90
181
% relative expression compared to control
Exposure time (s)

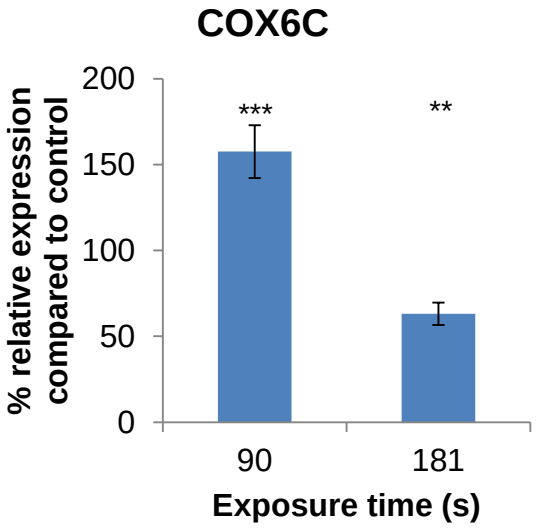
COX6C
200
150
100
50
0
***
**
90
181
% relative expression compared to control
Exposure time (s)

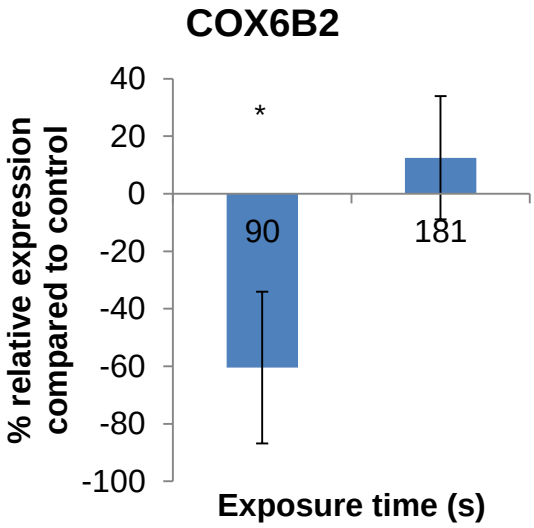
COX6B2
40
20
0
-20
-40
-60
-80
-100
*
90
181
% relative expression compared to control
Exposure time (s)

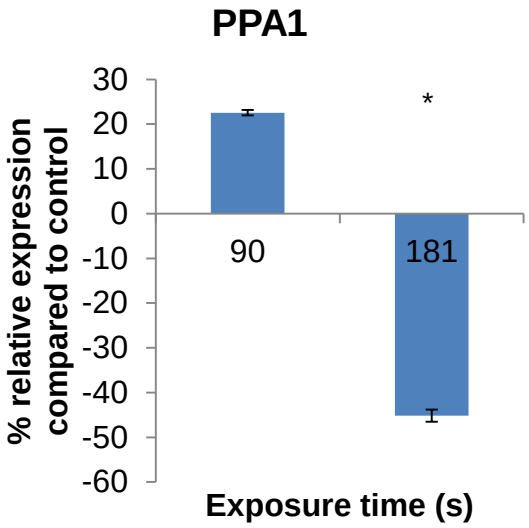
PPA1
% relative expression compared to control
30
20
10
0
-10
-20
-30
-40
-50
-60
*
90
181
Exposure time (s)

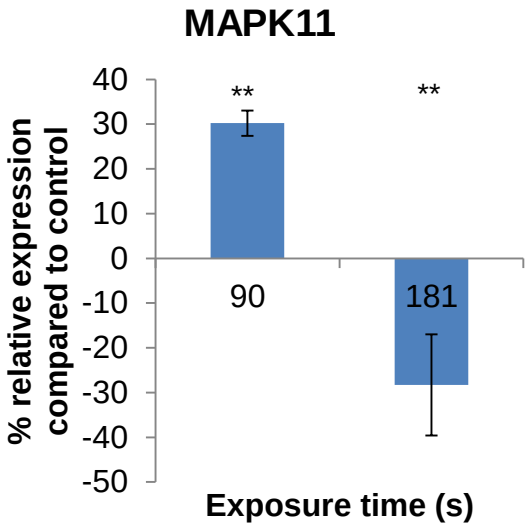
MAPK11
% relative expression compared to control
40
30
20
10
0
-10
-20
-30
-40
-50
**
**
90
181
Exposure time (s)

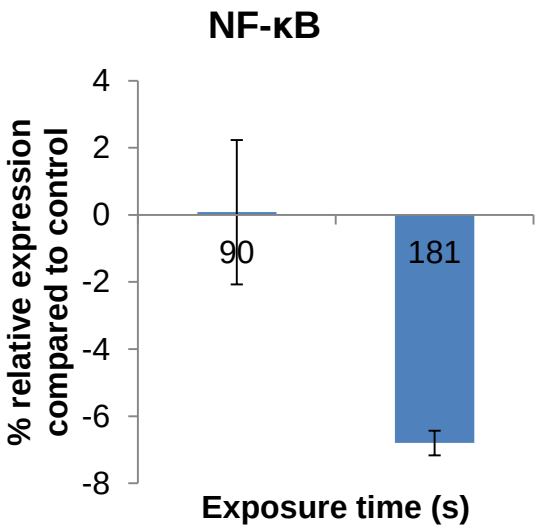
NF-κB
% relative expression compared to control
4
2
0
-2
-4
-6
-8
90
181
Exposure time (s)

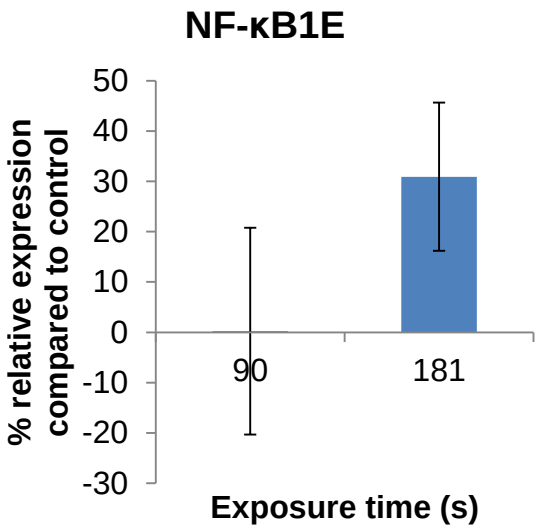
NF-κB1E
% relative expression compared to control
50
40
30
20
10
0
-10
-20
-30
90
181
Exposure time (s)

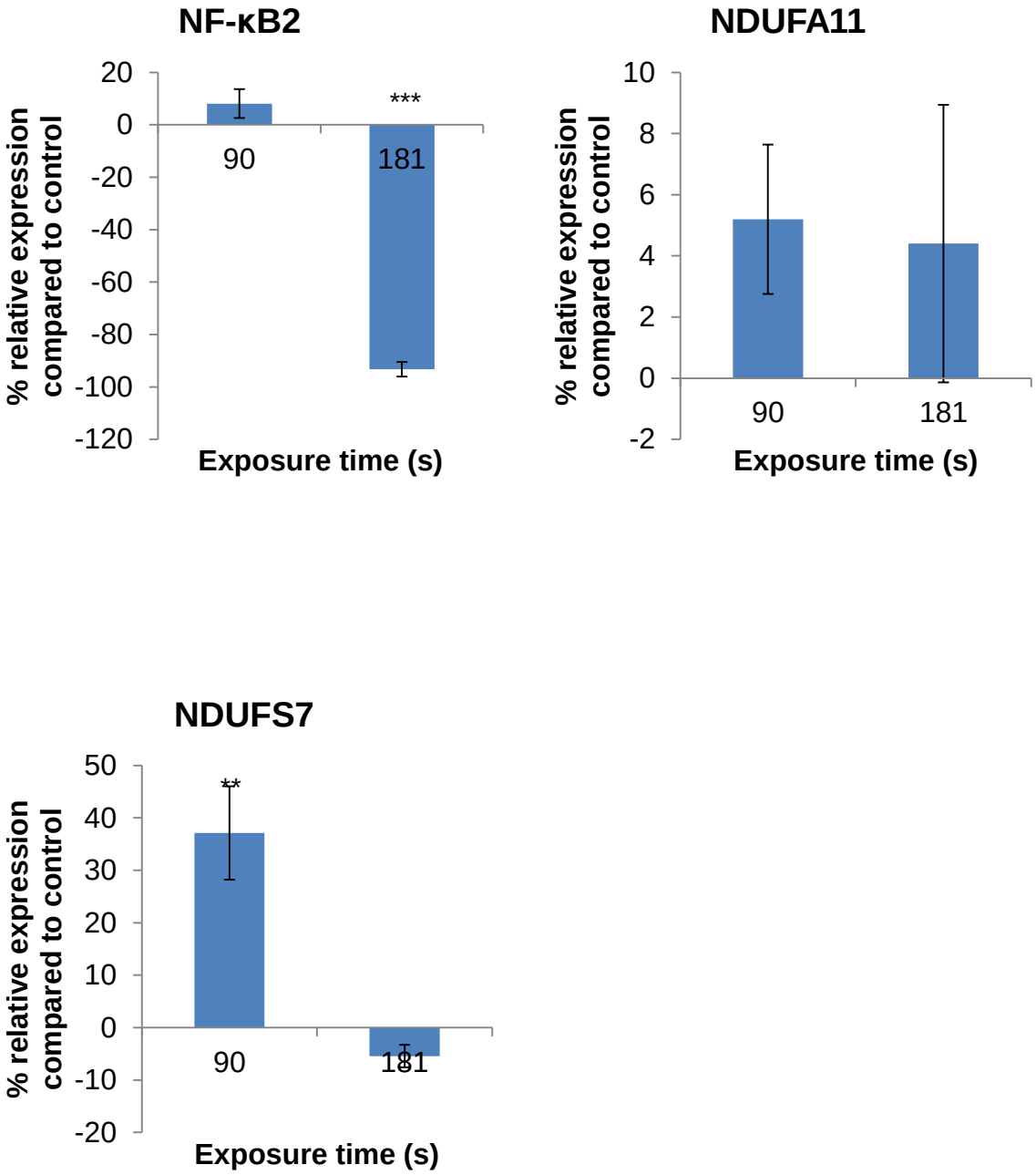

Figure 6.5: Expression level of genes of irradiated H400s with single dose 90 and 181s where the cells were harvested on day 3. Results are mean ± SD (n=3 in duplicate). *p<0.05, **p<0.01, ***p<0.001.

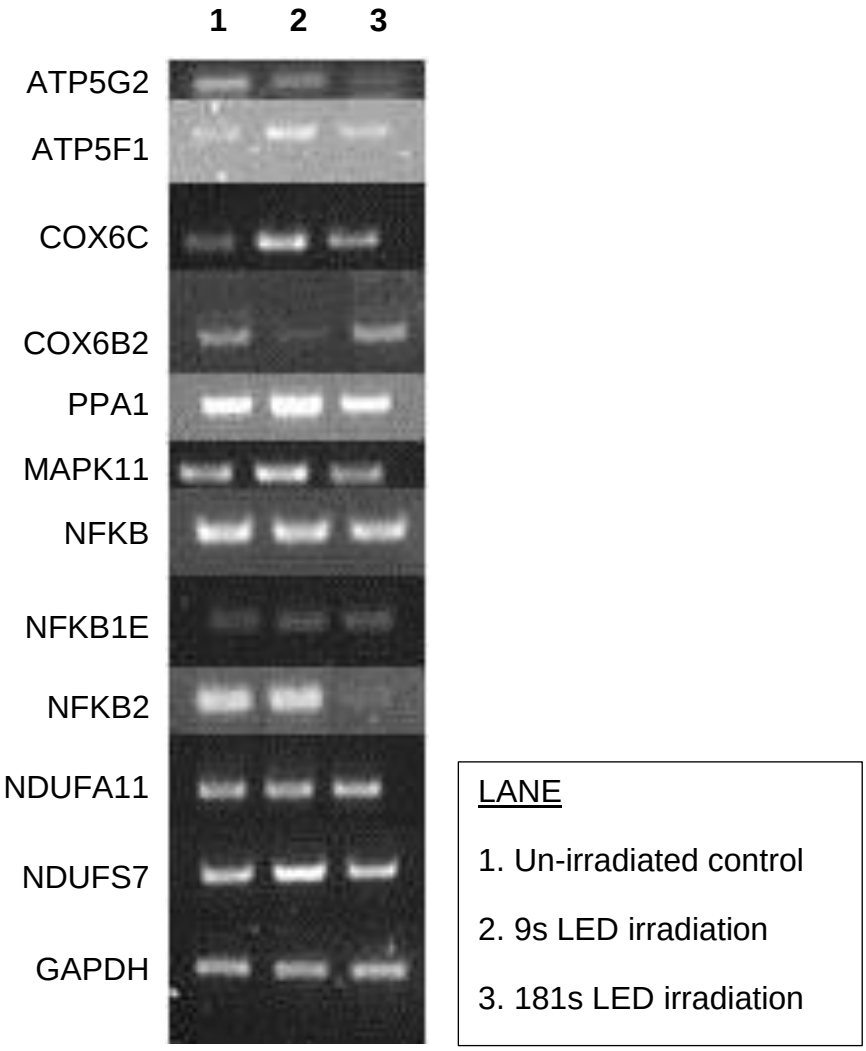

Figure 6.6: Diagram of agarose gel electrophoresis for PCR of H400 cell culture irradiated with single dose LED (n=3 in duplicate).

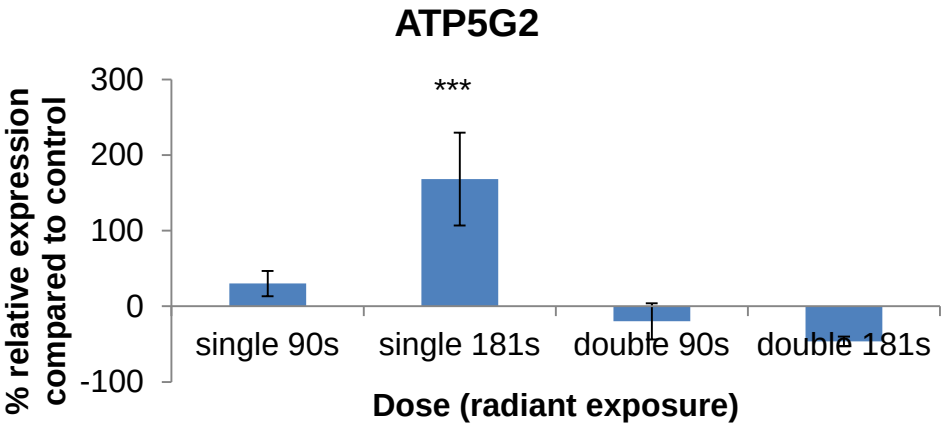
ATP5G2
% relative expression compared to control
300
200
100
0
-100
***
single 90s
single 181s
double 90s
double 181s
Dose (radiant exposure)

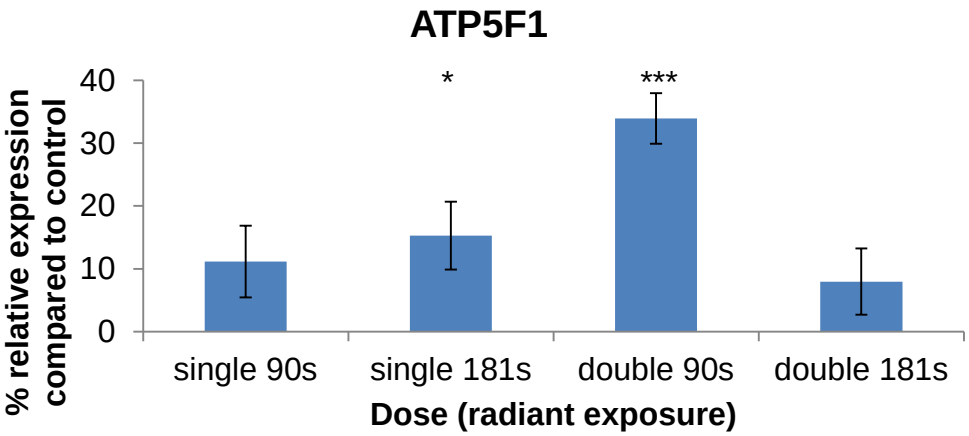
ATP5F1
% relative expression compared to control
40
30
20
10
0
*
***
single 90s
single 181s
double 90s
double 181s
Dose (radiant exposure)

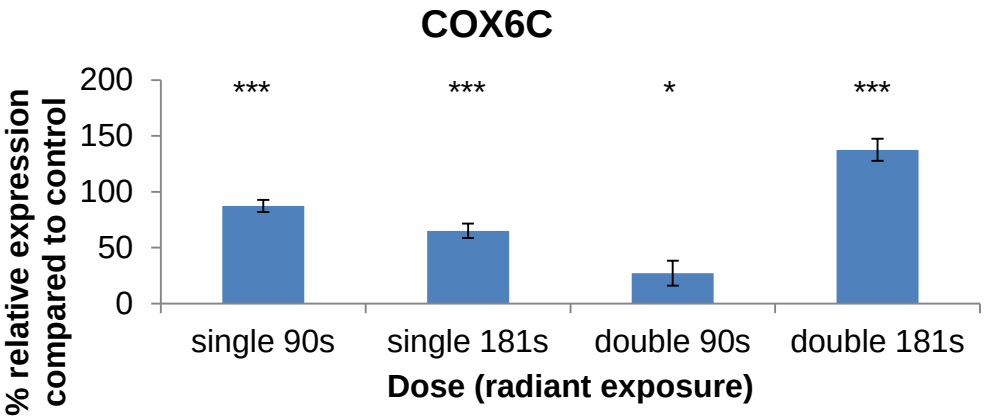
COX6C
% relative expression compared to control
200
150
100
50
0
***
***
*
***
single 90s
single 181s
double 90s
double 181s
Dose (radiant exposure)

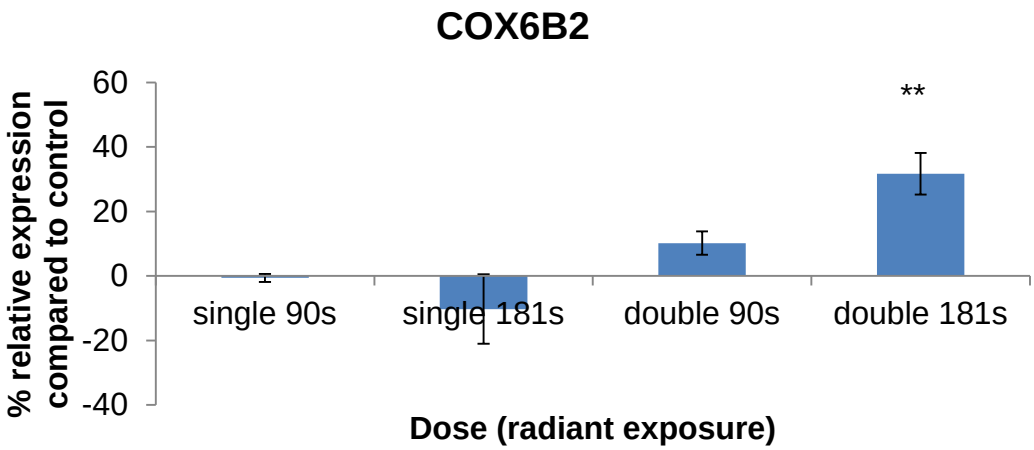
COX6B2
% relative expression compared to control
60
40
20
0
-20
-40
**
single 90s
single 181s
double 90s
double 181s
Dose (radiant exposure)

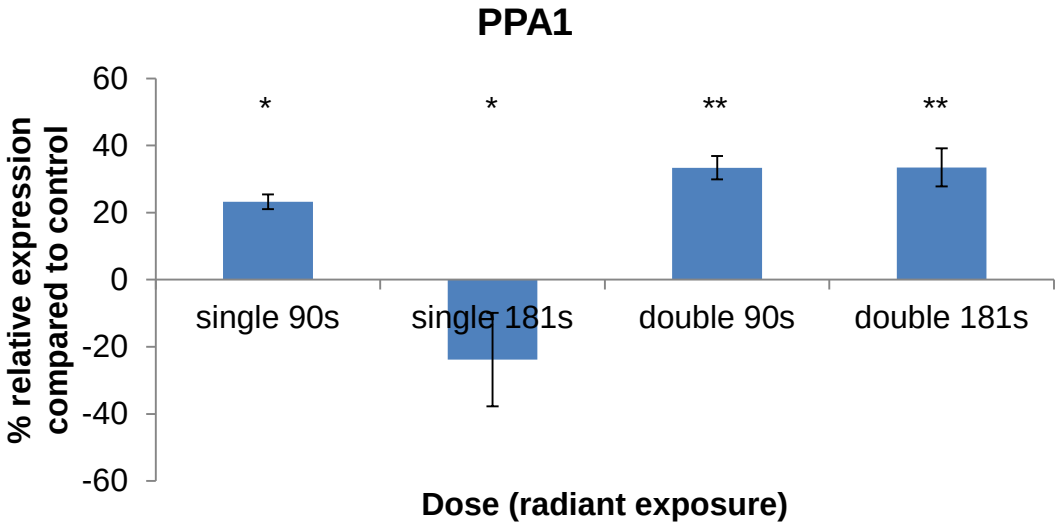
PPA1
% relative expression compared to control
60
40
20
0
-20
-40
-60
*
*
**
**
single 90s
single 181s
double 90s
double 181s
Dose (radiant exposure)

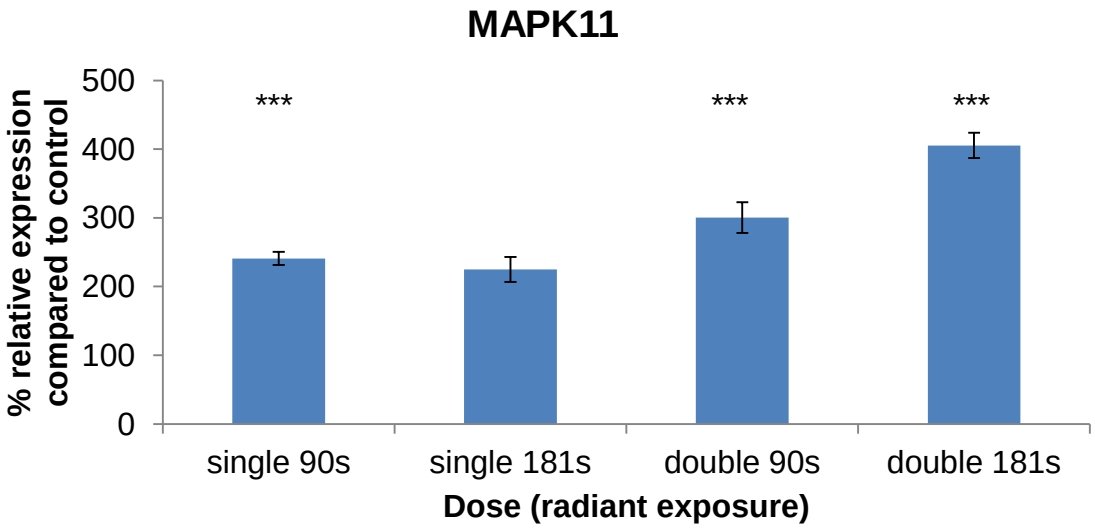
MAPK11
% relative expression compared to control
500
400
300
200
100
0
***
***
***
single 90s
single 181s
double 90s
double 181s
Dose (radiant exposure)

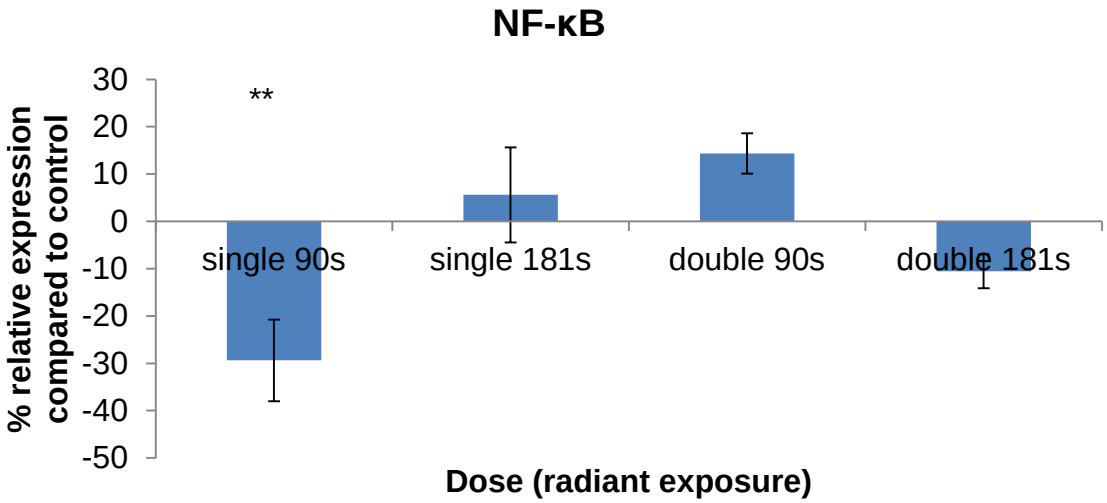
NF-κB
% relative expression compared to control
30
20
10
0
-10
-20
-30
-40
-50
**
single 90s
single 181s
double 90s
double 181s
Dose (radiant exposure)

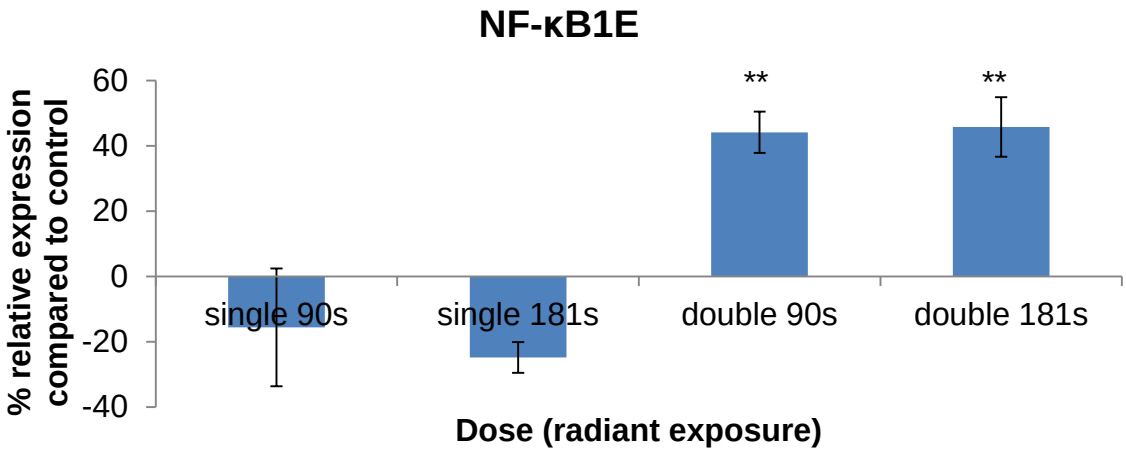
NF-κB1E
% relative expression compared to control
60
40
20
0
-20
-40
**
**
single 90s
single 181s
double 90s
double 181s
Dose (radiant exposure)

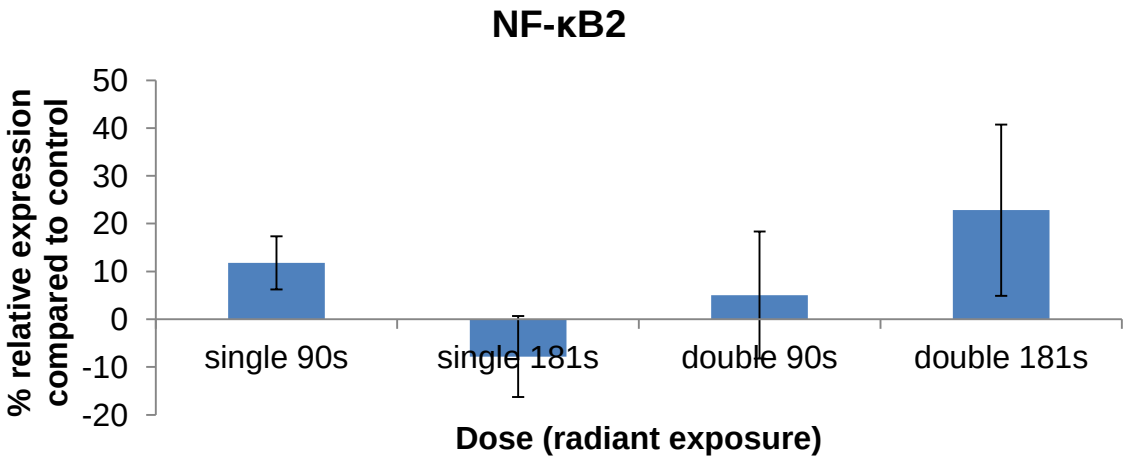
NF-κB2
% relative expression compared to control
50
40
30
20
10
0
-10
-20
single 90s
single 181s
double 90s
double 181s
Dose (radiant exposure)

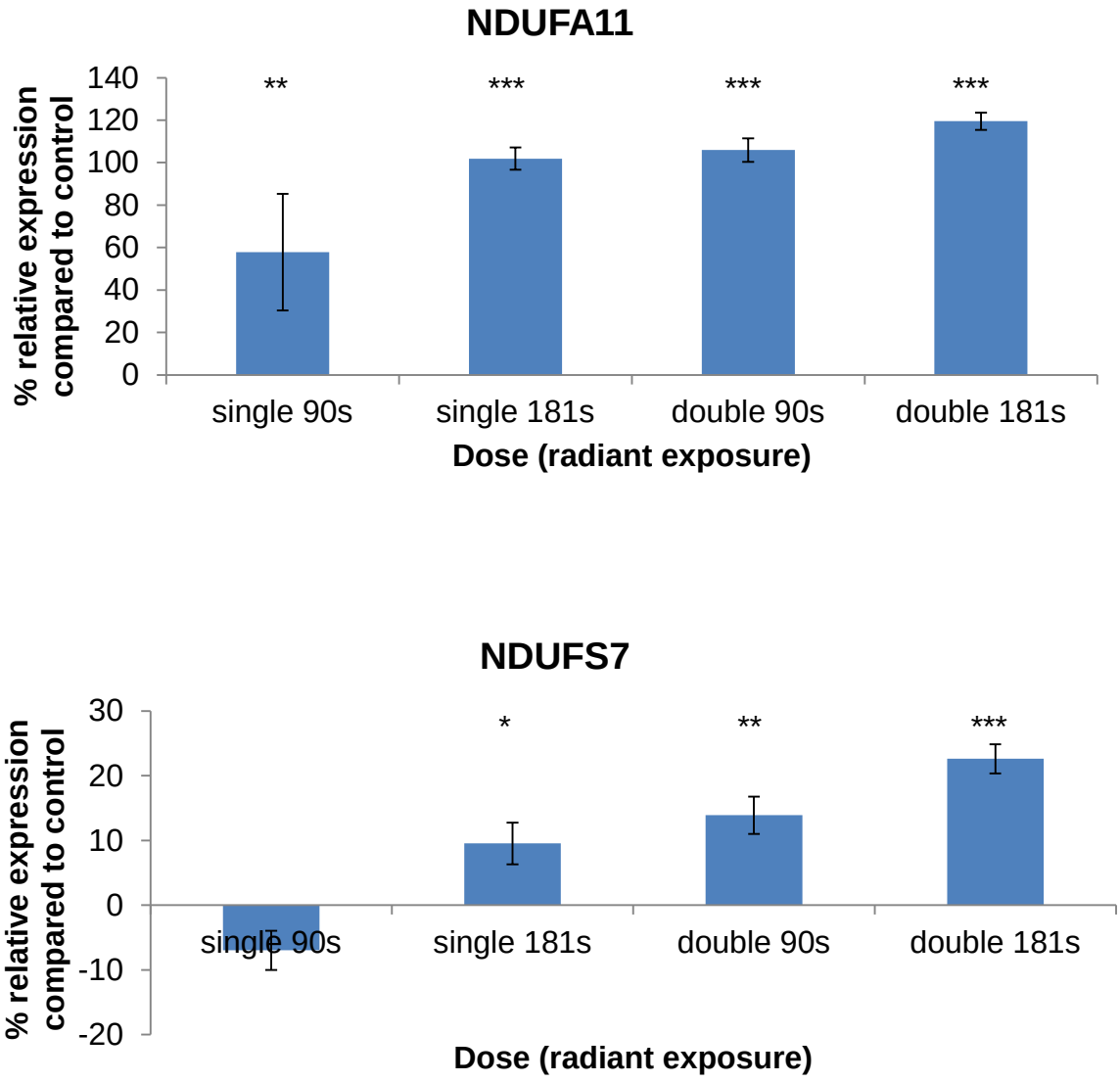

Figure 6.7: Relative gene expression changes of irradiated H400 cells with single or double dosing for either 90 or 181s. Cells were harvested on day 5. Results are mean ± SD (n=3 in duplicate). *p<0.05, **p<0.01, ***p<0.001.

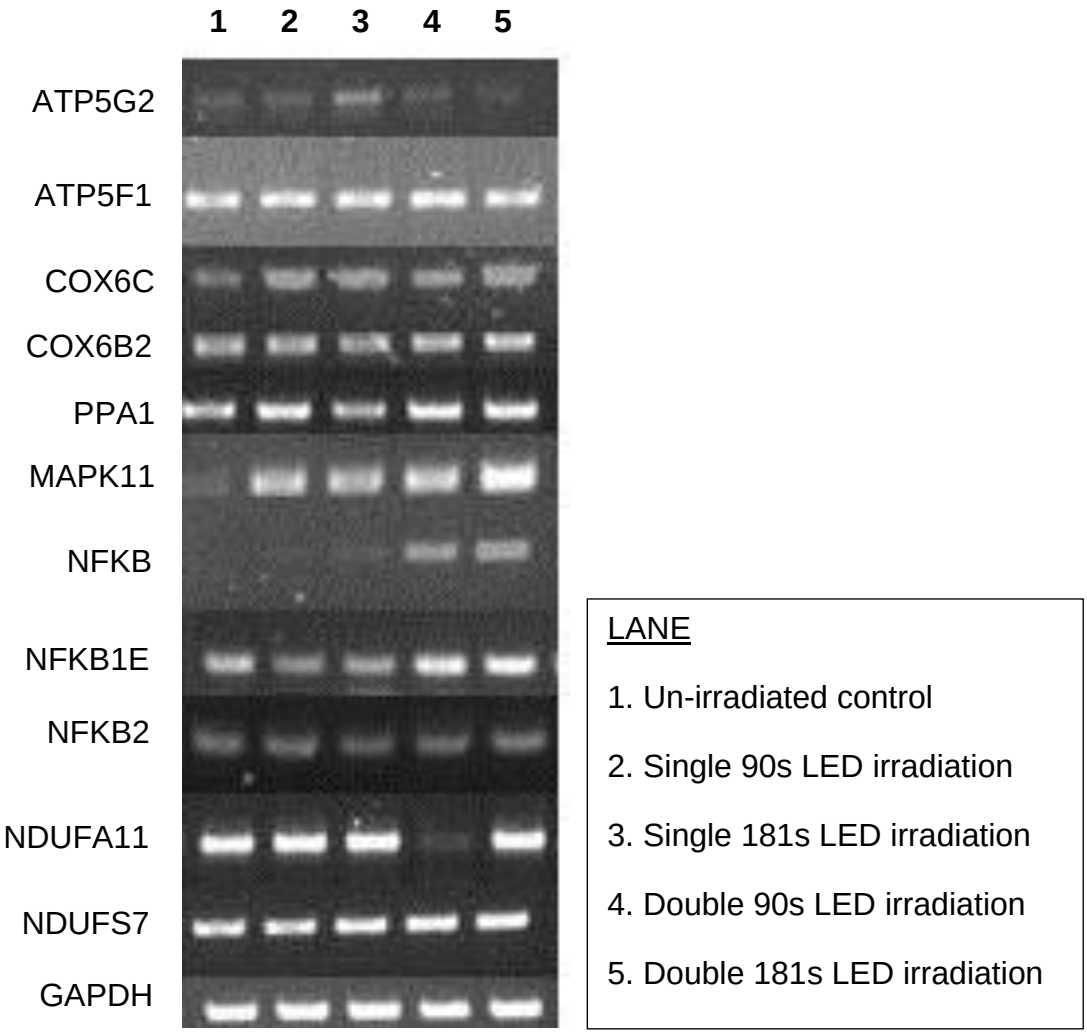

Figure 6.8: Representative gel electrophoresis image for gene expression following LED irradiation utilising single or double dosing with an exposure time of 90 or 181s. RNA harvested on day 5. Results are mean ± SD (n=3 in duplicate).

6.1.2.5 ELISA IL-8 detection following LED irradiation and bacterial stimulation

Previous data presented in this chapter suggested the inability of LED irradiation to inhibit NF-kB activation in H400 cells stimulated with *E. coli* LPS, which is a known activator of NF-kB and is therefore a useful control to ensure predicted cell behaviour. However *E. coli* is not clinically relevant in periodontal disease, so two key periodontal pathogens were utilised to determine pro-inflammatory cell activation via IL-8 (a surrogate marker of NF-kB activation).

IL-8 levels of H400 cells stimulated (by *F. nucleatum, P. gingivalis,* or non-stimulated control) and LED irradiated (or non-irradiated control) using a single or double dosing regimen for 90 or 181s (0.5 and 1J/cm^2) were examined on days 3 and 5 post irradiation.

An initial standard curve was performed using standard controls supplied within the manufacturer's kit (see Figure 5.11 for standard curve). Levels of IL-8 were compared to non-irradiated and non-stimulated controls (Figures 6.9, 6.10 and 6.11) results showed no statistically significant differences but some interesting trends were noted and will be discussed later.

(a)

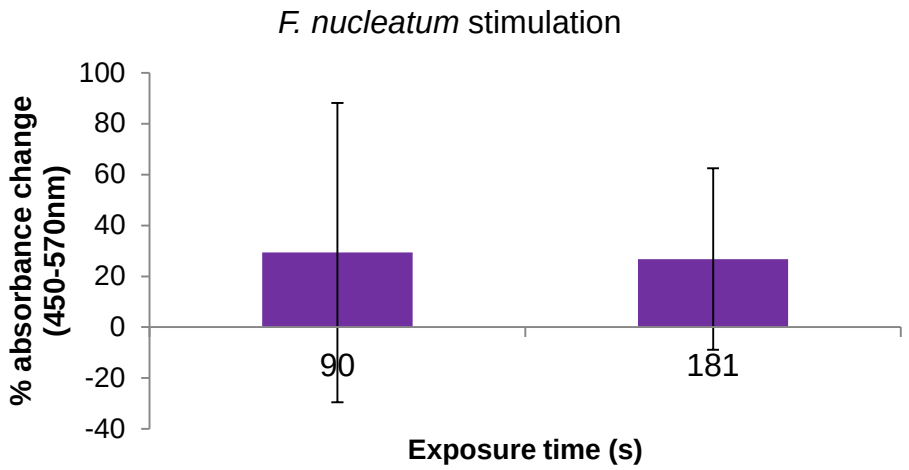

(b)

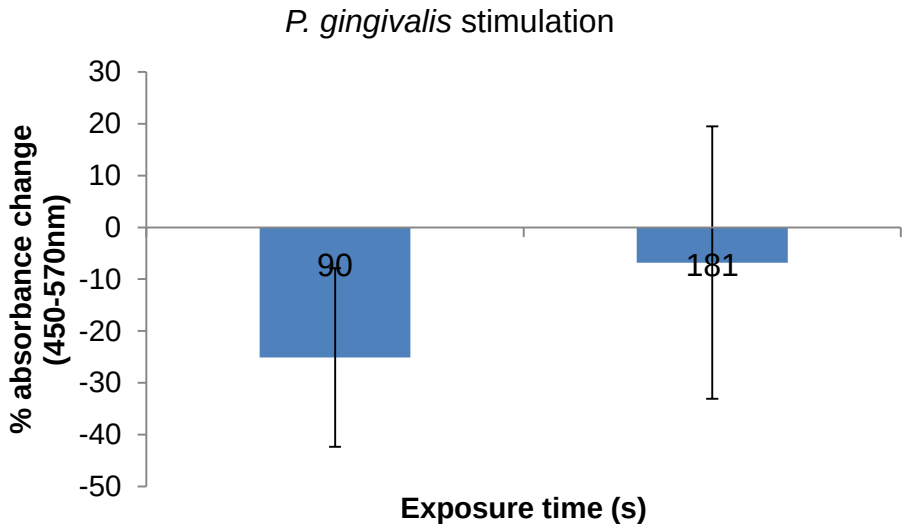

Figure 6.9: Diagram shows the relative changes in IL-8 production normalised to control for single dose LED irradiation with supernatant harvested at day 3. Results are mean ± SD (n=3 in single).

(a)

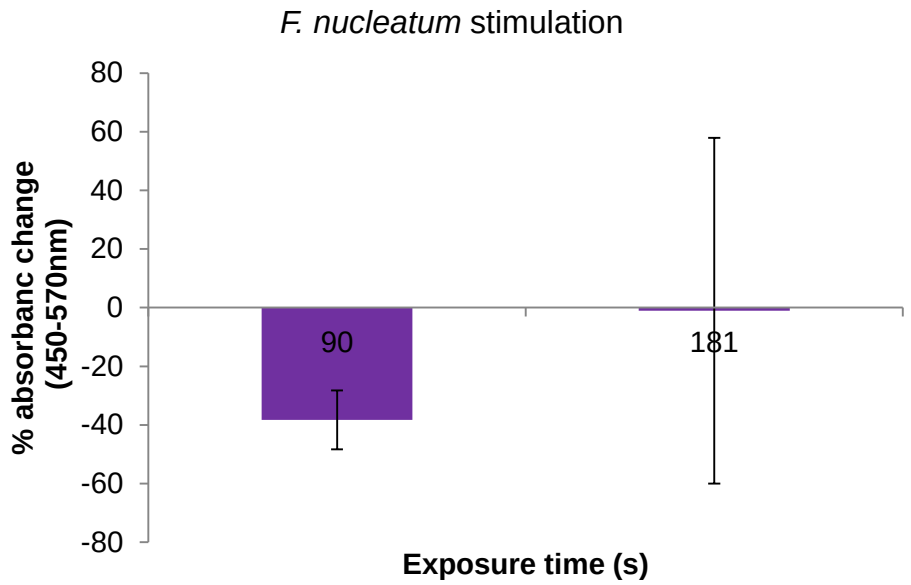

(b)

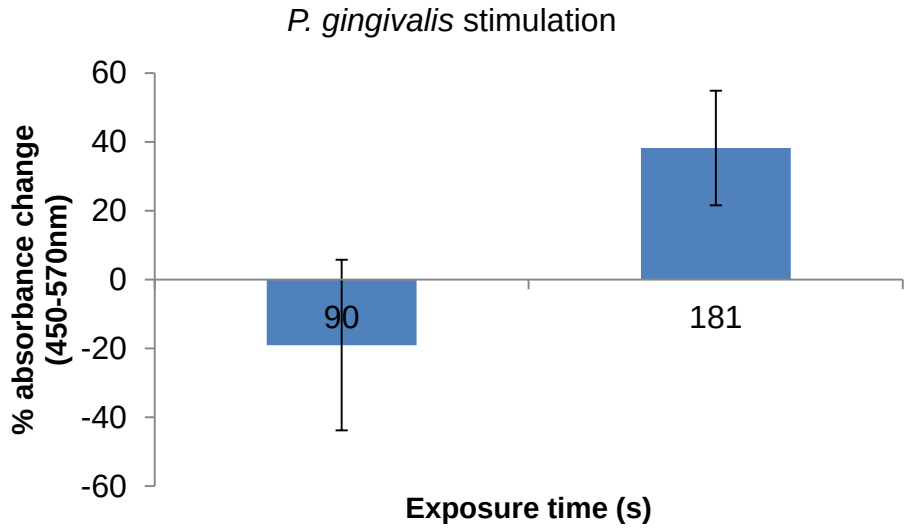

Figure 6.10: Illustrates the percentage change in IL-8 production for single dose LED irradiation with supernatant isolated at day 5. Results are mean ± SD (n=3 in single).

(a)

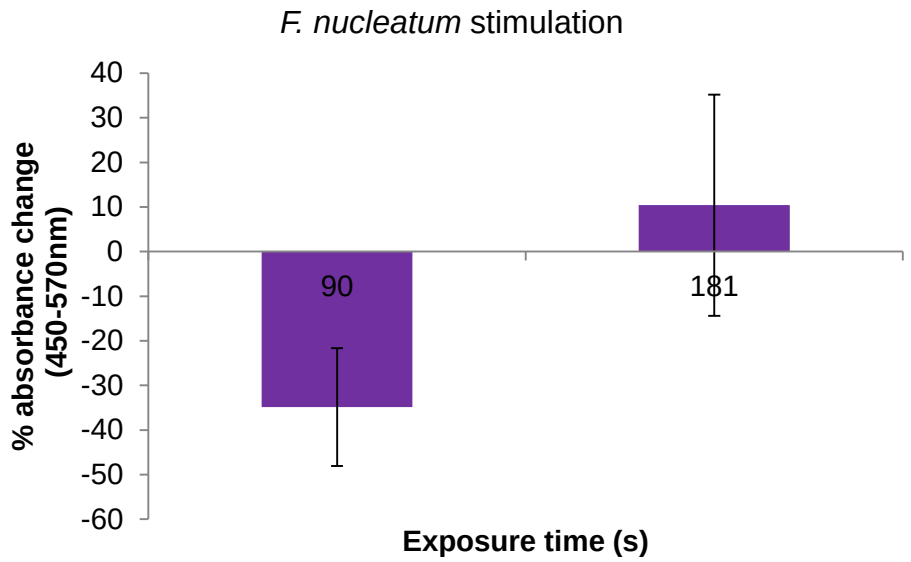

(b)

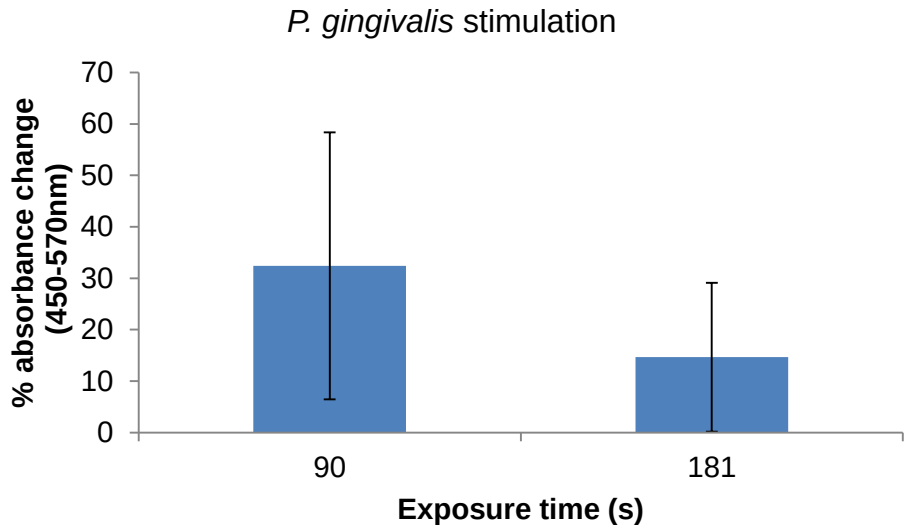

Figure 6.11: Data showing percentage change (compared to control) of IL-8 for double dose LED irradiation from supernatants harvested on day 5. Results are mean ± SD (n=3 in single).

6.2 Discussion

LED irradiation of H400 cells were performed utilising a similar experimental protocol to the laser experiments of the previous chapter, where the distance between LED and cell monolayer was 33mm. H400 cell were LED irradiated for either 90 or 181s (0.5 and 1J/cm^2 radiant exposure respectively), using both single and double dosing regimens. All data is presented as percentage of change compared to negative control.

The radiant exposure is an important parameter in irradiating cells and determination of the optimal value is central to ensuring delivery of a photostimulatory effect. Indeed excess radiant exposure can result in bioinhibitory effects (Barolet 2008). Pilot experiments were undertaken and described in Appendix 2, these indicated that irradiation of 90 or 181s which equates to 0.5 or 1J/cm^2 radiant exposure respectively in either a single or double dose protocol should be used in further experiments. Figure 6.1 presents the cell growth data for H400 cell cultures irradiated by LED at 33mm distance between the device and the cell monolayer. Day 3 (24h post-irradiation) cell counts with both experimental conditions showed increased cell number compared to non-irradiated controls whilst the cell count on day 5, showing the percentage was less for single dose 90 and 181s and double dose 90s but greater for double dose 181s. However, these data did not research statistical significance. MTT assay results demonstrated a similar pattern to the cell count data. MTT detection on day 3 was higher than control for 90 and 181s irradiation. MTT levels were greater for single dose 181s and double 90s irradiation on day 5 but this was non-significant.

Investigation of NF-kB activation in H400s cells LED irradiated for 181s (1J/cm^2) revealed that levels of activation was significantly higher in cells stimulated with *E. coli* LPS in the presence or absence of irradiation (Figure 6.3 and 6.4) (p<0.001). The 181s exposure time was chosen to perform this experiment based on the previous results from cell counts and the MTT assay even though the results obtained did not show significant different. It was also important to note that LED irradiation did not appear to stimulate NF-kB activation in the experimental conditions used. These data suggest that LED irradiation might not stimulate or inhibit activation of NF-κB in the parameters used in this experiment.

The downstream consequences of NF-kB activation is changes in gene expression so PCR was used to identify differential gene expression by investigating genes potentially closely associated with the mechanisms that deliver cellular changes post irradiation i.e. genes associated with NF-kB activation and cell respiratory function (i.e. ATP synthesis). Cells were investigated at 2 specific time points day 3 post single dose irradiation and day 5 for single and double dose experiments. Both of these conditions used 90 and 181s exposure times to be consistent with previous experiments. For the first time point (3 days single dosing), most of the genes, ATP5F1, COX6C, PPA1, MAPK11, NF-κB, NF-κB1E, NF-κB2, NDUFA11 and NDUFS7 were upregulated in cells irradiated with 90s exposure time (0.5J/cm^2) (Figure 6.5). This differed slightly in comparison to cell counts and the MTT assay where cells irradiated for 181s with a single dose produced a better response.

Results from the second time point, double dosage regime (Figure 6.7) showed more genes upregulated than those found utilising a single dose. The decision to investigate double dosing with LED irradiation was based on the studies of Li *et al.,* (2010), which published data indicating that double dosing regimens can significantly increase the proliferation rate of mesenchymal stem cells (MSCs) compared with a single dose irradiation. This study also suggested that the cellular effect of the red LED exposure were more obvious at low seeding cell density (Li *et al.,* 2010). Another study found that double dosing with 60s (224mJ/cm^2) using a red LED at days 1 and 4 on dental pulp cells (DPCs) described significant increases in cell growth, proliferation rates associated with increased ATP, nitric oxide (NO) and mitochondrial metabolic activity compared with a single dosing regimen (Holder *et al.,* 2012).

A pro-inflammatory cytokine, IL-8 was detected using ELISA upon stimulation with *F. nucleatum* or *P. gingivalis* and LED irradiation. Interestingly, IL-8 production was higher in cells irradiated with double dose for 90 and 181s after stimulation with *P. gingivalis*, but not with *F. nucleatum* (Figure 6.11) however this was not statistically significant. Milward *et al.,* (2012) demonstrated that IL-8, a surrogate marker of NK-κB activation was increased in epithelial cells after stimulation with *P. gingivalis* and *F. nucleatum* where highly significant of IL-8 secretion following *F. nucleatum* stimulation (Milward *et al.,* 2012).

A number of studies have shown significant increases in cell proliferation and up-regulation of cell processes post LED irradiation in a wide range of cell (AlGhamdi *et al.,* 2012, Karu 2010, Holder *et al.,* 2012).

It has been proposed that light delivered at appropriate doses will interact with the mitochondrial membrane following absorption by chromophores (Karu 2010, Oliveira *et al.,* 2011, Huang *et al.,* 2009). The concept of biphasic dose response indicates how important dose delivery is (Huang *et al.,* 2009, Chung *et al.,* 2012). Indeed a wide variety of studies have indicated that if light is delivered at sufficient dose and at the correct wavelength it produces downstream cellular effects (Schindl *et al.,* 2003, Holder *et al.,* 2012, Oliveira *et al.,* 2011, Lizarelli *et al.,* 2007, Chang *et al.,* 2013, Sgolastra *et al.,* 2013). However it is not always easy to compare the results of previous studies as the majority of them fail to adequately measure or report the parameters used in light delivery (Oliveira *et al.,* 2011) or even the source of light used.

CHAPTER 7: H400 RESPONSES TO 1ST GENERATION LED ARRAY IRRADIATION

7.1 H400 cell responses upon 1st generation LED array irradiation

7.1.1 Introduction

Previous chapters, 5 and 6 describe the H400s responses on laser and LED irradiation which were limited to two specific wavelengths reported in the literature as showing efficacy in enhancing cell proliferation i.e. 670 and 630nm. Although LED devices could be developed to investigate other wavelengths using the same experimental protocols as used in Chapter 6, this would be time consuming. Therefore ways of screening a wide range of wavelengths was sort. It was decided to develop 96 well plate based LED arrays in order to allow high throughput screening of multiple wavelengths and to identify optimal parameters for each cell type.

As a result a 1st generation array was developed by Dr M.A.Hadis member of Birmingham Photobiomodulation Research Group in conjunction with Electrical Engineering, University of Birmingham. This initial device utilised a series of wavelengths, 625, 650, 660, 670, 690, 780, 800, 810, 820 and 830nm (Figure 2.3). One of the challenges in developing this device was prevention of light contamination between wells, in order to overcome this issue the array included a black walled collimator and experiments used 96-well black plates to minimise this issue. Initial experiments to determine the optimum radiant exposure are described in Appendix 3. Each row of LED's at a specific wavelength has a different irradiance and in order to obtain the radiant exposure the exposure time for each wavelength was varied in order to deliver 2, 5 and 10J/cm^2 radiant exposure for single and double dosing regimens (see Table 2.7). For single dosing studies cells were irradiated 24h post

seeding, whilst for double dosing the cells received further irradiation 24h after first light exposure. Due to the small media volume and relatively few cells (in comparison to larger 35mm dishes used in previous experiments) and some initial pilot work which indicated the inaccuracy in cell counts it was decided to measure MTT as a indicator of cell number and to allow for high throughput screening.

7.1.2 MTT assay

MTT assay was performed to determine the H400 cell responses 24h post single and double irradiation utilising the 1st generation array. The graphs presented indicate percentage MTT increase compared to un-irradiated controls.

These results showed considerable variation between the different wavelengths investigated and the different radiant exposures used. For the majority of parameters tested light exposure has caused an across the board increase in MTT activity compared to non-irradiated controls, with the exception of 830nm 2J/cm^2 single and double dose, 780nm 5J/cm^2 single dose, 830nm 5J/cm^2 double dose, 830nm 10J/cm^2 single dose and 670nm 10J/cm^2 double dose which all produced slightly reduced levels of MTT in comparison to controls. For 2J/cm^2 single dose for the range of wavelengths tested none of the increases in MTT reached significance although peaks were seen around 625nm, 780nm, 810nm and 820nm. For 2J/cm^2 double dosing a significant increase was noted at 670nm. In the experiment using 5J/cm^2 radiant exposure and single dose again there were no significant increases, however peaks were seen at around 670nm, 690nm and 820nm. It was also noted with these experimental parameters that little change in MTT was detected at 650nm,

780nm and 830nm. Using double dosing at 5J/cm^2 also produced increases but not significant differences over non-irradiated controls, however peaks were seen at around 660nm, 690nm and 800nm, with 780nm and 830nm showing little difference in MTT over non-irradiated controls. When the experimental conditions were changed to deliver a radiant exposure of 10J/cm^2 a number of significant changes in MTT production could be seen, for single dosing significance was reached for 660nm, 670nm and 690nm, with maximum MTT change over control seen at 660nm. For 10J/cm^2 double dosing significant changes were seen at 650nm and 780nm.

So from these experiments using the range of wavelengths, radiant exposures and dosing regimens the conditions that show significant increases in MTT over non-irradiated controls are 670nm double dose 2J/cm^2; 660, 670, 690nm single dose 10J/cm^2; and 650 and 780nm double dose 10J/cm^2.

(a) single dose-2J/cm^2

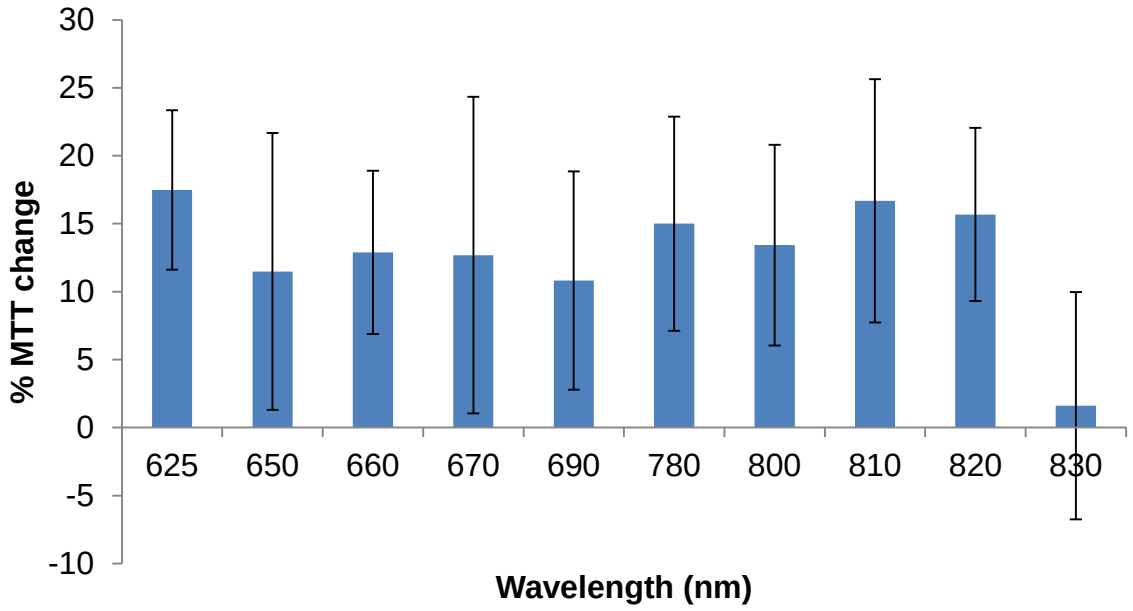

(b) double dose-2J/cm^2

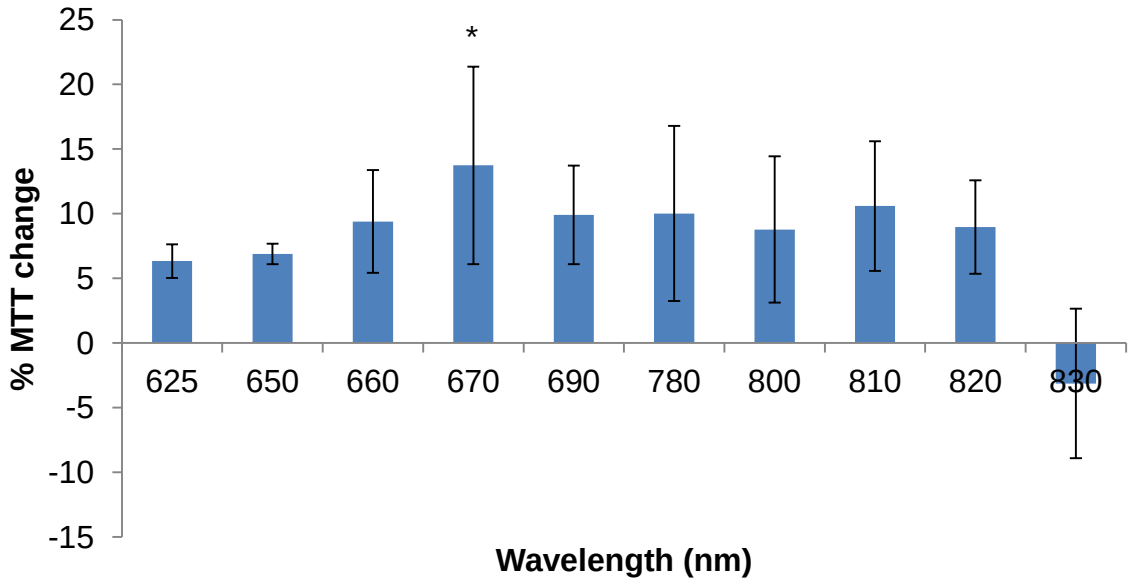

Figure 7.1: MTT levels in H400 cells exposed to LED array at 2J/cm^2 radiant exposure (a) single dose (n=5) and (b) double dose (n=4 in duplicate). Results are mean ± SD. *p<0.05.

(a) single dose-5J/cm^2

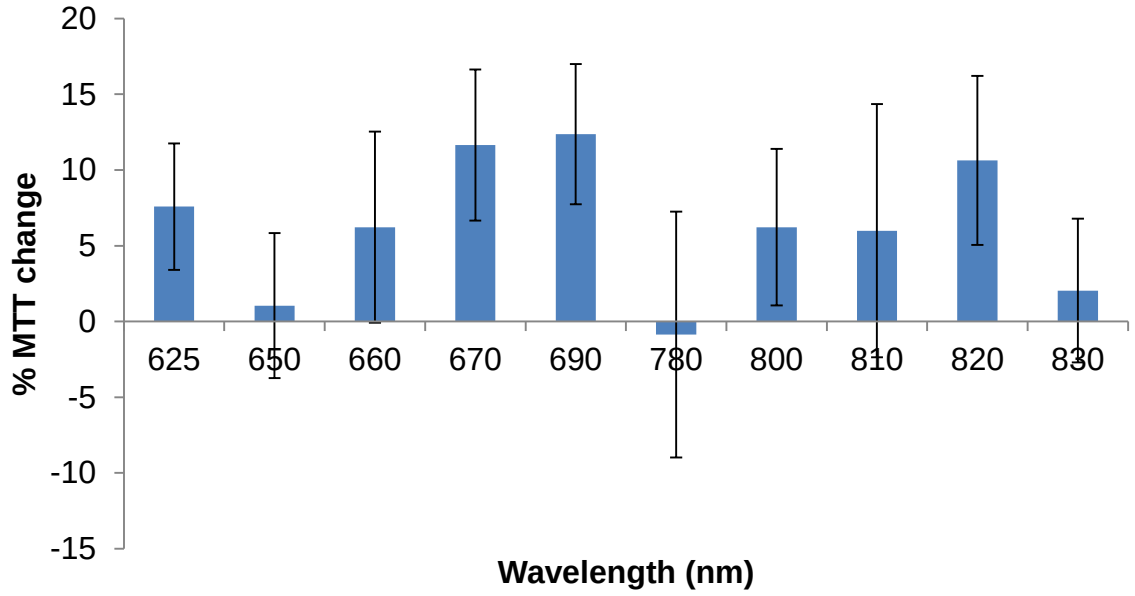

(b) double dose-5J/cm^2

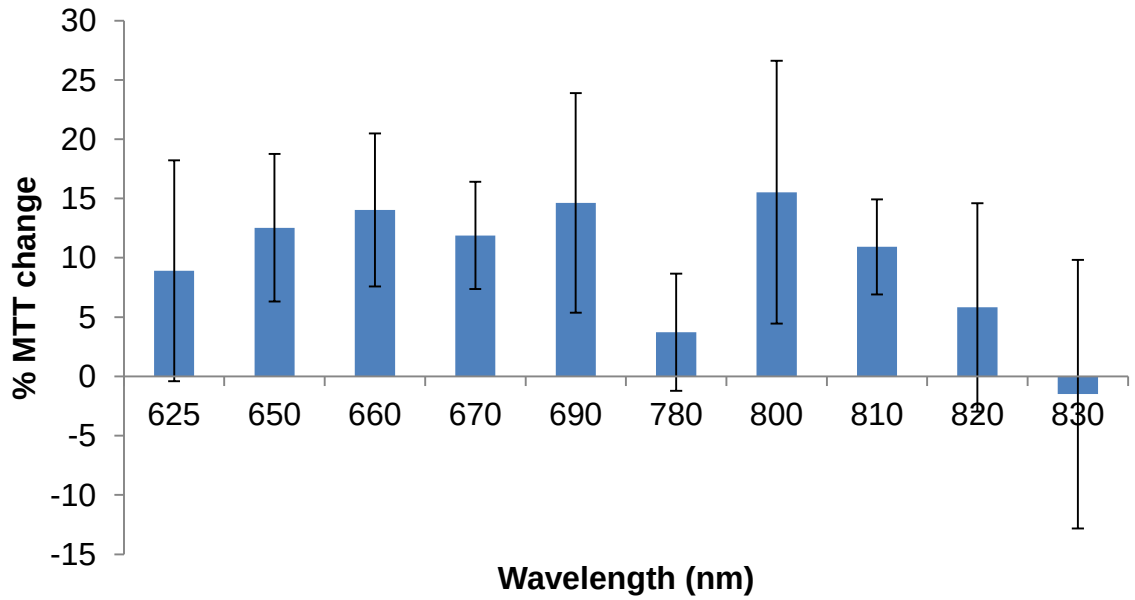

Figure 7.2: MTT levels in H400 cells irradiated with LED array (a) single and (b) double dosing at a radiant exposure of 5J/cm^2. Results are mean ± SD (n=4 in duplicate).

(a) single dose-10J/cm^2

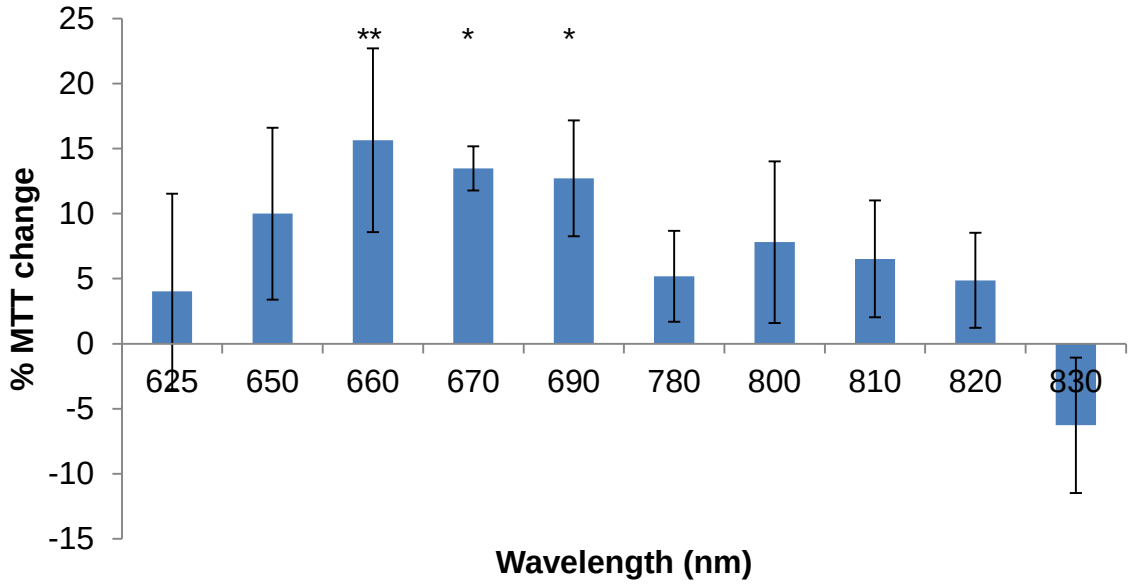

(b) double dose-10J/cm^2

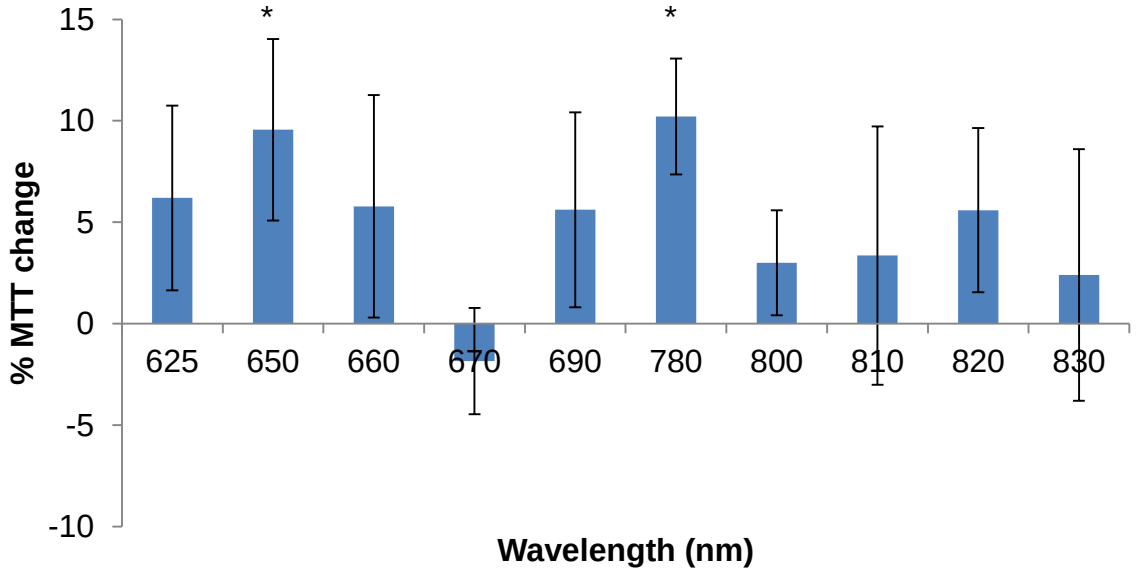

Figure 7.3: MTT levels in H400 cell irradiated with LED array at a radiant exposure of 10J/cm^2 in (a) single and (b) double dose regimes. Results are mean ± SD (n=4 in duplicate). *p<0.05, **p<0.01.

7.2 ROS detection of H400s by chemiluminescent Luminol

Irradiated H400 cell culture was examined for the level of ROS production using Luminol as describe in section 2.2.4.6.1. It was aimed to look at the level of production of ROS in H400 cells upon irradiation, however, the result showed unstable peaks for all conditions as illustrated in Figure 7. 4. Due to the results obtained, this approach may not be the best to assess the production of ROS in cell culture.

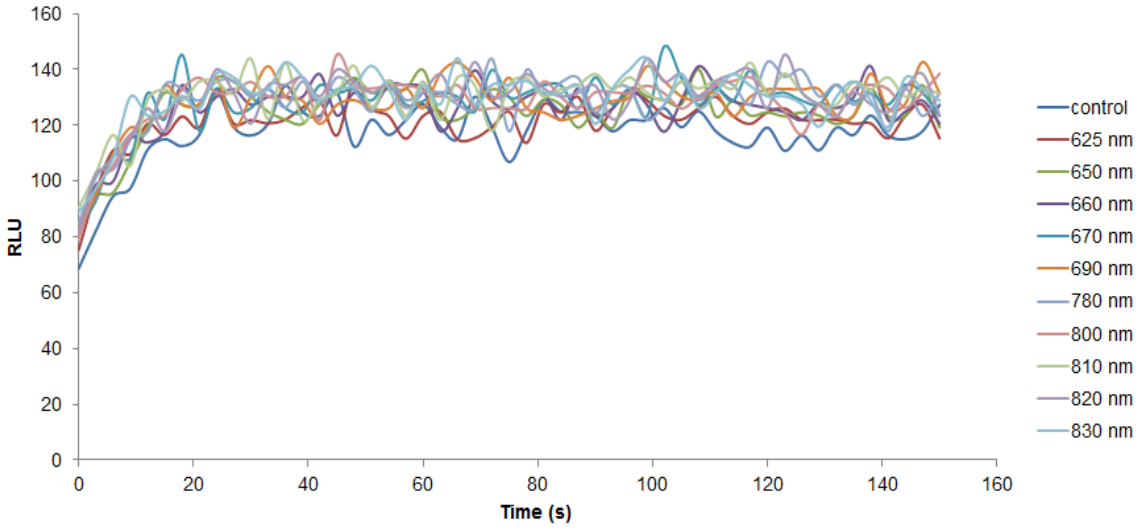

Figure 7.4: ROS level detection by Luminol upon 1st generation LED irradiation.

7.4 Discussion

This type of LED array has different irradiance value for each individual wavelength (Table 2.7) therefore in order to deliver radiant exposures of 2, 5 and 10J/cm^2 the exposure time needed to be adjusted for each wavelength in order to deliver the required radiant exposure. During irradiation, each LED for individual wavelength was switched on for a calculated time period (Table 2.7). The range of radiant exposures used (2, 5 and 10J/cm^2) was determined based on preliminary optimisation experiments (see Appendix 3). Double dosing was investigated as the literature indicated efficacy for example Li and colleagues (2010) illustrated double dosing using red LED increased rat bone marrow mesenchymal stem cell proliferation in comparison to a single dosing regimen with double at a radiant exposure of 2J/cm^2 triggered more proliferation and cytokine production (Li *et al.,* 2010). Another study by Wang *et al.,* (2015) observed significant wound healing in rat gingival fibroblasts when irradiated with 660nm LED light source at 5J/cm^2. These papers and initial pilot data support the irradiation parameters used in this thesis.

The use of LED arrays allows the rapid screening of a number of wavelengths at one time to determine optimal irradiation parameters for a particular cell type. However this method for screening cells has limitations. From the data it can be seen that there is considerable variability as seen by the error bars which can limit interpretation of data. There are potentially a variety of reasons for this variation including (a) the small volumes of media used in each of the micro wells, resulting in small errors in pipetting have potentially large downstream effects, (b) errors in initial cell seeding density would also potentially lead to similar errors.

The LED array also has problems in terms of the different irradiance each wavelength delivers requiring adjustment in exposure time to deliver a particular radiant exposure. Therefore it was decided that further refinement of the LED array was required to produce a multi-wavelength array with all wavelengths delivering the same irradiance thereby allowing a single exposure time to be used for all wavelengths in order to deliver a particular radiant exposure.

The following chapter describes the use of a second generation array delivering standardised irradiance.

CHAPTER 8: H400 AND NEUTROPHIL RESPONSES TO 2ND GENERATION LED ARRAY IRRADIATION

8.1 H400s responses

8.1.1 Introduction

This chapter describes the responses of H400 cells and primary neutrophils following LED irradiation using the 2nd generation array. This second generation array was designed to overcome the issues with non-standard irradiance delivered by the first generation array which required alteration of exposure time for individual wavelengths in order to control radiant exposure. This 2nd generation array had a standard irradiance of 24mW/cm^2 for each of the wavelengths used i.e. 400, 450, 525, 660, 740, 810, 830nm, in addition a white LED was included which generated a mixture of wavelengths. The first part of this chapter will report on H400 responses and the second on primary neutrophil responses.

8.1.2 Results

As with previous experiments a number of key biological markers were used to investigate H400 cell responses, i.e. MTT assay, BrdU assay, and cell counts. Another potentially interesting biological marker was added for this series of experiments i.e. ROS production, due to its importance in cell signalling / activation of an inflammatory response and its role in local tissue damage when found in excess in the periodontal lesion. ROS production was detected using CM-H_2DCFDA. Results are presented as a percentage increase in comparison of non-irradiated controls, with the exception of ROS production which used relative units.

8.1.2.1 MTT assay

Comparison between non-irradiated and irradiated H400 cells were examined following irradiation for 30, 60, 120, 24 and 480s (n=5) (Figure 8.1 a, b, c, d and e, respectively). These data show significant increases in MTT production for each of the irradiation time points used but there is variation in the wavelengths that deliver this increase for each time points. At 30s significant increases were seen for 400, 660, 740 and 810nm (largest increase). For 60s irradiation significant increases were seen for 450, 660nm and the white LED. At 120s irradiation of H400 cell significant increases in MTT were seen at 450, 525nm and white light. At an exposure time of 240s 525nm showed a decrease in MTT with significant increases seen for 740 & 810nm. Following 480s exposure 400nm showed a non-significant reduction in MTT compared with controls and a significant increase at 660nm. The most common wavelength to show an increase in MTT in these experiments were 660nm, 740nm, 450nm and white light.

(a) single dose-30s

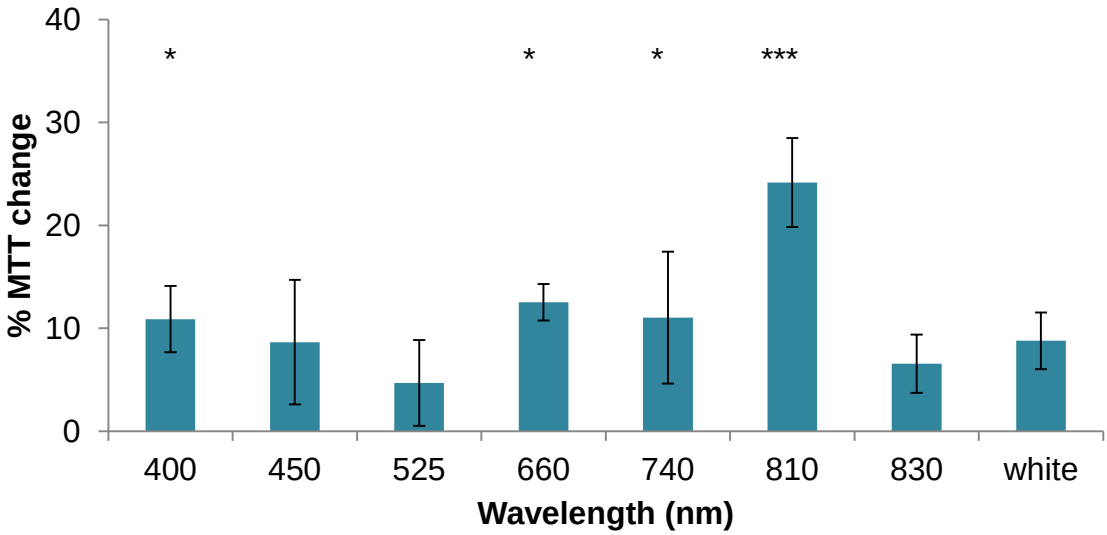

(b) single dose-60s

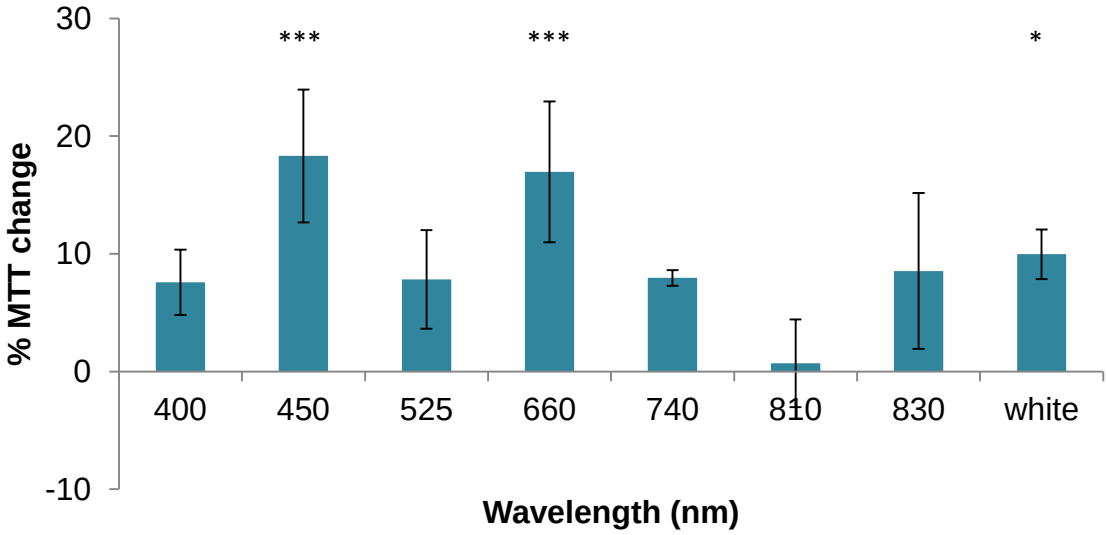

(c) single dose-120s

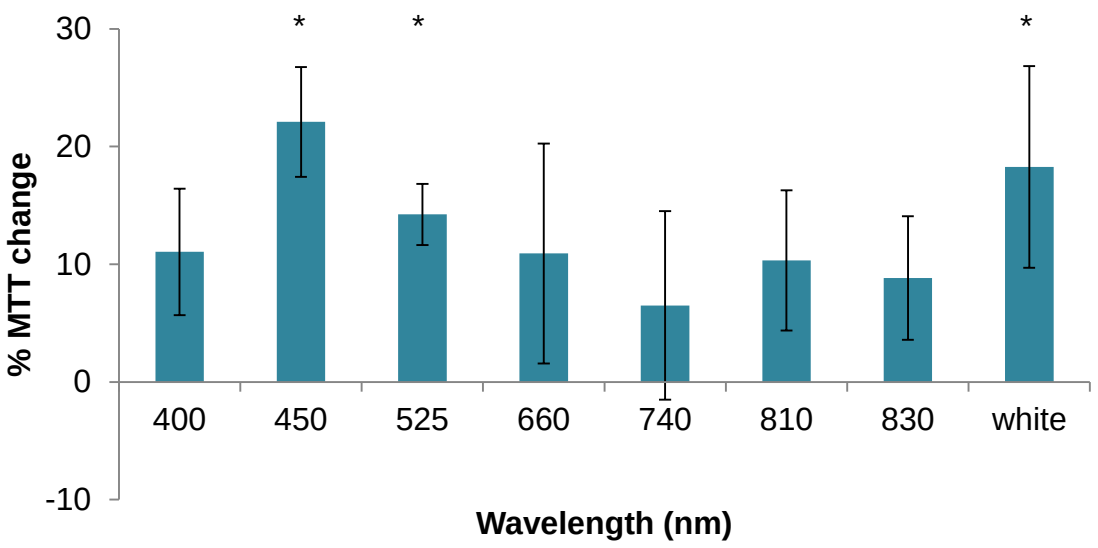

(d) single dose-240s

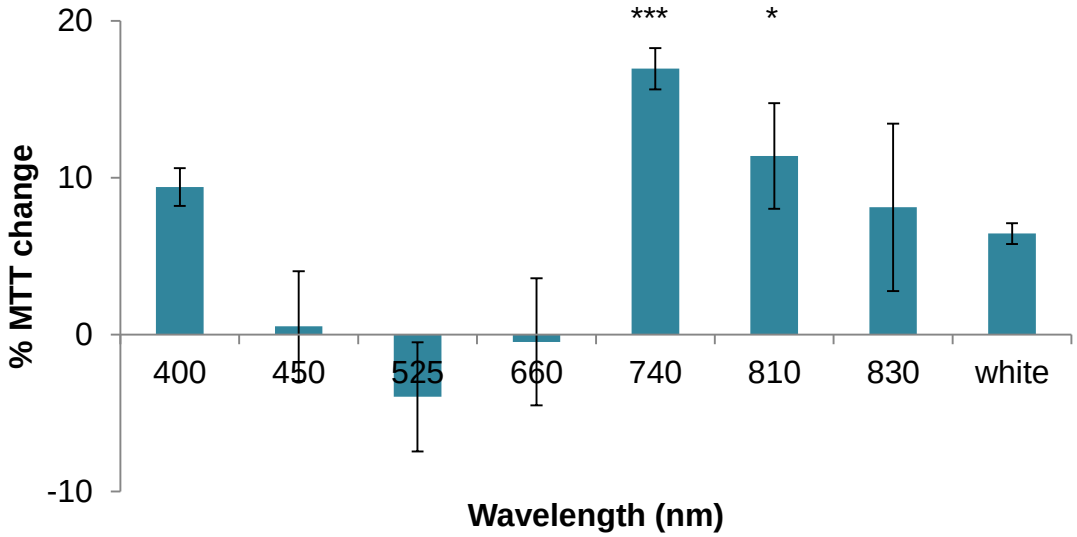

(e) single dose-480s

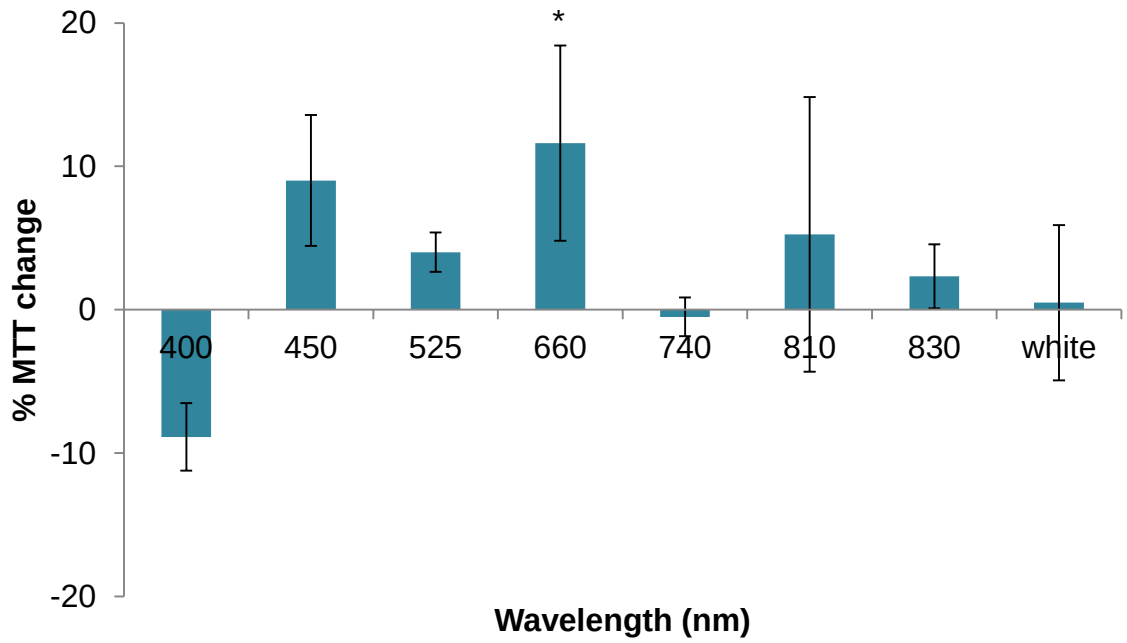

Figure 8.1: Single dose irradiation for (a) 30s (b) 60s (c) 120s (d) 240s (e) 480s. Data presented as percentage of MTT increase on day 2 (24h following irradiation) compared to the non-irradiated control. Results are mean ± SD (n=5 in duplicate). *p<0.05, ***p<0.001.

8.1.2.2 BrdU assay

BrdU levels were measured and represented as a percentage of the non-irradiated control. Following initial high throughput screening of H400 cells for MTT a number of significant results were obtained from these it was decided to look at BrdU levels using one of the exposure time points (480s). This exposure time was chosen to further analysis with BrdU and later cell count due to consistent MTT result obtained compared to other time point. Data generated from this experiment showed a significant increase of BrdU in H400 cells exposure to 660nm, this was the same wavelength that produced a significant increase in MTT (Figure 8.2).

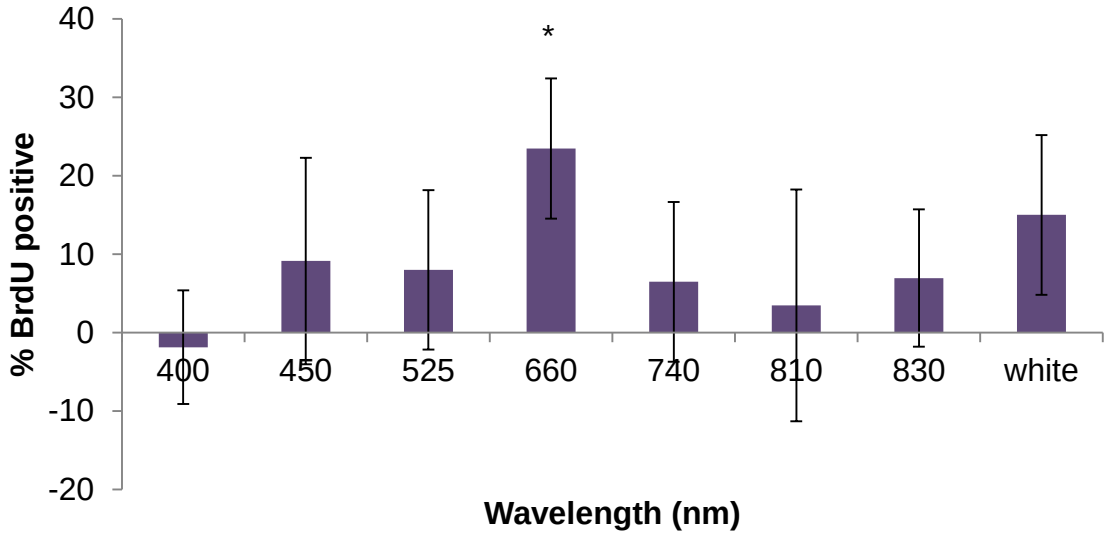

Figure 8.2: Percentage increase in BrdU positive H400 cells irradiated for 480s using the 2nd generation LED array. Results are mean ± SD (n=6 in single). *p<0.05.

8.1.2.3 Cell count

Following on from the initial high throughput screening using MTT and the results obtained for BrdU following an exposure time of 480s cell counts were performed on H400 cells. Results demonstrated a similar trend to both MTT and BrdU data with 660nm showing a significant increase in cell number when compared to non-irradiated controls. These data also indicated that cells irradiated at a wavelength of 525nm showed a significant increase in cell number (Figure 8.3).

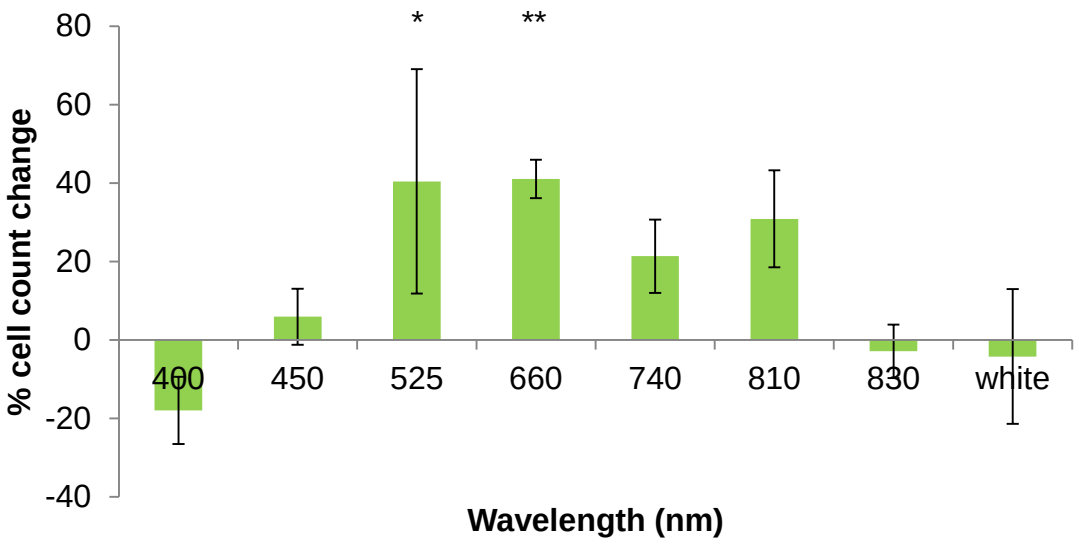

Figure 8.3: H400 cell counts following 2nd generation LED irradiation for 480s. Results are expressed as a percentage of control. Results are mean ± SD (n=6 in double). *p<0.05, **p<0.01.

8.1.2.4 ROS detection using CM-H_2DCFDA

Levels of ROS were determined in H400 cells 1, 2 and 4h post irradiation (Figure 8.4 a, b and c). ROS was determined using CM-H_2DCFDA (see Section 2.2.4.6.2). After 1h irradiation for 480s significant increases in ROS production were seen for 400, 450nm and white light. At 2h post irradiation significant increases were seen at 400nm and white light, however at 4h no significant changes over non-irradiated control were seen. For all 3 time points investigated there was a similar trend in ROS production for the different wavelengths investigated.

(a) 1h post 480s

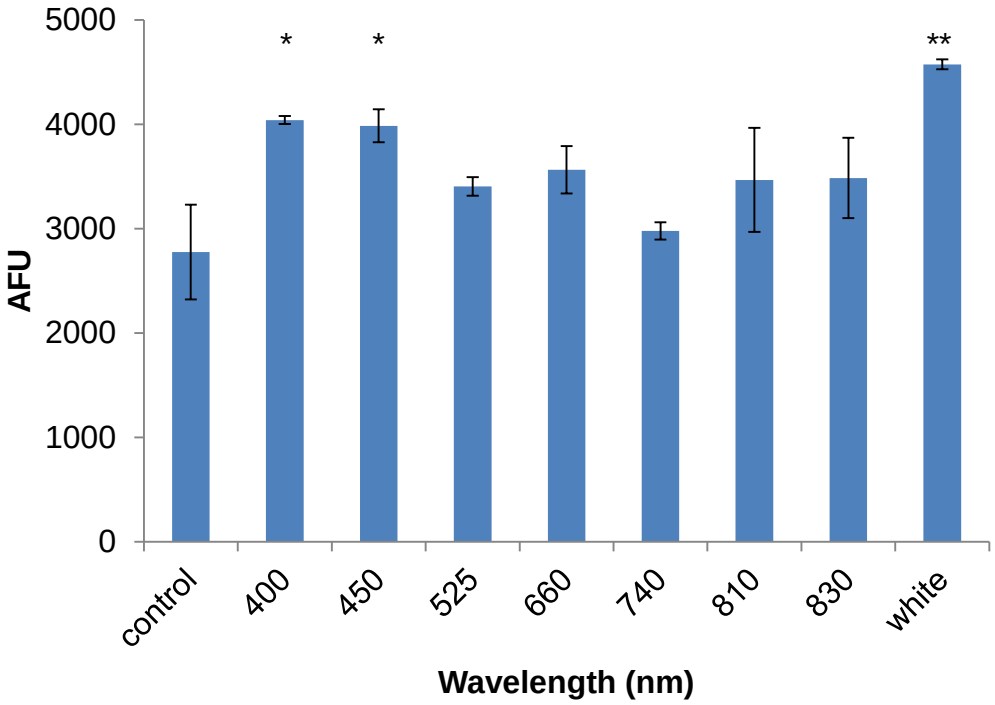

(b) 2h post 480s

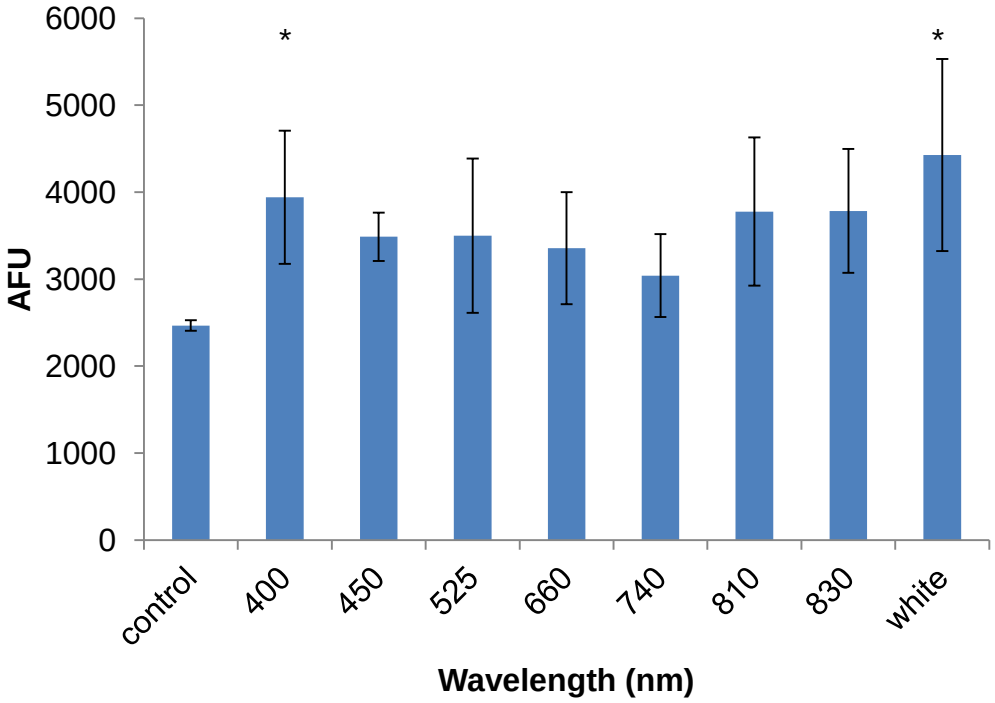

(c) 4h post 480s

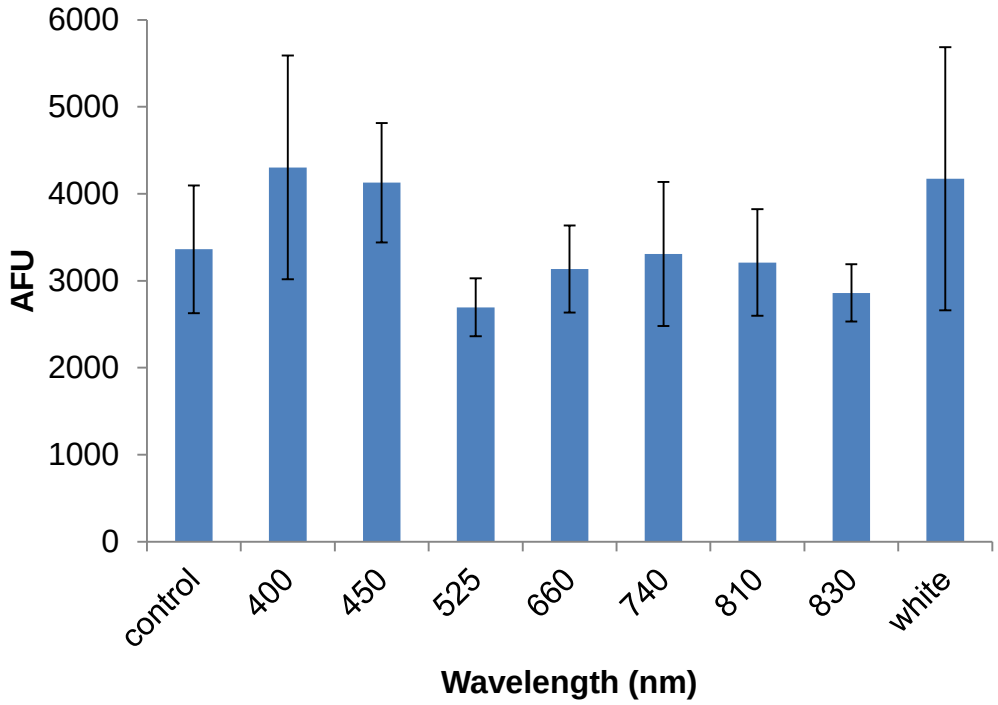

Figure 8.4: ROS production at (a)1h, (b) 2h and (c) 4h post 480s (11.6J/cm^2) irradiation with 2nd generation LED array. AFU: Arbitrary fluorescence units. Results are mean ± SD (n=4 in duplicate). *p<0.05, **p,0.01.

8.1.2.5 IL-8 production from stimulated H400 cells following irradiation

To investigate IL-8 production, ELISA was performed on media which was isolated from stimulated/non stimulated H400 cells exposed to 2nd generation LED array in comparison to non-irradiated controls (see Section 2.2.7). Data generated from this experiment indicated that irradiation appeared to have differential responses in terms of IL-8 production. In non-stimulated cells light irradiation resulted in reduction of IL-8 production at wavelengths 660, 740, 810, 830nm and white light (Figure 8.5 (a)). For cells stimulated with *F. nucleatum* reductions in IL-8 production were seen at 400, 660, 810nm and white light, increases in IL-8 were seen at 450 and 830nm (Figure 8.5 (b)). When H400 cells were stimulated with *P. gingivalis* reductions in IL-8 were seen at 400, 525, and 660nm, with increases at 740, 830nm and white light (Figure 8.5 (c)). The data presented here did not reach statistical significance.

(a) non-stimulated

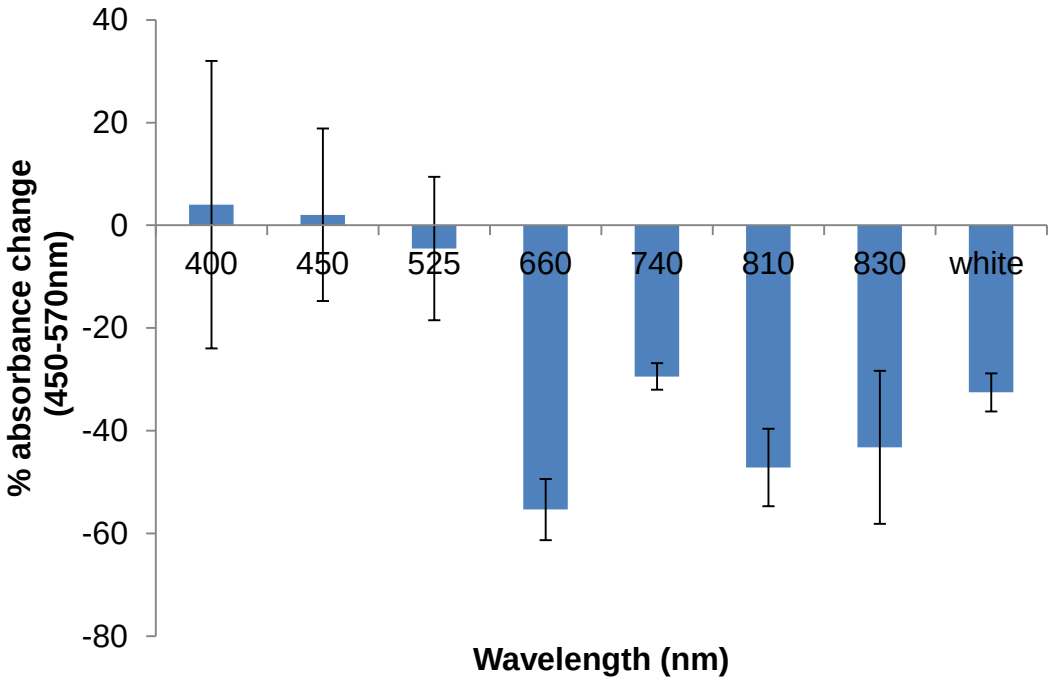

(b) stimulated-*F. nucleatum*

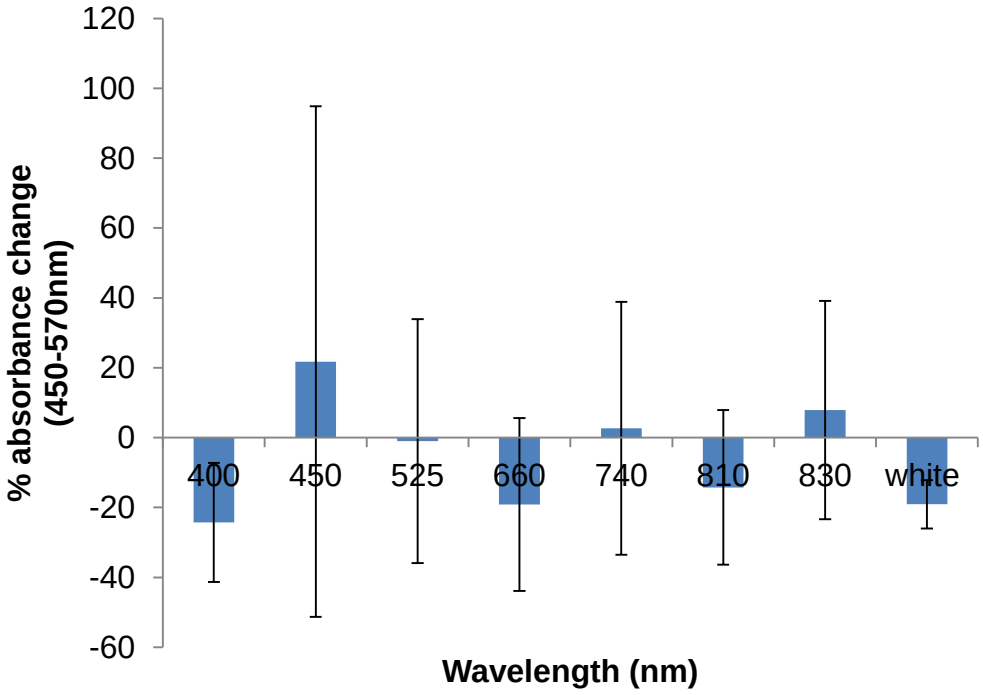

(c) stimulated-*P. gingivalis*

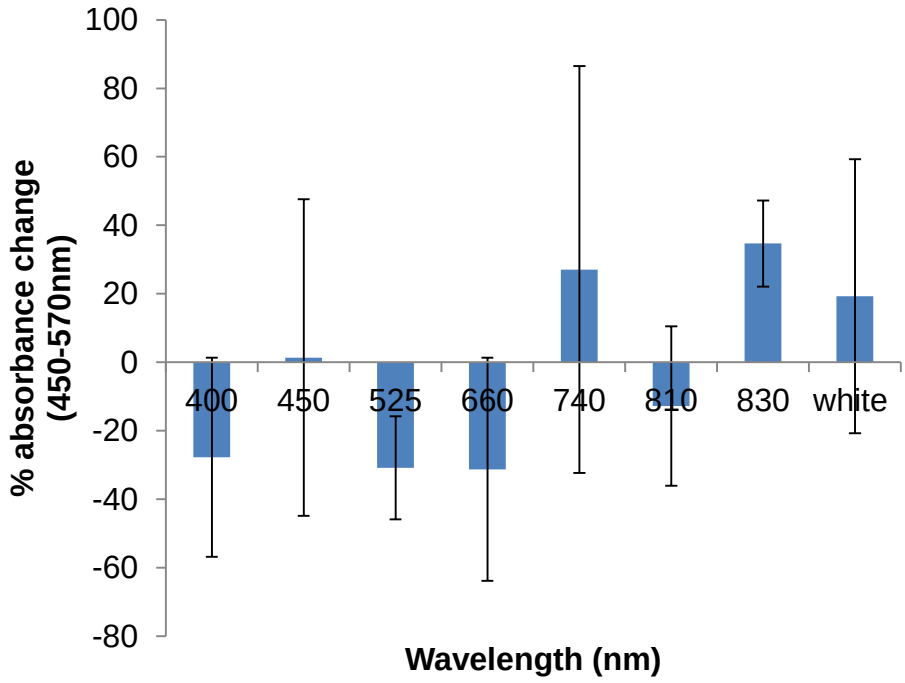

Figure 8.5: Percentage of IL-8 absorbance in H400 cells in comparison to non-irradiated controls. Cells were irradiated for 480s using the 2nd generation LED array; (a) non-stimulated (b) stimulated with *F. nucleatum* and (c) stimulated with *P. gingivalis*. Results are mean ± SD (n=3 in duplicate).

8.2 Neutrophils responses

8.2.1 Introduction

This experiment aimed to determine the effect of light irradiation using the 2nd generation array on neutrophil ROS production. This experiment used primary neutrophils harvested from healthy volunteers.

8.2.2 Results

ROS generation was assessed using a chemiluminescent assay (2.2.5.1) using Luminol, isoluminol and lucigenin for total ROS, extracellular ROS and superoxide, respectively. The assay used was supplemented by another assay (CM-H_2DCFDA) (2.2.5.2) to determine ROS production that was previously utilised to determine ROS production in H400 cells. Cell viability was also determined using an LDH assay (2.2.5.3).

8.2.2.1 Chemiluminescent ROS detection

Following neutrophil isolation and 480s LED array irradiation (11.6J/cm^2), ROS was analysed over a time-course of 180min following PMA stimulation. Results indicated that ROS production peak was seen in the non-irradiated controls with the lowest level seen in the neutrophils exposed to 660nm (Figure 8.6 (a)). Extracellular ROS release which was determined using isoluminol generated the biggest signal for ROS production approximately 30min following PMA stimulation, again the non-irradiated controls showed highest levels of ROS production and white light the lowest (Figure 8.6 (b)). Subsequent to PMA stimulation and irradiation, superoxide generation was

measured by lucigenin, again the non-irradiated controls showing highest levels of superoxide generation (Figure 8.6 (c)). Results are presented as relative light units (RLU). Statistical analyses were carried out for these three different assays using the highest peak of every curve. There was no statistically significant different of total ROS, extracellular ROS and superoxide.

8.2.2.2 CM-H_2DCFDA ROS detection

The quantification of ROS production following 480s (11.6J/cm^2) using the 2nd generation LED array and PMA stimulation which were quantified using the CM-H_2DCFDA assay indicated that ROS were gradually increased between upon stimulation, 10, 20, 30 and 60min after PMA stimulation (Figure 8.7). This level of ROS productions by PMA stimulation was compared with un-stimulated ROS which utilising PBS. The ROS produced lower in PBS. The result of this assay differed from the result of chemiluminescent assay where the ROS level increased in 30min. These result data of ROS detection by CM-H_2DCFDA showed no significant differences at all time points and wavelengths when compared to non-irradiated control. Data is presented as arbitrary fluorescence units (AFU).

(a) total ROS

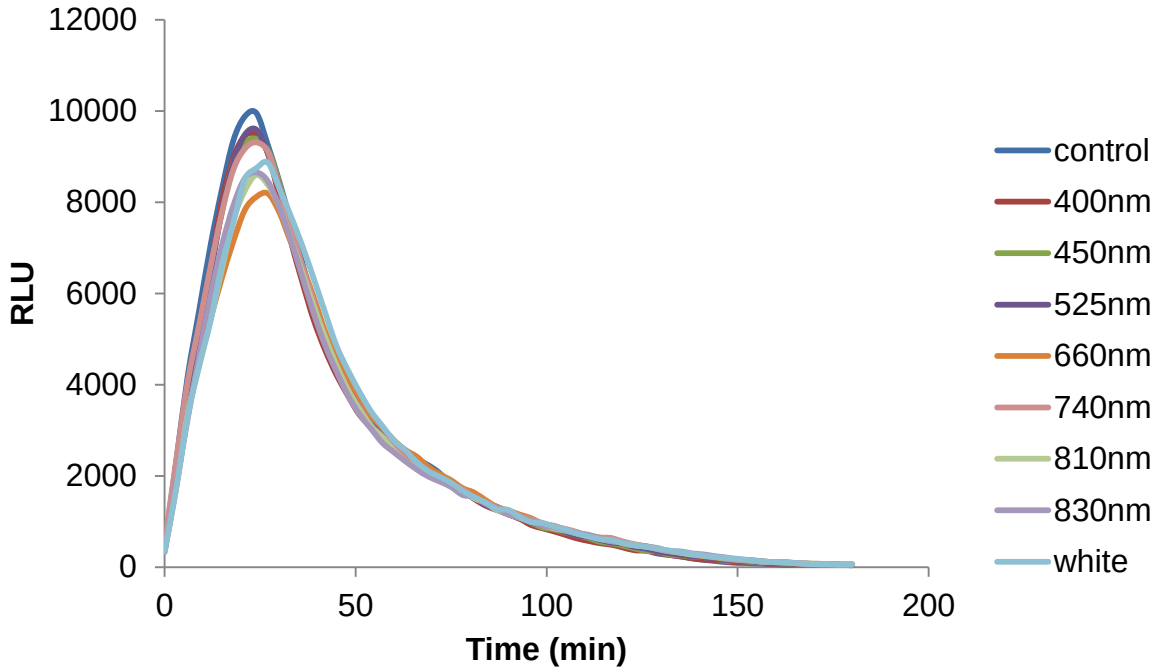

(b) extracellular ROS

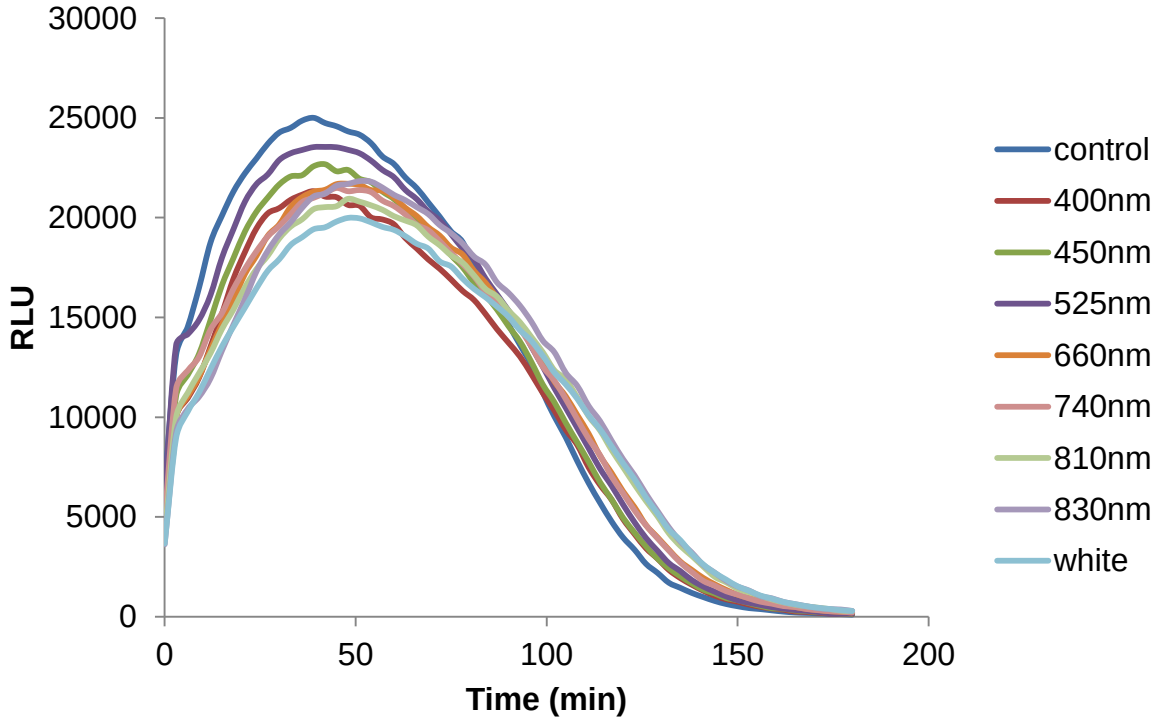

(c) superoxide

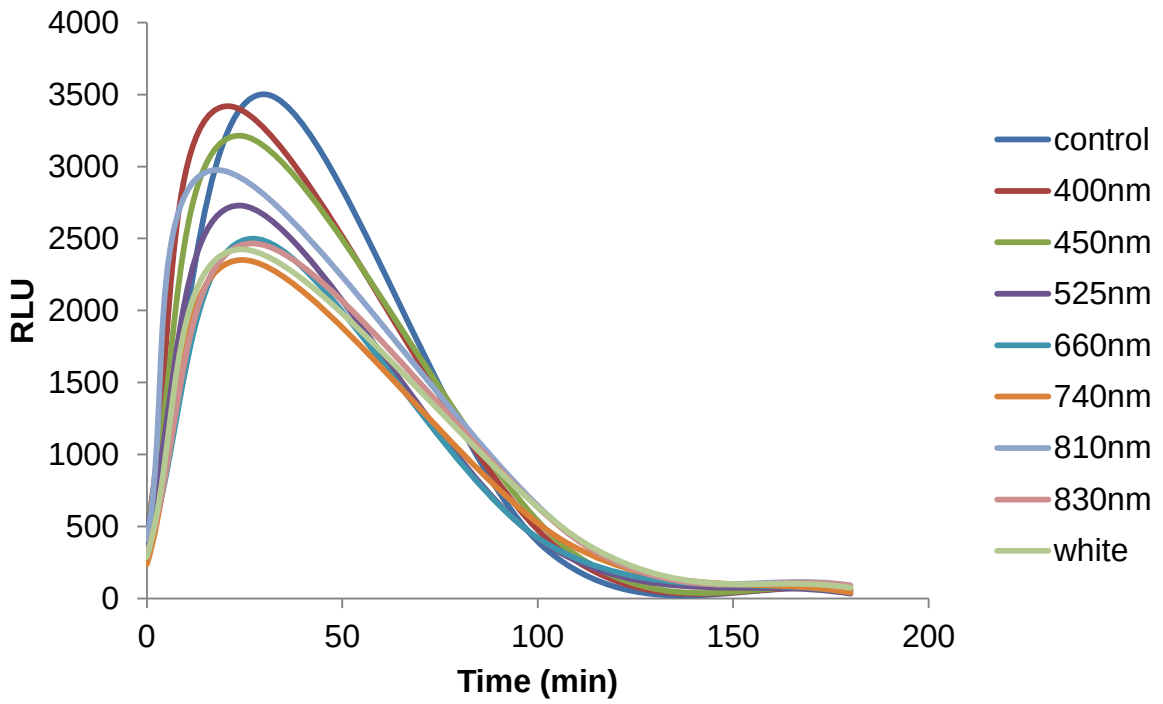

Figure 8.6: Real-time production of ROS production following irradiation (or non-irradiation – negative control) for 480s (11.6J/cm^2) with 2nd generation LED array (a) total ROS production (b) extracellular ROS production (c) superoxide production. RLU: relative light units (data presented in mean RLU, n=3 in duplicate).

(a) 0min after PMA

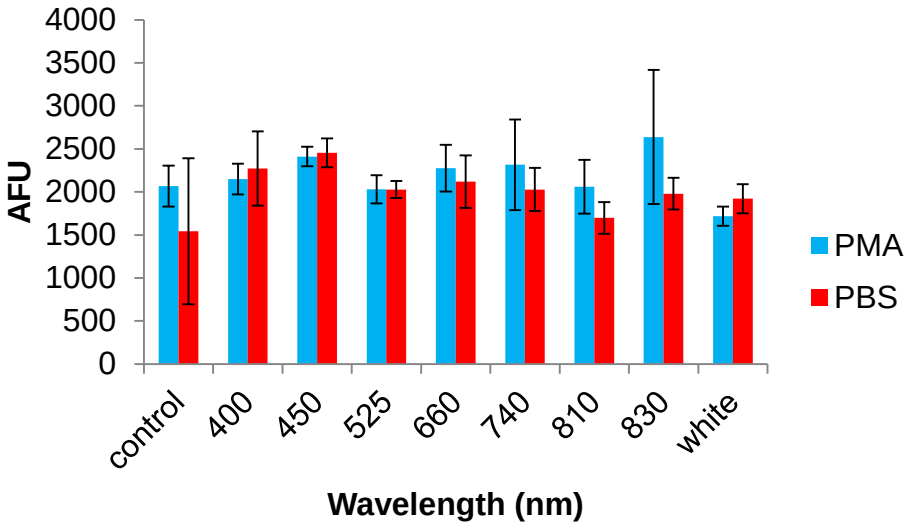

(b) 10min after PMA

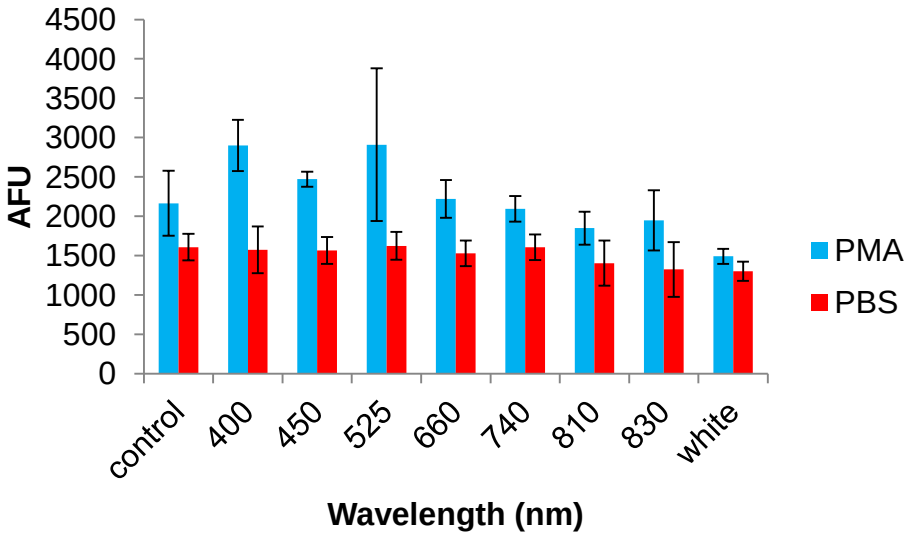

(c) 20min after PMA

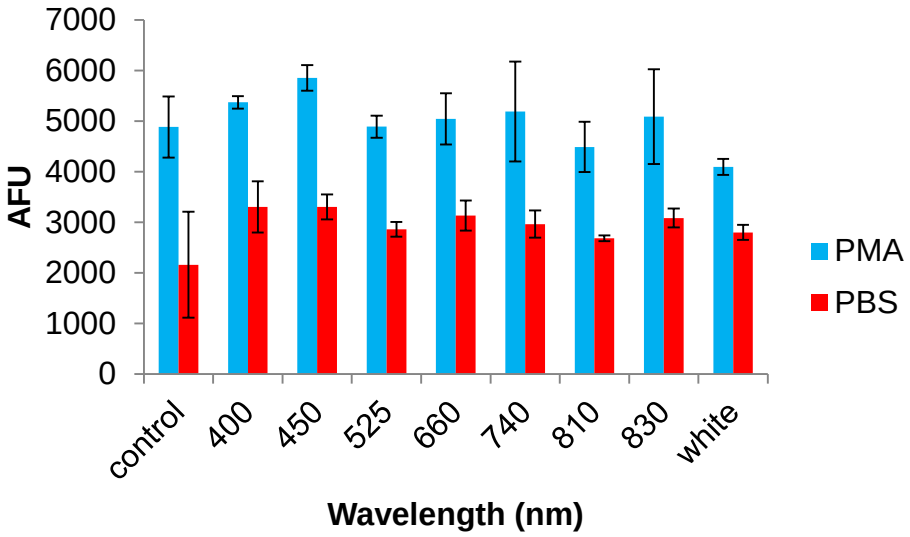

(d) 30min after PMA

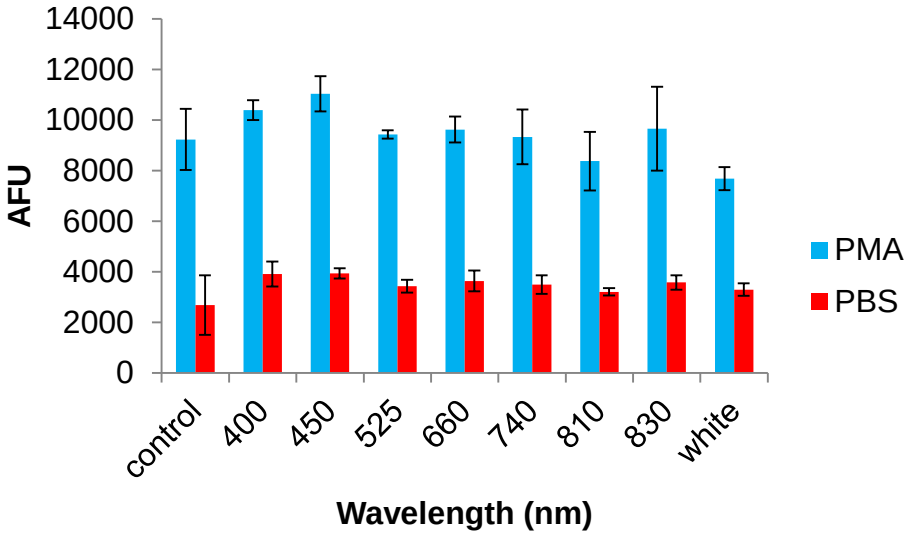

(e) 60min after PMA

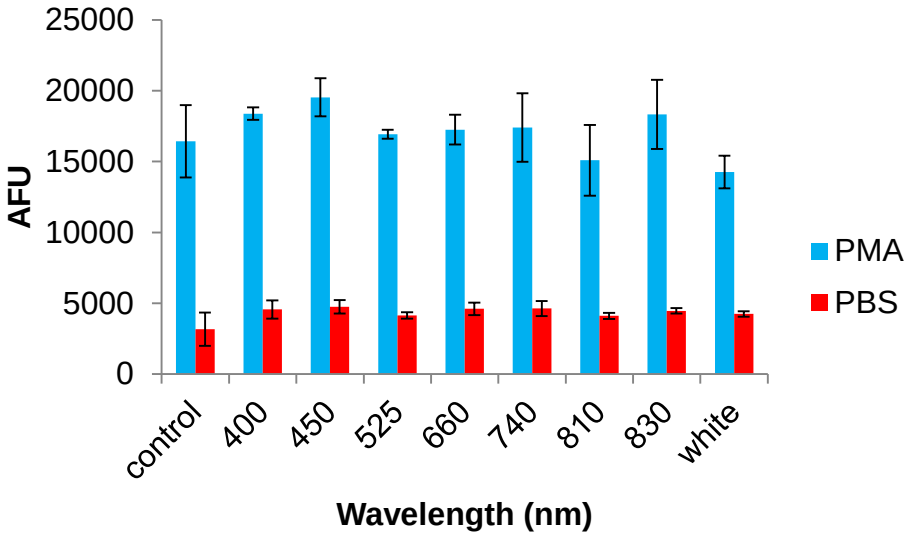

Figure 8.7: ROS release detection using CM-H_2DCFDA ROS detection marker. Plate was read at (a) 0, (b) 10, (c) 20, (d) 30 and (e) 60min upon PMA added. AFU: Arbitrary fluorescence units (Data presented in mean AFU, n=3 in duplicate).

8.2.2.3 LDH assay

This assay was used to determine any effects of irradiation on neutrophil viability, increases in LDH (lactate dehydrogenase) correlate with cell damage. The data generated showed no significant difference in LDH levels between non-irradiated and irradiated neutrophils, however there was a suggestion that the wavelengths used (apart from 400nm and white light) showed reduction in LDH release possibly suggesting that irradiation was increasing cell viability (Figure 8.8).

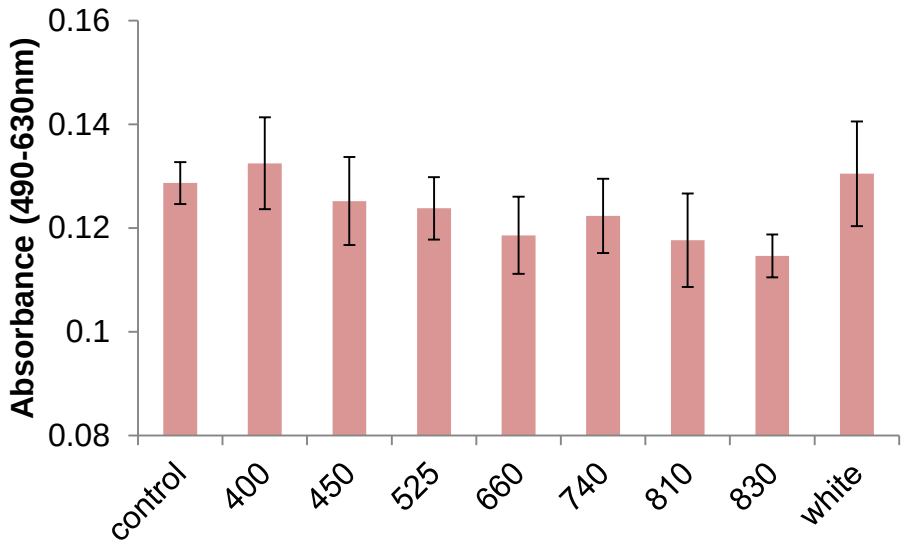

Figure 8.8: LDH release from neutrophils irradiated with the 2nd generation array (or non-irradiated control) for 480s (11.6J/cm^2). Results are mean ± SD (n=6 in duplicate).

8.3 Discussion

The 2nd generation LED array was developed as a further refinement of 1st generation LED array. This new array was able to deliver a standard irradiance value for each wavelength used (24mW/cm^2). This new array was used to investigate H400 cell and neutrophil responses following irradiation in comparison to non-irradiated controls. Both these cell types have an important role in the periodontal lesion. Epithelial cells having both barrier and pro-inflammatory roles and neutrophils exhibiting hyperactivity with respect to ROS production in patients with periodontitis. The ability to use light to modulate these responses may offer therapeutic benefits.

By irradiating H400s for 30, 60, 120, 240 and 480s using the 2nd generation array this delivered radiant exposures of 0.7, 1.5, 2.9, 5.8 and 11.6J/cm^2 respectively. Irradiation on neutrophils was undertaken using 480s time point only. Initial experiments indicated that one of the light parameters warranting further investigation was a wavelength of 660nm wavelength for 480s (11.6J/cm^2) this was therefore further investigated using different biological readouts.

Luminol, isoluminol and lucigenin signals in irradiated neutrophils demonstrated attenuated total ROS production, extracellular production and superoxide, respectively relative to non-irradiated control using PMA priming. A study by Fujimaki and co-workers (2003) reported on neutrophil ROS level in smoker and non-smokers. The result suggest that LLLT under certain conditions may have the ability to supress neutrophil ROS production in smokers and non-smokers (after longer incubation upon irradiation) where suggesting primed neutrophils in smokers may not be

amended to produce higher amount of ROS by irradiation whilst LLLT primed neutrophils in non-smokers (Fujimaki *et al.,* 2003). These data in total may suggest that LLLT may be able to beneficially modulate two important cell types in periodontal disease thereby offering the possibility of developing new LLLT based treatment regimens. However further investigation of H400 cell and neutrophil biological responses are required to elaborate optimal irradiation parameters for maximise patient benefit.

CHAPTER 9: GENERAL DISCUSSION

9.1 Introduction

This thesis proposed a role for low-level light therapy in modulation of epithelial cells and neutrophils in periodontal disease, by promoting healing and modulating inflammation. A number of stages were required to investigate this premise starting with an area that is often overlooked and inadequately research in a large proportion of the literature i.e. accurate and appropriate light characterisation to ensure correct dosing at a cellular level. This thesis goes on to investigate biological response initially using single light sources then to development of high throughput technology to allow screening on multiple light and biological parameters. All of which will elaborate on optimal conditions to deliver maximum biological and potential clinical benefit.

9.2 Parameters of light sources

As mentioned on several occasions light characterisation is often overlooked or utilises inappropriate/inadequate methodologies or misuses light characterisation terminology (Hadis *et al.,* 2016). Many reports have reported a 'biphasic dose response' for *in vivo* and *in vitro* experiments, resulting in the potential to miss the 'therapeutic window' and thereby provide no biological benefit, but importantly delivering no harm. It is therefore essential to identify the correct 'dose' to deliver optimal biological benefits. The Arndt Schulz model seen in Figure 9.1 suggests that insufficient or excess dose provides no benefit (Huang *et al.,* 2011).

The results presented in this thesis utilised well established and widely agreed criteria for light source characterisation including measurement of wavelength,

irradiance and beam profile which allows calculation of radiant exposure (Hadis *et al.,* 2015, Palin *et al.,* 2015). Each light source used including the 670nm laser, 630nm LED and the 1st and 2nd generation LED array were successfully characterised and important radiometric data obtained.

Another key parameter often overlooked is changes in temperature in the target cells during irradiation, some authors suggested that the effects of LLLT on temperature change was minimal and no significant effect on biological responses (Basford 1986, Basford 1995, Lee *et al.,* 2006, Hadis *et al.,* 2015). Controlling for temperature changes in LLLT is problematic, experiments conducted in this thesis aimed to determine the relevance of any changes in temperature in the experimental protocols used. Data suggested that temperature changes were small and were not responsible for the biological responses seen. In addition experimental conditions were designed wherever possible to minimise the possibility of temperature increases in the target cells, examples include increasing the distance from the light source to the cell monolayer and reducing exposure time. These findings were in agreement with findings published in 2015 which suggested temperature changes were minimal and were not responsible for the biological effects seen (Hadis *et al*., 2015).

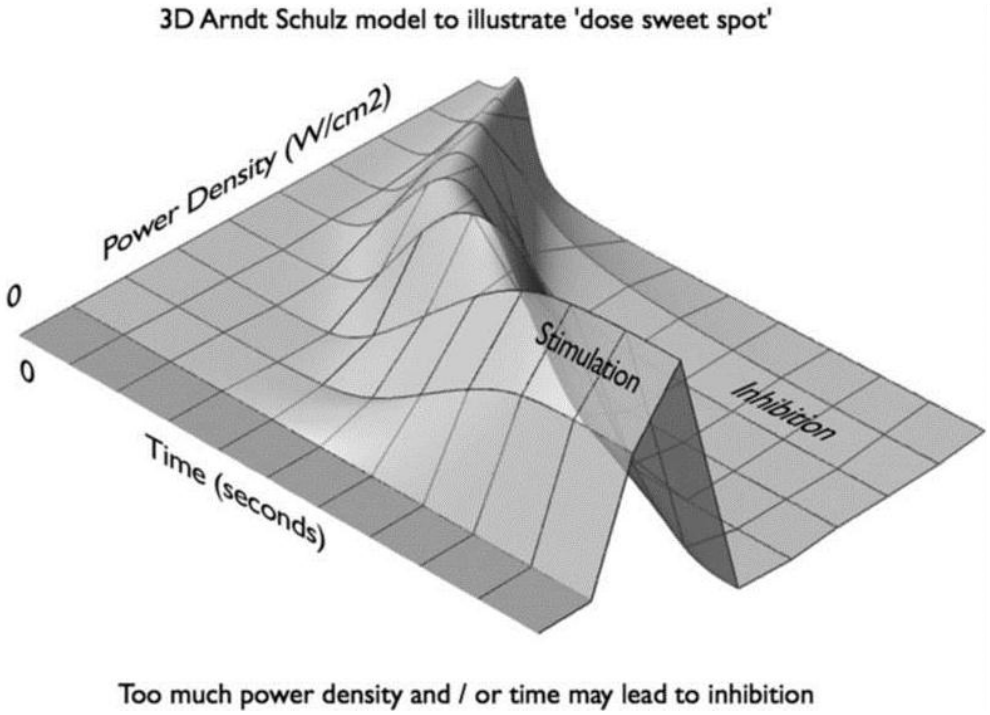

Figure 9.1: The Arnold-Schulz 3D model proposing a biphasic dose response for LLLT where optimal balance between radiant exposure (energy density) and time produces beneficial effect (Huang *et al.,* 2011). The diagram is adapted from Huang *et al.,* 2011.

The temperature experiments revealed that light affecting cells by irradiation, not by the temperature produced from the light. Maintaining stable temperature during irradiation is important to minimise any potential influence of cellular response due to raised temperature rather than as a direct effect of light. The experiment performed investigated temperature changes following removal of cell culture vessel from incubator (37^{o}C) and then irradiating cells (this mimics the experimental protocol used throughout this thesis). In the case non-irradiated control was included. These data indicated a small change in temperature and it is believed that the minimal increase in temperature from the laser, single LED or 1st generation LED array was unlikely to affect cell growth. This is because even though the temperature rose during exposure, it didn't reach the optimal temperature for cell growth (37^{o}C) with cells that remained at this temperature not demonstrating increased cellular activity when compared to irradiated cells (Figure 3.6, 3.7, 3.8 and 3.9) either met the optimum temperature for cell growth or below the temperature which is 37^{o}C. Therefore, the minimal heat produced by light source is unlikely to be a factor in any increase cell proliferation rate. As observed in Figure 3.7 and 3.8, the temperature rise was less than 5^{o}C. The temperature of cell culture slightly dropped upon taking out from the incubator to the bench for irradiation. Therefore, a slight increase of temperature during irradiation will tailor the culture to the essential temperature condition.

9.3 Epithelial cells proliferation

During this thesis a number of biological markers of cell proliferation were utilised to investigate irradiation responses. Ki-67 is a protein which is expressed during active

cell proliferation i.e. during cell cycle phases; G_1, S, G_2 and mitosis but is not expressed in resting cells (G_0), this therefore makes it a useful marker of proliferating cells (Scholzen & Gerdes 2000). Another measure of cell proliferation is the BrdU assay which determines BrdU incorporation into replicating DNA. Staining of irradiated H400s showed significantly higher incorporated BrdU detection following 6s (10J/cm^2) laser (Figure 5.5) and 480s (11.6J/cm^2) 2nd generation LED array irradiation (Figure 8.2). A further measure of cell proliferation is the MTT assay, this measures mitochondrial metabolic activity at short time points but a longer time points is used as a surrogate marker of cell number and viability (Sylvester 2011).

Assessment of MTT during this thesis showed significant increases in H400 cells irradiated for 120s (41J/cm^2) using the laser (Figure 5.4), single and double dosing using a radiant exposure of 10J/cm^2 using the 1st generation LED array at a number of wavelengths (Figure 7.3). Furthermore, the MTT absorbance significantly increased following irradiation between 30-480s (0.7-11.6J/cm^2 radiant exposure) at a range of wavelength using the 2nd generation LED array (Figure 8.1).

In addition, cell count data demonstrated relatively increase by 660nm 11.6J/cm^2 (480s) 2nd generation LED array irradiation (Figure 8.3). Also H400s irradiated by 100 and 120s laser (Figure 5.2).

While looking at H400s responses, the confluent H400 cell monolayer might produce excessive cell growth and lead to nutritional deficiency of supplemented growth media, and acidic pH and waste product accumulation, which all have a detrimental

effects effect on cell survival. These destructive factors should be avoided to prevent cell death and to have active cell growing (Milward 2010) to further examine the effect of light. The developed model systems of H400 cells which have been well characterised offer a useful study model and subsequent findings may have application in future dental treatment (Milward 2010).

All these data support the promise that LLLT using lasers or LED has the potential to enhance cell growth in H400 oral epithelial cells, however there is considerable differences in results with different wavelengths and radiant exposures, so further work is required to determine optimal conditions that could be translated into clinical use.

9.4 Activation of NF-κB

NF-κB translocation is a well-recognised marker of pro-inflammatory cellular activation. This thesis demonstrated activation of NF-kB following stimulation with *E. coli* LPS as widely reported in the literature, the introduction of irradiation with single LED light source at a wavelength of 630nm for 181s (1J/cm^2) did not significantly change NF-kB activation either in unstimulated or *E. coli* LPS stimulated cells (Section 6.1.2.3). The ability of LLLT to activate NF-kB as determined by immunocytochemistry staining was not seen in this study, however there are limitations in measuring cell activation by cell counting due to subjectivity of determining activation of NF-kB resulting in poor sensitivity of this technique.

A published study by Chen *et al.,* (2011) investigating activation of NF-κB via ROS in mouse embryonic fibroblasts following laser irradiation (810nm) showed significant activation of NF-κB with light exposure (Chen *et al*., 2011). So further work is required to screen other wavelengths and radiant exposures as well as using more sensitive measures of NF-kB activation.

9.5 Gene expression

Following NF-kB translocation to the nucleus (activation), a number of gene expression changes are initiated. NF-kB, a transcription factor for many genes, is involved in cell regulation and activated by ROS which has been found to be important in cell signalling pathways (Chen *et al*., 2011).Gene expression following laser and single LED were investigated and showed a number of interesting and significant changes. Genes ATP5G2 [subunit C2 (subunit 9)], ATP5F1 (subunit B1), COX6C (cytochrome c oxidase subunit VIc), PPA1 [pyrophosphate (inorganic) 1], MAPK11 (Mitogen-activated protein kinase 11-isoform of p38 MAPK), NF-κB, NF-κB1E, NDUFA11 [nicotinamide adenine dinucleotide (NADH) dehydrogenase (ubiquinone) 1 alpha subcomplex, 11] and NDUFS7 [NADH dehydrogenase (ubiquinone) Fe-S protein 7] showed increases in gene expression following laser irradiation while LED showed significant upregulation of ATP5F1, COX6C, PPA1, MAPK11 and NDUFS7. These data support the proposed mechanism for LLLT effects i.e. increasing cytochrome c oxidase activity and electron transport chain (ETC) resulting in increased in ATP synthesis (Masha *et al*., 2013, Wong-Riley *et al*., 2005, Karu & Kolyakov 2005).

There is evidence demonstrating LED irradiation decreased expression of pro-inflammatory cytokine, interleukin-8 (IL-8) where it increased when stimulated by *P. gingivalis* LPS (Choi *et al.,* 2012). This report supported the IL-8 expression result assessed by ELISA. Despite not significantly different, IL-8 was decreased in most of wavelengths irradiation in un-stimulated and stimulated H400 cells. Thus, it may be suggested that LED irradiation inhibit IL-8 release and potentially as an anti-inflammatory treatment management.

9.6 Human neutrophils

Level of neutrophil release is elevated in periodontitis patients to counter act the infected bacteria. Change of neutrophils production following light irradiation is yet elucidated. It is beneficial to explore the association between neutrophils production level and irradiation which may suggest an anti-inflammatory response. Experiment on neutrophils by chemiluminescense assay illustrated ROS release of un-irradiated neutrophils was demonstrated higher than irradiated and this finding showed that the irradiation might decrease production of ROS. Peripheral blood neutrophils produced higher levels of ROS in chronic periodontitis, furthermore underlying role of neutrophils in periodontology pathogenesis (Matthews *et al.,* 2007).

9.7 Future work

The findings observed in this study suggest the potential for low-level light therapy on enhancing epithelial growth and modulating neutrophil ROS production which may have efficacy in the management of periodontitis. This thesis has delivered some interesting results but more work is required to fully understand optimal conditions

required in periodontal disease. Details such as wavelength and radiant exposure need further refinement before the full translational benefit can be realised. Potential future work will include:

- The present study was performed using H400 cells an oral epithelial cell line, future work will investigate other key periodontal tissue cells including fibroblasts and osteoblasts which may respond to different wavelengths and radiant exposures. Indeed Vinck and colleagues (2003) previously showed an increased fibroblast proliferation rate in cultures irradiated by LED (Vinck *et al*., 2003). A further study described similar finding in cultured gingival fibroblast (Almeida-Lopes *et al*., 2001, Basso *et al*., 2012). This study has used an immortal cell line as a model of periodontal epithelium although widely characterised and used in this context it would be interesting to look a primary cells harvested from healthy and periodontal disease patients.

- The LED arrays are a reliable light source to high throughput screen cellular responses, they utilise 96 well plates, however due to the limited number of cells present in each well it is difficult to harvest sufficient RNA to perform gene expression analysis. Methods of overcoming this should be investigated, one such method would be the use of gene arrays or upscaling the arrays for use on 24 or 48 well plates may result in sufficient cells for gene expression analysis.

- Currently all experiments were performed on epithelial monolayers, this model system could be improved to better mimic the *in vivo* situation. This could be

achieved by the use of 3D organotypic systems and the introduction of mixed cell systems to help determine effects on cellular interaction.

- Once sufficient data is available to determine optimal irradiation parameters then it is proposed that efficacy could be determined initially in an animal periodontal disease model and ultimately in a human clinical trial following development of an approved prototype device. The ultimate outcome would be translation into a new therapeutic device to assist in the management of periodontal disease.

9.8 Concluding remarks

This thesis reports the investigation of low-level light irradiation in epithelial model system and the effects on primary neutrophils. The results obtained illustrate that low-level laser and LEDs have the capacity to stimulate and enhance cell proliferation, trigger gene expression changes and decrease ROS production which could play a vital role in reducing the excess inflammation and promoting healing in the periodontitis patients. Periodontal therapy has changed little in the last 60 years and it is proposed that low-level light therapy may offer potential as an adjunctive therapy in managing this prevalent disease.

REFERENCES

Ahmed, A. (2011). An overview of inflammation: mechanism and consequences. *Front Biol*, *6*(4), 274–281. doi:10.1007/s11515-011-1123-9

Akalın, F. A., Işıksal, E., Baltacıoğlu, E., Renda, N., & Karabulut, E. (2008). Superoxide dismutase activity in gingiva in type-2 diabetes mellitus patients with chronic periodontitis. *Arch Oral Biol*, *53*(1), 44–52. doi:http://dx.doi.org/10.1016/j.archoralbio.2007.07.009

Alberts, B., Johnson, A., Lewis, J., Raff, M., Roberts, K., & Walter, P. (2002). *Molecular Biology of The Cell.* (Fourth.). New York: Garland Science.

AlGhamdi, K., Kumar, A., & Moussa, N. (2012). Low-level laser therapy: a useful technique for enhancing the proliferation of various cultured cells. *Lasers Med Sci*, *27*(1), 237–249. doi:10.1007/s10103-011-0885-2

Almeida-Lopes, L., Rigau, J., Amaro Zângaro, R., Guidugli-Neto, J., & Marques Jaeger, M. M. (2001). Comparison of the low level laser therapy effects on cultured human gingival fibroblasts proliferation using different irradiance and same fluence*. *Lasers Surg Med*, *29*(2), 179–184. doi:10.1002/lsm.1107

Aas , J. A., Paster, B. J., Stokes, L. N., Olsen, I., & Dewhirst, F. E. (2005). Defining the normal bacterial flora of the oral cavity. *J Clin Microbiol, 43(11),* 5721-5732.

Avci, P., Gupta, A., Sadasivam, M., Vecchio, D., Pam, Z., Pam, N., & Hamblin, M. R. (2013). Low-level laser (light) therapy (LLLT) in skin: stimulating, healing, restoring. *Semin in Cutan Med Surg*, *32*(1), 41–52.

Baeuerle, P. A., & Henkel, T. (1994). Function and activation of NF-kappa B in the immune system. *Annu Rev Immunol*, *12*, 141–179. doi:10.1146/annurev.iy.12.040194.001041

Bals, R., & Hiemstra, P. S. (2004). Innate immunity in the lung: how epithelial cells fight against respiratory pathogens. *Eur Respir J*, *23*(2), 327–333. doi:10.1183/09031936.03.00098803

Barnes, P. J. (1997). Nuclear factor-κB. *Int J Biochem Cell Biol*, *29*(6), 867–870. doi:10.1016/s1357-2725(96)00159-8

Barnes, P. J., & Karin, M. (1997). Nuclear Factor-κB — A Pivotal Transcription Factor in Chronic Inflammatory Diseases. *N Engl J Med*, *336*(15), 1066–1071. doi:doi:10.1056/NEJM199704103361506

Barolet, D. (2008). Light-emitting diodes (LEDs) in dermatology. *Semin in Cutan Med Surg*, *27*(4), 227–38. doi:10.1016/j.sder.2008.08.003

Basford, J. R. (1986). Low-energy laser treatment of pain and wounds: hype, hope, or hokum? *Mayo Clin Proc, 61*, 671-675.

Basford J. R. (1995). Low intensity laser therapy: still not an established clinical tool. *Lasers Surg Med, 16*, 331-342

Basso, F. G., Pansani, T. N., Turrioni, A. P., Bagnato, V. S., Hebling, J., & de Souza Costa, C. A. (2012). In vitro wound healing improvement by low-level laser therapy application in cultured gingival fibroblasts. *Int J Dent*, *2012*, 719452. doi:10.1155/2012/719452

Bellezza, I., Mierla, A. L., & Minelli, A. (2010). Nrf2 and NF-κB and Their Concerted Modulation in Cancer Pathogenesis and Progression. *Cancers*, *2*(2), 483–497. doi:10.3390/cancers2020483

Beveridge, T. J. (2001). Use of the gram stain in microbiology. *Biotech Histochem*, *76*(3), 111–118.

Bezerra, S. C. (2015). Laser Phototherapy (660 nm) Can Be Beneficial for Reducing Gingival Inflammation in Prosthodontics. *Case Reports in Dentistry*, *2015*, 1–6. Retrieved from http://www.hindawi.com/journals/crid/2015/132656/abs/

Bjordal, J. M., Couppé, C., Chow, R. T., Tunér, J., & Ljunggren, E. A. (2003). A systematic review of low level laser therapy with location-specific doses for pain from chronic joint disorders. *J Physiother*, *49*, 107–116.

Bolton, P., Young, S., & Dyson, M. (1991). Macrophage responsiveness to light therapy with varying power and energy densities. *Laser Ther*, *3*(3), 105–111.

Carroll, J. D., Milward, M. R., Cooper, P. R., Hadis, M., & Palin, W. M. (2014). Developments in low level light therapy (LLLT) for dentistry. *Dental Materials : Official Publication of the Academy of Dental Materials*, *30*(5), 465–75. doi:10.1016/j.dental.2014.02.006

Cauwels, R. G., & Martens, L. C. (2011). Low level laser therapy in oral mucositis: a pilot study. *Eur Arch Paediatr Dent*, *12*(2), 118–123.

Chang, P. C., Chien, L. Y., Ye, Y., & Kao, M. J. (2013). Irradiation by light-emitting diode light as an adjunct to facilitate healing of experimental periodontitis in vivo. *J Periodontal Res*, *48*(2), 135–143. doi:10.1111/j.1600-0765.2012.01511.x

Chapple, I. L. C. (1997). Reactive oxygen species and antioxidants in inflammatory diseases. *J Clin Periodontal*, *24*, 287–296.

Chen, X.-L., Dodd, G., Thomas, S., Zhang, X., Wasserman, M. A., Rovin, B. H., & Kunsch, C. (2006). Activation of Nrf2/ARE pathway protects endothelial cells from oxidant injury and inhibits inflammatory gene expression. *Am J Physiol Heart Circ Physiol*, *290*(5), H1862–H1870. doi:10.1152/ajpheart.00651.2005

Chen, A. C., Arany, P. R., Huang, Y. Y., Tomkinson, E. M., Sharma, S. K., Kharkwal, G. B., … Hamblin, M. R. (2011). Low-level laser therapy activates NF-kB via generation of reactive oxygen species in mouse embryonic fibroblasts. *PLoS ONE*, *6*(7), e22453. doi:10.1371/journal.pone.0022453

Choi, H., Lim, W., Kim, I., Kim, J., Ko, Y., Kwon, H., … Kim, O. (2012). Inflammatory cytokines are suppressed by light-emitting diode irradiation of P. gingivalis LPS-treated human gingival fibroblasts: inflammatory cytokine changes by LED irradiation. *Lasers Med Sci*, *27*(2), 459–467.

Chor, A., de Azevedo, A. M., Maiolino, A., & Nucci, M. (2004). Successful treatment of oral lesions of chronic lichenoid graft-vs.-host disease by the addition of low-level laser therapy to systemic immunosuppression. *Eur J Haematol*, *72*(3), 222–224. doi:10.1046/j.0902-4441.2003.00202.x

Chung, H., Dai, T., Sharma, S. K., Huang, Y. Y., Carroll, J. D., & Hamblin, M. R. (2012). The nuts and bolts of low-level laser (light) therapy. *Ann Biomed Eng*, *40*(2), 516–533. doi:10.1007/s10439-011-0454-7

Clark, A. (2000). Post-transcriptional regulation of pro-inflammatory gene expression. *Arthritis Res*, *2*(3), 172–174. doi:10.1186/ar83

Clerehugh, V., Tugnait, A., & Genco, R. (2009). *Periodontology at a glance*. Wiley-Blackwell.

Conlan, M. J., Rapley, J. W., & Cobb, C. M. (1996). Biostimulation of wound healing by low-energy laser irradiation. A review. *J Clin Periodontol*, *23*(5), 492–496. Retrieved from http://www.ncbi.nlm.nih.gov/pubmed/8783057

Coussens, L. M., & Werb, Z. (2002). Inflammation and cancer. *Nature*, *420*(6917), 860–867. Retrieved from http://dx.doi.org/10.1038/nature01322

Dale, B. A. (2002). Periodontal epithelium: a newly recognized role in health and disease. *Periodontology 2000*, *30*(1), 70–78. doi:10.1034/j.1600-0757.2002.03007.x

Dall Agnol, M., Nicolau, R., de Lima, C., & Munin, E. (2009). Comparative analysis of coherent light action (laser) versus non-coherent light (light-emitting diode) for tissue repair in diabetic rats. *Lasers in Medical Science*, *24*(6), 909–916. doi:10.1007/s10103-009-0648-5

Davidson, J. M. (1992). *Wound repair*. (J. I. Gallin, I. M. Goldstein, & R. Synderman, Eds.)*Inflammation: Basic Principles and Clinical Correlates* (Second.). New York: Raven Press, Ltd.

Denis, T. G. S., & Hamblin, M. R. (2013). 4. History and Fundamentals of Photodynamic Therapy. In *Handbook of Photomedicine* (pp. 35–42).

Downes, A., & Blunt, T. P. (1877). Researches on the Effect of Light upon Bacteria and other Organisms. *Proc R Soc Lond*, *28*, 488–500.

Eduardo, F. de P., Bueno, D. F., de Freitas, P. M., Marques, M. M., Passos-Bueno, M. R., Eduardo, C. de P., & Zatz, M. (2008). Stem cell proliferation under low intensity laser irradiation: A preliminary study. *Lasers Surg Med*, *40*(6), 433–438. doi:10.1002/lsm.20646

Eke, P. I., Dye, B. A., Wei, L., Thornton-Evans, G. O., & Genco, R. J. (2012). Prevalence of Periodontitis in Adults in the United States: 2009 and 2010. *J Dent Res*, *91*(10), 914–920. doi:10.1177/0022034512457373

Ferrero-Miliani, L., Nielsen, O. H., Andersen, P. S., & Girardin, S. E. (2006). Chronic inflammation: importance of NOD2 and NALP3 in interleukin-1beta generation. *Clin Exp Immunol*, *147*(2), 227–235. doi:10.1111/j.1365-2249.2006.03261.x

Fork, R. L. (1971). Laser Stimulation of Nerve Cells in Aplysia. *Science*, *171*(3974), 907–908. doi:10.1126/science.171.3974.907

Fujimaki, Y., Shimoyama, T., Liu, Q., Umeda, T., Nakaji, S., & Sugawara, K. (2003). Low-Level Laser Irradiation Attenuates Production of Reactive Oxygen Species by Human Neutrophils. *J Clin Laser Med Surg*, *21*(3), 165–170.

Gao, X., & Xing, D. (2009). Molecular mechanisms of cell proliferation induced by low power laser irradiation. *J Biomed Sci*, *16*, 4. doi:10.1186/1423-0127-16-4

Gaspar, L. (2009). Professor Endre Mester, the Father of Photobiomodulation. *J Laser Dent*, *17*(3), 146–148.

Gerschman, J. A., Ruben, J., & Gebart-Eaglemont, J. (1994). Low level laser therapy for dentinal tooth hypersensitivity. *Aust Dent J*, *39*(6), 353–357.

Gilmore, T. D. (2006). Introduction to NF-[kappa]B: players, pathways, perspectives. *Oncogene*, *25*(51), 6680–6684. Retrieved from http://dx.doi.org/10.1038/sj.onc.1209954

Greathouse, D. G., Currier, D. P., & Gilmore, R. L. (1985). Effects of Clinical Infrared Laser on Superficial Radial Nerve Conduction. *Phys Ther*, *65*(8), 1184–1187. Retrieved from http://ptjournal.apta.org/content/65/8/1184.abstract

Greco, M., Guida, G., Perlino, E., Marra, E., & Quagliariello, E. (1989). Increase in RNA and protein synthesis by mitochondria irradiated with Helium-Neon laser. *Biochem Biophys Res Commun*, *163*(3), 1428–1434. doi:http://dx.doi.org/10.1016/0006-291X(89)91138-8

Griffen, A. N. N. L., Becker, M. R., Lyons, S. R., Moeschberger, M. L., & Leys, E. J. (1998). Prevalence of Porphyromonas gingivalis and Periodontal Health Status. *J Clin Microbiol*, *36*(11), 3239–3242.

Gupta, A., & Hamblin, M. R. (2013). 5. History and Fundamentals of Low-level Laser (Light) Therapy. In *Handbook of Photomedicine* (pp. 43–52).

Gursoy, H., Ozcakir-Tomruk, C., Tanalp, J., & Yilmaz, S. (2013). Photodynamic therapy in dentistry: A literature review. *Clin Oral Invest*, *17*, 1113–1125. doi:10.1007/s00784-012-0845-7

Haas, A. F., Isseroff, R. R., Wheeland, R. G., Rood, P. A., & Graves, P. J. (1990). Low-energy helium-neon laser irradiation increases the motility of cultured human keratinocytes. *J Invest Dermatol*, *94*(6), 822–826.

Hadis, M. A., Cooper, P. R., Milward, M. R., Gorecki, P., Tarte, E., Churm, J., & Palin, W. M. (2015). The effect of UV-Vis to near-infrared light on the biological response of human dental pulp cells. *Proc SPIE 9309, Mechanism For Low-Light Therapy X*,*930906 (March 5, 2015)*. doi:10.1117/12.2077645

Hadis, M. A., Zainal, S. A., Holder, M. J., Carroll, J. D., Cooper, P. R., Milward, M. R., & Palin, W. M. (2016). The dark art of light measurement : accurate radiometry for low-level light therapy. *Lasers Med Sci*. doi:10.1007/s10103-016-1914-y

Hallman, H. O., Basford, J. R., O'Brien, J. F., & Cummins, L. A. (1988). Does low-energy helium-neon laser irradiation alter "in vitro" replication of human fibroblasts? *Lasers Surg Med*, *8*(2), 125–129. doi:10.1002/lsm.1900080206

Hamblin, M. R., & Demidova, T. N. (2006). Mechanisms of Low Level Light Therapy. *Proc of SPIE*, *6140*, 614001–614012.

Hawkins, D. H., & Abrahamse, H. (2006). The role of laser fluence in cell viability, proliferation, and membrane integrity of wounded human skin fibroblasts following helium-neon laser irradiation. *Lasers Surg Med*, *38*(1), 74–83. doi:10.1002/lsm.20271

Hess, J., Angel, P., & Schorpp-Kistner, M. (2004). AP-1 subunits: quarrel and harmony among siblings. *J Cell Sci*, *117*(25), 5965–5973. doi:10.1242/jcs.01589

Holder, M. J., Milward, M. R., Palin, W. M., Hadis, M. A., & Cooper, P. R. (2012). Effects of Red Light-emitting Diode Irradiation on Dental Pulp Cells. *J Dent Res*, *91*(10), 961–966. doi:10.1177/0022034512456040

Houreld, N. N., Masha, R. T., & Abrahamse, H. (2012). Low-intensity laser irradiation at 660 nm stimulates cytochrome c oxidase in stressed fibroblast cells. *Lasers Surg Med*, *44*(5), 429–34. doi:10.1002/lsm.22027

How, K. Y., Song, K. P., & Chan, K. G. (2016). Porphyromonas gingivalis: An Overview of Periodontopathic Pathogen below the Gum Line. *Frontiers in Microbiology*, *7*(February), 53. doi:10.3389/fmicb.2016.00053

Huang, Y. Y., Chen, A. C., Carroll, J. D., & Hamblin, M. R. (2009). Biphasic dose response in low level light therapy. *Dose Response*, *7*(4), 358–383. doi:10.2203/dose-response.09-027.Hamblin

Huang, Y.-Y., Sharma, S. K., Carroll, J., & Hamblin, M. R. (2011). Biphasic dose response in low level light therapy - an update. *Dose-Response : A Publication of International Hormesis Society*, *9*(4), 602–18. doi:10.2203/dose-response.11-009.Hamblin

Igarashi, T., Nishino, K., & Nayar, S. K. (2005). The appearance of human skin. Technical report: CUCS-024-05, Department of Computer Science, Columbia University.

Igic, M., Kesic, L., Lekovic, V., Apostolovic, M., Mihailovic, D., Kostadinovic, L., & Milasin, J. (2012). Chronic gingivitis: the prevalence of periodontopathogens and therapy efficiency. *Eur J Clin Microbiol Infect Dis*, *31*(8), 1911–1915.

Jenkins, P. a, & Carroll, J. D. (2011). How to report low-level laser therapy (LLLT)/photomedicine dose and beam parameters in clinical and laboratory studies. *Photomed Laser Surg*, *29*(12), 785–7. doi:10.1089/pho.2011.9895

Karin, M., Liu, Z., & Zandi, E. (1997). AP-1 function and regulation. *Curr Opin Cell Biol*, *9*(2), 240–246.

Karu, T. (1989). Photobiology of low-power laser effects. *Health Phys*, *56*(5), 691–704. Retrieved from http://www.ncbi.nlm.nih.gov/pubmed/2651364

Karu, T. (1999). Primary and secondary mechanisms of action of visible to near-IR radiation on cells. *J Photochem Photobiol B*, *49*(1), 1–17. doi:http://dx.doi.org/10.1016/S1011-1344(98)00219-X

Karu, T. (2003). Low-Power Laser Therapy. *Biomedical Photonics Handbook*.

Karu, T. I. (2008). Mitochondrial Signaling in Mammalian Cells Activated by Red and Near-IR Radiation. *Photochem Photobiol*, *84*(5), 1091–1099. doi:10.1111/j.1751-1097.2008.00394.x

Karu, T. I. (2010). Multiple roles of cytochrome c oxidase in mammalian cells under action of red and IR-A radiation. *IUBMB Life*, *62*(8), 607–610. doi:10.1002/iub.359

Karu, T. I., & Kolyakov, S. F. (2005). Exact action spectra for cellular responses relevant to phototherapy. *Photomed Laser Surg*, *23*(4), 355–361. doi:10.1089/pho.2005.23.355

Karu, T. I., Pyatibrat, L. V, Kolyakov, S. F., & Afanasyeva, N. I. (2005). Absorption measurements of a cell monolayer relevant to phototherapy: Reduction of cytochrome c oxidase under near IR radiation. *J Photochem Photobiol B*, *81*(2), 98–106. doi:10.1016/j.jphotobiol.2005.07.002

Kishen, A., & Asundi, A. (2007). *Fundamentals and Applications of Biophotonics in Dentistry*. *Series on Biomaterials and Bioengineering*. London: Imperial College Press.

Konopka, K., & Goslinski, T. (2007). Photodynamic Therapy in Dentistry. *J Dent Res*, *86*(8), 694–707. doi:10.1177/154405910708600803

Konstan, M. W., & Berger, M. (1997). Current understanding of the inflammatory process in cystic fibrosis: Onset and etiology. *Pediatr Pulmonol*, *24*(2), 137–142. doi:10.1002/(sici)1099-0496(199708)24:2<137::aid-ppul13>3.0.co;2-3

Kreisler, M., Christoffers, A. B., Al-Haj, H., Willershausen, B., & d'Hoedt, B. (2002). Low level 809-nm diode laser-induced in vitro stimulation of the proliferation of human gingival fibroblasts. *Lasers Surg Med*, *30*(5), 365–369. doi:10.1002/lsm.10060

Lagan, K. M., Mc Donough, S. M., Clements, B. A., & Baxter, G. D. (2000). A case report of low intensity laser therapy (LILT) in the management of venous ulceration: potential effects of wound debridement upon efficacy. *J Clin Laser Med Surg*, *18*, 15–22.

Lee, J. M., & Johnson, J. A. (2004). An important role of Nrf2-ARE pathway in the cellular defense mechanism. *J Biochem Mol Biol*, *37*(2), 139–143. Retrieved from http://www.ncbi.nlm.nih.gov/pubmed/15469687

Lee, J.-M., Li, J., Johnson, D. A., Stein, T. D., Kraft, A. D., Calkins, M. J., … Johnson, J. A. (2005). Nrf2, a multi-organ protector? *The FASEB Journal*, *19*(9), 1061–1066. doi:10.1096/fj.04-2591hyp

Lee, H. S., Lee, D. H., Cho, S., & Chung, J. H. (2006). Minimal heating dose: a novel biological unit to measure infrared irradiation. *Photodermatol Photoimmunol Photomed, 22,* 148-152

Li, W. T., Leu, Y. C., & Wu, J. L. (2010). Red-light light-emitting diode irradiation increases the proliferation and osteogenic differentiation of rat bone marrow mesenchymal stem cells. *Photomed Laser Surg*, *28 Suppl 1*, S157–65. doi:10.1089/pho.2009.2540

Liang, H. L., Whelan, H. T., Eells, J. T., & Wong-Riley, M. T. T. (2008). Near-infrared light via light-emitting diode treatment is therapeutic against rotenone- and 1-methyl-4-phenylpyridinium ion-induced neurotoxicity. *Neuroscience*, *153*(4), 963–974. doi:10.1016/j.neuroscience.2008.03.042

Lins, R. D., Dantas, E. M., Lucena, K. C., Catao, M. H., Granville-Garcia, A. F., & Carvalho Neto, L. G. (2010). Biostimulation effects of low-power laser in the repair process. *An Bras Dermatol*, *85*(6), 849–855. Retrieved from http://www.ncbi.nlm.nih.gov/pubmed/21308309

Lizarelli, R. F. Z., Miguel, F. A. C., Villa, G. E. P., Filho, E. de C., Pelino, J. E. P., & Bagnato, V. S. (2007). Clinical Effects of Low-intensity Laser vs Light-emitting Diode Therapy on Dentin Hypersensitivity. *J Oral Laser Appli*. Retrieved from http://jola.quintessenz.de/jola_2007_02_s0129.pdf

Louis, K. S., & Siegel, A. C. (2011). Mammalian Cell Viability. In M. J. Stoddart (Ed.), *Mammalian Cell Viability: Methods and Protocols, Methods in Molecular Biology, vol 740* (Vol. 740, pp. 7–12). Totowa, NJ: Humana Press. doi:10.1007/978-1-61779-108-6

Maas-Szabowski, N., Stark, H.-J., & Fusenig, N. E. (2002). *Culture of Epithelial Cells*. (R. I. Freshney & M. G. Freshney, Eds.)*Culture of Specialized Cells*. Wiley-Liss, Inc.

Makhlouf, M., Dahaba, M., Tunér, J., Eissa, S., & Harhash, T. (2012). Effect of adjunctive low level laser therapy (LLLT) on nonsurgical treatment of chronic periodontitis. *Photomed Laser Surg*, *30*, 160–166.

Masha, R. T., Houreld, N. N., & Abrahamse, H. (2013). Low-intensity laser irradiation at 660 nm stimulates transcription of genes involved in the electron transport chain. *Photomed Laser Surg*, *31*(2), 47–53. doi:10.1089/pho.2012.3369

Matthews, J. B., Wright, H. J., Roberts, A., Ling-Mountford, N., Cooper, P. R., & Chapple, I. L. C. (2007). Neutrophil Hyper-responsiveness in Periodontitis. *J Dent Res*, *86*(8), 718–722. doi:10.1177/154405910708600806

Maver-Biscanin, M., Stipetic-Mravak, M., Jerolimov, V., & Biscanin, A. (2004). Fungicidal effect of diode laser irradiation in patients with denture stomatitis. *Lasers Surg Med*, *35*(4), 259–262.

Medzhitov, R. (2010). Inflammation 2010: New Adventures of an Old Flame. *Cell*, *140*(6), 771–776. doi:http://dx.doi.org/10.1016/j.cell.2010.03.006

Medzhitov, R. (2008). Origin and physiological roles of inflammation. *Nature*, *454*(7203), 428–435. Retrieved from http://dx.doi.org/10.1038/nature07201

Milward, M. R., Chapple, I. L., Carter, K., Matthews, J. B., & Cooper, P. R. (2012). Micronutrient modulation of NF-κB in oral keratinocytes exposed to periodontal bacteria. *Innate Immun, 0(0)*, 1-12.

Milward, M. R. (2010). *Oral epithelium in the pathogenesis of periodontitis*. *School of Dentistry, Unit of Periodontology*. University of Birmingham. http://etheses.bham.ac.uk/1007/1/Milward10PhD.pdf

Milward, M. R., Chapple, I. L., Wright, H. J., Millard, J. L., Matthews, J. B., & Cooper, P. R. (2007). Differential activation of NF-kappaB and gene expression in oral epithelial cells by periodontal pathogens. *Clin Exp Immunol*, *148*(2), 307–324. doi:10.1111/j.1365-2249.2007.03342.x

Mima, E. G. de O., Pavarina, A. C., Dovigo, L. N., Vergani, C. E., Costa, C. A. de S., Kurachi, C., & Bagnato, V. S. (2010). Susceptibility of Candida albicans to photodynamic therapy in a murine model of oral candidosis. *Oral Surg Oral Med Oral Pathol Oral Radiol Endod*, *109*(3), 392–401. doi:http://dx.doi.org/10.1016/j.tripleo.2009.10.006

Mohammed, I. F., Al-Mustawfi, N., & Kaka, L. N. (2007). Promotion of regenerative processes in injured peripheral nerve induced by low-level laser therapy. *Photomed Laser Surg*, *25*(2), 107–111. doi:10.1089/pho.2006.1090

Morgan, M. C., & Rashid, R. M. (2009). The effect of phototherapy on neutrophils. *Int Immunopharmacol*, *9*(4), 383–388. doi:10.1016/j.intimp.2009.02.001

Morita, H., Kohno, J., Hori, M., & Kitano, Y. (1993). Clinical application of low reactive level laser therapy (LLLT) for atopic dermatitis. *Keio J Med*, *42*(4), 174–176.

Mosmann, T. (1983). Rapid colorimetric assay for cellular growth and survival: Application to proliferation and cytotoxicity assays. *J Immunol Methods*, *65*(1–2), 55–63. doi:http://dx.doi.org/10.1016/0022-1759(83)90303-4

Naka, T., & Yokose, S. (2012). Application of Laser-Induced Bone Therapy by Carbon Dioxide Laser Irradiation in Implant Therapy. *Int J Dent*, *2012*, 1–8. doi:10.1155/2012/409496

Nanci, A., & Bosshardt, D. D. (2006). Structure of periodontal tissues in health and disease *. *Periodontology 2000*, *40*, 11–28.

Nathan, C. (2002). Points of control in inflammation. *Nature*, *420*(6917), 846–852. Retrieved from http://dx.doi.org/10.1038/nature01320

Needleman, I., McGrath, C., Floyd, P., & Biddle, A. (2004). Impact of oral health on the life quality of periodontal patients. *J Clin Invest*, *31*, 454–457. doi:10.1111/j.1600-051X.2004.00498.x

Nguyen, T., Sherratt, P. J., & Pickett, C. B. (2003). Regulatory mechanisms controlling gene expression mediated by the antioxidant response element. *Annu Rev Pharmacol Toxicol*, *43*, 233–260. doi:10.1146/annurev.pharmtox.43.100901.140229

Oliveira, C. F., Basso, F. G., Lins, E. C., Kurachi, C., Hebling, J., Bagnato, V. S., & de Souza Costa, C. A. (2011). In vitro effect of low-level laser on odontoblast-like cells. *Laser Phys Lett*, *8*(2), 155–163. doi:10.1002/lapl.201010101

Palin, W. M., Hadis, M. A., Milward, M. R., Carroll, J. D., & Cooper, P. R. (2015). Beam profile measurements for dental phototherapy: the effect of distance, wavelength and tissue thickness. *Proc SPIE 9309, Mechanisms for Low-Light Therapy X, 930905 (March 5, 2015)*. doi:10.1117/12.2077628

Palmer, R. M., Wilson, R. F., Hasan, A. S., & Scott, D. A. (2005). Mechanisms of action of environmental factors – tobacco smoking. *J Clin Periodontol*, *32*, 180–195. doi:10.1111/j.1600-051X.2005.00786.x

Palumbo, A. (2011). The Anatomy and Physiology of the Healthy Periodontium. Retrieved from http://cdn.intechopen.com/pdfs-wm/20289.pdf

Parker, S. (2007). Verifiable CPD paper: Low-level laser use in dentistry. *Br Dent J*, *202*(3), 131–138. Retrieved from http://dx.doi.org/10.1038/bdj.2007.75

Pfaffl, M. W. (2001). A new mathematical model for relative quantification in real-time RT-PCR. *Nucleic Acids Research*, *29*(9), 45e–45. doi:10.1093/nar/29.9.e45

Pihlstrom, B. L., Michalowicz, B. S., & Johnson, N. W. (2005). Periodontal diseases. *Lancet*, *366*(9499), 1809–1820. doi:http://dx.doi.org/10.1016/S0140-6736(05)67728-8

Pogrel, M. A., Chen, J. W., & Zhang, K. (1997). Effects of low-energy gallium-aluminum-arsenide laser irradiation on cultured fibroblasts and keratinocytes. *Lasers Surg Med*, *20*(4), 426–432. doi:10.1002/(sici)1096-9101(1997)20:4<426::aid-lsm8>3.0.co;2-s

Posten, W., Wrone, D. A., Dover, J. S., Arndt, K. A., Silapunt, S., & Alam, M. (2005). Low-Level Laser Therapy for Wound Healing: Mechanism and Efficacy. *Dermatol Surg*, *31*(3), 334–340. doi:10.1111/j.1524-4725.2005.31086

Prime, S. S., Nixon, S. V. R., Crane, I. J., Stone, A., Matthews, J. B., Maitland, N. J., … Scully, C. (1990). The behaviour of human oral squamous cell carcinoma in cell culture. *J Pathol*, *160*(3), 259–269. doi:10.1002/path.1711600313

Rangasamy, T., Cho, C. Y., Thimmulappa, R. K., Zhen, L., Srisuma, S. S., Kensler, T. W., … Biswal, S. (2004). Genetic ablation of Nrf2 enhances susceptibility to cigarette smoke–induced emphysema in mice. *J Clin Invest*, *114*(9), 1248–1259. doi:10.1172/jci21146

Roelandts, R. (2002). The history of phototherapy: Something new under the sun? *J Am Acad Dermatol*, *46*(6), 926–930. doi:http://dx.doi.org/10.1067/mjd.2002.121354

Roelandts, R. (2005). A new light on Niels Finsen, a century after his nobel prize. *Photodermatol Photoimmunol Photomed*, *21*(3), 115–117. doi:10.1111/j.1600-0781.2005.00160.x

Rood, P. A., Haas, A. F., Graves, P. J., Wheeland, R. G., & Isseroff, R. R. (1992). Low-energy helium neon laser irradiation does not alter human keratinocyte differentiation. *J Invest Dermatol*, *99*(4), 445–448.

Salahaldin, A. H., Abdulhadi, K., Najjar, N., & Bener, A. (2012). Low-Level Laser Therapy in Patients with Complaints of Tinnitus: A Clinical Study. *ISRN Otolaryngol*, *2012*, 1–5. doi:10.5402/2012/132060

Scannapeico, F. A., Bush, R. B., & Paju, S. (2003). Associations between periodontal disease and risk for atherosclerosis, cardiovascular disease, and stroke. A systematic review. *Ann Periodontol*, *8*(1).

Schindl, A., Merwald, H., Schindl, L., Kaun, C., & Wojta, J. (2003). Direct stimulatory effect of low-intensity 670 nm laser irradiation on human endothelial cell proliferation. *Br J Dermatol*, *148*(2), 334–336. doi:10.1046/j.1365-2133.2003.05070.x

Scholzen, T., & Gerdes, J. (2000). The Ki-67 protein: From the known and the unknown. *J Cell Physiol*, *182*(3), 311–322. doi:10.1002/(sici)1097-4652(200003)182:3<311::aid-jcp1>3.0.co;2-9

Schultz, M. (2008). Rudolf Virchow. *Emerg Infect Diseases*, *14*(9), 1480–1481. doi:10.3201/eid1409.086672

Scott, D. A., & Krauss, J. L. (2012). Neutrophils in periodontal inflammation. *Front Oral Biol*, *15*, 56–83. doi:10.1159/000329672.Neutrophils

Seymour, G. J., Ford, P. J., Cullinan, M. P., Leishman, S., & Yamazaki, K. (2007). Relationship between periodontal infections and systemic disease. *Clin Microbiol Infect*, *13*, 3–10. doi:10.1111/j.1469-0691.2007.01798.x

Sgolastra, F., Petrucci, A., Severino, M., Gatto, R., & Monaco, A. (2013). Lasers for the Treatment of Dentin Hypersensitivity: A Meta-analysis. *J Dent Res*. doi:10.1177/0022034513487212

Shivakumar, V., Sudhir, G., Priyadarshoni, Sp., & Shanmugam, M. (2012). Scope of photodynamic therapy in periodontics and other fields of dentistry. *J Interdiscip Dentistry*, *2*(2), 78. doi:10.4103/2229-5194.100598

Siebenlist, U., Franzoso, G., & Brown, K. (1994). Structure, regulation and function of NF-kappa B. *Annu Rev Cell Biol*, *10*, 405–455. doi:10.1146/annurev.cb.10.110194.002201

Signat, B., Roques, C., Poulet, P., & Duffaut, D. (1995). Role of Fusobacterium nucleatum in Periodontal Health and Disease. *Curr Issues Mol Biol*, *13*, 25–36.

Silva, T. A., Garlet, G. P., Fukada, S. Y., Silva, J. S., & Cunha, F. Q. (2007). Chemokines in Oral Inflammatory Diseases: Apical Periodontitis and Periodontal Disease. *J Dent Res*, *86*(4), 306–319. doi:10.1177/154405910708600403

Slot, D. E., Jorritsma, K. H., Cobb, C. M., & Van der Weijden, G. A. (2014). The effect of the thermal diode laser (wavelength 808-980nm) in non- surgical periodontal therapy: a systematic review and meta-analysis. *J Clin Periodontol*, n/a–n/a. doi:10.1111/jcpe.12233

Socransky, S., Haffajee, A., Cugini, M., Smith, C., & Kent Jr, R. (1998). Microbial complexes in subgingival plaque. *J Clin Periodontol*, *25*, 134–144.

Socransky, S. S., & Haffajee, A. D. (2005). Periodontal microbial ecology. *Periodontol 2000*, *38*, 135–187.

Sommer, A. P., Pinheiro, A. L., Mester, A. R., Franke, R. P., & Whelan, H. T. (2001). Biostimulatory windows in low-intensity laser activation: lasers, scanners, and NASA's light-emitting diode array system. *J Clin Laser Med Surg*, *19*(1), 29–33. doi:10.1089/104454701750066910

Sperandio, F. F., Simões, A., Corrêa, L., Aranha, A. C. C., Giudice, F. S., Hamblin, M. R., & Sousa, S. C. O. M. (2014). Low-level laser irradiation promotes the proliferation and maturation of keratinocytes during epithelial wound repair. *J Biophotonics*, *9999*(9999), 1–9. doi:10.1002/jbio.201400064

Suda, T. & Dexter, T. M. (1981). Effect of hydrocortisone on long-term human marrow cultures. *Br J Haematol, 48,* 661-664.

Sylvester, P. (2011). Optimization of the Tetrazolium Dye (MTT) Colorimetric Assay for Cellular Growth and Viability. In S. D. Satyanarayanajois (Ed.), *Drug Des Discov* (Vol. 716, pp. 157–168). Humana Press. doi:10.1007/978-1-61779-012-6_9

Tak, P. P., & Firestein, G. S. (2001). NF-kappaB: a key role in inflammatory diseases. *J Clin Invest*, *107*(1), 7–11. doi:10.1172/JCI11830

Uehara, A., & Takada, H. (2007). Functional TLRs and NODs in Human Gingival Fibroblasts. *J Dent Res*, *86*(3), 249–254. doi:10.1177/154405910708600310

Verma, I. M., Stevenson, J. K., Schwarz, E. M., Van Antwerp, D., & Miyamoto, S. (1995). Rel/NF-kappa B/I kappa B family: intimate tales of association and dissociation. *Genes & Development*, *9*(22), 2723–2735. doi:10.1101/gad.9.22.2723

Vinck, E. M., Cagnie, B. J., Cornelissen, M. J., Declercq, H. A., & Cambier, D. C. (2003). Increased fibroblast proliferation induced by light emitting diode and low power laser irradiation. *Lasers Med Sci*, *18*(2), 95–99. doi:10.1007/s10103-003-0262-x

Walsh, L. J. (1997). The current status of low level laser therapy in dentistry, Part 1. Soft tissue applications. *Aust Dent J*, *42*(4), 247–254. doi:10.1111/j.1834-7819.1997.tb00129.x

Wang, C.-Y., Tsai, S.-C., Yu, M.-C., Lin, Y.-F., Chen, C.-C., & Chang, P.-C. (2015). 660 nm LED Light Irradiation Promotes the Healing of the Donor Wound of Free Gingival Graft. *J Periodontol*, 1–17. doi:10.1902/jop.2015.140580

Weiss, R. A., McDaniel, D. H., Geronemus, R. G., Margaret, A. W., Karen, L. B., Munavalli, G. M., & Bellew, S. G. (2005). Clinical Experience with Light-Emitting Diode (LED) Photomodulation. *Dermatol Surg*, *31*, 1199–1205. doi:10.1111/j.1524-4725.2005.31926

White, D. A., Tsakos, G., Pitts, N. B., Fuller, E., Douglas, G. V. A., Murray, J. J., & Steele, J. G. (2012). Adult Dental Health Survey 2009: common oral health conditions and their impact on the population. *Br Dent J*, *213*, 567–572.

White, P. C. (2015). *The role of neutrophil extracellular traps in the pathogenesis of periodontal disease*. *School of Dentistry, Unit of Periodontology*. University of Birmingham. http://etheses.bham.ac.uk/6497/1/White16PhD.pdf

Wong-Riley, M. T. T., Liang, H. L., Eells, J. T., Chance, B., Henry, M. M., Buchmann, E., … Whelan, H. T. (2005). Photobiomodulation Directly Benefits Primary Neurons Functionally Inactivated by Toxins. *J Biol Chem*, *280*(6), 4761–4771. doi:10.1074/jbc.M409650200

Zhang, Y., Song, S., Fong, C. C., Tsang, C. H., Yang, Z., & Yang, M. (2003). cDNA microarray analysis of gene expression profiles in human fibroblast cells irradiated with red light. *J Invest Dermatol*, *120*(5), 849–857. doi:10.1046/j.1523-1747.2003.12133.x

APPENDIX

1. Optimisation of radiant exposure for laser irradiation

A pilot experiment was performed in order to optimise the radiant exposure (section 2.2.1.2) for subsequent laser irradiation. Initially, 60s exposure time was used at a distance at 0mm from the culture plate. The radiant exposure (dose) was calculated (Table 2.5) and this indicated that 60s irradiation at 0mm distance between laser and cell culture dish, resulted in a radiant exposure of 107J/cm^2. Initial results of 107J/cm^2 radiant exposure suggested a modification was required in laser dosage (radiant exposure) to optimise the biological response. Therefore subsequent experiments were performed using a reduced radiant exposure of 71J/cm^2 (which equates to 40s exposure time). These initial experiments allowed further refinement of the experimental protocol resulting in the use of a radiant exposure of 53J/cm^2 radiant exposure (30s). All these light exposures were performed 24h post cell seeding.

Following these pilot studies which aimed to determine the optimal light exposure conditions, the next set of experiments aimed to optimise the number of cells receiving light exposure during the irradiation. This was initially attempted by construction of a reflective light cover in order to reflect the laser light back towards the cell monolayer (Figure A1). Experiments investigated if this approach would increase the biological response in H400 cells. So experiments using (a) lid with reflective covering, (b) lid without reflective coating and (c) no lid during exposure were performed to investigate cell growth. Results indicated there was no increased cellular response following use of the reflective lid, therefore for subsequent experiments this experimental modification was not applied.

Table A1: Calculation of radiant exposure for the laser by irradiance value and time for initial experiment.

Type of light	Distance (mm)	Irradiance value (mW/cm^2)	Time (sec)	Radiant exposure (J/cm^2)
Laser	0	1788	60	107
			40	71
			30	53

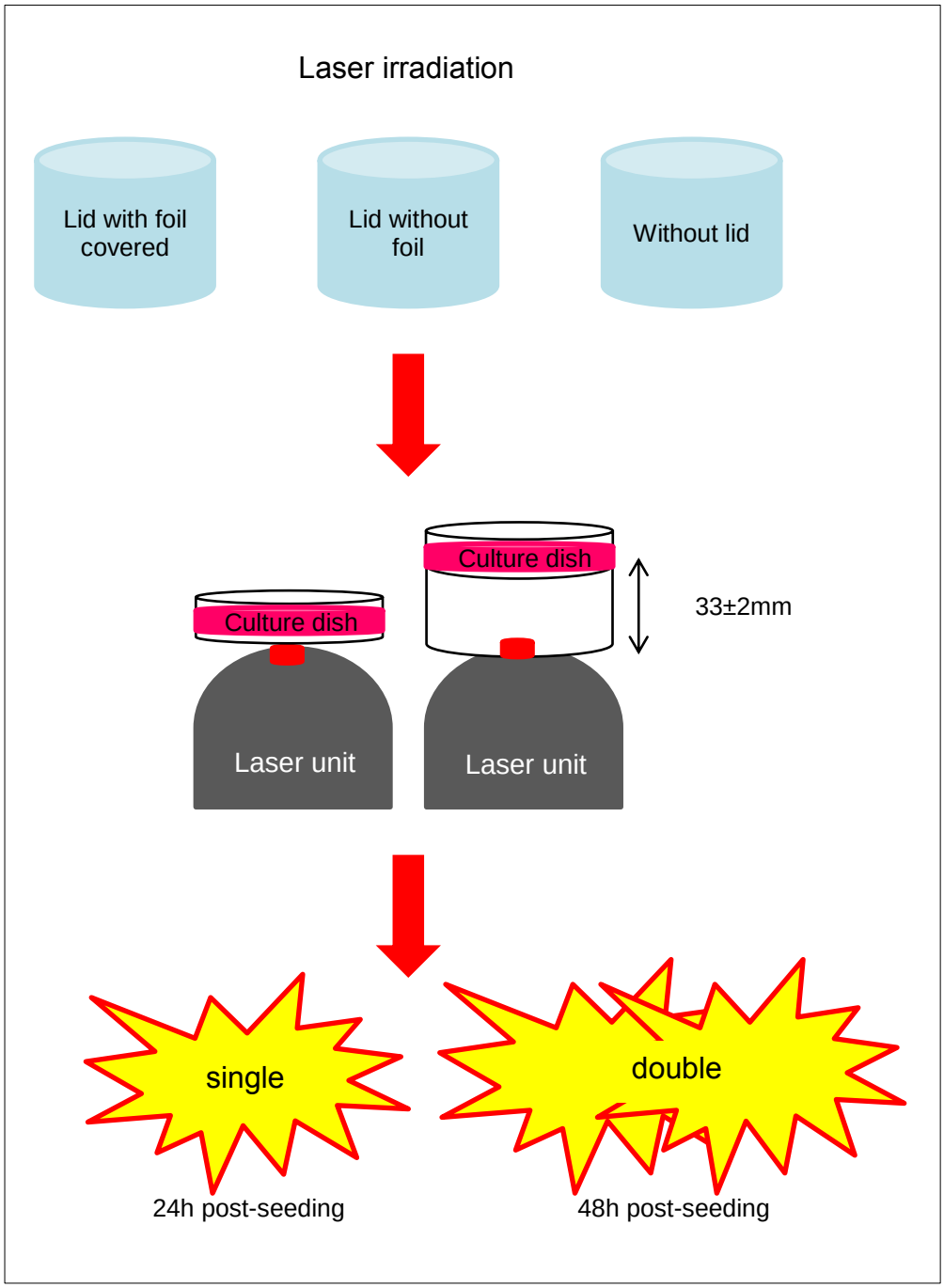

Figure A1: Diagram summarising the exposure regimes for laser irradiation.

2. Optimisation of radiant exposure for single LED irradiation

Initial experiments with single LED utilised 30s and 60s exposure times with 760mW/cm^2 of irradiance value (45 and 22J/cm^2) at 0mm distance. Results indicated that a radiant exposure, achieved by reducing the time of exposure, should be employed whilst using the same distance (0mm). Therefore, H400 cell cultures were irradiated with radiant exposures of 3, 5 and 8J/cm^2 (which equates to exposure times of 4, 7 and 11s, respectively) (Table A2). In addition this was compared with irradiation at a distance of 33mm which reduced radiant exposure and reduced potential for temperature increase as well as increasing the number of cells exposed. H400 cells were exposed at this increased distance for 7 and 30s which equates to radiant exposures of 0.038 and 0.16 J/cm^2, respectively. The two different exposure times (7 and 30s) showed different ranges of H400 cells proliferation. Later experiments with 7 and 30s utilising both single and double dosing regimens, generated data indicated that irradiation of 7s (0.038J/cm^2) with both single and double dosing regimens at the distance (33mm) provided significant results. Further experiments with the condition (7s - 0.038J/cm^2) demonstrated inconsistence data. Therefore, the irradiation regimens were further optimised by using 90 and 181s at 33mm distance (0.5 and 1J/cm^2 respectively). For all subsequent experimentation these conditions, single and double dosage regimes were employed because the cell growth rate with the conditions applied showed potential increases in cell proliferation (section 2.2.3.2).

Table A2: The radiant exposure for the single LED by irradiance value and time.

Type of light	Distance (mm)	Irradiance value (mW/cm^2)	Time (sec)	Radiant exposure (J/cm^2)
LED	0	760	4	3
			7	5
			11	8
			30	22
			60	45
	33	5.5	7	0.038
			30	0.16
			90	0.5
			181	1.0

3. Optimisation of radiant exposure for 1st generation LED array

Initial experiments for 1st generation LED array (section 2.2.3.3) utilised exposure times of 30, 45, 60, 75, 90 and 105s (Table A3). Results generated from cell growth suggested the need to decrease the exposure time (and therefore radiant exposure) to 8s (Table A3). This exposure time, produced statistically significant result.

However, due to the range of radiant exposures explored it was decided to standardise radiant exposure for each wavelength across the LED array to deliver 2, 5 and 10J/cm^2 of radiant exposure using a single dosage regime (see Table 2.8)

Table A3: Radiant exposure (J/cm^2) for each wavelength exposure time.

Quoted wavelength (nm)		625	650	660	670	690	780	800	810	820	830
Radiant exposure (J/cm^2)	30s	2.0	0.3	1.4	0.7	1.6	3.8	4.3	2.0	3.4	3.5
	45s	2.9	0.4	2.2	1.0	2.3	5.7	6.4	3.0	5.1	5.2
	60s	3.9	0.5	2.9	1.4	3.1	7.6	8.5	4.0	6.8	6.9
	75s	4.9	0.7	3.6	1.7	3.9	9.5	10.7	5.0	8.5	8.7
	90s	5.9	0.8	4.3	2.0	4.7	11.4	12.8	6.0	10.3	10.4
	105s	6.9	0.9	5.0	2.4	5.4	13.3	14.9	7.0	12.0	12.1
	8s	0.5	0.1	0.4	0.2	0.4	1.0	1.1	0.5	0.9	0.9

RESEARCH OUTPUT

Lasers Med Sci
DOI 10.1007/s10103-016-1914-y

REVIEW ARTICLE

The dark art of light measurement: accurate radiometry for low-level light therapy

Mohammed A. Hadis[1] · Siti A. Zainal[2] · Michelle J. Holder[2] · James D. Carroll[3] · Paul R. Cooper[2] · Michael R. Milward[2] · William M. Palin[1]

Received: 1 September 2015 / Accepted: 16 February 2016

Abstract Lasers and light-emitting diodes are used for a range of biomedical applications with many studies reporting their beneficial effects. However, three main concerns exist regarding much of the low-level light therapy (LLLT) or photobiomodulation literature; (1) incomplete, inaccurate and unverified irradiation parameters, (2) miscalculation of 'dose,' and (3) the misuse of appropriate light property terminology. The aim of this systematic review was to assess where, and to what extent, these inadequacies exist and to provide an overview of 'best practice' in light measurement methods and importance of correct light measurement. A review of recent relevant literature was performed in PubMed using the terms LLLT and photobiomodulation (March 2014–March 2015) to investigate the contemporary information available in LLLT and photobiomodulation literature in terms of reporting light properties and irradiation parameters. A total of 74 articles formed the basis of this systematic review. Although most articles reported beneficial effects following LLLT, the majority contained no information in terms of how light was measured (73 %) and relied on manufacturer-stated values. For all papers reviewed, missing information for specific light parameters included wavelength (3 %), light source type (8 %), power (41 %), pulse frequency (52 %), beam area (40 %), irradiance (43 %), exposure time (16 %), radiant energy (74 %) and fluence (16 %). Frequent use of incorrect terminology was also observed within the reviewed literature. A poor understanding of photophysics is evident as a significant number of papers neglected to report or misreported important radiometric data. These errors affect repeatability and reliability of studies shared between scientists, manufacturers and clinicians and could degrade efficacy of patient treatments. Researchers need a physicist or appropriately skilled engineer on the team, and manuscript reviewers should reject papers that do not report beam measurement methods and all ten key parameters: wavelength, power, irradiation time, beam area (at the skin or culture surface; this is not necessarily the same size as the aperture), radiant energy, radiant exposure, pulse parameters, number of treatments, interval between treatments and anatomical location. Inclusion of these parameters will improve the information available to compare and contrast study outcomes and improve repeatability, reliability of studies.

Keywords Radiometry · Low-level light therapy · Low-level laser therapy · LLLT · Photobiomodulation

✉ Mohammed A. Hadis
HadisM@bham.ac.uk

[1] Biomaterials Unit, School of Dentistry, College of Medical and Dental Sciences, University of Birmingham, St Chads Queensway, Birmingham, UK B4 6NN

[2] Oral Biology, School of Dentistry, College of Medical and Dental Sciences, University of Birmingham, St Chads Queensway, Birmingham, UK B4 6NN

[3] THOR Photomedicine Ltd, Chesham, UK

Introduction

'Low-level light therapy' (LLLT) or the recently accepted Medical Subject Heading (MeSH) term, photobiomodulation is the application of light typically within the wavelength range ~600–1000 nm to directly stimulate or inhibit cellular and biological processes. The application of low power (<500 mW; non-thermal and non-destructive) lasers or light-emitting diodes (LEDs; or even a combination of both) have shown therapeutic effects with a number of light parameters

Published online: 10 March 2016

that include irradiance, exposure time and total energy delivered.

Many studies have reported beneficial effects of LLLT following trauma in improving tissue healing [1], reducing inflammation [2], reducing oedema [3], restoring blood flow [4] and inducing analgesia [5] in a number of medical specialties that include musculoskeletal injuries, skin diseases, degenerative diseases, neuropathic pain syndromes and even traumatic brain injuries [1–8]. Favourable data for LLLT in other biomedical areas now also exists, which includes several dental specialties such as endodontics, maxillofacial surgery, oral pathology, oral surgery, orthodontics, pediatric, periodontics and prosthodontics [9] for a range of conditions including oral mucositis [10], dentine hypersensitivity [11] and candidiasis [12]. The application of LLLT may also prevent pain and protect muscles prior to strenuous exercise or trauma, which has significant implications for the wider use of this therapeutic technology as a pre-conditioning modality prior to surgical procedures [13].

Despite several thousand *in vitro* studies, *in vivo* studies and clinical trials reporting positive beneficial effects, articles exist where nil or negative effects have been reported, promoting controversy surrounding the effectiveness of LLLT [14–18]. In certain studies, non-significant effects can be attributed to several factors relating to dosimetry; too much or too little energy, irradiance and exposure time as well as pulse structure and insufficient irradiation area [14, 19, 20]. It is clear that there is a therapeutic window in terms of dosimetry and a biphasic dose response which has been likened to the Arndt-Schulz or hormesis curve [19]. Consequently, irradiation parameters are likely to be key to whether outcomes have a positive, nil or negative effect. Although LLLT parameters are known and have been previously defined in the literature, including specialised mandatory and volunteer laser safety international standards such as US Code of Federal Regulations, American National Standards Institute and the International Standards Manual and other laser safety books and review articles [21, 22], beam parameters are often not measured, calibration of measuring instruments are rarely verified, critical data is often unreported, and in some cases, there are elementary dose calculation errors, all of which leading to misinformation in the literature. The importance of correct measurement and reporting has been emphasised several times within the literature [23–28] and brief 'guidelines' on how to measure and report LLLT dose and beam parameters in clinical and laboratory studies has also been published [23, 29, 30].

The aims of this work are to (1) review the adequacy of reporting irradiation parameters in recent literature, (2) describe fundamental concepts and appropriate methodology for best practice in light property evaluation and (3) define the correct terminology for reporting radiometric parameters.

Methods

To assess the methods and variability of measuring and reporting LLLT irradiation parameters, and radiometric terminology used by researchers, a review of recent relevant literature was performed in PubMed. The following two searches where performed separately: (low and level and light and therapy) and (photobiomodulation). These specific search terms were used as 'LLLT' has been widely recognised and used as a MeSH term for many years, although more recently photobiomodulation has become accepted as a more appropriate description of the action of light on cellular behaviour. Following the literature searches, the results were filtered for 'full-text article', published in a 1-year period between 19th March 2014 and 19th March 2015 (Fig. 1) to ensure a manageable number of articles whilst assessing the latest methods used by researchers. Review articles, editorials, articles in languages other than English and those not relevant to LLLT or photobiomodulation, were excluded and duplicates removed. The selected articles were assessed in terms of the method employed to measure light properties, reporting of light properties (source, wavelength, power, pulse frequency and beam area) and reporting of irradiation parameters (irradiance, exposure time, radiant energy and radiant exposure).

Results

The initial search of the PubMed database resulted in 2295 and 177 articles according to the search terms employed (LLLT and photobiomodulation, respectively), which were filtered and screened (Fig. 1a, b) to 56 [31–86] and 18 [87–104] articles, respectively. Thus, a total of 74 articles formed the basis of this systematic review (Tables 1 and 2).

The majority (71/74; 96 %) of articles reported a positive effect following LLLT, with three articles [43, 70, 87] reporting nil effects following LLLT (Table 2) and none reporting negative effects. Of the 74 articles, 73 % (54/74) did not report methods for light measurement and relied on manufacturers' information. Only 5 % (4/74) of articles reported a full set of data for the parameters/information assessed in this review [83–86]. For articles that did report light measurement methods, the most common was using a power meter (22 %; 16/74), or equivalent. Remarkably, only six (6/74; 8 %) employed a method that was able to measure spectral properties such as wavelength [39, 45, 54, 67, 68, 83]. Two articles (3 %; 2/74) failed to report even manufacturers quoted wavelength [48, 61]. Other parameters which were not reported were power (41 %; 30/74), beam area (41 %; 30/74), irradiance (43 %; 32/74), exposure time (16 %, 12/74), radiant energy (74 %; 55/74) and radiant exposure (fluence; 16 %; 12/74), and these are detailed in Tables 1 and 2.

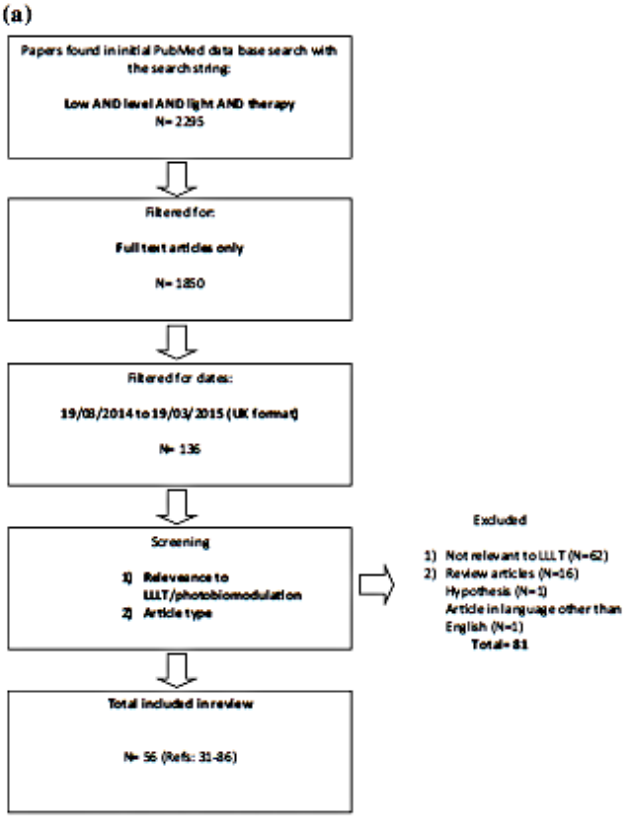

Fig. 1 a Flow chart of search strategy to identify articles for review using 'low and level and light and therapy.' b Flow chart of search strategy to identify articles for review using 'photobiomodulation'

Discussion

The need for the measurement and standardisation of reported irradiation parameters has previously been emphasised [22, 29, 30], and it was proposed that eight key beam parameters should be reported in all LLLT studies [29]: wavelength, power, irradiation time, beam area (at the skin or culture surface), pulse parameters (frequency), anatomical location (skin colour, target location, i.e. depth below skin), number of treatments and the interval between treatments. Whilst other radiometric parameters such as divergence, depth of field, beam polarisation, coherence length, beam profile and spectral width are also important, the authors of that paper suggested those parameters were the minimum necessary for a repeatable scientific study [29]. Thus, in agreement with that paper, a 'bare' minimum approach should be adopted when describing beam parameters and a more thorough approach should utilise more technically demanding techniques such as beam profiling. The importance of describing light parameters and treatment protocol has also been emphasised in several other publications [22–28]. Thus, the focus of this current study was to provide an overview of the fundamental concepts of light measurement and set the basis for a proper evaluation of light properties. Therefore, this study has reviewed the properties directly related to light rather than treatment protocol (anatomical location, number of treatments, interval between treatments).

In the current literature search, 96 % of articles reported positive effects of LLLT with only three articles [43, 70, 87] showing no beneficial effect following LLLT. However, the number of articles that report measured information regarding light properties and irradiation

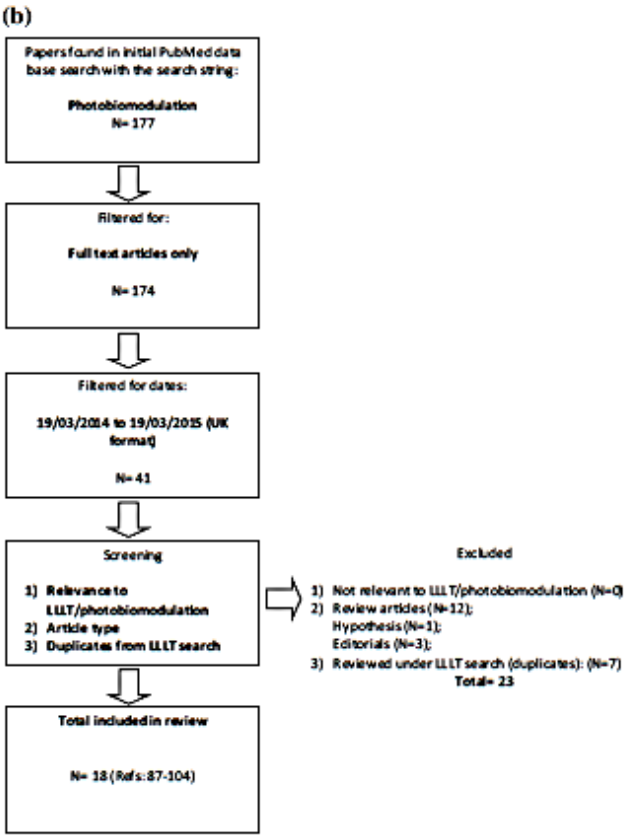

Fig. 1 (continued)

parameters was remarkably low (27 %; Table 1) considering that the physics of light forms a fundamental basis of this therapeutic process. Even when light is measured, the methods employed are not always adequate to fully assess light properties; only 8 % of articles reported a method that was capable of characterising the spectral (wavelength) light output [73–75, 80, 82, 102]. The most common light measurement method used power or energy meters (Table 1), which is obviously an improvement on nil measurement; however, these devices are known to have significant limitations, which is discussed in 'Photodiodes and power meters'.

Table 2 details the current state of light measurement and reporting of light parameters in LLLT studies where missing information does not allow for key parameters to be assessed. It is likely that these inadequacies are related to several factors that include expense of equipment, lack of expertise in equipment usage, poor appreciation of light properties and deficiencies of LLLT research standardisation. Consequently, this review continues by introducing fundamental concepts of light measurement and radiometric terms in attempt to explain their critical importance for LLLT research.

Light: the basics

Over recent centuries, units of measurement have been established for quantifying and reporting the multitude of parameters that describe the wavelength, irradiance and incident beam area, distribution and energy of light. These parameters have significance for LLLT research, and when used properly will fully describe the 'medicine' (the light source and its properties) and the 'dose' (the irradiation parameters/protocol) and will improve reproducibility and information between researchers, manufacturers and clinicians.

Table 1 The number of articles failing to report important LLLT/PBM parameters and information

Information not reported	References	Number articles for LLLT (total = 56)	Percentage (out of 56; %)	Percentage (out of 74 articles; %)	Number of articles for PBM (total = 18)	Percentage (out of 18; %)	Percentage (out of 74 articles; %)
LLLT articles							
Light source							
Light measurement method	[31–70]	40	71	73			
Wavelength	[48, 60]	2	3	3			
Source	[44, 54, 61]	3	5	8			
Power	[33, 34, 36, 40–42, 45, 48–50, 54, 58, 61–65, 67, 71–74]	22	39	41			
Pulse frequency	[33, 34, 36, 40, 42, 43, 45, 46, 48, 50, 51, 54–57, 59, 61–63, 67–70, 72–77]	30	54	52			
Beam area	[33, 34, 36, 40, 43, 45, 48–50, 54, 55, 58, 61–64, 67, 71–75, 77, 79]	24	43	41			
Irradiation parameters							
Irradiance	[31, 32, 38, 40, 43, 48, 51, 54, 55, 57, 58, 60, 62–64, 66, 68, 70, 76, 77, 80]	21	38	43			
Exposure time	[40, 50, 58, 61, 64, 70, 71, 74, 80]	9	16	16			
Energy (radiant)	[31, 33–36, 40–43, 45–50, 52–55, 58–65, 67–69, 71–75, 79, 81, 82]	40	71	74			
Radiant exposure	[38, 40, 49, 52, 54, 55, 63, 80]	8	14	16			
Articles with all information present	[83–86]	4	7	5			
Photobiomodulation articles							
Light source							
Light measurement method	[87–99]				14	77	73
Wavelength					0	0	3
Source	[95, 97, 100]				3	17	8
Power	[92, 94–98, 100, 101]				8	44	41
Pulse frequency	[88, 89, 93–98, 100–104]				13	72	52
Beam area	[92, 94, 95, 97, 98, 100]				6	33	41
Irradiation parameters							
Irradiance	[87, 89–91, 93, 95, 97, 99, 100, 102, 103]				11	61	43
Exposure time	[90, 93, 102]				3	16	16
Energy (radiant)	[87, 90–98, 100–104]				15	83	74
Radiant exposure	[89, 92, 98, 102]				4	22	16
Articles with all information present					0	0	5

Table 2 Reported irradiation parameters of recent (2014–2015) relevant literature in LLLT/photobiomodulation

Author/ref.	Method for light measurement	Light source	Dose	Conclusion
Low and level and light and therapy				
Wang et al. [34]	No info	Source, LED; wavelength, 660 nm; power, –; frequency, –; beam area, –	Irradiance, 3.5 mW/cm^2; time, 6–24 min; energy, –; radiant exposure, 0–20 J/cm^2	660 nm LED accelerated palatal wound healing, potentially via reducing reactive oxygen species production, facilitating angiogenesis and promoting provisional matrix and wound reorganisation.
Park et al. [36]	No info	Source, LED array; wavelength, 660 nm; power, –; frequency, –; beam area, –	Irradiance, 50 mW/cm^2; time, 10 min/day; 20 days; energy, –; radiant exposure, 30 J/cm^2	LLLT was a effective biostimulator of adipose derived stem cells in vascular regeneration
Moncib et al. [40]	No info	Source, erbium glass laser; wavelength, 1.550 nm; power, –; frequency, –; beam area, –	Irradiance, –; time, –; energy, 30–40 mJ; radiant exposure, –	Treatment of active acne with 1550 nm erbium glass laser is effective.
Kansal et al. [43]	No info	Source, GaAs; wavelength, 904 nm; power, 12 mW; frequency, –; beam area, –	Irradiance, –; time, 10 s × 10 irradiation × 10 days; energy, –; radiant exposure, 4.2 J/cm^2	No evidence of pathological changes in radiograph following LLLT.
Park et al. [45]	No info	Source, LED; wavelength, 660 nm; power, –; frequency, –; beam area, –	Irradiance, 50 mW/cm^2; time, 10 min/day; 20 days; energy, –; radiant exposure, 30 J/cm^2	LLLT is an effective biostimulator of sphenoid human adipose derived mesenchymal stem cells in tissue regeneration.
Imaoka et al. [48]	No info	Source, SuperLizer; wavelength, –; power, –; frequency, –; beam area, –	Irradiance, –; time, 20 min; energy, radiant exposure, 7.64 J/cm^2	The reduction of proinflammatory cytokine, IL-20 by LLLT suggests laser irradiation will be useful for rheumatoid arthritis therapy.
Lim et al. [49]	No info	Source, LED; wavelength, 635 nm; power, –; frequency, CW; beam area, –	Irradiance, 5 mW/cm^2; time, 1 h; energy, –; radiant exposure, –	Direct and indirect exposure with 635 nm light can inhibit activation of pro-inflammatory mediators and may be clinically useful as an anti-inflammatory tool.
Assis et al. [50]	No info	Source, LED; wavelength, 630 nm; power, –; frequency, –; beam area, –	Irradiance, 20 mW/cm^2; time, –; energy, –; radiant exposure, 0.5–3 J/cm^2	Low-level red LED light can enhance MC3T3-E1 cell proliferation and osteogenic differentiation when the cells are cultured for a relatively long time.
Bawins et al. [54]	No info	Source, –; wavelength, 356–530 nm; power, –; frequency, –; beam area, –	Irradiance, –; time, 15 min; energy, radiant exposure, –	Exposure to low-intensity incoherent red light after exposure to ionising radiation led to a decrease in the level of oxidative modification of protein and LPO products and diminished cellular manifestation of radiation sickness.
Ko et al. [55]	No info	Source, laser/LED; wavelength, 635 nm; power, 6 mW; frequency, –; beam area, –	Irradiance, –; time, 5 min (total); energy, –; radiant exposure, –	The use of low-level laser emitting toothbrush is a safe and effective treatment option for the management of dentine hypersensitivity.
Jun et al. [58]	No info	Source, Nd:YAG and Er:YAG; wavelength, 532 and 1064 nm; power, –; frequency, 2 and 10 Hz; spot size, 2 and 8 mm	Irradiance, –; time, –; energy, –; radiant exposure, 1.2–1.4 J/cm^2	Combined therapy and Q-switched Nd:YAG alone were effective in reducing light solar lentigines.
Hirotsuka et al. [61]	No info	Source, –; wavelength, –; power, –; frequency, –; beam area, –	Irradiance, 63–333 μW/cm^2; time, –; energy, –; radiant exposure, 2.76–36.13 J cm^{-2} day^{-1}	Artificial light phototherapy suppressed dextran sulphate sodium-induced colitis in mice by suppression of pro-inflammatory cytokines and promotion of anti-inflammatory cytokines.
Felici et al. [62]	No info	Source, laser; wavelength, 1.100–1.800 nm; power, –; frequency, –; spot size, 10 × 15 or 10 × 30 mm	Irradiance, –; time, 4–10 s; energy, 34–50 J; radiant exposure, 5–65 J/cm^2	The use of infared radiation represents a valid alternative to surgical lifting but cannot replace it.
Gold et al. [63]	No info	Source, LED array; wavelength, 405–460 nm; power, –; frequency, –; beam area, –	Irradiance, –; time, 10 min/zone; energy, –; radiant exposure:	The Silk'n Blue device is a safe efficacious at-home device for the treatment of mild to moderate inflammatory acne vulgaris.

Table 2 (continued)

Author/ref.	Method for light measurement	Light source	Dose	Conclusion
Fiorentzis et al. [64]	No info	Source, laser; wavelength, 500–1200 nm; power, –; frequency, 2.5 ms; beam area, –	Irradiance, –; time, –; energy, –; radiant exposure, 30–35 J/cm^2	Intense pulsed light therapy is a safe and effective treatment for telangiectasias and striae rubra, also in the complex clinical condition of Behçet's disease.
Wang et al. [67]	No info	Source, LED; wavelength, 660 nm; power, –; frequency, –; spot area, –	Irradiance, 3.5 mW/cm^2; time, 6–24 min; energy, –; radiant exposure, 5–20 J/cm^2	LED light irradiation at 660 nm accelerated palatal wound healing, potentially via reducing reactive oxygen species production, facilitating angiogenesis and promoting provisional matrix and wound reorganisation.
Wang et al. [69]	No info	Source, GaAlAs laser; wavelength, 808 nm; power, 170 mW; frequency, –; spot area, 3.8 cm^2	Irradiance, 44.7 mW/cm^2; time, 67.2–335.6 s; energy, –; radiant exposure, 3–15 J/cm^2 × 20	Results suggest that 808 nm LLLT at a low energy density (3 J/cm^2) and 8 J/cm^2 is capable of enhancing sciatic nerve regeneration following a crush injury.
Pinheiro et al. [70]	No info	Source, diode laser and LED; wavelength, 780 nm (laser), 850 nm (LED); power, 70 mW (laser), 150 mW (LED); frequency, –; spot area, 0.4 cm^2 (laser) and 0.5 cm^2 (LED)	Irradiance, –; time, –; energy, –; radiant exposure, 20 J/cm^2 (140 J/cm^2 total)	The use of biphasic synthetic micro-granular HA + Beta − TCP graft improved the repair of bone defects, associated or not with laser or LED light
Tsai et al. [71]	Power meter (Thorlabs, USA) to measure power densities	Source, GaAlAs; wavelength, 810 nm; power, –; frequency, CW; beam area, –	Irradiance, 20 mW/cm^2; time, –; energy, –; radiant exposure, 1.5 J/cm^2	LLLT moderately increased the uptake of mono-L-aspartyl chlorine(e6) and cellular ATP levels.
Gavish et al. [72]	LaserMate power-meter (coherent, Auburn group, Holland)	Source, diode laser; wavelength, 780 nm; power, –; frequency, –; beam area, –	Irradiance, 4 mW/cm^2; time, 9mins; energy, –; radiant exposure, 2.16 J/cm^2	LLLT prevented de-novo development of abdominal aortic aneurysms (AAA) and also arrested further progression of pre-induced AAA and its associated deterioration in the biochemical integrity of the aortic wall.
Dungel et al. [73]	USB2000 spectrometer (Ocean Optics, FL)	Source, LED; wavelength, 470 nm and 629 nm; power, –; frequency, –; beam area, –	Irradiance, 50 mW/cm^2; time, 10 min; energy, –; radiant exposure, 30 J/cm^2	LED treatment of ischemia challenged tissue improved early wound healing by enhancing angiogenesis irrespective of wavelength.
Taffinkli et al. [74]	Measured at Philips Research using a integrating sphere (Ulbricht)	Source, LED array; wavelength, 420 nm; power, –; frequency, –; beam area, –	Irradiance, 50 mW/cm^2; time, –; energy, –; radiant exposure, 0–90 J/cm^2	Observed effects are promising for a clinical use of blue light in the treatment or prevention of myofibroblast-mediated pathological condition such as tissue fibrosis and scleroderma or hypertrophic scarring.
Lanzafame et al. [77]	Ophir Nova Power meter (Model 30A-P-R-SH, Ophir Spiricon, UT)	Source, lasers and LEDs; wavelength, 655 nm; power, 5 mW; frequency, –; beam area, –	Irradiance, –; time, 25 min × 60; energy, 2.9 J/session; radiant exposure, 67 J/cm^2	LLLT of the scalp at 655 nm significantly improved hair counts in women with androgenetic alopecia.
Tedford et al. [80]	Power Meter (OptoTest OP710-Si), thermal-based power detector with meter (ophir LD40-150, Ophir Nova), Optical power and wavelength detector (ILX lightwave OHM-6810B) and amplified photodiode (Thorlabs PDA10A)	Source, laser diode; wavelength, 660, 808 and 940 nm; power, 50 mW–70 W; frequency, PW and CW, –; beam diameter, 30 mm	Irradiance, –; time, –; energy, –; radiant exposure, –	The 808-nm wavelength light demonstrated superior CNS tissue penetration.
Photobiomodulation				
Freire et al. [85]	No info	Source, laser (GaInPAl; 660 nm) and LED (670 nm); wavelength, 660 and 670 nm; power, 40 mW (laser), 150 mW (LED);	Irradiance, –; time, 30 s (laser) and 16 s (LED); energy, 1.6 J; radiant exposure, 4.8 J/cm^2 (laser) and 4 J/cm^2 (LED)	The best results were obtained from the preventive laser and LED photobiomodulation groups; both groups were effective in diminishing the oral mucositis lesions.

Table 2 (continued)

Author/ref.	Method for light measurement	Light source	Dose	Conclusion
		frequency, CW; beam area, 4 mm^2 (laser) and 0.5 cm^2 (LED)		
Larkin-Kaiser et al. [89]	No info	Source, laser; wavelength, 800 and 970 nm; power, 3 W; frequency, –; beam area, –	Irradiance, –; time, 4 min; energy, 360 J; radiant exposure, –	Applied to skeletal muscle before resistance exercise, NIR light therapy effectively attenuated strength loss.
de Carvalho et al. [90]	No info	Source, GaAlAs (660 nm, laser) and InGaAlP (630 nm, LED); wavelength, 660 and 630 nm; power, 40 mW (laser) and 150 mW (LED); frequency, CW; beam area, 4 mm^2 (laser) and 0.8 cm (LED) spot	Irradiance, –; time, –; energy, –; radiant exposure, 4.8 J/cm^2	Laser and LED photobiomodulation were effective in accelerating the healing of fumaric acid-induced oral ulcers in both clinical and histological aspects.
Ben Frenger et al. [92]	No info	Source, LED; wavelength, 470, 625, 660 and 850 nm; power, –; frequency, kHz range; beam area, –	Irradiance, 2.16–8.23 mW/cm^2; time, 3 min; energy, –; radiant exposure, –	Photobiomodulation using LED improved the sperm motility in asthenoteratospermia regardless of wavelength.
Ramalho et al. [93]	No info	Source, InGaAlP laser; wavelength, 660 nm; power, 50 mW; frequency, –; spot area, 0.028 cm^2	Irradiance, –; time, –; energy, –; radiant exposure, 3.57 J/cm^2	Low- and high-power lasers can contribute positively to all steps of the indirect restorative treatment period.
Turrioni et al. [94]	No info	Source, LED (InGaN); wavelength, 450, 630 and 840 nm; power, –; frequency, –; beam area, –	Irradiance, 88 mW/cm^2; time, 1 min 20 s and 8 min 40 s; energy, –; radiant exposure, 4 and 25 J/cm^2	The infrared LED irradiation at an energy density of 4 J/cm^2 and red LED at an energy density of 25 J/cm^2 were the most effective parameters for transdermal photobiomodulation of cultured endothelial-like cell.
Barbosa et al. [95]	No info	Source, –; wavelength, 670 nm; power, –; frequency, –; beam area, –	Irradiance, –; time, 3 min; energy, –; radiant exposure, 9 J/cm^2	Morphological image analysis was used to quantify the extent of vaso-obliteration in oxygen-induced retinopathic vascular growth, the preventive effect (by photobiomodulation) of exposure during tissue development to near-infrared light (670 nm) and the lack of adverse effects due to exposure to NIR light.
Tang et al. [97]	No info	Source, –; wavelength, 670 nm; power, –; frequency, –; beam area, –	Irradiance, –; time, 160 s/day (2–9 months); energy, –; radiant exposure, 25 J/cm^2	Photobiomodulation potentially offers a non-invasive and cost effective therapeutic option for patients with non-centre-involving diabetic macular oedema.
Ekizer et al. [98]	No info	Source, LED; wavelength, 618 nm; power, –; frequency, –; beam area, –	Irradiance, 20 mW/cm^2; time, 20 min (200 min total); energy, –; radiant exposure, –	Photobiomodulation therapy has the potential of accelerating orthodontic tooth movement and inhibitory effects on orthodontically induced resorptive activity.
Di Marco et al. [100]	Calibrated sensor (Quantum devices, Barnfield, Wisconsin)	Source, –; wavelength, 670 nm; power, –; frequency, –; spot area, –	Irradiance, –; time, 3 min; energy, –; radiant exposure, 4–4.5 J/cm^2	Detailed analysis suggests that there is a negative interaction between photobiomodulation and saffron when given simultaneously, with a consequent reduction of neuroprotection.
Pitchika et al. [102]	Integrating sphere (LMS-200, 20-in. diameter, Labsphere, USA) and Power meter (detector 818P-010-12, driver 1918-R, Spectra Physics Newport)	Source, laser diode; wavelength, 671 and 808 nm; power, 0.8 W at 671 nm and 1 W at 808 nm; frequency, –; spot area, 1 cm^2	Irradiance, –; time, –; energy, –; radiant exposure, –	Objective was to refine a possible treatment option for PD patients and validate the practicalities of light delivery and light dosimetry. The study demonstrates the possibility to illuminate deep brain tissue transcranially, transphenoidally and via different application routes.

Radiometry

Radiometry is the measurement of electromagnetic radiation between approximately 10 and 1,000,000 nm. Within these wavelengths are the ultraviolet (UV; <400 nm), visible (~400–700 nm), near-infrared (~700–1400 nm) and infra-red (IR; >1400 nm) bands. Since LLLT experiments typically involve the application of light in the visible red and near-infrared region of the electromagnetic spectrum, radiometric terms should be employed to describe light properties and irradiation parameters that adequately depict key information needed for repeatable and reliable results between researchers, manufacturers and clinicians, which will ultimately improve clinical outcomes. Table 3 represents a summary of correct key terms, quantities and units that should be used in LLLT, although commonly incorrect terminology is stated. For example, studies will often report radiant exposure using the term energy density which actually describes a volumetric parameter rather than the amount of energy applied to a given area [66, 105–108] or use ambiguous terms such as intensity [108], which in radiometry can lead to confusion with 'radiant intensity' (the radiant power emitted, reflected, transmitted or received). Likewise, in LLLT, the term intensity does not distinguish whether the light is measured as 'radiant exitance' which is the amount of light leaving (emitted) from a surface, or 'irradiance' which is the amount of light arriving (irradiated) onto a surface; a subtle, yet critical consideration for accurate measurement of incident light at a specimen surface such as treated tissue or cell culture areas ('Irradiance and radiant exitance'). Another example of a commonly used, largely ambiguous term is spot-size [39, 62, 91, 103] and the errors that may arise in assuming a circular beam area, which may not be representative of an elliptical laser speckle pattern ('Beam area'). These ambiguous terms can potentially lead to misinterpretation of dosing parameters and poor reproducibility of data and should be avoided.

Spectral quantities

Radiometric quantities often have a spectral (or wavelength) variable. The spectral variable describes the distribution of these quantities with respect to their representative wavelengths: the total irradiance of a light source is defined by the irradiance at each individual wavelength. Spectral measurements are particularly important for chemical or biological applications, as the knowledge of spectral content is often vital in choosing or interpreting the effects of a particular light source. This is potentially critical as popular work by Karu [109] suggests light of appropriate wavelength is absorbed by copper complexes within the mitochondrial enzyme, cytochrome *c* oxidase (CCO), which then causes the release of bound nitric oxide leading to further downstream cell signalling effects [110, 111]. Therefore, there must be an effective spectral overlap between the absorption of CCO and laser/LED emission for therapeutic LLLT. Consequently, not only is it important to characterise the spectral properties of the light source but also the absorbance profile of materials or tissue that can potentially absorb the therapeutic window of emitted light. It follows that accurate measurement and reporting of spectral information (peak wavelength, spectral irradiance, spectral half-width and absorption profiles) would confirm (or otherwise) the conclusions made in LLLT studies.

Light, quantities, units and symbols

Radiant energy

Electromagnetic radiation can be considered as both a wave and a particle (depending on how it is measured), which transports energy through space. This energy can be absorbed by physical objects and converted into other forms such as thermal or electrical energy (solar cells). For example, in photographic light meters, incident visible light causes electric current flow when the radiant light energy is transferred to electrons as kinetic energy, from which light power can be inferred

Table 3 Summary of quantities, symbols and units

Terminology commonly used	Correct terminology	Symbol	Equation of relation	Unit
Wavelength	Wavelength	λ		nm
Frequency	Pulse frequency	ν		Hz
Radiant energy	Radiant energy	Q		Joule, J
Energy density	*Not applicable*	u		J/cm^3
Energy density/fluence	Radiant exposure /(radiant) fluence	H	$\int E\,dt$	J/cm^2
Power (flux)	Power/radiant flux)	Φ	dQ/dt	watt, W
Spot size	Beam area	A		cm^2
Power density/intensity	Irradiance	E	$d\varphi/dA$	W/cm^2
Intensity	Radiant exitance	M		W/cm2
Exposure time/duration	Exposure time/duration	t		s

('Photodiodes and power meters'). Similarly, for LLLT, light is transferred to cells as radiant energy that modulates cellular responses via CCO absorption and is analogous to photosynthesis, whereby the action of light, and light alone, directly stimulates cell responses. Whilst radiant energy is important [112], the parameter alone is not enough to determine treatment efficacy since an infinite combination of irradiance and exposure could lead to similar radiant energies. Radiant energy is denoted as Q and expressed in *Joules* (J). Spectral radiant energy accounts for monochromatic (such as a single wavelength laser) and polychromatic sources (for example, lights which emit over a range of wavelengths) and is defined as radiant energy per unit wavelength interval at wavelength, λ:

$$Q_\lambda = \frac{dQ}{d\lambda} \tag{1}$$

The units of spectral radiant energy are *Joules per nanometre* (J/nm)

Radiant flux or radiant power

'Flux' or 'power' describes the time rate of flow of radiant energy. This is a parameter that is usually reported within LLLT literature through manufacturers' information or measured using power/energy meters (Tables 1 and 2). Metaphorically, this describes the 'potency' of the light and although important, does not provide adequate information concerning spectral and spatial distribution of the energy or the actual irradiance delivered to the target site. Lack of spatial information assumes uniform irradiance over the output area [113, 114], which can be far from accurate, especially considering the true irradiance across an active beam area (Fig. 2). This may differ according to the type of light source, e.g. the common elliptical profile of lasers (Fig. 2b) or the non-uniform irradiance distribution of LEDs (Fig. 2c) and the distance from the light tip to the target area. Although power or radiant flux should be reported, it only partially describes irradiation parameters that are necessary for complete information relevant to LLLT research. Radiant power or flux has units of *Joules per second* (J/s) *or watts* (W) and is defined as:

$$\phi = \frac{dQ}{dt} \tag{2}$$

The radiant flux per unit wavelength interval at wavelength, λ is given the term spectral radiant flux and is defined as:

$$\phi_\lambda = \frac{d\phi}{d\lambda} \tag{3}$$

and measured in *watts per nanometre* (W/nm).

Beam area

Beam area is often referred to as 'spot-size' in the LLLT literature [39, 62, 91, 103]. However, the term beam area should be preferred over spot-size and reported in *square centimetres*. The term spot is usually descriptive of a circular shape and size is ambiguous although units may remove ambiguity. As mentioned previously, lasers may emit an elliptical beam, which would significantly affect the area calculation (Fig. 2) and lead to misinterpretation of irradiation parameters. In cases where the beam area is non-circular, or of circular Gaussian, the beam area and/or diameter can be accurately determined using techniques such as beam profilometry which will be discussed in 'Light measurement/detectors'. Nonetheless, this review finds that a significant number of LLLT studies fail to report beam area (Tables 1 and 2), a key parameter that should be reported in all LLLT studies.

The radiant beam area acting on a target site is likely to significantly influence biological response in both *in vivo*, *in vitro* and clinical studies. Although systemic and local responses to LLLT irradiation have been reported [115] *in vivo*, beam area is also important for dosing and radiometric calculations. *In vitro*, a localised effect of light irradiation is likely to result in a significant biological response. Consequently, if the beam area is much smaller than the target culture area, then only a proportion of the host cells will be irradiated, attenuating the measured biological response and possibly resulting in a false-negative result. Therefore, a suggested good practice would be to ensure the whole culture well is irradiated evenly with a round, flat top beam.

Irradiance and radiant exitance

The radiant flux per unit area received by a surface from any direction can be termed irradiance (Fig. 3a). However, sometimes this is confusingly termed power density or intensity in the LLLT literature, and this does not distinguish between irradiance or light arriving (irradiance) or that leaving a surface (exitance). Irradiance is defined as:

$$E = \frac{d\phi}{dA} \tag{4}$$

where $d\phi$ is the radiant flux and dA is differential area. The measured flux can also be that leaving the surface from any direction due to emission and/or reflection (Fig. 3b) and is given the term radiant exitance and defined as:

$$M = \frac{d\phi}{dA} \tag{5}$$

where $d\phi$ is the radiant flux leaving and dA is differential area where $d\phi$ is leaving from. A possible use of this terminology in LLLT could be to describe reflection off biological tissue

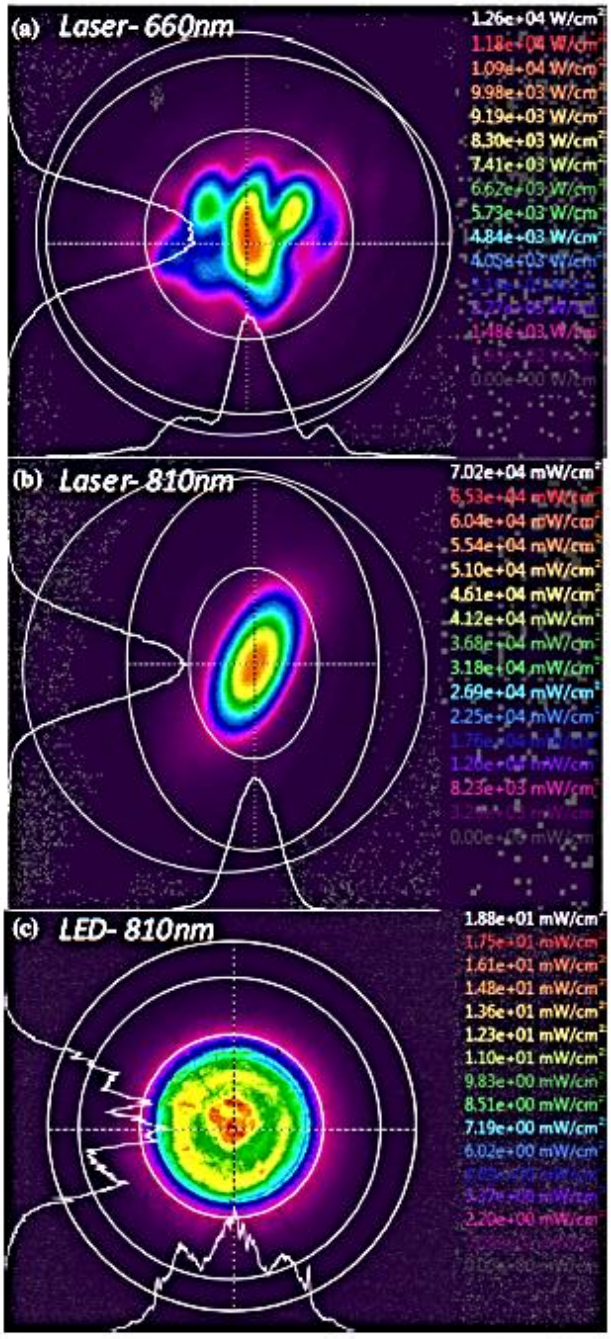

Fig. 2 Examples of spatial distribution of irradiance in lasers and LED lights where the highest to lowest irradiance is represented by the *rainbow colours*, *red* to *violet*, respectively, for **a** 660 nm laser, **b** 810 nm laser and **c** 810 nm LED

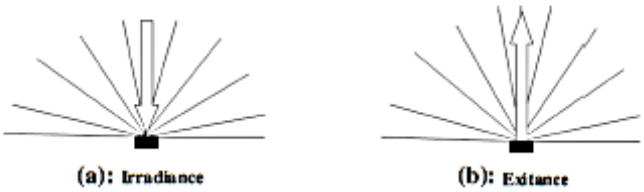

Fig. 3 The definitions of radiant flux density arriving (a irradiance) or leaving (b exitance) a surface (the *lines* represent rays of light travelling in the direction of the *arrow*)

such as dentine, bone and other tissues.

Irradiance can be measured in space and is usually measured in *watts per square centimetre*. This includes the surfaces of physical objects, i.e. tissue or cell culture samples, and the space occupied between them, i.e. air or through tissue thickness. This is particularly important when characterising lights that are highly divergent, as found in typical LED sources, or through tissue which is highly scattering.

Commonly, irradiance is not verified by researchers and only reported from manufacturers' quoted values or is calculated using values gained from inadequate measurement tools (Tables 1 and 2). Manufacturers' values are typically measured at the aperture or fibre tip, but because the beams are highly divergent, they are not useful for studies where the beam may be projected to a target such as in an in vitro study. Manufacturers' specific methods of measurement are also rarely divulged. Irradiation, *in vivo* or in *in vitro* cultures, likely occurs through tissue or culture plastics at distances greater than 0 mm. Therefore, replicating and measuring key light parameters at, or through, relevant targets at specific distances and geometry is far more accurate and clinically and experimentally relevant than using manufacturers' data alone.

Spectral irradiance is the radiant flux per unit wavelength interval at wavelength λ and can be defined for both irradiance and radiant exitance with the following equations:

$$E_\lambda = \frac{dE}{d\lambda} \tag{6}$$

$$M_\lambda = \frac{dM}{d\lambda} \tag{7}$$

Spectral irradiance is measured in *watts per square centimetre per nanometre*.

Exposure duration

Although the most straightforward irradiation parameter to measure, exposure time (s) is not always reported in the literature. Sixteen per cent (12/74) of articles reviewed in this study failed to report exposure duration (Tables 1 and 2), which is likely due to a common misconception that wavelength, flux (radiant energy) and fluence are all that are necessary to replicate a successful treatment [29]. Exposure duration is a key component of 'dose', which is the product of irradiance and exposure time and should always be separately defined (Section 'Radiant exposure and exposure reciprocity').

In addition to reporting exposure time, when multiple exposures are performed, the number of treatment sites, the number of exposures and the interval between exposures should also be reported in order to fully describe the treatment protocol [29, 30].

Radiant exposure and exposure reciprocity

The energy delivered per unit area of cells during light stimulation for LLLT is also an important parameter since the efficacy of the treatment would depend on the irradiance delivered over a given area. The quantity areal, measured in *joules per square centimetre* and is often incorrectly termed energy density, should only be used for volumetric energy deposition (J cm^{-3}). The proper terminology for the total amount of energy delivered per unit area is 'radiant exposure', or more commonly termed fluence in the LLLT literature, where H (the radiant exposure or fluence) is defined as the integral of the irradiance from Eq. 4

$$H = \int_0^T E\,dt \tag{8}$$

However, many researchers merely quote radiant exposure (sic. energy density) as an expression of dose within the literature with missing irradiance (W/cm^2) or exposure duration (s) values (or even both; Tables 1 and 2). This is potentially unreliable, as it assumes an inverse correlation between the effects of irradiance and exposure duration.

The Bunsen-Roscoe 'Law of Reciprocity' states that photochemical reactions will be independent of irradiance and exposure time with the effects being directly proportional to the total energy delivered [116–118]. Although it can be assumed that this law is valid for photochemical reactions within a certain dose range, photobiological responses of cells and tissue usually involve a sequence of interacting biological reactions making a linear dose-time relationship less likely. A true reciprocal relationship between irradiance and time would achieve similar therapeutic effects regardless of how radiant exposure was achieved (e.g. 20 s at 100 mW/cm^2 would exhibit similar therapeutic effects compared with 200 s at

10 mW/cm^2 or 80 s at 25 mW/cm^2). However, although an effective radiant exposure for a specific cell type is an important, and a largely unknown quantity in LLLT, the individual parameters (irradiance and time) are critical and should also be defined. Notably, if the irradiance is too low and/or the delivery time too short, any significant beneficial effect may not be realised or even reduced [19, 81]. Furthermore, if the irradiance is too high or the irradiation time is too long, any significant benefit may also be attributed to heat, or even sometimes produce inhibitory, rather than therapeutic effects [19, 68]. Thus, any useful concept of exposure reciprocity may not be applicable in biological systems such as LLLT, since treatment modalities may only be effective within a window of specific irradiation parameters [19]. However, using similar radiant exposure by varying the combination of irradiance and time, and its effect on stimulatory/inhibitory cell responses is not fully understood and warrants a systematic approach to further understanding of the photobiomodulation of different cell types.

Pulse frequency

The pulse frequency is the number of pulses of a repeating signal in a specific time frame and is usually measured pulse per second (Hz), thus pulse operation of lasers or LEDs is not classified as a continuous wave. This type of operation is beneficial for heat dissipation and to achieve high peak irradiances, but since there is an on/off period, dosing parameters such as radiant energy and radiant exposure are affected which may affect the efficacy of LLLT [52, 64, 68]. For example, if the irradiation was pulsed to deliver light at 0.5 s intervals, then only half the energy would be delivered compared with continuous delivery at similar irradiance and exposure time. Thus, when pulsing regimes are utilised, the peak irradiance should be defined along with pulse frequency and the on/off durations as previously recommended [29, 30].

Light measurement/detectors

Spectro(radio)meters

A spectrometer is an instrument used to measure the properties of light over specific portions of the electromagnetic spectrum and provides a useful system to analyse spectral characteristics critical for LLLT research. Spectrometers are coupled with flexible, transparent optical fibres of varying diameters made from high-quality glass that function as waveguides or light guides to transmit light between the two fibre ends. Opaline cosine correctors are usually attached, which have diffusing material apertures allowing light measurement normal to its surface with 180° field of view (Fig. 4a). Whilst cosine corrector probes provide a cheap, versatile, robust and reliable method of light measurement, the measurement accuracy is limited when analysing large light sources due to its small collection area and its 180° field of view. Alternatively, integrating spheres of varying diameter and port size (dependent upon the source size) can be used, which consist of hollow spherical cavities covered with diffuse white reflective coating. Spheres can be used to capture and measure light radiated in all directions from the light source as light scattered by the interior of the integrating sphere is evenly distributed over all angles (Fig. 4b). However, measurements using integrating spheres are limited by the size of the sphere and the size of the light source intended to be measured. Nevertheless, the fibres and cosine corrector (or integrating sphere) collectively become an optical probe, which can be calibrated using a photometric standard or calibrated light source to National Institute of Standards and Technology (NIST) standards providing an accurate measurement system known as a spectroradiometer.

Light is captured through the cosine corrector or integrating sphere and travels through the optical fibre into the spectrometer. The core of the spectrometer is formed by a diffraction grating which splits radiant light into its spectral components and projects the diffracted elements onto a detector. Computer software is used to calculate all radiometric, photometric and colourimetric quantities from spectral data. Two types of spectrometers exist, an array type, which has a fixed diffraction grating and a detector array, and a scanning spectrometer, which has a single detector and a rotating diffraction grating (Fig. 4c). Spectrometers are popular light measurement systems for many aspects of photonics research although rarely used in LLLT studies (Table 2). However, there are other limitations of fibre-coupled spectrometers which use cosine correctors and integrating spheres, primarily that power uniformity within the incident beam is assumed and the power distribution of light across the exit diameter of large light sources cannot be measured [114]. For example, using a typical cosine corrector diameter of 4 mm to measure an incident beam diameter of 10 mm, the outer 6 mm of the beam will not be captured by the sensor. Light sources used for LLLT typically have a Gaussian distribution and therefore if the irradiance is measured centrally, power is assumed to be equal over the whole area and the measured irradiance would be overestimated. Error is increased with the increasing ratio of beam diameter to probe diameter (or vice versa) and researchers need to cautiously interpret data in such situations. Ideally, researchers should employ methods that will adequately measure all of the light by considering the projected beam area on a target and the distance that the beam is applied from. For example, if LLLT studies are performed by irradiating culture dishes or tissue samples from a specific distance, then the experimental light measurement methods should simulate this to accurately analyse light properties at the target site (irradiance), i.e. measure light received by cells, not what the light outputs. The effects of absorption, scattering and

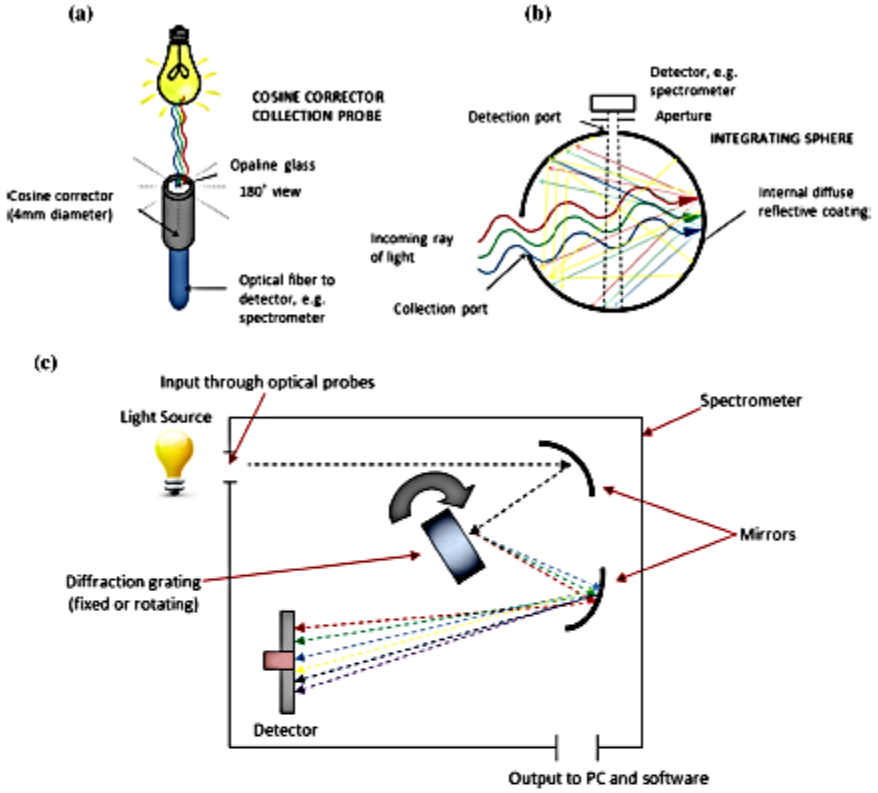

Fig. 4 Schematic representation of the internal workings of an **a** integrating sphere showing the 360° collection of light; **b** a cosine corrector probe allowing a 180° field of view; and **c** the internal workings of a UV–vis spectrometer

reflection by media, cell culture plasticware and other materials/tissue on spectral irradiance at the target site are critical and should be carefully considered, i.e. for cell culture work, the irradiance delivered on the culture area through plasticware should be measured to accurately determine the irradiance delivered to cells.

Spectrometers can also be used to measure absorption characteristics of specific cellular chromophores or photoreceptors localised in the mitochondria that are responsible for the absorption of light. A light source emitting multiple wavelengths is focused on to a sample which attenuates light through absorption, scattering and reflection of the incident light. The action spectra, a plot of relative effectiveness of different wavelengths, which is believed to mimic the absorption spectrum of CCO, has been reported by Karu et al. [119] and indicates several effective bands relating to the copper complexes of CCO. Thus, by recording this attenuation of light for various wavelengths, an absorption spectrum can be obtained and potential therapeutic windows for LLLT can be identified for specific tissue.

Photodiodes and power meters

A photodiode (detector) is responsive to optical input from UV to near infrared radiation and operates as a photoelectric converter generating a current that is proportional to the incident light. A photon of sufficient energy creates an electron hole pair by a mechanism known as the inner photoelectric effect that is dependent upon the efficiency of the photodiode. Quantum efficiency is dependent upon many factors, but in general if the energy of the photon is greater than the energy gap of the device, these photons will be absorbed very near the surface where the recombination rate is high and will contribute to a photocurrent. Thus, the photocurrent produced by the photodiode is proportional to the power of the light which can be measured directly by a 'power meter' which uses an operational amplifier circuit known as a transimpedance amplifier.

Although this type of measurement system is most popular within LLLT literature (Table 1), measurements from these devices should be interpreted cautiously. The spectral

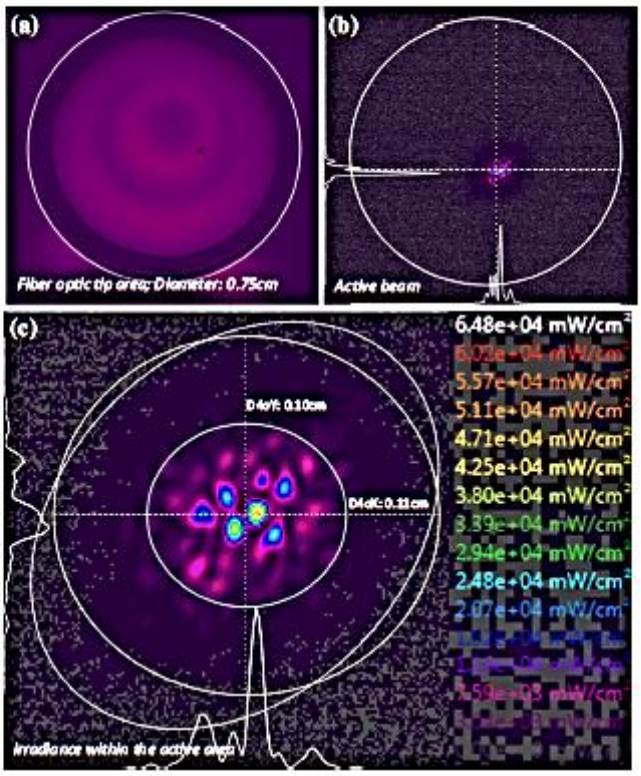

Fig. 5 A 2D beam profile image of a LLLT laser device: a an image of the actual tip area used for light delivery, b the actual active beam area and the location of the beam within the fibre optic tip and c the laser 'speckle' beam pattern of the devices and its active beam diameter/area

sensitivity differs with wavelength due to the quantum efficiency of the photodiode and generally has a better response at longer wavelengths. Thus, if broadband light sources are measured, the power emitted at short and longer wavelengths maybe be under- or over-estimated, respectively. Photodiodes also assume power uniformity across the beam and do not therefore effectively characterise the distribution of light for the same reasons described previously ('Spectro(radio)meters'). Although reproducible measurements can be made at the sub-picoampere regime, the response time is limited by the sensor size, which slows as surface area increases. Furthermore, the detectors are usually made from fragile or sensitive materials such as silicon (Si; 190–1100 nm), germanium (Ge; 400–1700 nm), indium gallium arsenide (InGa; 800–2600 nm), lead(II) sulphide (<1000–3500 nm) or mercury cadmium telluride (400–14000 nm) which can be prone to damage and therefore measurements usually must be made without contact with the detector. Consequently, even small distances are likely to result in a loss of power due to divergence which will reduce the measured power. More so and unlike spectrometers, photodiodes do not provide spectral information and are usually only limited to power readings (W) and crude irradiance measurements (W/cm^2) based on the sensor size or inputted tip or beam area values. However, photodiodes are relatively insensitive to temperature fluctuation (not critical for LLLT as low powered sources are used) and their main and unique advantage lies in their ability to measure very small optical powers which is specifically useful for basic light characterisation in LLLT studies.

Thermopiles

Thermopiles are essentially thermal sensors, which are best suited for measuring constant wave (CW) laser power, average power in pulsed lasers or the energy of long pulses. Thermopiles are robust, reliable and are a well-established method to measure light energy. They can be considered as an array of miniature thermocouple junctions connected in series as differential pairs. These differential pairs make up cold and hot junctions that are connected by alternating n-type and p-type materials. Thermopiles operate by using

temperature differences to create a voltage, which is correlated to the temperature gradient between the hot and cold junctions and proportional to the light energy. These systems are particularly useful for measuring high powered sources (>1 Watt) which can damage other types of sensors. Thermopiles are made from materials such as antimony (Sb), bismuth (Bi), poly-silicon gold (Au) or aluminininium (Al) and operate over a broad spectral range (200–20000 nm). Thermopiles tend to be more accurate than photodiodes but measurement sensitivity is reduced at low power. Since thermopiles work by using temperature gradients, they can be used to map irradiance distribution and offer uniform spatial response that is unaffected by changes in beam size, position or uniformity unlike photodiodes and spectrometer based systems which rely on inputted beam area values for irradiance calculation. However, although this type of sensor validly characterises the distribution of light and provides an accurate measure of important light properties such as irradiance and beam area, like the photodiode, it does not provide spectral information. Furthermore, response times are slow (generally a few seconds), which could be problematic in time-dependent experiments and thus are only really capable of measuring average powers. In addition, since the measurement is based on heat exchange, rapid fluctuations in housing temperature will decrease accuracy.

Charge coupled device cameras and beam profilometry

A charge coupled device (CCD) is an integrated circuit etched onto a silicon surface forming light sensitive elements called pixels. Photons incident on this surface generate charge that is converted into a digital copy of the light pattern. Following appropriate calibration, beam profilometry is very useful for characterisation and quantification of power distribution and irradiance of a given light source and has the advantages of both photodiodes (good response time and unaffected by temperature) and thermopiles (unaffected by beam diameter, good sensitivity and spatial distribution of power and irradiance, which can be used over a large range of power outputs). Light can be collected through lenses and directed onto the CCD sensor which then creates a digital image of the beam. Calibration using pre-determined power values may then be used to calculate the average power delivered to each pixel within the defined beam area to create a mapped irradiance image [120]. This is known as the top-hat factor and can be used to characterise the degree of spatial [114, 120–122] and spectral [123] uniformity of the power distribution. For system calibration, if the total measured power is calculated (using, for example, a photodiode or thermopile), the power received by each pixel in the detector's diode array can be calibrated to generate a 2- or 3-dimensional map of irradiance distribution across the active beam area. Therefore, the beam area can be accurately calculated rather than only measuring the light delivery tip diameter by crude methods such as calipers. For example, if the tip size of a LLLT laser device is much larger (7.5 mm diameter) than the actual beam diameter (~0.11 mm diameter; Fig. 5), erroneous irradiance values are inevitably obtained if the active beam area is assumed to be the same as the tip diameter. Thus, the need for standardised beam area calculation is required in LLLT, preferably using the ISO standard method (D4σ or second moment width; ISO 11145 3.5.2 [122]) or $1/e^2$ as suggested previously [29, 30].

Although CCD cameras and beam profilers are widely used for a variety of applications including dental research [114], this method has only been utilised in a limited number of LLLT studies [82, 120]. However, whilst beam profilers provide a relatively accurate measurement system, they are also unable to readily provide spectral information and are sensitive to spectral variation. Accurate and reliable test centres for LLLT research would have a suite of complimentary equipment including spectrometers or integrating spheres, photodiodes and beam profilers.

Safety requirements for LLLT

Whilst the perceivable dangers of LLLT are mainly related to retinal damage (both clinician and patient) and skin burn (mainly related to shorter UV wavelengths), the safety of LLLT is well documented in a number of standards such as US Code of Federal Regulations, American National Standards Institute and the International Standards Manual, and other laser safety books and review articles [21, 22]. This includes 'The Guidelines for Skin Exposure to Light' in the International Standards Manual (IEC-825) which states that an exposure of less than 200 mW/cm^2 is safe, and the marketing and the use of therapeutic LLLT is approved by the Food and Drug Administration. Preventative measures such as safety googles should always be utilised to minimise any risks and therapeutic devices may utilise high-powered light sources (>500 mW) may be spread over larger areas to fall within the recommended irradiance exposure limits. The operation of high-powered light sources may also be compensated by pulsing which may reduce the risk of any adverse effects caused by heating as discussed previously.

Recommendations

LLLT has generated markedly increasing interest in a wide variety of biomedical disciplines. However, researchers frequently report LLLT studies that have inadequate information regarding light properties and use ambiguous terminology. Thus, it is increasingly difficult to compare and contrast study outcomes, which hinders the progress in this field. Researchers working in LLLT should utilise a minimal set of

standard criteria for light measurement and reporting of radiometric data that are necessary for a repeatable scientific study and are sufficient to compare and contrast study outcomes. These include ten key parameter: wavelength, power, irradiation time, beam area (at the skin or culture surface), radiant energy, radiant exposure, pulse parameters, number of treatments, interval between treatments and anatomical location, which will improve the information available to other researchers. A similar approach is utilised in other biomedical research areas such as mesenchymal stromal stem cell (MSC) research which has a set of standard criterion to foster a more uniform characterisation of MSC and facilitate better exchange of data among investigators [124].

The measurement of light is fundamentally important for LLLT research, thus researchers should not merely rely on manufacturers information which is what is reportedly routinely practiced in many LLLT studies (Tables 1 and 2). Instead, researchers should use a combination of complimentary methods that will accurately describe the ten key parameters previously mentioned. For example, to describe the spectral output of a light source, spectrometer-based systems should be used, improving accuracy by employing integrating spheres to capture all of the light rather than cosine correctors. Similarly, to describe spatial distribution of power and irradiance, beam profilers or thermopiles could be employed. Further, as good practice, light property information should be fully reported in a standardised form as recommended previously [22, 29]. The terminology should also be consistent from study to study, which will make comparison and experimental repetition more straightforward. For example, instead of power density, the term irradiance should be used; instead of energy density, use radiant exposure or fluence, and so on (Table 3). Finally, the units should also be appropriately assigned, e.g. watts per square centimetre or milliwatts per square centimetre for irradiance depending on the output of the light source. Although these recommendations will probably require modification as new knowledge, technology and techniques unfold, they provide a minimal standard criteria that will facilitate a better exchange of information within LLLT which could 'drive' this field forward.

Conclusions

It is apparent that a relatively poor appreciation of radiometric properties exists within the literature associated with LLLT. Proper radiometric measurements are fundamental for this area of research and although it may appear straightforward, concepts and appropriate measurement techniques are commonly misunderstood, or ignored. Furthermore, the literature suffers greatly from missing information such as wavelength, power, pulse parameters, beam area, beam profile information, irradiance, exposure time, radiant exposure and evidence of calibrated measurement tools, making reliability questionable and reproducibility difficult all of which weakens the strength of conclusions potentially giving rise to false or nil results. The persistence of misunderstanding, inadequate experimentation and inaccurate reporting of radiometric data within LLLT literature has, and will continue to affect the reliability of LLLT information shared between scientists, manufacturers and clinicians. Ultimately, accurate measurements and reporting of light properties is essential to fully understand the potential beneficial biological mechanisms of LLLT, which could be achieved by following the recommendations of this review.

Acknowledgements This report is an independent research funded by the National Institute for Health Research (Invention for Innovation (I4I), Product Development Awards, II-LB-0712-20003). The views expressed in this publication are those of the author(s) and not necessarily those of the NHS, the National Institute for Health Research or the Department of Health.

References

1. Hopkins JT, McLoda TA, Seegmiller JG, Baxter DG (2004) Low-level laser therapy facilitates superficial wound healing in humans: a triple blind, sham controlled study. J Athl Train 39:226–229
2. Aimbire F, Albertini R, Pacheco MTT, Castro-Faria-Neto HC, Leonardo PSLM, Iversen VV, Martins L, Bjordal JM (2006) Low-level laser therapy induces dose-dependent reduction of TNFα levels in acute inflammation. Photomed Laser Surg 24: 33–37
3. Stergioulas A (2004) Low-level laser treatment can reduce edema in second degree ankle sprains. J Clin Laser Med Surg 22:125–128
4. Avci P, Gupta A, Sadasivam M, Vecchio D, Pam Z, Pam N, Hamblin MR (2013) Low-level laser (light) therapy (LLLT) in skin: stimulating, healing and restoring. Semin Cutan Med Surg 32:41–52
5. Brosseau L, Welch V, Wells G, Tugwell P, de Bie R, Gam A, Harman K, Shea B, Morin M (2000) Low level laser therapy for osteoarthritis and rheumatoid arthritis: a metaanalysis. J Rheum 27:1961–1969
6. Jackson Streeter (2001) Method for treating musculoskeletal injuries. US Patent 6267780 B1
7. Kneebone WJ (2006) Practical applications of low level laser therapy. Prac Pain Mangament
8. Xuan W, Vatansever F, Huang L, Wu Q, Xuan Y, Dai T, Ando T, Xu T, Huang Y-Y, Hamblin MR (2013) Transcranial low-level laser therapy improves neurological performance in traumatic brain injury mice: effect of treatment repetition regimen. PLoS One 8:e53454
9. Milward MR, Holder MJ, Palin WM, Hadis MA, Carroll JD, Cooper PR (2014) Low level light therapy (LLLT) for the

treatment and management of dental and oral diseases. Dent Update 41:763–772
10. Bensadoun RJ, Nair RG (2012) Efficacy of low level laser therapy (LLLT) in oral mucositis: what we have learned from randomized studies and meta-analyses? Photomed Laser Surg 30:191–192
11. Umberto R, Claudia R, Gaspare P, Gianluca T, Alessandro DV (2012) Treatment of dentine hypersensitivity by diode laser: a clinical study. Int J Dent 2012:858950
12. Basso FG, Oliveira CF, Fontana A, Kurachi C, Bagnato VS, Spolidório DM, Hebling J, de Souza Costa CA (2011) In vitro effect of low-level laser therapy on typical oral microbial biofilms. Braz Dent J 22:502–510
13. Agrawal T, Gupta G, Rai V, Carroll J, Hamblin MR (2014) Pre conditioning with low-level laser (light) therapy: light before the storm. Dose Response 12:619–649
14. Tunér J, Hode L (1998) It's all in the parameters: a critical analysis of some well-known negative studies on low-level laser therapy. J Clin Laser Med Surg 16:245–248
15. Tunér J and Hode L (2010) The new laser therapy handbook, chapter 13.1—are all the negative studies really negative? Prima Books
16. Jang H, Lee H (2012) Meta-analysis of pain relief effects by laser irradiation on joint areas. Photomed Laser Surg 30:1–13
17. Tumilty S, Munn J, McDonough S, Hurley DA, Basford JR, Baxter GD (2009) Low level laser treatment of tendinopathy: a systematic review with meta-analysis. Photomed Laser Surg 00: 1–14
18. Bjordal JM, Couppé CRT, Tunér J, Ljunggren EA (2003) A systematic review of low level laser therapy with location-specific doses for pain from chronic joint disorders. Aust J Physiother 49:107–116
19. Huang YY, Chen ACH, Carroll JD, Hamblin MR (2009) Biphasic dose response in low level light therapy. Dose Response 7:358–383
20. Ilic S, Leichliter S, Streeter J, Oron A, DeTaboada L, Oron U (2006) Effects of power densities, continuous and pulse frequencies, and number of sessions of low-level laser therapy on intact rat brain. Photomed Laser Surg 24:458–466
21. Sliney DH, Wolbarsht ML (1980) Safety with lasers and other optical sources: a comprehensive handbook. Plenum Press
22. Sliney DH (2007) Radiometric quantities and units used in photobiology and photochemistry: recommendations of the Commission Internationale de l'Eclairge (International Commission on Illumination. Photochem Photobiol 83:425–432
23. Tang E, Arany P (2013) Photobiomodulation and implants: implications for dentistry. J Periodontal Implant Sci 43:262–268
24. Rojas JC, Gonzalez-Lima F (2013) Neurological and psychological applications of transcranial lasers and LEDs. Biochem Pharmacol 86:447–457
25. Chung H, Dai T, Sharma SK, Huang YY, Carroll JD, Hamblin MR (2012) The nuts and bolts of low-level laser (light) therapy. Annu Biomed Eng 40:516–533
26. Peplow PV, Chung TY, Baxter GD (2010) Laser photobiomodulation of cells in culture: a review of human and animal studies. Photomed Laser Surg 28:S3–S40
27. Enwemeka CS (2011) The relevance of accurate comprehensive treatment parameters in photobiomodulation. Photomed Laser Surg 29:783–784
28. Hashmi JT, Huang YY, Osmani BZ, Sharma SK, Naeser MA, Hamblin MR (2010) Role of low-level laser therapy in neurorehabilitation. PM R 12:S292–S305
29. Jenkins PA, Carroll JD (2011) How to report low-level laser therapy (LLLT)/photomedicine dose and beam parameters in clinical and laboratory studies. Photomed Laser Surg 29:785–787
30. Stuck BE (1993) Measuring and reporting physical parameters in laser biomodulation research. SPIE 1883. Low-energy effects on biological systems. doi:10.1117/12.148024
31. Massotti FP, Gomes FV, Mayer L, de Oliveira MG, Baraldi CE, Ponzoni D, Puricelli E (2015) Histomorphometric assessment of the influence of low-level laser therapy on peri-implant tissue healing in the rabbit mandible. Photomed Laser Surg 33:123–128
32. Burger E, Mendes AC, Bani GM, Brigaglo MR, Santos GB, Malaquias LC, Chavasco JK, Verinaud LM, de Camargo ZP, Hamblin MR, Sperandio FF (2015) Low-level laser therapy to the mouse femur enhances the fungicidal response of neutrophils against Paracoccidioides brasiliensis. PLoS Negl Trop Dis 9: e0003541
33. Park IS, Mondal A, Chung PS, Ahn JC (2015) Prevention of skin flap necrosis by use of adipose-derived stromal cells with light-emitting diode phototherapy. Cytotherapy 17:283–292
34. Wang CY, Tsai SC, Yu MC, Lin YF, Chen CC, and Chang PC (2015) 660 nm LED light irradiation promotes the healing of the donor wound of free gingival graft. J Periodontol 1–17
35. Dixit S, Agrawal PR, Sharma DK, Singh RP (2014) Closure of chronic non healing ankle ulcer with low level laser therapy in a patient presenting with thalassemia intermedia: case report. Indian J Plast Surg 47:432–435
36. Park IS, Mondal A, Chung PS, Ahn JC (2015) Vascular regeneration effect of adipose-derived stem cells with light-emitting diode phototherapy in ischemic tissue. Lasers Med Sci 30:533–541
37. Hwang MH, Shin JH, Kim KS, Yoo CM, Jo GE, Kim JH, Choi H (2015) Low level light therapy modulates inflammatory mediators secreted by human annulus fibrosus cells during intervertebral disc degeneration in vitro. Photochem Photobiol 91:403–410
38. Herpich CM, Leal-Junior EC, Amaral AP, Tosato Jde P, Gikria IP, Garcia MB, Barbosa BR, El Hage Y, Arruda ÉE, Gomes CÁ, Rodrigues MS, de Sousa DF, de Carvalho PT, Bussadori SK, Gonzalez Tde O, Politti F, Biasotto-Gonzalez DA (2014) Effects of phototherapy on muscle activity and pain in individuals with temporomandibular disorder: a study protocol for a randomized controlled trial. Trials 15:491
39. de Brito Vieira WH, Bezerra RM, Queiroz RA, Maciel NF, Parizotto NA, Ferraresi C (2014) Use of low-level laser therapy (808 nm) to muscle fatigue resistance: a randomized double-blind crossover trial. Photomed Laser Surg 32:678–685
40. Moneib H, Tawfik AA, Youssef SS, Fawzy MM (2014) Randomized split-face controlled study to evaluate 1550-nm fractionated erbium glass laser for treatment of acne vulgaris—an image analysis evaluation. Dermatol Surg 40:1191–1200
41. Derlacz A, Protasiewicz M, Rola P, Podgorska K, Szymczyszyn A, Gutherc R, Poręba R, Doroszko A (2014) Effects of intravascular low-level laser therapy during coronary intervention on selected growth factors levels. Photomed Laser Surg 32:582–587
42. Takhtfooladi MA, Shahzamani M, Takhtfooladi HA, Moayer F, Allahverdi A (2015) Effects of light-emitting diode (LED) therapy on skeletal muscle ischemia reperfusion in rats. Lasers Med Sci 30:311–316
43. Kansal A, Kittur N, Kumbhojkar V, Keluskar KM, Dahiya P (2014) Effects of low-intensity laser therapy on the rate of orthodontic tooth movement: a clinical trial. Dent Res J (Isfahan) 11: 481–488
44. Xuan W, Agrawal T, Huang L, Gupta GK, and Hamblin MR (2014) Low-level laser therapy for traumatic brain injury in mice increases brain derived neurotrophic factor (BDNF) and synaptogenesis. J Biophotonics
45. Park IS, Chung PS, Ahn JC (2014) Enhanced angiogenic effect of adipose-derived stromal cell spheroid with low-level light therapy in hind limb ischemia mice. Biomaterials 35:9280–9289
46. Zigmond E, Varol C, Kaplan M, Shapira O, Melzer E (2014) Low-level light therapy induces mucosal healing in a murine model of

dextran-sodium-sulfate induced colitis. Photomed Laser Surg 32: 450–457
47. Marques JM, Pacheco-Soares C, Da Silva NS (2014) Evaluation of the photobiomodulation in L929 cell culture. Exp Biol Med (Maywood) 239:1638–1643
48. Imaoka A, Zhang L, Kuboyama N, Abiko Y (2014) Reduction of IL-20 expression in rheumatoid arthritis by linear polarized infrared light irradiation. Laser Ther 23:109–114
49. Lim W, Choi H, Kim J, Kim S, Jeon S, Zheng H, Kim D, Ko Y, Kim D, Sohn H, Kim O (2015) Anti-inflammatory effect of 635 nm irradiations on in vitro direct/indirect irradiation model. J Oral Pathol Med 44:94–102
50. Asai T, Suzuki H, Kitayama M, Matsumoto K, Kimoto A, Shigeoka M, Komori T (2014) The long-term effects of red light-emitting diode irradiation on the proliferation and differentiation of osteoblast-like MC3T3-E1 cells. Kobe J Med Sci 60: E12–E18
51. Cunha MJ, Esper LA, Sbrana MC, de Oliveira PG, do Valle AL, de Almeida AL (2014) Effect of low-level laser on bone defects treated with bovine or autogenous bone grafts: in vivo study in rat calvaria. Biomed Res Int 2014:104230
52. Leal-Junior EC, Johnson DS, Saltmarche A, Demchak T (2014) Adjunctive use of combination of super-pulsed laser and light-emitting diodes phototherapy on nonspecific knee pain: double-blinded randomized placebo-controlled trial. Lasers Med Sci 29: 1839–1847
53. Khoo NK, Shokrgozar MA, Kashani IR, Amanzadeh A, Mostafavi E, Sanati H, Habibi L, Talebi S, Abouzaripour M, Akrami SM (2014) In vitro therapeutic effects of low level laser at mRNA level on the release of skin growth factors from fibroblasts in diabetic mice. Avicenna J Med Biotechnol 6:113–118
54. Bavrina AP, Monich VA, Malinovskaya SL, Ermolaev VS, Druzhinin EA, Kuznetsov SS (2014) Correction of after effects of ionizing radiation by exposure to low-intensity light. Bull Exp Biol Med 156:663–664
55. Ko Y, Park J, Kim C, Park J, Baek SH, Kook YA (2014) Treatment of dentin hypersensitivity with a low-level laser-emitting toothbrush: double-blind randomised clinical trial of efficacy and safety. J Oral Rehabil 41:523–531
56. Aliodoust M, Bayat M, Jalili MR, Sharifian Z, Dadpay M, Akbari M, Bayat M, Khoshvaghti A, Bayat H (2014) Evaluating the effect of low-level laser therapy on healing of tentomized Achilles tendon in streptozotocin-induced diabetic rats by light microscopical and gene expression examinations. Lasers Med Sci 29:1495–1503
57. Führer-Valdivia A, Noguera-Pantoja A, Ramírez-Lobos V, Solé-Ventura P (2014) Low-level laser effect in patients with neurosensory impairment of mandibular nerve after sagittal split ramus osteotomy. Randomized clinical trial, controlled by placebo. Med Oral Patol Oral Cir Bucal 19:e327–e334
58. Jun HJ, Kim SM, Choi WJ, Cho SH, Lee JD, Kim HS (2014) A split-face, evaluator-blind randomized study on the early effects of Q-switched Nd:YAG laser versus Er:YAG micropeel in light solar lentigines in Asians. J Cosmet Laser Ther 16:83–88
59. Novaes RD, Gonçalves RV, Cupertino MC, Araújo BM, Rezende RM, Santos EC, Leite JP, Matta SL (2014) The energy density of laser light differentially modulates the skin morphological reorganization in a murine model of healing by secondary intention. Int J Exp Pathol 95:138–146
60. Hochman B, Pinfildi CE, Nishioka MA, Furtado F, Bonatti S, Monteiro PK, Antunes AS, Quiseregatto PR, Liebano RE, Chadi G, Ferreira LM (2014) Low-level laser therapy and light-emitting diode effects in the secretion of neuropeptides SP and CGRP in rat skin. Lasers Med Sci 29:1203–1208
61. Hiratsuka T, Inomata M, Goto S, Oyama Y, Nakano T, Chen CL, Shiraishi N, Noguchi T, Kitano S (2014) Phototherapy with artificial light suppresses dextran sulfate sodium-induced colitis in a mouse model. J Gastroenterol Hepatol 29:749–756
62. Felici M, Gentile P, De Angelis B, Puccio L, Puglisi A, Felici A, Delogu P, Cervelli V (2014) The use of infrared radiation in the treatment of skin laxity. J Cosmet Laser Ther 16:89–95
63. Gold MH, Biron JA, Sensing W (2014) Clinical and usability study to determine the safety and efficacy of the Silk'n Blue Device for the treatment of mild to moderate inflammatory acne vulgaris. J Cosmet Laser Ther 16:108–113
64. Fioramonti P, Fino P, Ponzo I, Ruggieri M, Onesti MG (2014) Intense pulsed light in the treatment of telangiectasias: case report of Behçet's disease with superficial vascular involvement. J Cosmet Laser Ther 16:124–128
65. Huang YY, Nagata K, Tedford CE, Hamblin MR (2014) Low-level laser therapy (810 nm) protects primary cortical neurons against excitotoxicity in vitro. J Biophotonics 7:656–664
66. Ammar TA (2014) Monochromatic infrared photo energy versus low level laser therapy in patients with knee osteoarthritis. J Lasers Med Sci 5:176–182
67. Wang CY, Tsai SC, Yu MC, Lin YF, Chen CC, Chang PC (2015) Light-emitting diode Irradiation promotes donor site wound healing of the free gingival graft. J Periodontol 86:674–681
68. Leite SN, Andrade TA, Masson-Meyers Ddos S, Leite MN, Enwemeka CS, Frade MA (2014) Phototherapy promotes healing of cutaneous wounds in undernourished rats. An Bras Dermatol 89:899–904
69. Wang CZ, Chen YJ, Wang YH, Yeh ML, Huang MH, Ho ML, Liang JI, Chen CH (2014) Low-level laser irradiation improves functional recovery and nerve regeneration in sciatic nerve crush rat injury model. PLoS One 13:e103348
70. Pinheiro AL, Soares LG, Marques AM, Aciole JM, de Souza RA, Silveira L Jr (2014) Raman ratios on the repair of grafted surgical bone defects irradiated or not with laser (λ780 nm) or LED (λ850 nm). J Photochem Photobiol B 138:146–154
71. Tsai SR, Yin R, Huang YY, Sheu BC, Lee SC, Hamblin MR (2015) Low-level light therapy potentiates NPe6-mediated photodynamic therapy in a human osteosarcoma cell line via increased ATP. Photodiagn Photodyn Ther 12:123–130
72. Gavish L, Beeri R, Gilon D, Rubinstein C, Berlatzky Y, Bulut A, Reissman P, Gavish LY, Gertz SD (2014) Arrest of progression of pre-induced abdominal aortic aneurysm in apolipoprotein E-deficient mice by low level laser phototherapy. Lasers Surg Med 46:781–790
73. Dungel P, Hartinger J, Chaudary S, Slezak P, Hofmann A, Hausner T, Strassl M, Wintner E, Redl H, Mittermayr R (2014) Low level light therapy by LED of different wavelength induces angiogenesis and improves ischemic wound healing. Lasers Surg Med 46: 773–780
74. Taflinski L, Demir E, Kauczok J, Fuchs PC, Born M, Suschek CV, Oplländer C (2014) Blue light inhibits transforming growth factor-β1-induced myofibroblast differentiation of human dermal fibroblasts. Exp Dermatol 23:240–246
75. Teuschl A, Balmayor ER, Redl H, van Griensven M, Dungel P (2015) Phototherapy with LED Light modulates healing processes in an in vitro scratch-wound model using 3 different cell types. Dermatol Surg 41:261–268
76. Nadur-Andrade N, Dale CS, Santos AS, Soares AM, de Lima CJ, Zamuner SR (2014) Photobiostimulation reduces edema formation induced in mice by Lys-49 phospholipases A2 isolated from Bothrops moojeni venom. Photochem Photobiol Sci 13:1561–1567
77. Lanzafame RJ, Blanche RR, Chiacchierini RP, Kazmirek ER, Sklar JA (2014) The growth of human scalp hair in females using visible red light laser and LED sources. Lasers Surg Med 46:601–607

78. Panhoca VH, de Fatima Zanirato Lizarelli R, Nunez SC, Pizzo RC, Grecco C, Paolillo FR, Bagnato VS (2015) Comparative clinical study of light analgesic effect on temporomandibular disorder (TMD) using red and infrared led therapy. Lasers Med Sci 30: 815–822
79. Ferraresi C, de Sousa MV, Huang YY, Bagnato VS, Parizotto NA, Hamblin MR (2015) Time response of increases in ATP and muscle resistance to fatigue after low-level laser (light) therapy (LLLT) in mice. Lasers Med Sci 30:1259–1267
80. Tedford CE, DeLapp S, Jacques S, Anders J (2015) Quantitative analysis of transcranial and intraparenchymal light penetration in human cadaver brain tissue. Lasers Surg Med 47:312–322
81. Ferraresi C, Kaippert B, Avci P, Huang YY, de Sousa MV, Bagnato VS, Parizotto NA, Hamblin MR (2015) Low-level laser (light) therapy increases mitochondrial membrane potential and ATP synthesis in C2C12 myotubes with a peak response at 3–6 h. Photochem Photobiol 91:411–416
82. Burland M, Paris L, Quintana P, Bec JM, Dioulouflet L, Sar C, Boulhaddaoui H, Charlot B, Braga Silva J, Chammas M, Sieso V, Valmier J, and Bardin F (2014) Neurite growth acceleration of adult dorsal root ganglion neurons illuminated by low-level light emitting diode light at 645 nm. J Biophotonics 30
83. Ferraresi C, Dos Santos RV, Marques G, Zangrande M, Leonaldo R, Hamblin MR, Bagnato VS, Parizotto NA (2015) Light-emitting diode therapy (LEDT) before matches prevents increase in creatine kinase with a light dose response in volleyball players. Lasers Med Sci. doi:10.1007/s10103-015-1728-3
84. Ferraresi C, Beltrame T, Fabrizzi F, Nascimento ES, Karsten M, Francisco CO, Borghi-Silva A, Catai AM, Cardoso DR, Ferreira AG, Hamblin MR, Bagnato VS, and Parizotto NA (2015) Muscular pre-conditioning using light-emitting diode therapy (LEDT) for high-intensity exercise: a randomized double-blind placebo-controlled trial with a single elite runner. Physiother Theory Pract 1–8
85. Gupta A, Keshri GK, Yadav A, Gola S, Chauhan S, Salhan AK, Bala and Singh S (2014) Superpulsed (Ga-As, 904 nm) low-level laser therapy (LLLT) attenuates inflammatory response and enhances healing of burn wounds. J Biophotonics
86. Fazilat F, Ghoreishian M, Fekrazad R, Kalhori KA, Khalili SD, Pinheiro AL (2014) Cellular effect of low-level laser therapy on the rate and quality of bone formation in mandibular distraction osteogenesis. Photomed Laser Surg 32:315–321
87. de Jesus VC, Beunes G, Paraguassú GM, Ramalho LM, Pinheiro AL, Ramalho MJ, Rodriguez TT (2015) Influence of laser photobiomodulation (GaAlAs) on salivary flow rate and histomorphometry of the submandibular glands of hypothyroid rats. Lasers Med Sci 30:1275–1280
88. Sperandio FF, Simões A, Corrêa L, Aranha AC, Giudice FS, Hamblin MR, Sousa SC (2014) Low-level laser irradiation promotes the proliferation and maturation of keratinocytes during epithelial wound repair. J Biophotonics. doi:10.1002/jbio.201400064
89. Larkin-Kaiser KA, Christou E, Tillman M, George S, Borsa PA (2015) Near-infrared light therapy to attenuate strength loss after strenuous resistance exercise. J Athl Train 50:45–50
90. de Carvalho FB, Andrade AS, Rasquin LC, de Castro IV, Cangussu MC, Pinheiro AL, dos Santos JN (2015) Effect of laser (λ 660 nm) and LED (λ 630 nm) photobiomodulation on formocresol-induced oral ulcers: a clinical and histological study on rodents. Lasers Med Sci 30:389–396
91. Tomimura S, Silva BP, Sanches IC, Canal M, Consolim-Colombo F, Conti FF, De Angelis K, Chavantes MC (2014) Hemodynamic effect of laser therapy in spontaneously hypertensive rats. Arq Bras Cardiol 103:161–164
92. Ban Frangez H, Frangez I, Verdenik I, Jansa V, Virant KI (2015) Photobiomodulation with light-emitting diodes improves sperm motility in men with asthenozoospermia. Lasers Med Sci 30:235–240
93. Ramalho KM, de Freitas PM, Correa-Aranha AC, Bello-Silva MS, Lopes RM, Eduardo CP (2014) Lasers in esthetic dentistry: soft tissue photobiomodulation, hard tissue decontamination, and ceramics conditioning. Case Rep Dent 2014:927429
94. Turrioni AP, Basso FG, Alonso JR, de Oliveira CF, Hebling J, Bagnato VS, de Souza Costa CA (2015) Transdentinal cell photobiomodulation using different wavelengths. Oper Dent 40: 102–111
95. Barbosa M, Natoli R, Valter K, Provis J, Maddess T (2014) Integral-geometry characterization of photobiomodulation effects on retinal vessel morphology. Biomed Opt Express 5:2317–2332
96. Havlucu U, Bölükbaşı N, Yeniyol S, Cetinel S, Ozdemir T (2014) Effects of LPT and BioOss® as single and combined treatment in an experimental model of bone defect healing in rats. J Oral Implantol. doi:10.1563/aaid-joi-D-13-00310
97. Tang J, Herda AA, Kern TS (2014) Photobiomodulation in the treatment of patients with non-center-involving diabetic macular oedema. Br J Ophthalmol 98:1013–1015
98. Elkizer A, Uysal T, Güray E, Akkuş D (2015) Effect of LED-mediated-photobiomodulation therapy on orthodontic tooth movement and root resorption in rats. Lasers Med Sci 30:779–785
99. Freire Mdo R, Freitas R, Colombo F, Valença A, Marques AM, Sarmento VA (2014) LED and laser photobiomodulation in the prevention and treatment of oral mucositis: experimental study in hamsters. Clin Oral Investig 18:1005–1013
100. Di Marco F, Di Paolo M, Romeo S, Colecchi L, Fiorani L, Spana S, Stone J, Bisti S (2014) Combining neuroprotectants in a model of retinal degeneration: no additive benefit. PLoS One 9:e100389
101. Montoro LA, Turrioni AP, Basso FG, de Souza Costa CA, Hebling J (2014) Infrared LED irradiation photobiomodulation of oxidative stress in human dental pulp cells. Int Endod J 47: 747–755
102. Pitzschke A, Lovisa B, Seydoux O, Zellweger M, Pfleiderer M, Tardy Y, Wagnières G (2015) Red and NIR light dosimetry in the human deep brain. Phys Med Biol 60:2921–2937
103. Amaroli A, Parker S, Dorigo G, Benedicenti A, Benedicenti S (2015) Paramecium: a promising non-animal bioassay to study the effect of 808 nm infrared diode laser photobiomodulation. Photomed Laser Surg 33:35–40
104. Naeser MA, Zafonte R, Krengel MH, Martin PI, Frazier J, Hamblin MR, Knight JA, Meehan WP 3rd, Baker EH (2014) Significant improvements in cognitive performance post-transcranial, red/near infrared light-emitting diode treatments in chronic, mild traumatic brain injury: open-protocol study. J Neurotrauma 31:1008–1017
105. do Nascimento RX, Callera F (2006) Low-level laser therapy at different energy densities (0.1–2.0 J/cm^2) and its effects on the capacity of human long-term cryopreserved peripheral blood progenitor cells for the growth of colony-forming units. Photomed Laser Surg 24:601–604
106. Altan BA, Sokucu O, Toker H, Sumer Z (2014) The effect of low-level laser therapy on orthodontic tooth movement: metrical and immunological investigation. JSM Dent 2:1040
107. Lanzafame RJ, Stadler I, Kurtz AF, Connelly R, Peter TA, Brondon P, Olson D (2007) Reciprocity of exposure time and irradiance on energy density during photoradiation on wound healing in a murine pressure ulcer model. Lasers Surg Med 39: 534–542
108. Kheshie AR, Alayat ASM, Ali MME (2014) High intensity versus low-level laser therapy in the treatment of patients with knee osteoarthritis: a randomized controlled trial. Lasers Med Sci 29: 1371–1376

109. Karu TI (2010) Multiple roles of cytochrome c oxidase in mammalian cells under action of red and IR-A radiation. IUBMB Life 62:607–610
110. Karu TI, Pyatibrat LV, Afanasyeva NI (2005) Cellular effects of low power laser therapy can be mediated by nitric oxide. Laser Surg Med 36:307–314
111. Karu TI (2008) Mitochondrial signaling in mammalian cells activated by red and near-IR radiation. Photochem Photobiol 84: 1091–1099
112. Enwemeka CS (2009) Intricacies of dose in laser phototherapy for tissue repair and pain relief. Photomed Laser Surg 27:387–393
113. Vayshenker I, Li X, Livigni DJ, Scott TR and Cromer CL (2000) NIST measurement services: optical fiber power meter calibrations at NIST. NIST Spec Publ 250–54
114. Price RBT, Rueggeberg FA, Labrie D and Felix CM. Irradiance uniformity and distribution from dental light curing units. J Esthet Restor Dent, 2010; 22: 86:103
115. Pinheiro ALB, Oliveira MG, Martins PPM, Ramalho LMP, de Oliveira MAM, Novaes Junior A, Nicolau RA (2001) Biomodulatory effects of LLLT on bone regeneration. Laser Ther 13:73–79
116. Bunsen R, Roscoe HE. Photochemische Untersuchungen. Pggendorff's Annalen, 1855; 96: 373–394, 1857; 100: 43–88 and 781–516, 1857; 101: 235–263, 1859; 108: 193–2073
117. Nussbaum EL, Lilge L, Mazzulli T (2003) Effects of low level laser therapy (LLLT) of 810 nm upon in vitro growth of bacteria: relevance of irradiance and radiant exposure. J Clin Laser Med Surg 21:283–290
118. Bunsen RW, Roscoe HE (1862) Photochemical researches—part V. On the measurement of the chemical action of direct and diffuse sunlight. Proc R Soc London 12:7
119. Karu TI, Kolyakov SF (2005) Exact action spectra for cellular responses relevant to phototherapy. Photomed Laser Surg 23: 355–361
120. Palin WM, Hadis MA, Milward MR, Carroll JD and Cooper PR (2015) Beam profile measurements for dental phototherapy: the effect of distance, wavelength and tissue thickness. Proc SPIE9309. Mechanisms for low-light therapy X, 930905. doi: 10.1117/12.2077628
121. Vandewalle KS, Roberts HW, Rueggeberg FA (2008) Power distribution across the face of different light guides and its effect on composite surface microhardness. J Esthet Restor Dent 20:108–117
122. LBA-USB Beam Profiler User Guide. Logan, UT: Ophir-Spiricon; 2006
123. Price RB, Labrie D, Rueggeberg FA, Felix CA (2010) Irradiance differences in the violet (405 nm) and blue (460 nm) spectral ranges among dental light-curing units. J Esthet Restor Dent 22: 363–377
124. Dominici M, Le Blanc K, Mueller I, Slaper-Cortenbach I, Marini F, Krause D, Deans R, Keating A, Prockop D, Horwitz E (2006) Minimal criteria for defining multipotent mesenchymal stromal cells. The International Society for Cellular Therapy Position Statement. Cytotherapy 8:315–317

CONFERENCES

1. 47th Meeting of the Continental European Division of the International Accociation for Dental Research, Antalya, Turkey; October 15-17, 2015.

   Oral presentation. Abstract title: The effect of 660nm LED irradiation on human oral epithelial cell *in vitro*.

2. EuroPerio8, London, UK; June 3-6, 2015.

   Poster presentation. Abstract title: Effect of Low-Level Light Exposure on Human Oral Epithelial Cells.

3. BSP Autumn Conference, Birmingham, UK; September 21-23, 2014.

   Poster presentation. Abstract title: Potential for Low-Level Light Therapy in Periodontal Disease Management.